Physics Reports 575 (2015) 1–71

Contents lists available at ScienceDirect

Physics Reports

journal homepage: www.elsevier.com/locate/physrep

Tracing and controlling electronic dynamics in atoms and molecules by attosecond pulses

Liang-You Peng [a,b,*], Wei-Chao Jiang [a,1], Ji-Wei Geng [a,1], Wei-Hao Xiong [a,1], Qihuang Gong [a,b,*]

[a] State Key Laboratory for Mesoscopic Physics and Department of Physics, Peking University, Beijing 100871, China
[b] Collaborative Innovation Center of Quantum Matter, Beijing 100871, China

ARTICLE INFO

Article history:
Accepted 7 February 2015
Available online 24 February 2015
editor: J. Eichler

ABSTRACT

In this review, we will focus on the theoretical aspects in observing and controlling the electronic dynamics in few-electron atoms and molecules by attosecond pulses in different circumstances. In particular, we will first review the main theoretical methods and concepts in strong field and attosecond physics, and then discuss a number of topics including generation of xuv light sources, the probe and steering of the electron motion in the combination of xuv and IR pulses, the photoionization time delay, the electron–electron correlation dynamics in multiple-electron atoms and molecules, etc. Although the present review mainly concentrates on the theoretical aspects, in each section we will also give a brief account of the related experimental implications and implementations for those which have been demonstrated so far or which will be experimentally feasible in the near future.

Contents

* Corresponding authors.
E-mail addresses: liangyou.peng@pku.edu.cn (L.-Y. Peng), qhgong@pku.edu.cn (Q. Gong).

[1] These authors equally contribute to this work.

http://dx.doi.org/10.1016/j.physrep.2015.02.002
0370-1573/

1. Introduction

To acquire the internal structures and constituents of microscopic matters stands for one of the main pursuits of physics, chemistry, and biology. Traditionally, particle scattering or collision has been used to get these knowledge by measuring the scattered particles or the broken fragments. The earliest scattering experiments went back to 1880–1890s by Goldstein and Thomson in studying the nature of electric discharge in a high-vacuum cathode-ray tube, with subsequent studies using the rays of positive particles as a method of chemical analysis [1]. In addition, Thomson attempted to estimate the number of electrons inside an atom in his plum pudding model from measurements of the scattering of light. Thomson's student, Rutherford, followed this route to discover the nuclear nature of atoms by deflecting alpha particles passing through a thin metal foil in his lab during 1908–1913 [2,3]. Actually, the analysis of scattering or collision phenomena plays an important role in nearly every investigation into the world of microcosm. In fact, most of the detailed information on particle structure and interaction is inferred from scattering experiments in high energy physics and nuclear physics.

However, only knowing the structures and constituents of matter is far from being enough. People have been keen on watching how the constituent particles move and interact with each other as a function of time. In another word, to understand and further control the internal dynamics of microscopic matter is an everlasting dream of scientists. Usually, the dynamics happens on an ever faster time scale, which makes its observation and control not an easy task because one needs a 'camera' that is fast enough to capture its evolution. The monitoring of the dynamics is often realized in a pump–probe scheme. The first prototype pump–probe experiment was carried by Toepler in 1864 to observe the evolution of the shock wave using two short light sparks with a time delay controlled by a circuit in the microsecond time regime [4]. Subsequently, Abraham and Lemoine [5] improved the pump–probe spectroscopy by generating the pump and probe flash from a same spark with the delay varied by the difference of the optical path length between them. Their scheme achieved synchronism between the two flashes and thus improved the time resolution, which was however ultimately limited by the flash duration itself. Therefore, the direct observation of even faster motions on the microscopic scale had been hindered by the incoherent light sources in the nanosecond regime for almost six decades until the invention of lasers in 1960 [6]. Ever since then, there has been several crucial stages of technological revolutions which have made the durations of optical laser pulses become

shorter and shorter until the single-cycle limit [7,8]. These new short light pulses have made it possible for scientists to trace and control the fast motions on the atomic and molecular levels, e.g., monitoring the breakage of a chemical bond in real time by pump–probe method using femtosecond laser pulses [9,10].

At the same time, the pulse compression and amplification technologies have continually increased the peak intensity of a laser pulse to an extent that the external force exerted by the laser electric field on the electron is comparable with or many times larger than the internal Coulomb force that binds the atoms and molecules together [11,12]. The matter in gas phase or condensed phase can even be turned into a plasma, in which the electrons and protons can be accelerated to an extremely high energy in the relativistic regime [13–15]. To an extreme case, the current and future high power lasers make it feasible to explore the realm of relativistic quantum dynamics, quantum electrodynamics, and nuclear and particle physics [16]. In the present review, we will restrain ourselves from discussing the aforementioned topics of laser–particle acceleration and relativistic quantum dynamics.

In the pump–probe scheme, the pulse duration of a laser pulse used to watch and control the microscopic dynamics needs to be comparable or shorter than the typical time scale of the dynamics itself. Meanwhile, the intensity of the laser pulse must be strong enough to induce a nonlinear response to the system under scrutiny. The mature and stable technologies in femtosecond pulses have guaranteed the great success in many branches of femtosecond sciences in physics [17], chemistry [18], biology [19], micromachining [20], etc. Unlike the atomic and molecular dynamics in the femtosecond and picosecond regime, the electronic motion inside atoms and molecules is usually in the attosecond regime,[2] whose direct supervision and control is *usually* beyond the reach of even the single-cycle optical laser pulses (e.g., for a 800 nm laser, the period is about 2.6 fs). Therefore, one needs coherent attosecond pulses [23,24] for such purposes, which have luckily become available in several laboratories worldwide since 2001 [25–27]. Nowadays, the majority of the attosecond light sources are generated through the highly nonlinear interaction of atoms and molecules in gas phase with strong femtosecond laser pulses in the intensity range of 10^{12}–10^{16} W/cm^2. Nevertheless, there are other well established facilities, such as synchrotron radiation [28] and free electron lasers [29], which can provide very versatile sources in a broad frequency range and possibly with a much higher photon flux [30,31]. However, these sources usually cannot provide short and stable enough pulses for direct probe and control of the electronic motion in real time.

Investigations over dynamics of atoms and molecules in gas phase with strong femtosecond laser pulses have played fundamental roles in the generation and applications of attosecond pulses and in our general understanding of laser–matter interactions in the nonrelativistic regime. From a theoretical point of view, the underlying mechanisms can be first understood in a single atom and molecule level with the temporary neglecting of the macroscopic effects caused by a dense gas. For these purposes, in the last 20 years or so, a three-step model [32,33] has been successfully used to transparently explain many strong field phenomena. In the scenario of this three-step model, the electron in atoms or molecules first tunnels through the distorted Coulomb potential barrier into the continuum; it then propagates in the combined field of the laser pulse and the ionic core; when the laser electric field reverses its direction, the accelerated electron has a certain probability to return to the vicinity of the ionic core, where recombination can happen to emit high-order harmonic photons or elastic/inelastic scattering may take place to induce single or multiple ionization and atomic excitation. For the case of molecules, dissociation or Coulomb explosion may also happen because of the recollision process.

It is obvious that the above recollision of the ionizing electron with the core within an optical cycle bridges the traditional collision physics and the optical physics in the strong field regime [34]. Actually, compared with the traditional particle scattering, the reunion of collision and optical physics possesses overwhelming advantages, such as temporal and spatial coherence and high current flux. Because the high-order harmonic generation (HHG) process contains information of the initial atomic or molecular orbital and the returning wave packets, HHG spectroscopy has been established and applied to image the orbital or to probe the internal dynamics [35–37]. Similarly, if the returning electron is elastically scattered off the atomic or molecular core, the high energy electrons also encode the structural and dynamical information of the core at the instance of the recollision [38,39]. The strong field physics has allowed us to probe and control the molecular structures and dynamics in an unprecedented temporal and spatial resolution.

In the past three decades or so, intensive experimental and theoretical studies were carried out to understand a lot of important strong field phenomena [40–42], such as above-threshold ionization (ATI) [43–45], high-order harmonic generation [46–49], double or multiple ionization [50–55], dissociative ionization [56–60], molecular imaging [35,36,61–63], molecular alignment [64,65], Coulomb explosion [66–73], etc. In addition, quantum control of these processes have been realized by tuning the laser parameters (such as the central wavelength, the peak intensity, and the pulse duration) or by using a multiple laser pulses scheme [74,75]. In particular, when the laser pulse duration approaches a few-cycle limit, the carrier envelope phase (CEP) becomes another important knob to control these processes [76–78], especially the controlled emission of electrons/photons or controlled molecular dissociation [45,79–83].

However, the main purpose of the present review is to discuss the progress of tracing and controlling the electronic motion inside atoms and molecules after the availability of the attosecond pulses. The generation of such short pulses are mostly based on the aforementioned high-order harmonic generation. One of the conspicuous features of the HHG spectra is that it contains a plateau in which harmonic yields of each order harmonic have a comparable amplitude and definite phases

[2] However, note that, the electronic dynamics of highly lying Rydberg states is in the range of picoseconds or nanoseconds, which can be well controlled by microwave pulses or shaped electric pulses, see e.g., Refs. [21,22].

among them. People theoretically proposed that one can utilize these wonderful properties to generate laser pulses (or pulse trains) on the attosecond time scale [84–91]. Eventually, thanks to a number of breakthroughs in the laser technologies and xuv optics, single attosecond pulse [25] or attosecond pulse trains [26] were both experimentally demonstrated in 2001. In the following time of more than a decade, different schemes of attosecond pulse generation have been theoretically proposed and some of them are experimentally demonstrated, with essential goals of a controllable attosecond light sources with a shorter duration, a higher photon flux, and preferably a higher repetition rate [92,93].

Although the present attosecond sources available in laboratories can hardly been applied to a direct attosecond pump and attosecond probe experiment, a lot of new insights into the electronic dynamics in atoms, molecules, and condensed matter have been unprecedentedly acquired experimentally by using attosecond pulses as a pump and a femtosecond pulse as a probe, or vice versa, with a wonderful synchronization of both pulses controlled in a precision within a few attoseconds [94]. The availability of single attosecond pulse or attosecond pulse trains has enabled the experimental scrutiny of many fundamental electron processes that are out of reach by femtosecond pulses alone, such as the dynamics of Auger processes [95], electron tunneling in atoms [96], charge transport dynamics in condensed matter [97], coherent EUV emission in the single-cycle limit [98], time delay in photoelectric effects from different shells of atoms [99], direct observation of valence electron movement [100,101], and the control of the optical and electric properties of dielectrics [102,103], etc. On the theoretical side, there have been many other proposals which potentially enable us to trace and control the electronic motion inside atoms, molecules, and solids [104–115]. In the present review, we wish to present a self-contained brief review of the new concepts, new methods, and the new insights in attosecond physics, with emphasis on how one can trace and control the electronic motion inside atoms and molecules. At the same time, relevant experimental demonstrations or their feasibilities in the near future will be discussed in an appropriate context.

The rest of the review is arranged as follows. In Section 2, we will give a brief introduction to the theoretical and numerical methods in strong field and attosecond physics. Then, the theoretical and experimental aspects of attosecond light sources will be discussed in Section 3, at the end of which we will mention the applications of HHG spectroscopy in the molecular structures and dynamical information. In Section 4, we then proceed to present how one can probe and control the electronic dynamics with the combination of xuv and/or IR pulses, mostly in the context of attosecond streaking. The availability of the attosecond streaking technique has allowed one to ask the fundamental question such as how long it takes for a photoionization to occur, we thus discuss the photoionization time delays for atoms, molecules and solids in Section 5. In Section 6, we deal with more complicated cases of two-electron atoms and molecules, emphasizing the probe and control of the electron correlation dynamics by xuv pulses. In this section, theoretical methods pertaining to the two-electron atoms and molecules will be also surveyed. Finally, in Section 7, we will give a short summary and outlook.

Note that atomic units (a.u.) will be used throughout this review unless otherwise stated. In the system of atomic units, the following four quantities are all assumed to be unit, including the mass of an electron m_e, the amount of charge carried by an electron $|e|$, the reduced Planck's constant $\hbar$, and the Coulomb's constant $1/(4\pi\varepsilon_0)$. Explicitly, one has $m_e = |e| = \hbar = 1/(4\pi\varepsilon_0) = 1$. However, we keep the sign of the electron charge to be -1 in all the formulation.

2. Theoretical concepts and numerical methods

In the attosecond physics, it is important to understand the underlying dynamics of atoms and molecules interacting with strong femtosecond laser pulses. This is true because of several apparent reasons. Firstly, both the electronic and atomic dynamics under interaction with attosecond and/or femtosecond laser pulses are governed by the same equation of motion, i.e., the time-dependent Schrödinger equation, with the atom–field interaction described semiclassically. By *semiclassically*, we mean that the atoms or molecules are treated quantum mechanically while the light is classically described by the vector and scalar potential of the electromagnetic field. Secondly, as mentioned in the last section, the majority of the current technologies of attosecond light sources are based on high-order harmonic generation, i.e., the emitting of high energy photons when atoms and molecules are exposed to intense femtosecond laser pulses. Therefore, the development and improvement of attosecond pulses critically rely on how well one can shape and control the driving femtosecond laser pulses. Thirdly, many strong field processes are initialized by the same first step, i.e., the tunneling ionization of an electron. It is well known that the ionization rate in an electric field exponentially depends on the field strength, which means that the tunneling ionization in strong IR fields happens within a very small fraction of an optical period when the laser electric field acquires its maxima. Therefore, the tunneling process of an electron is in the attosecond domain. After its tunneling, the electron will propagate in the laser field and pick up a significant amount of kinetic energy from the field. After the laser electric field reverses its sign, the electron has a probability to recombine to or recollide with the ionic core, where both processes also happen in the subfemtosecond domain. Because of these facts, one can actually probe and control some of the fast electronic and atomic dynamics *without* usage of attosecond pulses. For example, by extracting accurate differential elastic scattering and photo-recombination cross sections [116–118], one can carry out molecular imaging [35,62,119].

To sum up, understanding the ionization dynamics caused by an intense infrared laser pulse is the doorway to understand the electronic dynamics in the attosecond time scale. Thus we will present the main theoretical concepts and numerical methods in strong field and attosecond physics in this section. Traditionally, the theoretical methods in strong field physics can be classified to three main categories, i.e., analytical or semi-analytical approaches; classical and semiclassical methods; direct numerical solution of the time-dependent Schrödinger equation (TDSE).

When the laser-interaction is *weak*, time-dependent or time-independent perturbation theories represent the first type of useful analytical methods. In particular, perturbation theories are applicable in the case of few-photon single or double ionization of atoms by xuv or attosecond light sources. Combined with other methods, they have played important roles in interpreting many attosecond phenomena.

One of the most prevailing tool of the semi-analytical approaches is Keldysh–Faisal–Reiss (KFR) theory, i.e., the so-called strong field approximation (SFA) [120–122]. It is worth pointing out that, for the emitted high energy photons or electrons, Frolov and coworkers [118,123–141] have developed analytical methods based on the time-dependent effective range (TDER) theory. Their methods can give quantitatively accurate differential photon or electron spectra when compared with the results of TDSE calculations. In recent years, Tolstikhin and coworkers [142–157] have made great progress in developing a theory which can treat the Coulomb and laser field on the equal footing and thus can produce quantitatively correct results almost in the whole electron spectrum region when the adiabatic condition is satisfied.

In many cases, SFA can achieve qualitative agreement with the *ab initio* TDSE results or experimental measurements, especially for the case of negative ions ([158,159] and references therein) for the high energy rescattering electrons [45,160] and for cutoff region of HHG [44,161]. However, severe discrepancies were recently observed when compared the SFA results with experimental or TDSE data, particularly in the low energy regime. The neglect of the Coulomb potential in the ionization of neutral atoms in the SFA leads to these discrepancies, which include Coulomb-asymmetries in elliptically polarized fields [162–164], the holography patterns observed in photoelectron momentum distributions [165–170], frustrated tunneling ionization [171–174], near-threshold radial structures [175–177], and the low-energy structure at long wavelengths [178–186].

A simple and intuitive way to consider both the role of the laser field and Coulomb potential is the purely classical method, in which one numerically solves time-dependent Newton's equation (TDNE) of the electron. TDNE calculations can be carried out over a wide range of laser parameters where most experiments have been carried out (see Ref. [50] and references therein).

Another widely used method is the semiclassical scheme [164,174,187–190], in which the initial conditions of the electron for classical propagation are prescribed by a quantum tunneling formula [191]. This type of semiclassical method, usually called classical trajectory Monte Carlo (CTMC) simulation, has achieved great success in interpreting many experimental results, but some quantum features such as interferences in the spectra cannot be captured by these models. Very recently, a quantum trajectory Monte Carlo (QTMC) was proposed to successfully interpret the interference patterns observed in the experiments [192,193]. QTMC is a generalization of the CTMC by adding a phase to each trajectory from the classical action, based on the Feynman path integral [194].

The most quantitatively accurate method to investigate the dynamics of atomic and molecular ionization in strong laser fields is to solve the corresponding TDSE in its full dimensions. Numerical solution to TDSE for a multielectron atom or molecule is in most cases a formidable task. Luckily, for some of the strong field processes, the single-active-electron approximation (SAE), can be usually applied, which means the atoms are modeled by an effective potential optimized to reproduce energies of the ground state and singly excited states. For instance, good agreement was achieved by comparing the experimental spectra for argon with those calculated by TDSE [195].

Numerical solutions to TDSE plays very important roles in femtosecond and attosecond physics. It is a benchmark tool to test different kinds of approximate theories and to compare with experimental measurements. However, TDSE calculations can be very computationally demanding, especially for high intensity, large wavelength, long pulse duration, or elliptically polarized laser pulses.

Please note that each of the aforementioned methods has its own range of applicability with different strengths and drawbacks. Therefore, for a full and clear understanding of a specific problem, one usually needs to simultaneously use more than one method. In the rest of this section, we will introduce the basic concepts in the strong field and attosecond physics and give an outline of the different theoretical methods mentioned above. We will first present the atom–field minimal coupling Hamiltonian, which is followed by a general introduction of the time-dependent perturbation theory for the case of weak interaction Hamiltonian. Then we move on to the other opposite when the atom–field coupling is very strong. In this case, classical and semiclassical methods can be effectively applied. Particularly, we briefly introduce the classical simple man's model, in which crude approximations are made by neglecting the atomic Coulomb field. It can incredibly provide intuitive pictures of many strong field phenomena. Then we briefly illustrate the semiclassical methods in which the laser field and the Coulomb effects are taken into account on equal footing. In addition, we will introduce how to describe quantum interference in the semiclassical model. The counterpart of quantum mechanical method in the case of intense field coupling is the strong field approximation, which is a semi-analytical approach. By using the concept of quantum orbits, the SFA amplitude can be reformulated by a sum over saddle points. In this case, a fully quantum-mechanical generalization of the classical orbits of the simple-man model that retains the intuitive appeal of the former, but allows for quantum interference and quantum tunneling incorporated. Next, we briefly introduce numerical methods for TDSE and briefly illustrate how to extract physical observable from the wave function. Note that, in many circumstances, the TDSE simulations act as exact numerical experiments to validate other approximative methods and to quantitatively compare with the experimental measurements, provided that reliable algorithms and efficient computer codes are guaranteed. However, solution to the TDSE sometimes works like a black box and lacks direct physical insights into the underlying dynamics. Nevertheless, one can carry out a series of calculations under different laser parameters so that the main underlying mechanisms for a physical process can be surely identified.

At the end of this section, we will turn to briefly introduce two important schemes in the attosecond physics, namely, the RABBITT (reconstruction of attosecond beating by interference of two-photon transitions) technique and the attosecond streaking. These two techniques have been playing very important roles in probing and controlling the electronic dynamics.

2.1. Atom–field interaction Hamiltonian

The Hamiltonian of an electron in the electromagnetic field can be derived from a local gauge invariance argument [196]. In this subsection, we will follow the route described by Scully to present the atomic-field interaction Hamiltonian [196]. The motion of a free electron is described by the Schrödinger equation in atomic unites

$$-\frac{1}{2}\nabla^2\Psi(\mathbf{r},t)=i\frac{\partial\Psi(\mathbf{r},t)}{\partial t}, \tag{1}$$

such that $P(\mathbf{r},t)=|\Psi(\mathbf{r},t)|^2$ gives the probability of finding the electron at position $\mathbf{r}$ and time t. Note that, under the transform $\Psi(\mathbf{r},t)\rightarrow\Psi(\mathbf{r},t)\exp\ (i\chi)$ (where χ is a constant), P remains unchanged and $\Psi(\mathbf{r},t)\exp\ (i\chi)$ is also a solution to Eq. (1). However, if one allows χ to vary locally, i.e., $\Psi(\mathbf{r},t)\rightarrow\Psi(\mathbf{r},t)\exp\ [i\chi(\mathbf{r},t)]$, the above Schrödinger equation needs to be modified as

$$H(\mathbf{r},t)\Psi(\mathbf{r},t)\equiv\left\{-\frac{1}{2}[\nabla+i\mathbf{A}(\mathbf{r},t)]^2-U(\mathbf{r},t)\right\}\Psi(\mathbf{r},t)=i\frac{\partial\Psi(\mathbf{r},t)}{\partial t}, \tag{2}$$

in order to satisfy the local gauge transform invariance so that $\Psi(\mathbf{r},t)\exp\ [i\chi(\mathbf{r},t)]$ remains a solution to the modified Schrödinger equation Eq. (2). $H(\mathbf{r},t)$ is the so-called minimal coupling Hamiltonian. Along with the wave function transform, one simultaneously requires that

$$\mathbf{A}(\mathbf{r},t)\rightarrow\mathbf{A}(\mathbf{r},t)-\nabla\chi(\mathbf{r},t), \tag{3}$$

$$U(\mathbf{r},t)\rightarrow U(\mathbf{r},t)+\frac{\partial}{\partial t}\chi(\mathbf{r},t). \tag{4}$$

The functions $\mathbf{A}(\mathbf{r},t)$ and $U(\mathbf{r},t)$ are identified as the vector and scalar potentials of the electromagnetic field, which are of course gauge-dependent. The gauge-independent quantities are the classical electric and magnetic fields

$$\mathbf{E}(\mathbf{r},t)=-\frac{\partial\mathbf{A}}{\partial t}-\nabla U, \tag{5}$$

$$\mathbf{B}(\mathbf{r},t)=\nabla\times\mathbf{A}. \tag{6}$$

For an electron bounded by a Coulomb potential $V(\mathbf{r})$, the minimal coupling Hamiltonian $H(\mathbf{r},t)$ in Eq. (2) is then changed to

$$H(\mathbf{r},t)=-\frac{1}{2}[\nabla+i\mathbf{A}(\mathbf{r},t)]^2+U(\mathbf{r},t)+V(\mathbf{r}), \tag{7}$$

which can be reduced to a simpler form as

$$H(\mathbf{r},t)=-\frac{1}{2}[\nabla+i\mathbf{A}(t)]^2+V(\mathbf{r}), \tag{8}$$

if the radiation gauge [$U(\mathbf{r},t)=0$ and $\nabla\cdot\mathbf{A}=0$] is used and the dipole approximation can be made by a Taylor expansion of the vector potential $\mathbf{A}(\mathbf{r},t)\approx\mathbf{A}(t)\exp\ (-i\mathbf{k}\cdot\mathbf{r}_0)$ when the atomic size is much smaller than the wavelength of the field.

For the time-dependent Schrödinger equation with Hamiltonian Eq. (8), if one defines $H_{\rm at}=-\frac{1}{2}\nabla^2+V(\mathbf{r})$ and makes a further transformation of

$$\Psi(\mathbf{r},t)=\exp\ [i\mathbf{A}(t)\cdot\mathbf{r}]\Phi(\mathbf{r},t), \tag{9}$$

the corresponding time-dependent Schrödinger equation is then given by

$$i\frac{\partial\Phi(\mathbf{r},t)}{\partial t}=[H_{\rm at}+\mathbf{r}\cdot\mathbf{E}(t)]\,\Phi(\mathbf{r},t), \tag{10}$$

where the interaction Hamiltonian is referred as in the length gauge: $H_{\rm int}^{\rm L}=\mathbf{r}\cdot\mathbf{E}(t)$.

On the other hand, the Schrödinger equation can also be written into

$$i\frac{\partial\Psi(\mathbf{r},t)}{\partial t}=[H_{\rm at}+\mathbf{p}\cdot\mathbf{A}(t)]\,\Psi(\mathbf{r},t), \tag{11}$$

by expanding the square of the brackets and neglecting the A^2 term since it only contributes a global phase to the wave function. In this case, the interaction Hamiltonian is referred as in the velocity gauge: $H_{\rm int}^{\rm V}=\mathbf{p}\cdot\mathbf{A}(t)$.

2.2. Time-dependent perturbation theory

Time-dependent perturbation theory, which was originally developed by Dirac [197,198], is quite suitable to study the effects of a time-dependent perturbation $V(t)$ applied to a time-independent Hamiltonian H_0. In this section, we review the basic idea of time-dependent perturbation theory and the procedure to obtain the perturbative amplitude of the transition from an initial bound state to the continuum.

Perturbation theory can be formulated elegantly in the interaction picture (also known as the Dirac picture), in which the state vectors and the operators are defined as unitary transformation to those same operators and state vectors in the Schrödinger picture. The total Hamiltonian in the Schrödinger picture is divided into two parts

$$H = H_0 + V(t), \tag{12}$$

where H_0 is the time-independent part and $V(t)$ is the time-dependent part. A state vector in the interaction picture is defined as

$$|\Psi_{\rm I}(t)\rangle = e^{iH_0 t}\,|\Psi(t)\rangle\,. \tag{13}$$

An operator in the interaction picture is defined as

$$O_{\rm I} = e^{iH_0 t} O e^{-iH_0 t}. \tag{14}$$

Since the operators commute with differentiable functions of themselves, the time-independent Hamiltonian H_0 stays the same in the interaction picture as in the Schrödinger picture. Usually the time-dependent interaction Hamiltonian $V(t)$ does not commute with H_0, so the interaction Hamiltonian $V_{\rm I}(t)$ in the interaction picture and the interaction Hamiltonian $V(t)$ in the Schrödinger picture are usually different.

The evolution of the state vector obeys

$$i\frac{\partial}{\partial t}\,|\Psi_{\rm I}(t)\rangle = V_{\rm I}(t)\,|\Psi_{\rm I}(t)\rangle\,, \tag{15}$$

and the evolution of the time-dependent operator obeys

$$i\frac{\partial}{\partial t} O_{\rm I}(t) = [O_{\rm I}(t), H_0]\,. \tag{16}$$

The state vector $\Psi_{\rm I}(t)$ can be related to the initial vector $\Psi_{\rm I}(t_0)$ by the propagator (time-evolution operator) $U_{\rm I}(t, t_0)$, i.e. $\Psi_{\rm I}(t) = U_{\rm I}(t, t_0)\Psi_{\rm I}(t_0)$. According to Eq. (15), it is not difficult to see that the propagator obeys the following differential evolution equation

$$i\frac{\partial}{\partial t} U_{\rm I}(t, t_0) = V_{\rm I}(t) U_{\rm I}(t, t_0). \tag{17}$$

The initial condition of Eq. (17) is $U_{\rm I}(t_0, t_0) = I$, where I is the unit operator. Solution of Eq. (17) can be formally expressed as

$$U_{\rm I}(t, t_0) = I - i\int_{t_0}^{t} d\tau V_{\rm I}(\tau) U_{\rm I}(\tau, t_0). \tag{18}$$

Now we assume that $V_{\rm I}(t)$ is just a small perturbation. Then we seek for the solution of Eq. (18) in the form of the sum of the powers of $V_{\rm I}(t)$. For the zeroth-order solution, the result can be given by

$$U_{\rm I}^{(0)}(t, t_0) = I, \tag{19}$$

which can be obtained be setting $V_{\rm I}(t) = 0$ in the right side of Eq. (18). This zeroth-order solution is now fed back into the right side of Eq. (18) to develop a first-order solution:

$$U_{\rm I}^{(1)}(t, t_0) = I - i\int_{t_0}^{t} dt_1 V_{\rm I}(t_1), \tag{20}$$

which in turn is fed back into the right side of Eq. (18) to develop a second-order solution:

$$U_{\rm I}^{(2)}(t, t_0) = I - i\int_{t_0}^{t} dt_1 V_{\rm I}(t_1) + (-i)^2 \int_{t_0}^{t} dt_2 \int_{t_0}^{t_1} dt_1 V_{\rm I}(t_2) V_{\rm I}(t_1). \tag{21}$$

Iterating this procedure, we thus obtain

$$U_{\rm I}(t, t_0) = \sum_{k=0}^{\infty} U_{\rm I}^{(k)}(t, t_0), \tag{22}$$

where

$$U_{\rm I}^{(k)}(t,t_0)=(-i)^k\int_{t_0}^{t}dt_k\int_{t_0}^{t_k}dt_{k-1}\ldots\int_{t_0}^{t_1}dt_1V_{\rm I}(t_k)V_{\rm I}(t_{k-1})\ldots V_{\rm I}(t_1). \tag{23}$$

Now we seek for the connection between the propagator $U_{\rm I}(t,t_0)$ in the interaction picture and the propagator $U(t,t_0)$ in the Schrödinger picture. For an initial state vector $|\Psi(t_0)\rangle$ in the Schrödinger picture, we firstly translate it to the interaction picture $|\Psi_{\rm I}(t_0)\rangle=e^{iH_0t_0}|\Psi(t_0)\rangle$. Then we apply the propagator $U_{\rm I}(t,t_0)$ in the interaction picture to $|\Psi_{\rm I}(t_0)\rangle$ to get $|\Psi_{\rm I}(t)\rangle$. Finally we translate the state vector $|\Psi_{\rm I}(t)\rangle$ in the interaction picture to the state vector $|\Psi(t)\rangle$ in the Schrödinger picture. This procedure leads to

$$|\Psi(t)\rangle=e^{-iH_0t}U_{\rm I}(t,t_0)e^{iH_0t_0}|\Psi(t_0)\rangle\,. \tag{24}$$

Thus,

$$\begin{aligned}U(t,t_0)&=e^{-iH_0t}U_{\rm I}(t,t_0)e^{iH_0t_0}\\&=\sum_{k=0}^{\infty}e^{-iH_0t}U_{\rm I}^{(k)}(t,t_0)e^{iH_0t_0}\\&=\sum_{k=0}^{\infty}U^{(k)}(t,t_0),\end{aligned} \tag{25}$$

where we have defined that

$$\begin{aligned}U^{(k)}(t,t_0)=e^{-iH_0t}U_{\rm I}^{(k)}(t,t_0)e^{iH_0t_0}&=(-i)^k\int_{t_0}^{t}dt_k\int_{t_0}^{t_k}dt_{k-1}\ldots\int_{t_0}^{t_1}dt_1e^{-iH_0t}V_{\rm I}(t_k)V_{\rm I}(t_{k-1})\ldots V_{\rm I}(t_1)e^{iH_0t_0}\\&=(-i)^k\int_{t_0}^{t}dt_k\int_{t_0}^{t_k}dt_{k-1}\ldots\int_{t_0}^{t_1}dt_1\\&\quad\times e^{-iH_0(t-t_k)}V(t_k)e^{-iH_0(t_k-t_{k-1})}V(t_{k-1})\ldots e^{-iH_0(t_2-t_1)}V(t_1)e^{-iH_0(t_1-t_0)}.\end{aligned} \tag{26}$$

Suppose the initial state vector is the eigenstate of the time-independent Hamiltonian H_0 with eigenvalue of E_i, and we denote that $|\Psi(t_0)\rangle=|E_i\rangle$. With the interaction of the perturbation $V(t)$, the system has probability to translate to the other eigenstate $|E_f\rangle$ of Hamiltonian H_0 with eigenvalue of E_f. The corresponding transition amplitude is expressed as

$$A_{fi}(t)=\langle E_f|\,U(t,t_0)\,|E_i\rangle\,. \tag{27}$$

The first-order transition amplitude can be expressed as

$$\begin{aligned}A_{fi}^{(1)}(t)&=\langle E_f|\,U^{(1)}(t,t_0)\,|E_i\rangle\\&=-i\int_{t_0}^{t}dt_1\,\langle E_f|\,e^{-iH_0(t-t_1)}V(t_1)e^{-iH_0(t_1-t_0)}\,|E_i\rangle\\&=-ie^{-i(E_f-E_i)(t-t_0)}\int_{t_0}^{t}dt_1e^{i(E_f-E_i)t_1}\,\langle E_f|\,V(t_1)\,|E_i\rangle\\&=-ie^{-i\omega_{fi}(t-t_0)}\int_{t_0}^{t}dt_1e^{i\omega_{fi}t_1}\,\langle E_f|\,V(t_1)\,|E_i\rangle\,,\end{aligned} \tag{28}$$

where we have defined that $\omega_{fi}=E_f-E_i$.

Let us consider a periodic perturbation, $V(t)=e^{\epsilon t}Ve^{-i\omega t}$. The parameter ϵ is a small positive number, so that the periodic perturbation is gradually turned on from the initial time $t_0=-\infty$. We look at times much smaller than $1/\epsilon$. In this case, the first-order transition amplitude can be further given by

$$\begin{aligned}A_{fi}^{(1)}(t)&=\lim_{t_0\to-\infty}-ie^{-i\omega_{fi}(t-t_0)}\int_{t_0}^{t}dt_1e^{i(\omega_{fi}-\omega-i\epsilon)t_1}\,\langle E_f|\,V\,|E_i\rangle\\&=\lim_{t_0\to-\infty}-\frac{e^{-i(\omega t-\omega_{fi}t_0)}e^{\epsilon t}}{\omega_{fi}-\omega-i\epsilon}\,\langle E_f|\,V\,|E_i\rangle\,,\end{aligned} \tag{29}$$

and the corresponding transition probability is

$$\begin{aligned}P^{(1)}(t)&=\left|A_{fi}^{(1)}(t)\right|^2\\&=\frac{e^{2\epsilon t}}{(\omega_{fi}-\omega)^2+\epsilon^2}\left|\langle E_f|V\,|E_i\rangle\right|^2.\end{aligned} \tag{30}$$

The transition rate is then given by

$$R^{(1)}(t) = \frac{dP^{(1)}(t)}{dt} = \frac{2\epsilon e^{2\epsilon t}}{(\omega_{fi}-\omega)^2+\epsilon^2}\left|\langle E_f|V|E_i\rangle\right|^2. \tag{31}$$

In the limit of $\epsilon \to 0$, we have the following identity

$$\lim_{\epsilon\to 0}\frac{2\epsilon}{(\omega_{fi}-\omega)^2+\epsilon^2} = 2\pi\delta(\omega_{fi}-\omega), \tag{32}$$

so Eq. (31) can be expressed as

$$R^{(1)}(t) = 2\pi\delta(\omega_{fi}-\omega)\left|\langle E_f|V|E_i\rangle\right|^2. \tag{33}$$

This expression is known as Fermi's Golden Rule.

Next, we consider the second-order perturbation. Inserting $U^{(2)}(t,t_0)$ into Eq. (27), we obtain the second-order transition amplitude

$$A_{fi}^{(2)}(t) = \left\langle E_f\right| U^{(2)}(t,t_0)\left|E_i\right\rangle = -\int_{t_0}^{t}dt_2\int_{t_0}^{t_2}dt_1\left\langle E_f\right| e^{-iH_0(t-t_2)}V(t_2)e^{-iH_0(t_2-t_1)}V(t_1)e^{-iH_0(t_1-t_0)}\left|E_i\right\rangle. \tag{34}$$

In the above expression, between the operator $V(t_2)$ and $e^{-iH_0(t_2-t_1)}$, one can insert a unit operator $I=\sum_k|E_k\rangle\langle E_k|$, where $|E_k\rangle$ is the eigenvector of H_0 with eigenvalue of E_k. Then the second-order transition amplitude can be reformulated as

$$A_{fi}^{(2)}(t) = -e^{-i\omega_{fi}(t-t_0)}\sum_k\int_{t_0}^{t}dt_2\int_{t_0}^{t_2}dt_1 e^{i\omega_{fk}t_2}e^{i\omega_{ki}t_1}\left\langle E_f\right| V(t_2)\left|E_k\right\rangle\left\langle E_k\right| V(t_1)\left|E_i\right\rangle, \tag{35}$$

where $\omega_{fk}=E_f-E_k$ and $\omega_{ki}=E_k-E_i$. Again, we apply the same periodic perturbation, $V(t)=e^{\epsilon t}Ve^{-i\omega t}$, to the second-order perturbation. In this case,

$$A_{fi}^{(2)}(t) = \frac{e^{-i(2\omega t-\omega_{fi}t_0)}e^{i2\epsilon t}}{\omega_{ki}-2\omega-i2\epsilon}\sum_k\frac{\langle E_f|V|E_k\rangle\langle E_k|V|E_i\rangle}{\omega_{ki}-\omega-i\epsilon}. \tag{36}$$

Similar to the previous derivation in the first-order perturbation, in the case that $\epsilon\to 0$, the transition rate for the second-order perturbation can be given by

$$R^{(2)}(t) = 2\pi\delta(\omega_{fi}-2\omega)\left|\sum_k\frac{\langle E_f|V|E_k\rangle\langle E_k|V|E_i\rangle}{\omega_{ki}-\omega}\right|^2. \tag{37}$$

Generally, the kth-order transition amplitude can be expressed as

$$A_{fi}^{(k)}(t) = (-i)^k e^{-i\omega_{fi}(t-t_0)}\sum_{m_1,m_2\ldots m_{k-1}}\int_{t_0}^{t}dt_k\ldots\int_{t_0}^{t_2}dt_1 \times e^{i\omega_{fm_{k-1}}t_k}\ldots e^{i\omega_{m_1i}t_1} \times\langle E_f|V(t_k)\left|E_{m_k}\right\rangle\ldots\langle E_{m_1}|V(t_1)\left|E_i\right\rangle. \tag{38}$$

In the case that a periodic perturbation is applied, the transition rate for the kth-order perturbation can be given by

$$R^{(k)}(t) = 2\pi\delta(\omega_{fi}-k\omega)\left|\sum_{m_1m_2\ldots m_{k-1}}\frac{\langle E_f|V\left|E_{m_{k-1}}\right\rangle\ldots\langle E_{m_1}|V|E_i\rangle}{\left[\omega_{m_{k-1}i}-(k-1)\,\omega\right]\ldots\left(\omega_{m_1i}-\omega\right)}\right|^2. \tag{39}$$

2.3. Classical or semiclassical description

When the laser–atom interaction is sufficiently strong, the perturbation theory starts to break down. For the case of intense IR pulses, the electron motion can be qualitatively described classically in the combined force of the Coulomb field

and the laser electric field. According to the quantum–classical correspondence principle, the classical canonical Hamiltonian can be readily inferred from Eq. (10) to be

$$H(\mathbf{r}, t) = \frac{1}{2}\mathbf{p}^2 + V(\mathbf{r}) + \mathbf{r}\cdot\mathbf{E}(t). \tag{40}$$

The equation of motion can thus be deduced from the canonical Hamiltonian equation to be

$$\ddot{\mathbf{r}} = -\nabla V(\mathbf{r}) - \mathbf{E}(t). \tag{41}$$

Many strong field processes can be qualitatively understood by solving the above Newton's equation. One of the advantages of the classical description is that one can fully trace the trajectories of the electron in the phase space so that the underlying mechanism can be intuitively interpreted. This method relies on the numerical solution to the time-dependent Newton's equation (TDNE) [50,199,200].

However, the ionization process of atoms and molecules is intrinsically a quantum mechanical one because of the electron tunneling in the distorted Coulomb barrier in the presence of the external laser field. There exist semiclassical methods which incorporate the tunneling concept in the ionization process, which will be discussed later. The usual semiclassical methods cannot describe the interference phenomena in the quantum mechanics. Here, we introduce a method to prescribe a phase from the classical action for each of the classical trajectory, based on the Feynman path integral. This can wonderfully reproduce the interference patterns predicted by the pure quantum mechanical description.

2.3.1. Simple man's model

Simple man's model [32,33,201] with an intuitive physics picture successfully explains the cutoff energy of the plateau electrons in above threshold ionization process and cutoff region of the HHG spectrum. In this model, the electron first enters the continuum by the optical field ionization usually depicted by the tunneling through a potential formed by the combined laser and Coulomb field. Once the electron appears at the tunnel exit (which is usually small and is ignored in the simple man's model), the laser field will take over and drive the electron away from the ion core. The Coulomb potential is neglected in this picture and the electron's motion is governed by the laser field.

For the simplicity of illustration, we assume a linearly polarized laser pulse along the x-axis. Then the Newton's equation of the classical motion is given by

$$\ddot{x} = -E_{\mathrm{IR}}(t). \tag{42}$$

Another important approximation is that at the tunnel exit the initial velocity along the laser polarization direction is assumed to be zero. Then according to Eq. (42), the electron's velocity can be obtained as

$$v(t) = A_{\mathrm{IR}}(t) - A_{\mathrm{IR}}(t_0), \tag{43}$$

in which t_0 is the time when the electron appears at the tunnel exit, $A_{\mathrm{IR}}(t) = A_0 f(t)\sin(\omega t)$ is the vector potential of the laser field. By integrating the velocity over time, we obtained the electron's trajectory

$$x(t) = \int_{t_0}^{t} A_{\mathrm{IR}}(\tau)\, d\tau + A_{\mathrm{IR}}(t_0)(t - t_0). \tag{44}$$

Without considering the long-range Coulomb potential, the electrons can be clarified into direct electrons and rescattered electrons in each half laser cycle. The electrons tunneling before the laser maximum will be directly pulled away by the laser field, and this kind of electrons are called direct electrons. The velocity in Eq. (43) consists of a constant term, which is the drift momentum measured at the detector for direct electrons, and an oscillating term, which is related to the ponderomotive energy when averaged over a cycle of the laser field, i.e.,

$$U_{\mathrm{p}} = A_0^2/4, \tag{45}$$

where A_0 is the peak value of the laser vector potential. For the case of a linearly polarized laser, the drift energy of the direct electrons is between 0 and $2U_{\mathrm{p}}$.

Alternatively, a significant fraction of the electrons released after the laser maximum will be driven back to the ion and scattered by the nucleus one or several times and they are termed as rescattered electrons. The rescattering effect will give rise to high-order above-threshold ionization (HATI) [202] for elastic scattering, nonsequential double ionization (NSDI) [203,204] for inelastic scattering, and high-harmonic generation [161] for recombination. Assuming the electron rescatters with its parent ion at t_1, The kinetic energy of the electron at the time of its return is $E_1 = \frac{1}{2}[A_{\mathrm{IR}}(t_1) - A_{\mathrm{IR}}(t_0)]^2$. Maximizing this energy under the condition $x(t_1) = 0$ yields the maximum return energy of $3.17\,U_{\mathrm{p}}$, which corresponds to the cutoff photon energy $3.17\,U_{\mathrm{p}} + I_{\mathrm{p}}$ in the HHG process. For some returned electrons backscatter by 180°, these electrons can achieve energies as high as $10.007\,U_{\mathrm{p}}$.

2.3.2. CTMC simulation

The simple man's model, although successful in providing many useful qualitative predictions, has not been able to provide a quantitative description with the experimental data due to the shortcoming in handling the Coulomb potential

of the parent ion. A widely used approach to interpret the experimental data and to investigate the Coulomb effect is the semiclassical sampling method or the classical trajectory Monte Carlo simulations [187–190,205,206]. The CTMC simulations based on the three-step model are widely used due to: (i) their numerical simplicity, (ii) the intuitive physical picture of strong-field phenomena, (iii) and the fact that the Coulomb potential is incorporated on an equal footing with the laser field in the propagation process.

Briefly, in the CTMC model, we randomly sample the electron's tunneling time at the tunnel exit, which is derived from the Landau's effective potential theory [207]. The tunneled electrons have a Gaussian-like distribution on the transverse momentum perpendicular to the instantaneous laser field and a zero longitudinal momentum along the instantaneous laser field. Each electron trajectory is weighted by the ADK [191] ionization rate

$$W(t_0, v_\perp^i) = W_0(t_0) W_1(v_\perp^i), \tag{46}$$

in which

$$W_0(t_0) \propto |\left(2I_p\right)^2 / E(t_0)|^{2/\sqrt{2I_p}-1} \exp\left[-2\left(2I_p\right)^{3/2} / |3E(t_0)|\right] \tag{47}$$

determines the ionization rate with respect to the tunneling time and

$$W_1(v_\perp^i) \propto [\sqrt{2I_p} / |E(t_0)|] \exp\left[\sqrt{2I_p}(v_\perp^i)^2 / |E(t_0)|\right] \tag{48}$$

gives the initial lateral momentum distribution. In above $E(t_0)$ is the laser electric field, $v_\perp^i$ is the randomly sampled initial transverse momentum. After sampling the initial conditions of all the electrons, their classical motion in the combined laser and Coulomb fields is governed by the Newton's equation $\ddot{\mathbf{r}} = -\mathbf{r}/r^3 - \mathbf{E}(t)$ until the laser is turned off, where r is the distance from the electron to the nucleus. For the electrons with positive energies, we obtain their final momentum at the detector by using the Kepler's formula. In the final step, we put the electrons with similar final momenta into a bin, whose probability is added by each electron's weight in the bin $|M|_{\text{bin}}{}^2 = \sum_j W(t_0, v_\perp{}^j)$, where j is the jth electron in this bin. The CTMC models have been successfully used to explain various strong-field phenomena [52,171,184,208–212].

2.3.3. QTMC method

The CTMC methods has achieved greatly success in explaining the experimental results, however the main flaw of this method is that the quantum mechanical interference effects are absolutely ignored in this model, which limits the power of this method. For this purpose, we encode a phase for each tunneled electron trajectory with Feynman path-integral approach, which is called quantum trajectory Monte Carlo [192,193] simulation. The main idea to the Coulomb correction of the phase is the same with the Coulomb corrected strong field approximation (CCSFA) method [213,214,181,215], but QTMC model is more efficient. Instead of solving the enormous saddle point equations for different final momenta, the initial condition for the classical propagation is the same with those of the CTMC methods.

The Coulomb corrected phase of the jth electron trajectory can be expressed as

$$S_j = \int_{t_0}^{\infty} \left[\mathbf{v}^2(t)/2 - 1/|\mathbf{r}(t)| + I_p\right] dt. \tag{49}$$

The electrons located in the same bin will interfere with each other and the probability of each bin is determined by adding coherently the trajectories in that bin

$$|M|_{\text{bin}}{}^2 = \left|\sum_j \sqrt{W(t_0, v_\perp{}^j)} \exp\left(-iS_j\right)\right|^2. \tag{50}$$

We show the comparison of the QTMC simulation with the experimental data and the TDSE calculation in Fig. 1, which illustrates good qualitative agreement between different methods. Using the QTMC model, we can investigate the Coulomb effects to the direct and rescattered electrons by analyzing the initial coordinates of all of the tunneled electrons in a half laser cycle that contribute to the final momentum distribution. Fig. 2 shows the initial transverse momentum and the tunneling phase for the tunneled electrons for three spots in the first ATI ring [Fig. 1(b) P1–P3]. There are three types of trajectories contributing to the interference structures. The first two types of trajectories are the rescattered electrons R1 and directly ionized electrons D1, both of which can be qualitatively described in the SFA. Another type of trajectory appears with a small negative initial transverse momentum and the momentum changes its direction at the detector, which is defined as R2. These three types of trajectories will show constructive or destructive interference patterns within the ATI rings [Fig. 2]. The initial tunneling coordinates of the photon electron angular distributions (PADs) of ATI can be resolved by the QTMC model. This model has established the classical correspondence of the quantum dynamics. The underlying electron dynamics of ATI patterns on a subcycle time scale can be described using the QTMC model.

2.4. Strong field approximation

Now we turn to the full quantum mechanical description of the strong field ionization process. Here we want to briefly introduce the SFA approach. For detail reviews, we refer the readers to Refs. [44,45]. Considering an atom initially in the

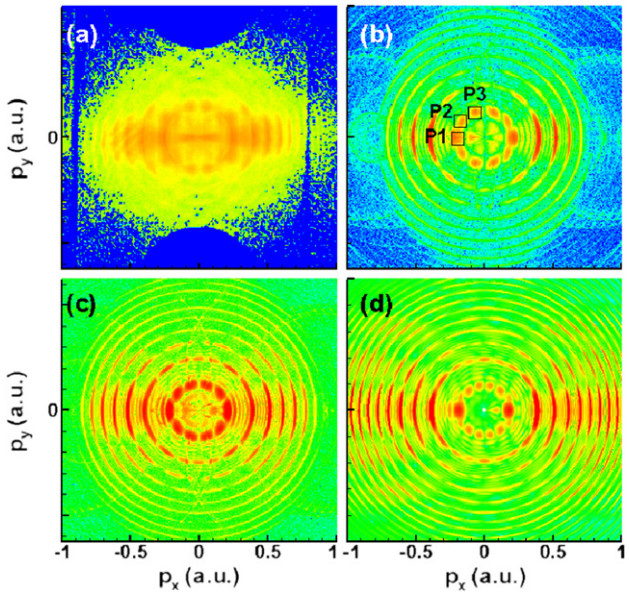

Fig. 1. (Color) The photoelectron angular distribution of Xe at the intensity of $I = 7.5 \times 10^{13}$ W/cm^2 (795 nm): (a) experimental measurement, (b) the QTMC simulated results. (c) and (d) shows the momentum spectrum of H atoms calculated respectively by QTMC and TDSE at the intensity of $I = 1 \times 10^{14}$ W/cm^2 (800 nm).
Source: Figures (a) and (b) are adapted from Ref. [192].

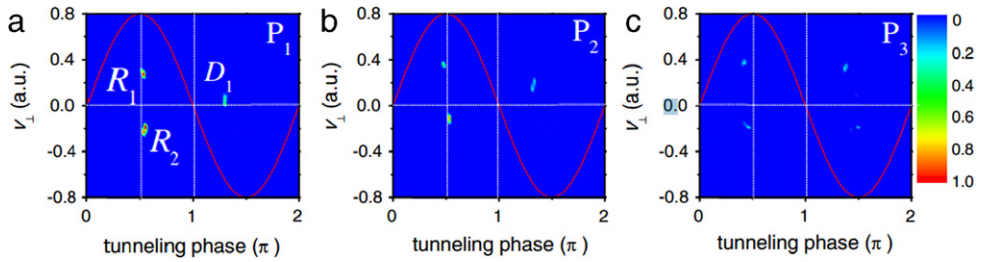

Fig. 2. (Color) The initial transverse momentum of the first-order ATI electrons in a laser cycle with respect to the tunneling phase for the ATI node: (a) P1, (b) P2, and (c) P3, respectively marked in Fig. 1(b). In (a), R1 and R2 indicate the group of the rescattered electrons with a larger and smaller transverse momentum, respectively. D1 indicates the direct electrons.
Source: Taken from Ref. [192].

bound state $|\Psi_0(t)\rangle = |\Psi_0\rangle e^{iI_p t}$. The laser-induced transition amplitude from the initial to the continuum state $\left|\Psi_p(t)\right\rangle$ in the dipole approximation is given by

$$M_{\mathbf{p}}(t_f, t_i) = -i \int_{t_i}^{t_f} d\tau \left\langle \Psi_{\mathbf{p}}(t_f) \right| U(t_f, \tau) H_{\text{Int}}(\tau) |\Psi_0(\tau)\rangle , \tag{51}$$

where $U(t_f, \tau)$ is the full time-evolution operator from the initial time t_i to a final time t_f. One essential step of SFA is the replacement of the final state $\left\langle \Psi_{\mathbf{p}}(t_f) \right|$ by $\left\langle \Psi_{\mathbf{p}}^{\text{V}}(t_f) \right|$, which is the eigenstate of a free electron in an external field, i.e., the Volkov states. In the non-relativistic limit and the length gauge, the Volkov states reads

$$\left|\Psi_{\mathbf{p}}^{V}(t)\right\rangle = |\mathbf{p} + \mathbf{A}(t)\rangle \exp\left[-\frac{i}{2}\int_0^t d\tau \left[\mathbf{p} + \mathbf{A}(t)\right]^2\right]. \tag{52}$$

Then the exact transition amplitude Eq. (51) can be approximated by

$$M_{\mathbf{p}}^0 = -i \int_{-\infty}^{\infty} dt_0 \langle \mathbf{p} + \mathbf{A}(t_0) | \mathbf{r} \cdot \mathbf{E}(t_0) |\Psi_0\rangle e^{iS(t_0)}, \tag{53}$$

with $S(t) = \int_0^t d\tau \left[\frac{1}{2}(\mathbf{p} + \mathbf{A}(\tau))^2 + I_{\text{p}}\right]$. The physical content of this substitution is that, after the electron has been promoted into the continuum at time t_0, its motion is fully governed by the laser field and the electron no longer feels the Coulomb potential. So the amplitude Eq. (53) describes the "direct" electrons.

Being generalized to account for the effects of rescattering [44,45], SFA can be used to describe the high-energy ATI spectra and the HHG process. The rescattering amplitude for high energy ATI is given by

$$M_{\mathbf{p}}^{1}=-\int_{-\infty}^{\infty}dt_{1}\int_{-\infty}^{t_{1}}dt_{0}\int d\mathbf{k}\left\langle \Psi_{\mathbf{p}}^{\mathrm{V}}\left(t_{1}\right)\right|V\left(r\right)\left|\Psi_{\mathbf{k}}^{\mathrm{V}}\left(t_{1}\right)\right\rangle \times\left\langle \Psi_{\mathbf{k}}^{\mathrm{V}}\left(t_{1}\right)\right|\mathbf{r}\cdot\mathbf{E}\left(t_{0}\right)\left|\Psi_{0}\left(t_{0}\right)\right\rangle . \tag{54}$$

The matrix element for emission of a photon with a frequency Ω in the HHG process by the strong-field approximation is

$$M\left(\Omega\right)\sim-\int_{-\infty}^{\infty}dt_{1}\int_{-\infty}^{t_{1}}dt_{0}\int d\mathbf{k}\exp\left[iS_{\Omega}\left(t_{1},t_{0},\mathbf{k}\right)\right]\times m\left(t_{1},t_{0},\mathbf{k}\right), \tag{55}$$

in which $m\left(t_{1},t_{0},\mathbf{k}\right)=\left\langle \Psi_{0}\left(t\right)\right|\mathbf{r}\left|\mathbf{k}+\mathbf{A}\left(t_{1}\right)\right\rangle \left\langle \mathbf{k}+\mathbf{A}\left(t_{0}\right)\right|\mathbf{r}\cdot\mathbf{E}\left(t_{0}\right)\left|\Psi_{0}\left(t_{0}\right)\right\rangle$. The main difference between ATI and the HHG process is in the phase term

$$S_{\Omega}\left(t_{1},t_{0},\mathbf{k}\right)=\int_{t_{1}}^{\infty}d\tau\left(I_{\mathrm{p}}-\Omega\right)-\frac{1}{2}\int_{t_{0}}^{t_{1}}d\tau\left[\mathbf{k}+\mathbf{A}\left(\tau\right)\right]+\int_{-\infty}^{t_{0}}d\tau I_{\mathrm{p}}. \tag{56}$$

The physical implication of Eqs. (54) and (55) is that the electron goes to the continuum at some time t_0, then propagates in the continuum subject to the laser field, until at the later time t_1 it returns to the range of the binding potential and rescatters to the final Volkov state for ATI electrons or recombines with the ion core for emission of a photon with a frequency Ω in the HHG.

The integral of the transition amplitude for direct and rescattered situation, or the HHG process, can all be approximated by the saddle point method, which is endowed with an intuitive picture of quantum orbits [194,216]. In saddle point method the transition amplitude recasts in the form of a sum over saddle points

$$M=\sum_{n}a_{n}e^{iS\left(t_{n}^{s}\right)}, \tag{57}$$

where a_n is an amplitude and t_n^s is determined by the saddle point equations. t_n^s is usually complex because $I_{\mathrm{p}}>0$ and the real part of t_n^s is referred to the time when an electron reaches the tunnel exit. In particular, the saddle points for rescattered ionization and the HHG process are given by the solutions of the three equations

$$\left[\mathbf{k}+\mathbf{A}\left(t_{0}\right)\right]^{2}=-2I_{\mathrm{p}}, \tag{58}$$

$$\left(t_{1}-t_{0}\right)\mathbf{k}=-\int_{t_{0}}^{t_{1}}d\tau A\left(\tau\right), \tag{59}$$

$$\left[\mathbf{k}+\mathbf{A}\left(t_{1}\right)\right]^{2}=\begin{cases}\left[\mathbf{p}+\mathbf{A}\left(t_{1}\right)\right]^{2}, & \text{for ATI}\\ 2\left(\Omega+I_{\mathrm{p}}\right), & \text{for HHG.}\end{cases} \tag{60}$$

These equations physically ensure energy conservation in the process of tunneling, the condition that the electron returns, and elastic scattering when the electron returns to the parent ion for ATI or recombines to produce a harmonic photon with energy Ω.

The saddle points define quantum orbits in the position space in which the electron departs from the ion and returns to it to rescatter or recombine. The real parts of these orbits are very closely related to the trajectories of the simple man's model. The momentum spectrum can be interpreted by the interference of different trajectories. The concept of quantum orbits establish a bridge between the quantum and the classical mechanics and pave the way to the Coulomb correction to SFA [181,213–215].

2.5. Numerical solution of time-dependent Schrödinger equation

The time-dependent Schrödinger equation is one of the most important partial differential equations (PDEs). It is well known that analytic solutions of PDEs are only possible for simple cases or under very restrictive conditions. For many practical and realistic problems, numerical methods are usually the only means of solution. The main purpose of a numerical method is to solve a PDE on a discrete set of points within the temporal and spatial domains. The first step of numerical solution to a PDE is to discretize the space-time to obtain a finite set of algebraic equations. Since we have introduced discretization on a finite grid, we can only get an approximate solution of the original PDE whatever methods we use. The most important numerical methods are finite difference, finite elements, spectral methods, or combinations of them.

A successful numerical scheme should be *stable*, *convergent*, and *consistent*. By "stable", we mean that the solution stays bounded during the whole solution procedure; by "convergent", we mean that the numerical solution tends to the real solution as the mesh size and the time step approach zero; a method is "consistent" if the truncation error tends to zero as the mesh size and the timestep go to zero. Generally if a numerical scheme is consistent, then stability is a necessary and sufficient condition to achieve convergence. A scheme which is stable but not consistent may converge to a solution of a different equation.

During the process when a PDE is discretized on grids and solved numerically, we are bound to introduce some errors. *Truncation error* is introduced by the finite approximation of the derivatives. *Discretization error* is due to the replacement of the continuous equation with a discretized one. *Round-off error* is due to the finite number of digits used in the numerical representation on computers.

There exist many different schemes of solving TDSE, depending on the specific problem being investigated. Among these methods, they differ in how one discretizes the spatial and temporal coordinates. A complete survey of these TDSE methods are beyond the scope the present review. Some very early theoretical studies of the strong field physics through direct numerical solution to TDSE can be found in Ref. [217–233] and references therein.

2.5.1. Discretization for space coordinates

To be able to solve the TDSE, we need to express the Hamiltonian as a matrix. One approach is the use of grid-based methods, in which the space coordinates are divided into a sequence of grid points. Only the values of the wave function at the grid points are stored. The derivative operators are approximated by finite difference techniques. The grid-based methods have the favorable property that all operators are very sparse, i.e. operators that are local in space remain local in this representation, and derivative operators typically couple only a few adjacent grid points. This allows for efficient computation of the matrix–vector products representing the action of operators on a wave function. On the other hand, in grid-based methods, it often requires a high number of grid points to achieve converged results.

Another approach is the use of basis-set methods, in which the wave function is represented by the coefficients of a (typically orthonormal) basis set $|b_i\rangle$. The basis set $|b_i\rangle$ is usually chosen according to the particular physical problem. Thus, the number of the basis functions required can be much fewer than the number of grid points necessary in a grid-based approach. On the other hand, in the basis-set methods, the matrix element $\langle b_i| O \left|b_j\right\rangle$ of an operator can be very complex, and the resulting matrix representations of the operators are often far from being sparse, even for local operators such as potentials $V(x)$.

The finite difference algorithm is a grid-based method, and easy to program and implement. In addition, it is very stable for large scale computation such as two-electron problem [234,235] or the strong mid-infrared physics [118,141]. The time propagation in the finite difference scheme has been successfully implemented by the split-operator [236,237] or the Arnoldi method [238–242].

For example, for the centered five-point difference case, the first and second derivative of a function $u(x)$ is respectively given by [243]

$$\frac{du(x)}{dx} = \frac{1}{12\Delta x}[u(x-2\Delta x) - 8u(x-\Delta x) + 8u(x+\Delta x) - u(x+2\Delta x)] + O(\Delta x^5), \tag{61}$$

and

$$\frac{d^2u(x)}{dx^2} = \frac{1}{12(\Delta x)^2}[-u(x-2\Delta x) + 16u(x-\Delta x) - 30u(x) + 16u(x+\Delta x) - u(x+2\Delta x)] + O(\Delta x^4), \tag{62}$$

where Δx is the grid spacing.

There are methods, in which some of the features of both grid-based and basis-set approaches are combined. One such approach is the finite element discrete variable representation (FE-DVR) [244]. We will introduce the FE-DVR method in more detail in the following.

The space coordinates are firstly divided into a series of finite elements, the boundaries $x^{(i)}$ of which are marked as

$$x_{\min} \le x^{(1)} < x^{(2)} < \cdots < x^{(\mathrm{Nelem})} \le x_{\max}. \tag{63}$$

$x_{\min}$ and $x_{\max}$ are the boundaries of the space coordinate x, and they can be defined according to the particular problems. If x represents a rectangular coordinate, one can choose $x_{\min} = -x_{\max}$. If x represents a radial coordinate, naturally $x_{\min} = 0$. $x_{\max}$ is usually chosen large enough to guarantee that the wave function beyond $x_{\max}$ can be safely treated to be zero, otherwise one needs to use absorbing boundary conditions to avoid nonphysical reflections. In each element, we further define a series of discrete variable representation (DVR) basis functions [245–248]. The DVR method provides a link between analytic basis set methods and the pure grid based methods. The DVR basis functions in the element $x^{(i)} \le x \le x^{(i+1)}$ are defined as,

$$f^{(i,m)}(x) = \frac{L^{(i,m)}(x)}{\sqrt{w^{(i,m)}}}, \quad 1 \le m < N, \tag{64}$$

where the Lagrange interpolation polynomials are defined as

$$L^{(i,m)}(x) = \begin{cases} \prod_{k\neq m} \dfrac{x - x^{(i,k)}}{x^{(i,m)} - x^{(i,k)}}, & x^{(i)} \le x^{(i,1)} \le x \le x^{(i,N)} \le x^{(i+1)} \\ 0, & \text{otherwise.} \end{cases} \tag{65}$$

In the above, the index i represents the ith element; $x^{(i,k)}$ and $w^{(i,k)}$ are the points and weights corresponding to the Gauss quadrature, respectively. Several types of Gauss quadratures are frequently employed [243]. In the Gauss–Legendre

quadrature, no point coincides with the endpoints of the integral interval. In the Gauss–Radau quadrature, one of the endpoints is included as a quadrature point and the other is excluded, i.e. $x^{(i,1)} > x^{(i)}$ and $x^{(i,N)} = x^{(i+1)}$. In the Gauss–Lobatto quadrature, two of the points are constrained to coincide with the endpoints, i.e. $x^{(i,1)} = x^{(i)}$ and $x^{(i,N)} = x^{(i+1)}$. Usually, the Gauss–Lobatto quadrature is chosen to build FE-DVR basis functions. In the Gauss quadrature, the integral of an arbitrary function $g(x)$ in the interval $x^{(i)} \le x \le x^{(i+1)}$ is approximated to be

$$\int_{x^{(i)}}^{x^{(i+1)}} g(x)dx \approx \sum_{k=1}^{N} g(x^{(i,k)})w^{(i,k)}. \tag{66}$$

The weights $w^{(i,k)}$ and points $x^{(i,k)}$ of the Gauss quadrature in an arbitrary integral interval $x^{(i)} \le x \le x^{(i+1)}$ can be inferred by the weights $\omega^{(k)}$ and points $t^{(k)}$ of the Gauss quadrature in the integral interval $-1 \le x \le 1$,

$$w^{(i,k)} = \frac{x^{(i+1)} - x^{(i)}}{2}\omega^{(k)}, \tag{67}$$

$$x^{(i,k)} = \frac{x^{(i+1)} - x^{(i)}}{2}t^{(k)} + \frac{x^{(i+1)} + x^{(i)}}{2}. \tag{68}$$

To insure the continuity of the wave function at the boundaries of two adjacent finite elements, we define the bridge functions as

$$f^{(i,N)}(x) = \frac{L^{(i,N)}(x) + L^{(i+1,1)}(x)}{\sqrt{w^{(i,N)} + w^{(i+1,1)}}}. \tag{69}$$

Those FE-DVR basis functions defined above are orthonormalized in the Gauss quadrature. When any function $g(x)$ is expanded by the FE-DVR basis functions

$$g(x) \approx \sum_{i,m} g_{i,m} f^{(i,m)}(x), \tag{70}$$

the expansion coefficient for the basis function $f^{(i,m)}(x)$ is directly related to the value of the function $g(x)$ at the point $x^{(i,m)}$

$$g_{i,m} = \begin{cases} \dfrac{g(x^{(i,m)})}{\sqrt{w^{(i,m)}}}, & m \ne N \\ \dfrac{g(x^{(i,N)})}{\sqrt{w^{(i,N)} + w^{(i+1,1)}}}, & m = N. \end{cases} \tag{71}$$

Another attractive feature is that the potential matrix is diagonal and the elements are equal to the potential values at the grid points, i.e.

$$V_{(i,m),(j,n)} = \int f^{(i,m)}(x)V(x)f^{(j,n)}(x)dx = V(x^{(i,m)})\delta_{i,j}\delta_{m,n}. \tag{72}$$

Similar conclusions hold for other local operators, such as the electron–laser interaction operator in the length gauge.

In the FE-DVR basis, the kinetic energy matrix is not diagonal but rather sparse, and the matrix elements are analytically known. A wave function that is expanded in terms of the FE-DVR basis functions will be continuous at the finite element boundaries, but will not have continuous derivatives. However, the derivative of the wave function need not be continuous to correctly define the kinetic energy [244]. The matrix element of the second derivative operator in the FE-DVR basis can be evaluated as [244]

$$\int f^{(i,m)}(x)\frac{d^2}{dx^2}f^{(j,n)}(x)dx = -\left(\delta_{i,j} + \delta_{i,j\pm1}\right)\int dx\frac{d}{dx}f^{(i,m)}(x)\frac{d}{dx}f^{(j,n)}(x). \tag{73}$$

The integral in the right side of the above equation can be evaluated by the Gauss quadrature. To complete this, the following equations will be useful,

$$\frac{dL^{(i,m)}(x)}{dx} = \sum_{p\ (p\ne m)} \frac{1}{x^{(i,m)} - x^{(i,p)}} \prod_{k(k\ne m,p)} \frac{(x - x^{(i,k)})}{x^{(i,m)} - x^{(i,k)}}, \tag{74}$$

$$\frac{dL^{(i,m)}(x^{(i'm')})}{dx} = \begin{cases} \delta_{ii'}\dfrac{1}{x^{(i,m)} - x^{(i,m')}} \displaystyle\prod_{k\ne m,m'} \frac{(x^{(i,m')} - x^{(i,k)})}{x^{(i,m)} - x^{(i,k)}}, & m' \ne m \\ \delta_{ii'}\displaystyle\sum_{k\ne m} \frac{1}{x^{(i,m)} - x^{(i,k)}}, & m' = m. \end{cases} \tag{75}$$

If the Gauss–Lobatto quadrature is used in the finite element, Eq. (75) can be further reduced in the case of $m' = m$,

$$\frac{dL^{(i,m)}(x^{(i,m)})}{dx} = \frac{\delta_{m,N}}{2w^{(i,N)}} - \frac{\delta_{m,1}}{2w^{(i,1)}}. \tag{76}$$

2.5.2. Time propagation method

Formally, the solution of the TDSE can be expressed as

$$\Psi(t) = \hat{T} \exp\left[-i \int_{t_0}^{t} H(t')dt'\right] \Psi(t_0), \tag{77}$$

where $\hat{T}$ is the time-ordering operator, and $U(t, t_0) = \hat{T} \exp\left[-i \int_{t_0}^{t} H(t')dt'\right]$ is the time evolution operator. Direct evaluation of the above equation is cumbersome, since the time evolution operator has to be expanded in a Dyson series to represent the time-ordering. However, for small time intervals Δt the Hamiltonian can be assumed to be time-independent, thus one has

$$U(t + \Delta t, t) \approx \exp\left[-iH(t)\Delta t\right], \tag{78}$$

and

$$\Psi(t + \Delta t) \approx \exp\left[-iH(t)\Delta t\right] \Psi(t). \tag{79}$$

The wave function at arbitrary time t can be obtained by iterating Eq. (79) from the initial wave function at time t_0. For many practical problems, the exponential in Eq. (79) cannot be evaluated exactly but there are many propagation schemes that provide different approximations [249,250]. In the following, we only introduce the Lanczos algorithm in more detail.

Lanczos algorithm is related to the Krylov subspace, which is generated by the repeated action of H on a normalized initial state Ψ_0. The set of the basis functions in the Krylov subspace is

$$K_{N+1} = \left\{|\Psi_0\rangle, H|\Psi_0\rangle, H^2|\Psi_0\rangle, \ldots, H^N|\Psi_0\rangle\right\}. \tag{80}$$

A new orthonormal set can be formed using the Gram–Schmidt orthogonalization procedure,

$$Q_{N+1} = \{|q_0\rangle, |q_1\rangle, |q_2\rangle, \ldots, |q_N\rangle\}. \tag{81}$$

Usually N is chosen to be much smaller than the dimension of the matrix representation of H. Generally, the matrix representation of a non-Hermitian operator in the subspace Q_{N+1} is an upper Hessenberg matrix. The Hamilton is Hermitian operator, for which the matrix representation in the subspace Q_{N+1} is tridiagonal. Employing this character of the Hermitian operator, the procedure to construct the orthonormal subspace Q_{N+1} can be reduced with the following three-term recurrence relation

$$|q_0\rangle = |\Psi_0\rangle, \tag{82}$$
$$\beta_0 |q_1\rangle = H|q_0\rangle - \alpha_0 |q_0\rangle, \tag{83}$$
$$\beta_j |q_{j+1}\rangle = H|q_j\rangle - \alpha_j |q_j\rangle - \beta_{j-1} |q_{j-1}\rangle, \tag{84}$$

where $|\Psi_0\rangle$ is normalized and

$$\alpha_j = \langle q_j| H |q_j\rangle, \tag{85}$$
$$\beta_j = \left\| H|q_j\rangle - \alpha_j |q_j\rangle - \beta_{j-1} |q_{j-1}\rangle \right\| = \langle q_{j-1}| H |q_j\rangle = \langle q_{j+1}| H |q_j\rangle. \tag{86}$$

Both α_j and β_j are real. The matrix of the Hamiltonian operator in the subspace Q_{N+1} is represented as

$$H_{ij}^{(Q)} = \langle q_i| H |q_j\rangle = \begin{pmatrix} \alpha_0 & \beta_0 & 0 & \cdots & 0 \\ \beta_0 & \ddots & \ddots & \ddots & \vdots \\ 0 & \ddots & \ddots & \ddots & 0 \\ \vdots & \ddots & \ddots & \ddots & \beta_{N-1} \\ 0 & \cdots & 0 & \beta_{N-1} & \alpha_N \end{pmatrix}. \tag{87}$$

Now, the propagation of the wave function is performed in the subspace Q_{N+1}. The eigenvector $|Z_i\rangle$ and the eigenvalue h_i of $H_{ij}^{(Q)}$ can be obtained by a direct diagonalization. The propagation operator in the subspace Q_{N+1} is then expressed as

$$U^{(Q)} = \exp\left(-iH^{(Q)}\Delta t\right) \tag{88}$$
$$= \sum_l \exp\left(-ih_l \Delta t\right) |Z_l\rangle \langle Z_l|. \tag{89}$$

Applying propagation operator $U^{(Q)}$ to the initial wave function $|\Psi_0\rangle \equiv |\Psi(t)\rangle = |q_0\rangle$, one obtains the propagated wave function in the subspace Q_{N+1},

$$|\Psi(t+\Delta t)\rangle = \sum_l \langle Z_l \mid q_0\rangle \exp\ (-ih_l\Delta t)\,|Z_l\rangle \tag{90}$$

$$\equiv \sum_{k=0}^{N} a_k\,|q_k\rangle\,, \tag{91}$$

where

$$a_k = \sum_l \langle Z_l \mid q_0\rangle \exp\ (-ih_l\Delta t)\,\langle q_k \mid Z_l\rangle\,. \tag{92}$$

The representation of the propagated wave function in the whole space can be obtained by actually calculating the summation in Eq. (91).

Since $|q_k\rangle$ are linear combinations of $H^k\,|\Psi_0\rangle$, Eq. (91) is actually a Nth order polynomial expansion of the exponential in Eq. (78). In contrast to a standard Nth order Taylor or Chebyshev expansion, the unitarity of the propagation operator is conserved.

2.5.3. Extraction of physical observables

By numerical solution of TDSE, the time-dependent wave function is known at any time during the interaction with the external laser pulses. According to the quantum mechanics, one can in principle extract any physical quantities needed. The most important observables to extract are the photon emission spectra and the differential momenta of electrons or ions.

The calculations of the HHG spectra is rather simple. One can evaluate the expectation values of the acceleration (or the dipole if the initial state depletion is not severe[3]) of the electron at a sequence of time points during the wave function propagation. According to the classical electrodynamic theory of radiation, one obtains the HHG spectra by making a Fourier transform of the time-dependent acceleration. One can also get some time information of the photon emission by making a Gabor transform or wavelets analysis [252].

The extraction of electron momentum spectra is more demanding than the HHG spectra. For an accurate computation of the electron spectra, one usually needs to solve a corresponding time-independent Schrödinger equation to get the continuum states and the relevant phase shifts [253–256] at any momentum for a large number of partial waves. This is straightforward for a single electron atom, under the SAE approximation, but becomes not so easy even for the simplest one-electron molecule. For two-electron atoms or molecules, the exact scattering states are not known at all so that one needs to use approximative methods such as the product of a single-electron continuum or to develop other numerical strategies such as exterior complex scaling (ECS) [257,258].

2.6. Two important schemes in attosecond physics

Now, we turn to introduce two important setups in the attosecond physics, namely, the RABBITT and the attosecond streaking, which have been playing central roles in attosecond physics to probe and control the electronic dynamics.

2.6.1. RABBITT technique

If an intense femtosecond laser pulse is focused on an atomic gas jet, the nonlinear electronic response of the medium causes the generation of high order harmonics of the laser field. The harmonic spectrum consists of a series of narrow peaks separated by twice the frequency of the driving field, and it can extend far into the extreme ultraviolet regime. When many-cycle IR pulses are used for the harmonic generation, the corresponding attosecond pulses appear as a pulse train. Paul *et al.* performed [26] the first experiment on the characterization of an attosecond pulse train (APT) by means of the RABBITT (reconstruction of attosecond beating by interference of two-photon transitions) technique [259–261].

The electric field of an attosecond pulse train can be expressed as

$$E_{\mathrm{xuv}}(t) = \sum A_q \cos\left(\omega_q t + \varphi_q\right). \tag{93}$$

Full characterization of this APT means to determine the amplitude A_q of each component and the relative phase variation of φ_q. A_q can be straightforwardly determined from the measurement of the HHG spectra using an xuv spectrometer and the relative phase can be obtained by recording sidebands in the two-color (xuv + IR) photoelectron spectra. The RABBITT technique relies on the atoms ionized by the harmonics in the presence of an IR field at a relatively low intensity. The

[3] When the laser intensity is so high that there is significant amount of ionization from the initial state, the HHG spectra calculated from the electron dipole will have a large background due to the divergent contribution to the dipole by the ionizing electronic wavepackets. The HHG signal in this case will be immersed under the background. However, calculations of HHG using the electron acceleration can resolve this problem, see detailed discussions in Ref. [251].

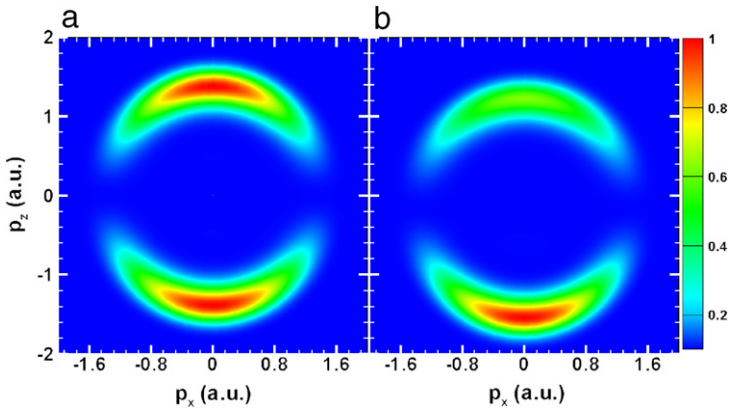

Fig. 3. (Color) Illustration of the principle of the attosecond streaking spectra. (a) The electron momentum distribution of H atom ionized by a 200 as (attosecond) pulse with a central frequency of 1.5 a.u. and a peak intensity of 1×10^{14} W/cm^2. (b) The electron momentum distribution created by the attosecond pulse combined with a 3-cycle 780 nm IR pulse with a peak intensity of 3×10^{12} W/cm^2. The attosecond pulse is placed at the center of the IR pulse which leads to a maximum momentum shift about 0.16 a.u. When one continuously changes the time delay between the two pulses, one can get a typical streaking spectrogram [cf., Fig. 18(b)].

photoelectron spectra then contain side bands, owing to absorption of one of the harmonics accompanied by the absorption or stimulated emission of one IR photon. Each side band q contains interfering contributions from the two neighboring odd harmonics $(q-1)\,\omega$ and $(q+1)\,\omega$. The yield of the side bands can be expressed as a function of the xuv–IR time delay Δt:

$$S_q \sim \cos\left(2\omega_{\rm IR}\Delta t + \varphi_{q-1} - \varphi_{q+1} + \varphi_{\rm atomic}\right), \tag{94}$$

where $\varphi_{\rm atomic}$ is an intrinsic complex phase of the transition matrix elements and can be obtained from the established theory with a high precision [26]. Measuring the sideband yield as a function of Δt allows one to extract the relative phase of these two harmonics. Performing this procedure for all harmonics then allows one to reconstruct the xuv pulse envelope.

2.6.2. Attosecond streaking

Different from the RABBITT technique which relies on the use of an IR dressing field at a perturbative intensity, the attosecond streaking technique [262–264] exploits on the non-linearity of a moderately strong IR laser field which exchanges many IR photons with the electron after it has been set free in the continuum by the attosecond pulse. This streaking dynamics can very often be treated semiclassically. For an attosecond streaking setup, a linearly polarized laser field (typically in the IR spectral region) is split into a stronger and a weaker beam, with the former acting as the generation field for the attosecond pulse and the latter one as the streaking field. This assures perfect synchronization between the two pulses with the usage of time delay line. The electron momentum distribution at the detector experiences a shift that depends on the relative timing between the liberation event by the attosecond pulse and the streaking laser pulse. The principle of the attosecond streaking can be easily explained in a classical picture. Assuming the electron is released by the attosecond pulse at the time t_0 and at this moment the electron has a momentum $\mathbf{p}_0$ which is determined by $E_0 = p_0^2/2 = \omega_{\rm xuv} - I_{\rm p}$. Neglecting the role of the Coulomb potential, the electron's subsequent motion is governed by the IR field only. According to the Newton's equation, the motion of the electron can be expressed by $\mathbf{v}(t) - \mathbf{p}_0 = -\int_{t_0}^{t} \mathbf{E}_{\rm IR}(\tau)\, d\tau$. When the IR laser is passed, the electron momentum at the detector is

$$\mathbf{p} = \mathbf{p}_0 - \mathbf{A}_{\rm IR}(t_0), \tag{95}$$

where $\mathbf{A}_{\rm IR}(t_0)$ is the IR vector potential at the released time t_0, corresponding to the momentum shift of the electron acquired from the IR field (see the illustration in Fig. 3). Thereby, the time of creation of the electron in the continuum is mapped to a velocity displacement that depends on the vector potential of the IR laser. Note that, in writing down Eq. (95), we assume that the electron is ionized instantaneously. For the discussion of photoionization time delays, please see Section 5.

From a point view of the quantum mechanics, one can start at the ionization of an atom by an xuv field alone, with the neglect of the polarization and ionization by the IR pulse. According to the perturbation theory, the amplitude of detecting an electron with an asymptotic momentum $\mathbf{p}$ is given by

$$a_{\mathbf{p}} = -i\int_{-\infty}^{\infty} dt \mathbf{d}_{\mathbf{p}} \cdot \mathbf{E}_{\rm xuv}(t) \exp\left[i\left(W + I_{\rm p}\right)t\right], \tag{96}$$

where $\mathbf{E}_{\rm xuv}(t)$ is the electric field, $W = \mathbf{p}^2/2$ is the final electron energy, $\mathbf{d}_{\mathbf{p}}$ is the dipole transition operator from the ground state to the continuum state. Eq. (96) gives the connection between an xuv field and the electron wavepacket it generates in the continuum. By synchronizing with a co-linearly polarized IR laser field, the electron ionized by the xuv pulse can be accelerated or decelerated by the IR field. When the photon energy of the xuv pulse is much larger than the

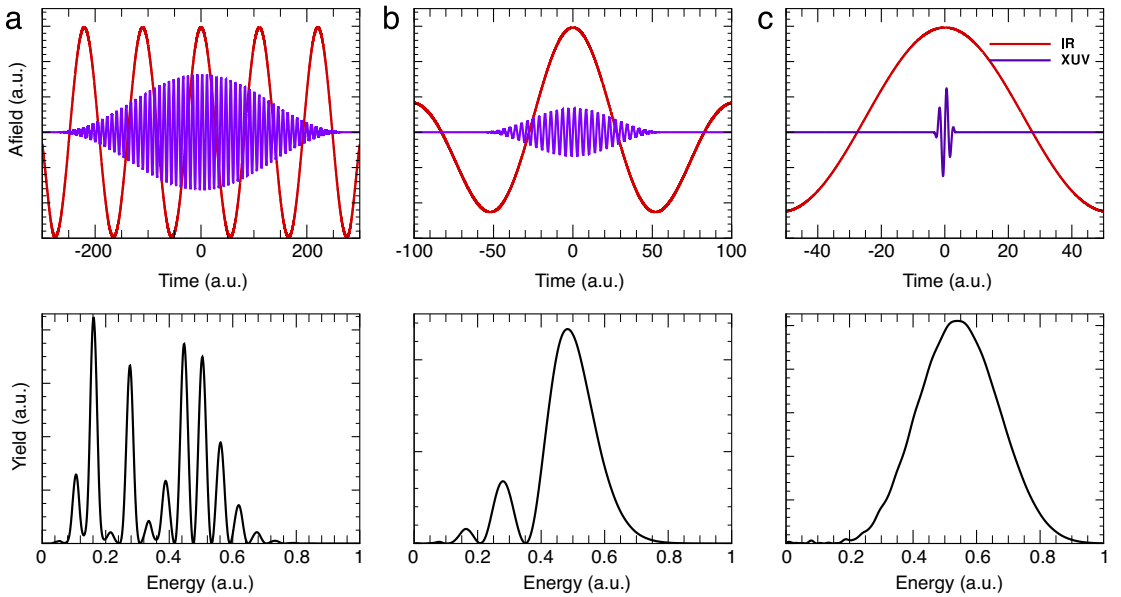

Fig. 4. (Color) Illustration of xuv–IR interaction with different xuv pulse durations. We show the electron energy spectrum along the laser polarization direction for different durations of xuv pulses, calculated by TDSE [the IR intensity is $I = 1 \times 10^{14}$ W/cm^2 (800 nm) and the central energy of the xuv pulse is 1.3 a.u.].

ionization potential of the atom, neglecting the Coulomb potential after the birth of the electron is a good approximation. Strong field approximation can be applied to describe the propagation process in the IR laser field [265,266]. If the intensity of laser field is just moderately intense, which means that the IR field itself cannot induce significant ionization signal, the motion of electron after the ionization by the xuv pulse is governed by the IR field. The continuum wave function can then be described by the Volkov state. The transition amplitude to a final continuum state $|\mathbf{p}\rangle$ in the combined xuv and IR field is given by

$$a_{\mathbf{p}}(\tau) = -i\int_{-\infty}^{\infty} dt \mathbf{d}_{\mathbf{v}(t)} \cdot \mathbf{E}_{\mathrm{xuv}}(t-\tau) \exp\left\{i\left[I_{\mathrm{p}}t - \int_{t}^{+\infty} dt' \mathbf{v}^2\left(t'\right)/2\right]\right\}, \tag{97}$$

where $\mathbf{v}(t) = \mathbf{p} + \mathbf{A}(t)$ is the instantaneous momentum of the free electron in the laser field. Reformulating Eq. (97), we obtain:

$$a_{\mathbf{p}}(\tau) = -i\int_{-\infty}^{\infty} dt \exp\left[i\phi(t)\right] \mathbf{d}_{\mathbf{v}(t)} \mathbf{E}_{\mathrm{xuv}}(t-\tau) \exp\left[i\left(W + I_{\mathrm{p}}\right)t\right], \tag{98}$$

where $\phi(t) = -\int_{t}^{+\infty} dt' \left[\mathbf{v}\cdot\mathbf{A}\left(t'\right) + \mathbf{A}^2\left(t'\right)/2\right]$. Comparing Eq. (98) with Eq. (97), we find that the combined IR field plays a role of a phase modulator. For a linearly polarized laser field $\mathbf{E}_{\mathrm{IR}}(t) = \mathbf{E}^0_{\mathrm{IR}}(t)\cos(\omega_{\mathrm{IR}}t)$ with a slowly-varying envelope, the corresponding vector potential can be expressed as $\mathbf{A}_{\mathrm{IR}}(t) = -\mathbf{E}^0_{\mathrm{IR}}(t)/\omega_{\mathrm{IR}}\sin(\omega_{\mathrm{IR}}t)$. Under these approximations, $\phi(t)$ can be expressed analytically.

Basically, according to the different durations of the xuv pulses, there are three different regimes of the IR–xuv interactions as illustrated in Fig. 4. All these phenomena can be analyzed by Eq. (98). When the duration of the xuv pulse covers several periods of the optical laser field [Fig. 4(a)], the oscillations $\phi(t)$ result in the energy spectrum consisting some sidebands separated by one photon energy of the optical field [267]. This interference phenomenon was experimentally investigated [268] recently and can be used to precisely reconstruct the detailed long duration X-ray profile [269]. For xuv pulses which are on the order of half an optical period as shown in [Fig. 4(b)], the energy spectra consist of several larger interference peaks, which are due to interference of electrons emitted at different moments of the IR pulse [270,267] with the same value of the IR vector potential. When the duration of the xuv pulse is much shorter than a half cycle of the laser pulse, the electron ionized by the xuv pulse is streaked by the laser field and the energy spectrum is a broadened smooth curve [Fig. 4(c)].

3. Attosecond light sources

The development of new light sources continuously improve our understanding and controlling of dynamics on the microscopic level. In turn, new knowledge of light–matter interaction and creative technologies in controllable light waves have produced brand new coherent light sources in a wide range of frequency domain. By confining light energy in a tiny

spatial focus within a very short time interval, one can study the nature and dynamics of matter under extreme conditions. Our quest of even shorter and stronger pulses are relentless since they can bring us new field we have never seen. Here we will review the development of laser sources whose durations drop from femtosecond down to attosecond time scale.

In the late 1980s, laser pulses with a duration of a few cycles with very high peak intensities became available because of pulse compression and chirped pulse amplification techniques [271–273]. Nowadays, Ti:sapphire lasers centered around 800 nm is widely available in many laboratories. The shortest pulse duration of such pulses approaches a single optical cycle with an optical period around 2.7 fs in the Fourier transform limit [94].

In order to overcome the barrier of generation subfemtosecond pulses, many proposals have been continually put forward since the early 1990s. The basic idea towards attosecond pulses is the same as the generation of femtosecond pulses: a wide range of phase locked different ultraviolet frequencies can be applied to synthesize attosecond pulses, in the same way that visible frequencies are used to get femtosecond pulses. Thus before generating attosecond pulses we should get the coherent light source in the high frequency range. To get these frequency components, there are three main proposals in that time to generate sub-femtosecond or attosecond pulses.

The first kind of proposal is to exploit Fourier synthesizer by a superposition of different frequencies from separate lasers synchronized by a nonlinear phase locking [85,274,275]. This method works fine in the visible regime in which light can be controlled easily including the phase and can be synthesized from different wavelengths to get a short pulse [101]. As we can see, to get a shorter pulse, short laser wavelength is necessary. If we want to get an attosecond pulse, the central photon energy usually should be high and a wide frequency bandwidth is necessary. The second kind of method is to use the cascade stimulated Raman scattering (CSRS) to generate the comb of equidistant frequencies [276–286]. The third kind of method is to use the higher energy part of the high-order harmonic generation in gas phase [84,86], which turns out to have been successful in generation of single attosecond pulses or attosecond pulse trains.

Since the harmonic generation process is quite successful in generating attosecond pulses, we will focus on this kind of method. Harmonic generation is a non-linear frequency up conversion effect when the driving laser is intense. Frequency up conversion was first observed by Franken, immediately after the invention of the laser when he focused a ruby laser into a quartz crystal [287]. This subsequent development of nonlinear optics benefited from the elegant perturbation treatment by Bloembergen and coworkers [288]. In low order harmonic regime, the harmonic generation process was studied in the 1960s in the context of laser–plasma interaction [289]. However, in 1981, quite high order of harmonics up to 28th order was first observed [290] and a plateau structure ranging from 16th to 42nd order was identified [291], both from the plasma produced by CO_2 lasers. In rare gases, harmonics up to 7th order was observed by a quadrupled Nd:YAG laser in 1978 [292] and by an intense KrF laser in 1983 [293]. By an even stronger KrF lasers, in 1987, harmonics of up to 17th (far beyond the prediction of the perturbation theory) was observed in Ne, together with strong fluorescence emissions from the excited levels for different species of noble gases [46]. After these experiments, in the infrared region, Wildenauer employed iodine-laser radiation at 1315 nm and observed 11th order of harmonic in 1987 [294]. Soon after this, very nice experiments were carried out at 1064 nm for noble gases and a plateau structure was identified [47], similar to the one observed earlier in the dense plasma [291]. Higher order of HHG was subsequently observed [295–298]. Even higher order of emission has continuously been observed experimentally to a very high energy of 1.6 keV [299], roughly corresponding to 5000 times of the fundamental photon energy.

Nowadays in the xuv range, free electron lasers (FELs) [30] is another popular kind of coherent light sources. Compared with HHG, FEL can get high intensity xuv pulses, but longer pulse durations in the femtosecond time scale, although there are many efforts towards shorter pulses [300]. HHG can lead to attosecond pulses down to tens of attosecond and it is a table-top light source while the FELs in xuv range are large facilities. There is one step further from coherent xuv light sources to attosecond light sources, as we will discuss in Section 3.2. For the HHG process, when the driving laser intensity gets high, the gas will be turned into plasma. The interaction then becomes laser–plasma interaction and can generate harmonics [301–304] as well. This process could be another way towards strong attosecond pulses but it is also hard to achieve.

In this section, we will first discuss the fundamental physics of high-order harmonic generation of atoms and molecules in gas phase. Then we will review how one can get a single attosecond pulse or attosecond pulse trains and how to characterize the attosecond pulses. Finally, by measuring the HHG spectra, one can actually access the electronic or molecular dynamics in some circumstances. Therefore, in the last part of this section, we will review these kinds of high harmonic spectroscopy, which has been established and proved to be quite successful in unveiling the underlying dynamics in many strong field processes.

3.1. High-order harmonic generation

A typical spectrum of HHG for H atom, calculated by the TDSE, is shown in Fig. 5. This atom is radiated by a 1600 nm, 1×10^{14} W/cm^2 mid-IR laser pulse whose pulse duration is 4 cycle with a flap-top shape. The harmonic spectrum from atoms and molecules in gas phase consists of three main ranges from low to high photon energy as indicated in this figure, i.e., below threshold harmonics (BTH) [305–310], plateau regime, and cutoff regime. The interpretation of this process can use the simple man's model discussed before. The electron is first ionized from the atom or molecule, then it will be accelerated in the laser field, the electron has a certain probability to recombine with the parent ion after the laser field reverses its direction. This recombination process will emit a photon whose energy is the summation of the electron kinetic energy and the ionization potential. The electron kinetic energy can be approximately calculated through the classical Newton's

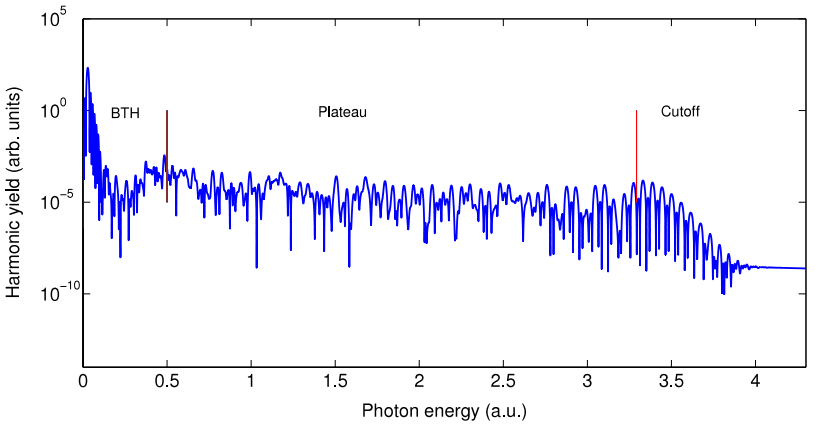

Fig. 5. (Color) Typical harmonic spectrum from H atom with a driving laser of wavelength 1600 nm at the peak intensity of 1×10^{14} W/cm^2, three different areas are indicated in the spectrum.

equation. Electrons tunneling out at different instants have different energies whose minimum is zero and maximum is $3.17U_p$, which corresponds to the cutoff photon energy $3.17U_p + I_p$. This can explain the harmonic yield in the plateau regime and the cutoff regime. But for the BTH, the Coulomb potential must be involved and it becomes difficult to deal with. Making use of the excited states of the potential, relative strong but low frequency harmonic emission can be observed [311].

The emitted light in HHG provides a wide frequency range of coherent light sources. In the harmonic generation process, the phase of emitted photon critically depends on the driving laser. The photon phase consists of phases from the three steps, these steps are identical for all atoms. This means for different atoms, they emit photons with the same phase if the phase matching condition is satisfied. This can make HHG a way to produce coherent xuv light sources. Through chirp compensation of the generated harmonics, short pulses can be generated [27]. Recently, with the development of optical parametric amplifier technique attention has been paid towards harmonic generation from mid-IR driving laser [312]. Through long wavelength driving laser, even higher frequency pulses can be in principle generated [313]. But unfortunately, both theoretical [130,134,314–322] and experimental investigations [323,324] show that the harmonic generation efficiency drops quickly towards a longer wavelength pulse.

The classical model can only give the relative yield and cannot describe the interference structure in the harmonic spectrum. The SFA was proposed in 1994 [161], where an analytical solution to TDSE was presented [44,161,325]. In the SFA, the harmonic yield can be expressed as Eq. (55) and its saddle point form in Eq. (57). The quantum trajectories can be considered as classical trajectories with a phase accumulated [326,327]. This kind of trajectories may correspond to the same kinetic energy but with a different phase accumulated in the propagation. The superposition of these trajectories can lead to the interference structures. Usually in the harmonic spectrum of a long driving laser pulse, there are two trajectories (usually called the short trajectory and the long trajectory) with different phases within half an optical cycle and the process repeats every half cycle. Then there are two kinds of interference structures in the spectrum. Both of them can be observed in the cutoff regime in Fig. 5. The first kind of interference has a larger interference space while the other kind shows small peaks spaced by 2ω.

The first kind of interference happens at every half optical cycle, i.e. the interference between two shortest trajectories. The two shortest trajectories happen within one optical cycle and we call them a short trajectory and a long trajectory respectively according to the travel time. The electrons with a short trajectory recombine to the core almost immediately after ionization while those with a long trajectory return to the core after about one optical cycle. Apparently these two kinds of electrons has different phases when they recombine to the core. The interferences between these two kinds of trajectories can be observed in the harmonic yield by changing U_p. This kind of interference structure can be observed both in the dependence on the laser intensity [161] and the wavelength [316], and can be used to differentiate these two kinds of trajectories. Recently, this kind of the interference structures can be observed in the BTH regime both in experiments [305,306] and theories [307–309].

The second kind of interference spaced by 2ω usually lead to the fact that only odd harmonics can be observed. This happens due to the harmonic emission process repeat itself every half cycle. The phase difference for these different emission times constructively interfere for odd harmonics while destructively for even harmonics. To observe the even harmonics, one should break the symmetry of two half optical cycles, e.g., by adding another laser pulse with different frequency or by using oriented molecules etc. [328].

The SFA is very efficient in interpreting the emission process. The model gives not only a qualitatively explanation of harmonic generation, but also for a clear picture of this process. Making use of this model, we can manipulate electrons in the first two steps [329–336] and to get a controllable light source [75,332,337–340]. We can use the recombination step to detect the atomic or molecular structure.

In the SFA, different trajectories with different energies return back to the core at different times. And this will encode atto-chirp [341] of the emitted light and cause the broadening in the time domain. The propagation process gives the electron

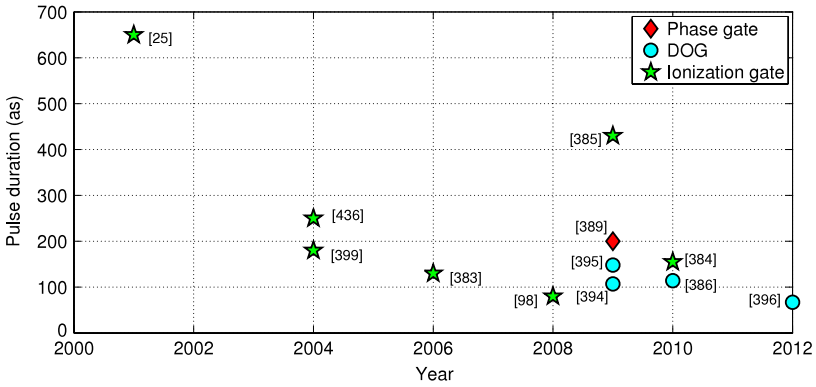

Fig. 6. (Color) Measured pulse duration of attosecond pulses since its first generation in 2001. Different methods are indicated by different symbols. The bracketed number near each point indicates the numbering of the reference for that particular experiment.

a phase corresponding to the time during which the electron travels. Through controlling this process, an interferometer in this scale has been proposed, which can be used as a method for space-time characterization of attosecond pulses [342]. The ionization process is also time dependent for different trajectories, and the instant when the electron gets out of the barrier can be determined [343].

As a process towards new light sources through the harmonic generation, we can get a tunable xuv source [344] or single attosecond pulse [345–355]. For now, the main problem lies in the strength and stability of attosecond light sources. The solution of these problems proposed for now is mainly based on the controlling of ionization and acceleration step of this model.

3.2. Generation of attosecond pulses

As recognized in 1990 [356], the wide spectrum generated through HHG can be used to synthesize laser pulses with duration of attosecond time scale. From another point of view, the harmonic emission happens in a short time range in the classical picture. The emission of photons happens in the attosecond time scale, the synthesis of these harmonics generates light pulses within this time scale as well. To get the synthesized pulse, one can insert an filter in the far field to select some of the harmonics, the superposition of these filtered harmonics leads to attosecond pulse bursts in the time domain [26,25,357]. Since 2001, lots of efforts have been made towards shorter and more reliable attosecond light sources, for a recent review, see [92,93,358]. The emission accident happens every half cycle, thus the attosecond pulse repeats itself every half cycle of the driving pulse and forms an attosecond pulse train. There are several experimental groups who have very successfully used attosecond pulse trains (including those spaced by a full and a half laser cycle) to explore dynamics in atoms and molecules [359–382]. In this section, we only focus on the generation and characterization of a single attosecond pulse as it is more preferred in a future pump–probe scheme.

To get a single attosecond pulse, we need a gate to pick one attosecond pulse from the pulse train. Usually, we manipulate the driving laser pulse to select single attosecond pulse from the harmonic generation process itself. Towards a single attosecond pulse, there are a lot of theoretical proposals as mentioned before, but only some of them made a success in experiments. The successful selection of a single attosecond pulse can be achieved both in the time domain and in the space domain, corresponding to a temporal gating and a spatio-temporal gating respectively. Temporal gating makes use of the driving laser pulse which is shaped in the time domain. The harmonic process happens in a temporal gate selected by ionization rate (ionization gating and amplitude gating) [98,383–388], phase match condition [389,390], or ellipticity which includes polarization gating [391,392], double optical gating (DOG) [393,394], and generalized double optical gating (GDOG) [395,396].

The development of attosecond pulse duration from different techniques are shown in Fig. 6. In the last decade, the pulse duration drops from 650 as to 67 as. In the early years, the cutoff regime [397–399] of CEP stable few-cycle driving laser was adopted to synthesize a single attosecond pulse. For a few-cycle driving laser, the signal of the cutoff regime mainly comes from the ionization at the peak of electric field and this method is called ionization gating. The ionization gating applies a short driving pulse to generate high harmonics. If we filter the cutoff energy in the spectrum, a single burst can be selected. Furthermore, if the driving laser intensity is high enough to be close to the saturation intensity, the harmonic burst after the peak can be further suppressed, and thus a wider spectrum is available for a shorter pulse [384]. The problem of this method is that the cutoff regime usually only covers a short range of spectrum. For an even shorter pulse, a broader bandwidth is necessary. And one needs that the whole harmonic spectrum can be effectively made use of. To achieve this goal, the schemes of DOG [393,394,400] and GDOG [395,396,401] were proposed.

The laser field for DOG and GDOG has a time varying ellipticity. From the picture of the three-step model, the elliptically polarized driving laser can induce a force laterally and the electron would probably miss the core when it is supposed to recombine. The harmonic yield thus drops with a Gaussian distribution versus the laser ellipticity, corresponding to the distribution of initial lateral velocity. This kind of method forms a gate within which the driving laser field is linearly

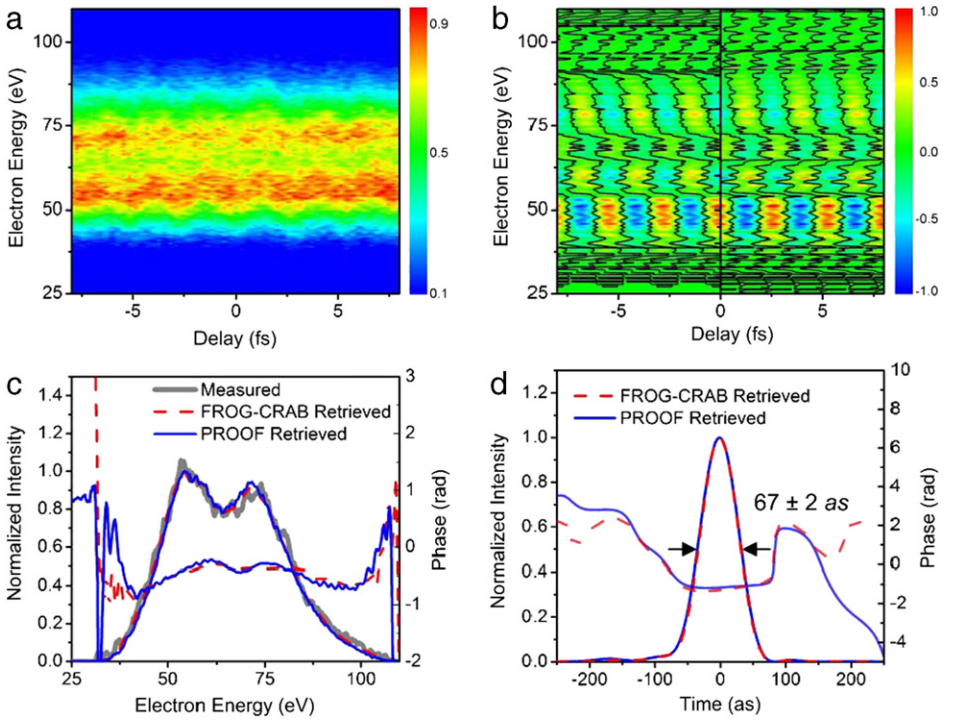

Fig. 7. (Color) Characterization of a 67 as xuv pulse. (a) Streaked photoelectron spectrogram obtained experimentally. (b) Filtered trace (left) from the spectrogram in (a) and the retrieved trace (right). (c) Photoelectron spectrum obtained experimentally (thick solid) and retrieved spectra and spectral phases from PROOF (solid) and FROG-CRAB (dashed). (d) Retrieved temporal profiles and phases from PROOF (solid) and FROG-CRAB (dashed).
Source: Taken from Ref. [396].

polarized, while otherwise it is elliptically polarized. Then the harmonic burst during the gate is selected as a single attosecond pulse. For this purpose, the polarization gating was first proposed, the driving laser pulse is combined with two circularly polarized pulses with counter-rotating polarization direction. There is a deficit of this method, the atoms are mostly ionized before the pulse reaches the time window, and the intensity of generated light is relatively low because the driving laser intensity is limited by the ionization saturation. A way to partially solve this problem is the double optical gating technique. Double gating means another gating technology, the temporal gating, is applied at the same time. The traditional temporal gating includes another light with a twice frequency to shape the temporal structure of the laser field. The shaped laser field only has one maximum every cycle where the ionization rate is large, and the attosecond burst happens only once each laser cycle and the ionization rate is reduced significantly. For now, DOG can generate the shortest single attosecond pulse down to 67 as measured in the experiment [396]. The measured results are shown in Fig. 7. The GDOG further reduces the ionization rate before the gate compared with the DOG. Instead of counter-rotating circularly polarized field, GDOG induces a counter-rotating ellipticity polarized field.

Recently, the spatio-temporal gating technology was proposed in 2012 for the harmonic generation in laser–plasma interaction [402]. Instead of time varying temporal profile, the spatio-temporal gating technology has a time-varying direction of wave-front. For the harmonics generated in gas phase, the propagation direction of the generated pulses is the same as the driving laser. When the driving laser has a rotating propagation direction, so does the harmonic. To get one separated pulse from the pulse trains, one just needs to select the field in the real space of the far field. This method has also been successfully applied in the harmonic generation of the laser gas interaction [403].

3.3. Characterization of attosecond pulses

The characterization of attosecond pulses is difficult, because it is impossible to detect such a short pulse in the xuv range using the usual optical means for the femtosecond laser pulses [404,405]. The autocorrelation traditionally used for the 800 nm laser pulse cannot be applied here as there is not a suitable material generating double frequency in the xuv region. Thus, new technology to measure the pulse duration is necessary. In addition, the characterization of an attosecond pulse can help to compensate the attochirp and lead to a shorter pulse. As the attochirp is considered as the main problem for getting a Fourier limited pulse. The characterization of an attosecond pulse needs the intensity and phase of all the frequencies in the spectra. Recently, the space distribution can also be characterized [342]. The measurements of a single attosecond pulse can be divided into *in situ* and *ex situ* according to when we characterize the pulse. If the characterization

happens after the pulse is generated, we call it *ex situ* measurement. While if we get the information about the pulse at the same time when the pulse is generated, it is called *in situ* measurement.

Ex situ measurements come with the generation of attosecond pulses in the early years. This method observes the electron spectrum after the interaction of attosecond pulses and atoms. When atoms are radiated by attosecond pulses, the electron momentum distribution can be calculated easily. Besides, the emission time of these electrons are limited within the attosecond pulse. Making use of these information, one can extract the phase information of the attosecond pulse from the momentum distribution observed.

The *ex situ* method comes from the measurements of femtosecond pulses. For attosecond pulse trains, the intensity can be detected from the CCD. Due to the separated frequency distribution, the characterization of the pulse train can be done if we know the related phase between these certain harmonic orders. To detect these phases, a relative simple method by reconstruction of attosecond beating by interference of two-photon transitions (RABBIT) can be applied. In the RABBIT scheme [26], the electrons ionized by the attosecond pulses trains can absorb or emit infrared photons and exhibit some interference structures. From these interference structures, the phase of harmonic orders in the pulse train can be retrieved. The RABBIT technique can only apply for odd harmonic while the improved Phase Retrieval by Omega Oscillation Filtering (iPROOF) [406] is suitable for both odd and even harmonics.

For the single attosecond pulse generated, the measurement is more difficult due to its continuous spectrum. The phase should be retrieved for every frequency sampled. A method called FROG-CRAB [407,408] is generalized from the FROG technology. The basic idea of this method is as follows. It is apparent that the phase information cannot be acquired if only the spectra are known. However, if the temporal pulse is gated before the detection, one can get more information about the temporal profile by moving the position of the gate. Through making use of all the delayed data, it is possible to get the whole temporal profile. The gate used for femtosecond pulses is the second harmonic generation (SHG) crystal. For attosecond pulses, no suitable crystal is available. The gate comes from the attosecond streaking scheme, in which the infrared laser can then act as a phase gate to the final momentum distribution [cf., Eq. (98)]. By changing the delay between the attosecond pulse and the infrared pulse, one can measure the electron momentum spectrum at different gating time. The algorithm called the principal component generalized projections algorithm (PCGPA) [409], as used in FROG, can then be used to retrieve the phase of the whole xuv spectrum.

The retrieve algorithm of FROG-CRAB assumes a central momentum approximation for the attosecond pulse. For an extremely short pulse, this assumption breaks down. Some alternative methods are necessary, the method of phase retrieval by omega oscillation filtering (PROOF) [410] has been developed. The PROOF method uses the same data as the FROG, but a different retrieve algorithm [411,406]. Without the assumption of the central frequency, this algorithm filters the frequency range around the infrared frequency to manipulate the detected spectra. From the filtered spectrum, the phase information can be retrieved through a slightly different method.

The *in situ* method characterizes attosecond pulses at the same time when they are generated [342]. This kind of method adds another weak driving pulse whose frequency is twice as the fundamental driving pulse. The additional laser pulse breaks the symmetry of the half-cycle emission and even harmonics emerge. When the harmonics are generated, detecting the generated intensity ratio between even and odd harmonics from the two laser pulses can reveal much information about the quantum trajectories deduced from the SFA. Changing the time delay between the two driving lasers, trajectories deduced can help to measure the harmonic spectra. When the *in situ* method was first presented, the time when electron is ionized can be determined as well as the intrinsic attochirp. These information can also help to compress the attosecond pulses. Recently, the *in situ* method was further developed by using the second pulse with a small propagation angle with respect to the driving laser [412]. From the theory of SFA, the added angle can separate the spatial distribution in the far field with different propagation angle. Thus, the spatial distribution can be retrieved through PCGPA for all energies.

3.4. High-order harmonic spectroscopy

The HHG process is a powerful way to probe the molecular structures or electronic dynamics. As mentioned before, the third step can be applied to detect the atoms or molecules as a single photon process. Traditionally if we want to detect the physical quantity like the single photon ionization cross section, we have to scan the energy range we are concerned with. While for the HHG process we do not need to scan the energy since the electron wavepacket returns to the core with an energy range from zero to the cutoff energy. All the energy information can be detected in the harmonic spectrum. This scheme is called high harmonic spectroscopy (HHS) (for a recent review see [114,413]). HHS detects the atoms or molecules using only a single IR pulse. Here in this subsection, we will review some progress in applications of HHS. The basic idea comes from the fact that the harmonic spectrum can be factorized as $S(\omega) = W(k)d(k)$, where $W(k)$ indicates the returning wavepacket and $d(k)$ is the recombination dipole [414,415]. The latter is approximately given by: $d(k) \approx \langle \Psi_g | r | \Psi_c \rangle$, which contains much information about the ground state wavefunction Ψ_g. Using this relation, on can extract $d(k)$ from the experimental measurement and retrieve the atomic or molecular information from it. This dipole element can give us information about the internuclear distance, the photon ionization cross section (PICS), the molecular orbital, the nuclear motion, and the electron–hole dynamics etc.

For static information such as the internuclear distance, the PICS, and the molecular orbitals, the harmonic generation process can be considered as a time independent process as one ignores the evolution of the core after ionization. On the contrary, if we consider the nuclear motion or electronic motion during the acceleration, the harmonic generation can be

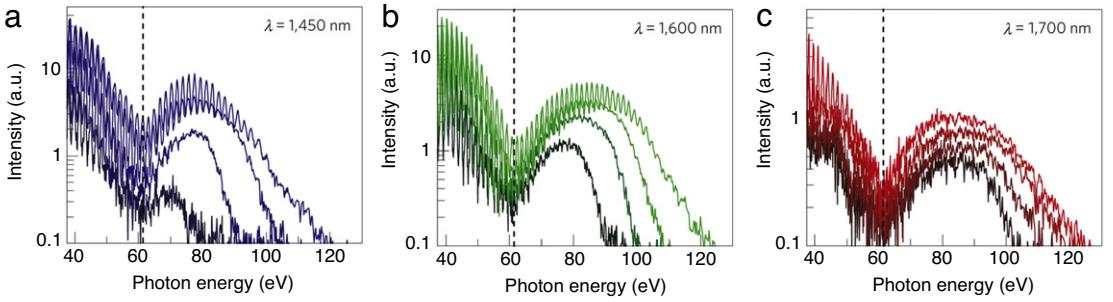

Fig. 8. (Color) High-order harmonic spectra measured in aligned CO_2 molecules for different pulse intensities and wavelengths. The xuv emission from CO_2 molecules was measured at a fixed delay $\tau = 21.1$ ps between the aligning and generating pulses (corresponding to maximum molecular alignment), for different driving laser wavelength λ and peak intensity I: a, $\lambda = 1450$ nm, $I = 1.0\ 1.7 \times 10^{14}$ W/cm^2; b, $\lambda = 1600$ nm, $I = 0.9\ 1.5 \times 10^{14}$ W/cm^2; c, $\lambda = 1700$ nm, $I = 1.0\ 1.4 \times 10^{14}$ W/cm^2.
Source: Adapted from Ref. [427].

regarded as a pump–probe scheme. In a pump–probe experiment, the pump pulse excites the system, and the probe pulse projects the excited system to a final state which can be easily detected. From the final state detection, we can retrieve the intermediate state through methods based on some theories. To get better retrieval results, the description of the probe process should be as accurate as possible. The proposed scheme treats the tunneling ionization as the pump, and the recombination as probe. The system changes its state with time after ionization and the travel time of electrons corresponds to the time delay. After the recombination, we can detect the photon emitted. Here in HHS, we can measure the intensity and phase of $S(\omega)$ and $W(k)$, and then calculate $d(k)$. We know that different harmonic orders correspond to different excursion times, which means we can get different signals from various time delays in the spectrum. Through this principle, we can detect nuclear motion and electron–hole dynamics for several simple cases.

When returning to the core, the electron can be rescattered as well. The rescattering generates electrons whose momentum spectra can be measured. These electrons can interfere with those direct ionized ones and form a holography structure in the momentum spectrum [165,167,414]. From the holography structure, information about the core can also be retrieved. But the scattered electrons will be affected by the Coulomb potential and the laser pulse. Due to the complexity of the momentum spectrum, the pump–probe schemes using electrons has developed more slowly than the high harmonic spectroscopy.

3.4.1. Two-center interference and PICS

In the HHG process, the generated spectrum are mainly determined by the recombination of the quantum electronic wavepackets to the atomic or molecular ionic core [416]. Information about the atom or molecule can be extracted from HHG as long as the recombination step is taken into consideration. The recombination process is a single photon process and the harmonic yield is proportional to the PICS [33]. When the returning electron wave-packet can be approximated by a plane wave, the harmonic spectrum is then directly related to the PICS. The Cooper minimum [417–420] and the giant enhancement [134,421,422] due to the collective electron effect can be observed through the harmonic spectra.

For aligned molecules, the ground state wavefunction can be approximately treated as a linear combination of atomic orbitals and a minimum can naturally arise in the dipole element $d(k)$ for some certain continuum wavepacket $\Psi(k)$. This kind of two-center interference minimum has been observed in the harmonic spectra in both theories [423] and experiments [424,425]. However, multichannel effects may get involved and cause an intensity dependent minimum, e.g., in CO_2 [426]. Multichannel effects come from the ionization from different molecular orbitals. Commonly, one would think only HOMO orbital is involved in the HHG process due to the exceptional decrease of the ionization rate with the ionization potential according to the ADK theory. But for an 800 nm laser usually applied in the experiments, the tunneling ionization is not the only ionization mechanism. It turns out that HOMO-1 and HOMO-2 orbitals can also get involved. New pathways towards the same photon energy can lead to interferences. These interference minimum may cause confusions with the two-center interference. This effect can be avoid through using long wavelength driving lasers [427]. Fig. 8 shows the results of intensity-dependent harmonic spectra whose minimum does not change with the laser intensity. This interference minimum can reflect the internuclear distance if we assume the ground state is a linear combination of atomic orbitals. The minimum can be observed in any alignment angle in different harmonic energies. If the intensity and phase information of harmonics are measured in different alignment angles, the assumption of linear combination is no more necessary and the molecular orbitals can be extracted directly through tomography, which will be discussed in the following.

3.4.2. Tomography of molecular orbitals

The first successful application of HHS scheme is the tomography reconstruction of molecular orbitals [35]. In this work, they reconstructed the HOMO of N_2 and provided us a new method to detect the molecular structure. In practice, they measured the harmonic intensity and phase of harmonic emission $S(\omega, \theta)$, and calibrated the wavepacket $W(k, \theta)$ by a reference atom. Full information about the dipole elements $d(k, \theta)$ can be extracted. The dipole elements with different

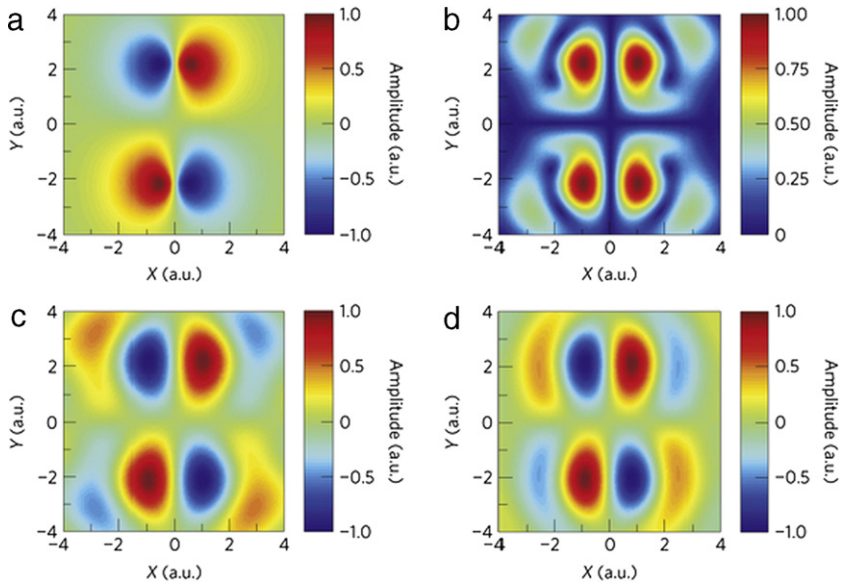

Fig. 9. (Color) HOMO orbital reconstruction of molecule CO_2. a, Bidimensional projection of the HOMO in CO_2 calculated with a quantum chemistry program. b, Absolute value of the HOMO wavefunction reconstructed from the experimental data according to the strong field approximation. c, HOMO image retrieved from the experimental data following the generalized tomographic procedure described in the text. d, Calculated effects of the limited spatial frequencies sampled in the experiment on the HOMO image shown in a. The *Z* axis, not shown, is perpendicular to the figure.
Source: Taken from Ref. [427].

harmonic energies and different angles between the laser polarization and the molecular alignment direction forms a two-dimension function. In the plane wave approximation, the Fourier transformation of this function gives the value of wavefunction in the real space.

There are some issues deserving more careful consideration, including applicability of the plane wave approximation, the multi-channel effects, and so on. These problems hinder the generalization of this method towards other kinds of molecules. Several improvements have been made after this work, these improvements mainly aimed at the unsolved problems. The HOMO-1 of N_2 can be reconstructed if the plane wave approximation was slightly modified [428]. And for the CO_2, an 800 nm laser pulse can easily ionize electrons in HOMO-1 and HOMO-2 orbitals. The reconstruction of HOMO of CO_2 shown in Fig. 9 was achieved recently by making use of a long wavelength laser pulse to avoid ionization from other orbitals [427]. This kind of reconstruction still needs more improvement to become a universal method as it works well only for several molecules. For the reconstruction proposed above, harmonic phase between different alignment angles cannot be measured and this is just an approximation. Recently, by making use of mixed gas, harmonic phase difference between different alignment angles can also be retrieved [429]. This can improve the quality of tomography reconstruction.

4. Electron dynamics in the combined xuv and IR fields

The availability of laser pulses in the extreme ultraviolet range with sub-femtosecond duration, i.e., attosecond pulse [25] or pulse trains [26] offers a new route to the direct observation of the fundamental dynamics of atoms and molecules on their natural time scale. These results sparked the emergence of a new field of attosecond science [94,430–435], which is now rapidly gaining ground worldwide.

The ideal way to trace and control the electron's motion is to perform attosecond pump–probe experiments [104–108, 110,112–115], in which a first attosecond pump pulse electronically excites an atom or a molecule of interest, thereby triggering an ultrafast electronic process, then a second time-delayed attosecond probe pulse extracts a signal from the system containing information about the time evolution that has been taking place.

The above attosecond pump and attosecond probe experiment requires a suitable xuv nonlinearity when the pulses are sufficiently strong. However, for the large xuv photon energy, the multiphoton ionization cross section is dramatically low, which puts a very strong limitation to characterize the attosecond pulse by the autocorrelation method, not to mention to trace and control the electronic dynamics.

In order to overcome the above difficulties, usually a few-cycle IR laser pulse with a controlled waveform [387], which can induce a highly nonlinear process, is applied to either initialize or probe the electronic dynamics. This kind of state of the art pump–probe experiment is mostly performed by using a combination of an attosecond pulse or pulse trains with a strong IR laser pulse. The role of the IR laser field has been either to ionize electrons from the excited states or to modulate the electrons in the continuum ionized by the attosecond pulse, or to initialize a dynamics with the subsequent electronic dynamics probed by the attosecond pulses [100]. With these kinds of techniques, many

important progresses have been made either in characterizing laser pulses or in observing and controlling the fast dynamics inside atoms and molecules. For the laser pulse diagnosis, the intensity profile of the isolated attosecond pulse can be retrieved [25] and the direct measurement of a few cycle IR pulse has been demonstrated [387,436]. The trace of the movement of electrons on the subatomic scale has been shown in many studies [95,110,371,399, 437–440]. As for a molecule, control of the electron localization in the molecular dissociation was realized [441]. The photoelectric effect in the condensed-matter systems was observed in a time resolution of attosecond regime for the first time [97]. By exploiting the interferences occurring between electronic wave packet replicas produced by the attosecond pulse train, one can infer some information of the atomic wavefunction such as phase [365]. A large number of fundamental electronic processes such as laser induced tunneling and Auger decay process have also been achieved [96,101]. One can also carry out a real time trace of the laser-driven electron acceleration process [442]. What is more, the synchronization of the attosecond and IR pulses with a precision of few attosecond allows one to ask the fundamental question of how long it takes for a photoelectric process to happen. The photoionization time-delays have been measured in atoms and solids [97,99,438,443]. More recently, control of the optical and electrical properties of dielectrics [102,103] and characterization of the ultrashort free-electron pulses [444] have been experimentally demonstrated.

The measurement of streaking spectrum of the electrons in the combined xuv–IR pulses has been by far the most successful and most versatile approach to the attosecond time-resolved spectroscopy. Nevertheless, one of the flaw of these methods is that the strong IR field may create a significant background of electrons through the strong-field ionization process. Other new methods to investigate the attosecond electronic dynamics are the all-optical approach of attosecond time-resolved transient absorption spectroscopy [100,445–449], and the attosecond angular streaking method [450,451]. Instead of detecting ions or electrons, the transient absorption spectroscopy detects the photons of the probe attosecond pulse that has transmitted through the sample as a function of the pump–probe delay [434] with no intrinsic need for the presence of a *strong* IR laser pulse and allows to directly probe the bound to bound transitions. While the transient absorption is a well-known measurement technique in the femtosecond domain [452–455], it was only recently extended into the attosecond regime using isolated attosecond pulses [100] to the real-time observation of valence electron motion of krypton ions. Autoionization of Argon atoms was also studied experimentally by the transient absorption spectroscopy with isolated attosecond pulses [445]. Transient absorption spectroscopy with APTs can give more insights of the interferences of transiently bound electron wave packets [446], which is performed in a helium experiment [366] with APTs (the photon energy is below the ionization threshold of He) in a synchronized IR laser field. The ionization probability is found to strongly oscillate with the delay between the IR and attosecond pulse twice per IR laser cycle.

The attosecond angular streaking [450] is a completely different approach which does not require attosecond pulses to trigger the electron dynamics. Classically speaking, the asymptotic momentum observed at the detector is determined by $\mathbf{p} = -\mathbf{A}(t_0)$ if the rescattering process is not considered, where t_0 is a certain release time of the electron relative to the laser field. This leads a time to momentum correspondence. For a linearly polarized laser pulse most of the electrons drift to the laser polarization direction and in a half cycle the direct and the rescattered electrons can reach the same final momentum, which obstructs the extraction of the corresponding time to momentum relation. By employing a nearly circularly polarized laser pulse (the rescattering process is largely suppressed) in which the electric field vector rotates in the polarization plane so the electrons that are ionized at different times will be deflected to different directions in the polarization plane. The instant of ionization is so that mapped to the final angle of the momentum vector in this plane. Different from the attosecond streaking which maps the electron's release time to the electron's final momenta, in the angular streaking, time is mapped to the emission angle of the electrons. The attoclock technique was applied to investigated the tunneling time in the tunnel ionization of helium [209], to determine the natural coordinates of the laser-induced tunneling current flow [456], and to measure the release time in the sequential double ionization [457].

The majority of attosecond experiments performed so far is to utilize the two-color xuv–IR experiments, in which the time delay between the two pulses can be controlled within attosecond time-resolution and serve as a fast clock to many dynamics processes inside atoms and molecules. Due to the prevailing applications of this type of experiments, in this section we will concentrate on this two-color xuv–IR pump–probe technique and the theoretical background will be illustrated and several typical proof of principle experiments will be reviewed. Specifically, we will first introduce two of the experiments in which the role of the IR field is to ionize the excited electrons that populated by the attosecond pulse. The first is the real time observation of the laser induced tunneling in atoms and the second one is a novel interferometric pump–probe experiment that was performed to probe the temporal evolution of bound electron wave packets of helium atoms. Attosecond streaking experiments or theoretical proposals, in which the role of the IR field is to control the electrons ionized by the attosecond pulses, is introduced in the next subsection. Three different attosecond streaking regimes are discussed according to the intensity of the streaking IR field. Most of the experiments are performed with a relatively low intensity of IR field, which is supposed to be weak enough not to ionize the target atoms, but strong enough to impart substantial momentum shift to the photoelectrons liberated by the xuv pulse. The information of the electronic dynamics is encoded in the streaking spectrogram when the time delay between two pulses is scanned. With a slightly higher IR intensity the motion of some low energy electrons ionized by the attosecond pulse can be controlled to recollide with the ionic core, inducing many interesting interferences structures. If the IR intensity is further increased, the IR pulse itself will induce significant ionized electrons which may interfere with the electrons ionized by the xuv pulse, provided that their probabilities are comparable [458]. Actually, using this type of interference spectra, there has been a theoretical proposal to fully characterize the single attosecond pulse [459].

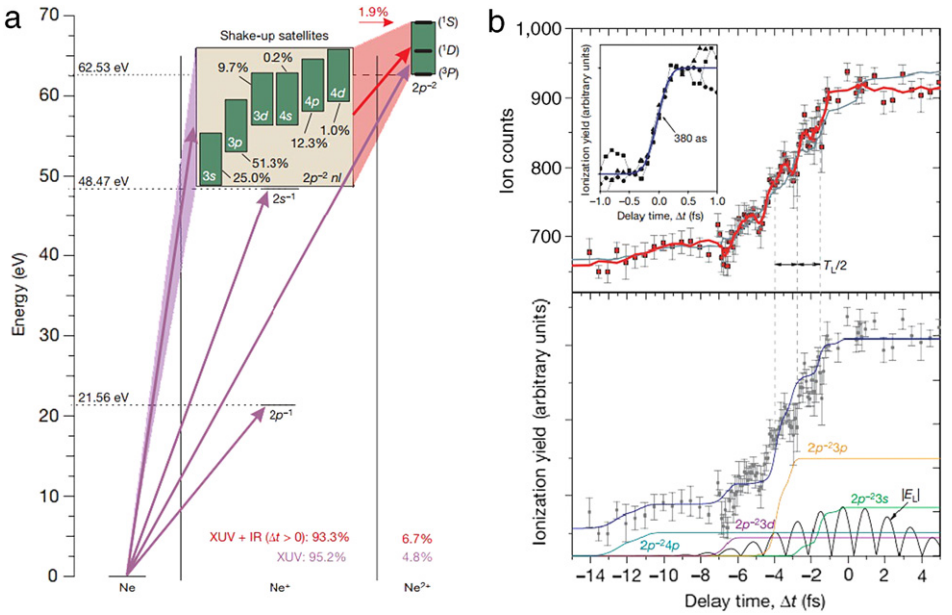

Fig. 10. (Color) (a) The plotted levels represent energies required to ionize and possibly excite a neutral Ne atom from its ground state. (b) The measured Ne^{2+} yield shows a step-like structure as a function of the time delay, indicating a real-time observation of the laser induced tunneling ionization. *Source:* Adapted from Ref. [96].

4.1. xuv–IR pump–probe experiments

4.1.1. Real-time observation of the laser induced tunneling

Tunneling is a pure quantum mechanical phenomenon where a particle penetrates through a potential barrier that it classically cannot surmount. Quantum tunneling plays an essential role in many physical processes and has important applications to various modern devices such as the tunnel diode and the scanning tunneling microscope. Many strong field processes of atoms and molecules initialize with or are closely related to the tunneling of an electron from the distorted ionic potential barrier. According to the pioneering work by Keldysh [120], photoionization is distinguished by two limiting cases depending on the value of Keldysh parameter $\gamma = \sqrt{I_p/2U_p}$. Specifically, tunneling ionization takes place when $\gamma \ll 1$ while multiphoton ionization dominates when $\gamma \gg 1$. In the adiabatic picture, the electron Keldysh time is negligible compared with the change of the laser electric field. The electron tunnels through a static or quasi-static barrier formed by the electric field and the binding potential of the atom. Particularly, in tunneling ionization the ionization rate strongly varies with the electric field and peaks when the magnitude of the electric field reaches a maximum. When $\gamma \sim 1$, the electron will tunnel through a moving barrier and acquires energy under the barrier [460–462] and various non-adiabatic effects are expected to emerge in this situation. Many effects associated with tunneling are still under debate.

By drawing on the newly developed tools of attosecond metrology, Uiberacker et al. [96] performed an experiment to observe distinct steps of ionization with each lasting several hundreds of attoseconds in real-time. This experiment provides the first direct insight into the dynamics of electron tunneling and reveals how light-field-induced tunneling can be exploited for the real-time observation of intra-atomic or intramolecular motion of electrons. In their experiment, Ne atoms were exposed to 250 as xuv pump pulse with a central energy of 90 eV and a time-delayed 750 nm laser field with intensity $I_0 = 7 \times 10^{13}$ W/cm^2. Fig. 10(a) shows the level structures and transitions relevant to this experiment. A few fractions of the Ne^+ ions ionized by the xuv pulse populate to several quantum states in the valence band by shakes-up process, from which electrons can be freed by the IR probe. By scanning the delay between the xuv pulse and IR field, different shake-up states depleted sequentially by the laser-field ionization can be distinguished [Fig. 10(b)]. The experimental data is compared with the analytic nonadiabatic theories [460] and numerical calculations, reasonable agreement is obtained. The observed Ne^{2+} ion yield is mainly increased within approximately one and a half IR cycles and is separated to several sharp steps by half a laser cycle, which is a strong evidence of the laser induced tunneling process. Moreover, the main shake-up states are depleted at IR intensities corresponding to a Keldysh parameter up to about three, which suggests that the tunneling picture may still hold at intensities more commonly associated with the multiphoton regime.

4.1.2. Characterization of attosecond electron wave packets

In the above experiment [96], the IR field is used to ionize the excited electrons populated by the shake-up process and the ion yield is recorded to be analyzed. Recently Mauritsson et al. [371,440] performed a similar pump–probe experiments. Instead of investigating the ion yield and the tunneling process, in their experiment the electrons momentum distribution

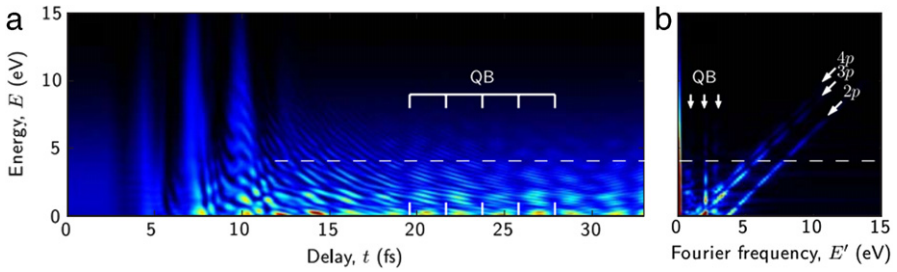

Fig. 11. (Color) (a) Calculated photoelectron spectra in He as a function of delay between the attosecond pulse (180 as, 24 eV) and the IR pulse (6 fs, $I = 1 \times 10^{13}$ W/cm^2). Interference fringes are clearly seen where the attosecond pulse precedes the IR probe. (b) Fourier transform of the photoelectron spectrum allows the identification of the states that form the bound wave packets. The beat signals from the 2p, 3p and 4p states can be seen as vertical lines while the direct–indirect interference gives rise to contributions at an angle of 45°.
Source: Taken from Ref. [371].

is recorded by a velocity map imaging spectrometer and they focused on the interference patterns between the continuum photoelectrons and the bound electrons. A broadband attosecond pulse with a central photon energy near the ionization threshold of helium is used to coherently excite an electron wave packets consisting of a superposition of bound and continuum p states. After the xuv isolated attosecond pulse has passed, the continuum electron wave packet rapidly moves away from the atom, while the bound wave packets displays radial oscillations. The bound part of the wave packets is finally ionized by a few-cycle IR pulse (which is locked in phase to the attosecond pulse) and interfere with the previously created continuum wave packets in the observed photoelectron spectra. In addition, simultaneous excitation of several bound states leads to quantum beats in the ionization signal. The continuum electron wave packet ionized by the attosecond pulse serves as a "reference" beam, which can interfere with the "signal" continuum electron wave packet ionized from an unknown Rydberg state by the delayed IR pulse. The analysis of the interference patterns obtained by measuring the photoelectron spectrum as a function of delay allows us to determine the spectral components of the bound wave packets. The accumulated phase difference between the"reference" and "signal" wave packets can be approximated by

$$\Delta\varphi\left(E_{\text{continuum}}, t_{\text{IR}} - t_{\text{xuv}}\right) \approx \left(E_{\text{continuum}} - E_{\text{Rydberg}}\right)\left(t_{\text{IR}} - t_{\text{xuv}}\right). \tag{99}$$

Fig. 11(a) shows the TDSE calculated energy spectrum $S\left(E, t_{\text{IR}} - t_{\text{xuv}}\right)$ along laser polarization axis as a function of the time delay between the two pulses. Different components of the excited wave packets can be extracted by a Fourier analysis of this delay dependent photoelectron signal $S\left(E, t_{\text{IR}} - t_{\text{xuv}}\right)$. From the Fourier transformed photoelectron spectra [Fig. 11(b)], quantum beats signal between different bound states, and the bound state energy can be identified. Moreover, the populations and relative phases of the Rydberg wave packet excited by the isolated attosecond pulse can be extracted. This proof-of-principle experiment paves the way to characterize the temporal evolution of unknown bound or quasi-bound electron wave packets with a high spectral and temporal resolution.

4.2. Attosecond streaking

The main principle of attosecond streaking technique is introduced in the theoretical part Section 2.6. The IR laser field is supposed to be weak enough not to significantly ionize the sample, but strong enough to impart substantial momentum shift to the photoelectrons liberated by the xuv pulses. Usually the central energy of the xuv pulse is much larger than the bound energy of the atoms or molecules. The photoelectron ionized by the xuv pulses can be considered to go to the continuum directly and the influence of the ionic potential can be neglected. Generally, the usual attosecond streaking involves momentum shifts of high-energy photoelectrons [25,262,399]. However, when photoelectrons ionized by the xuv attosecond pulse have low initial kinetic energies, the moderately strong IR field can be applied to control the continuum-electron dynamics by inducing electron scattering from the residual ion [109,463–465]. Even stronger IR field will cause significant ionization signal by itself [458]. In this case, the interference between the IR ionized electrons and xuv-ionized IR-streaked electrons can give more interesting physics and may find its application [459]. In this subsection, these three regimes will be discussed in details.

4.2.1. Attosecond electron wave packet interferometry

As mentioned before, the characterization of attosecond pulse trains using RABBITT requires IR intensities to be relatively low with simultaneous absorption or stimulated emission of one IR photon. The attosecond streaking scheme at a higher IR intensity, usually used for an isolated attosecond pulse, can also be used to APTs. The large ponderomotive momentum shifts induced by the IR laser field can create interferences among photoelectrons ejected by different sequences of attosecond pulses in the train. The interference patterns can be applied to characterize the electronic wave packet created in this process, as experimentally demonstrated in 2006 [365]. In the experiment [365], angular and energy-resolved momentum distributions of photoelectrons were measured for Ar, which was exposed to a train of attosecond pulses in the presence of a IR laser field with an intensity of $I = 2.5 \times 10^{13}$ W/cm^2. The electrons ionized by two attosecond pulses of the train

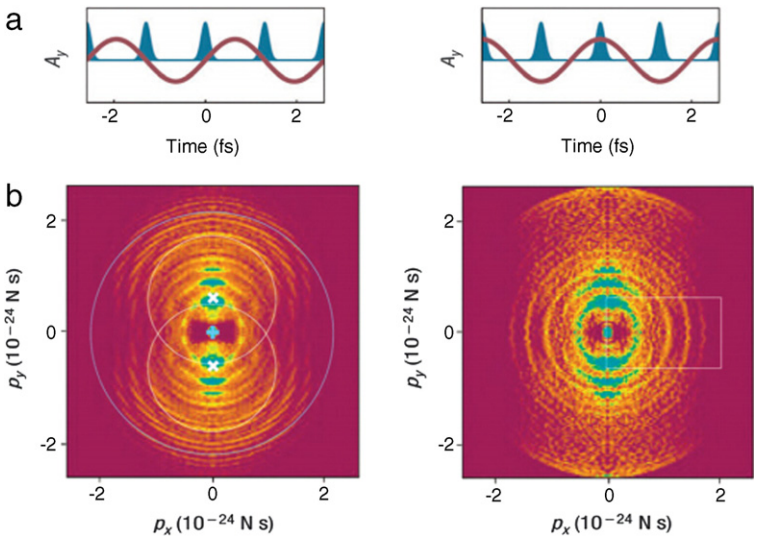

Fig. 12. (Color) (a) Two relative delays between the xuv and the IR field, i.e., the APTs coincide with a zero (left panel) or a maximum (right panel) of the corresponding IR vector potential. (b) The corresponding experimental measured momentum distribution at these two different relative delays. The central energy of the APTs is 11 eV and the peak intensity of the IR field is $I = 2.5 \times 10^{13}$ W/cm^2. For the former situation the fringes resulting from the interference of consecutive electron wave packets are circles centered on the p_y axis, which allows to determine the IR laser intensity. For the later case the interference patterns in the white rectangle allow to determine of the symmetry of the continuum momentum wave function.
Source: Adapted from Ref. [365].

separated by half the IR laser period will be streaked by the IR field and will interfere when their final momenta overlap. When the electron wave packets are formed in the presence of an IR field at zero crossings of the vector potential [Fig. 12(a) left], there is no streaking but the two electron wave packets will accumulate different phases in the IR field, which is very similar with the Young's double-slit experiment. By using the strong field approximation [466] (further development can be found in [467,468]), the phase difference between two consecutive electron wave packets is given by

$$\Delta\Phi_k = \pi - \frac{W\pi}{\omega_{\mathrm{IR}}} + (-1)^k \frac{2A_0 p_y}{\omega_{\mathrm{IR}}}, \tag{100}$$

where k is an integer, $W = \mathbf{p}^2/2 + I_{\mathrm{p}} + U_{\mathrm{p}}$ is the total energy absorbed by the electrons, and A_0 is the peak value of the laser vector potential. The position of the maxima of the interference pattern between two consecutive wave packets can then be derived by

$$\frac{1}{2}\left[p_x^2 + \left(p_y - (-1)^k \frac{2A_0}{\pi}\right)^2\right] = (2n+1)\,\omega_{\mathrm{IR}} - I_{\mathrm{p}} + \left(\frac{8}{\pi^2} - 1\right) U_{\mathrm{p}}, \tag{101}$$

where p_x and p_y is respectively the photoelectron momentum perpendicular to and parallel with the laser polarization direction. The maxima of the interferences correspond to circles centered at $(p_x = 0, p_y = \pm\frac{2A_0}{\pi})$, which can be used to determine the intensity of the IR field, and their radii allow us to cross-check the value of the ponderomotive shift.

On the other hand, when the attosecond pulses instead coincide with the maxima and minima of the vector potential [Fig. 12(a) right], the momentum transfer from the IR field is maximal but opposite in the direction for the two wave packets. In this case, there is no difference in the accumulated phase from the IR field and the phase difference between two wave packets is simply given by

$$\Delta\Phi_k = \pi - \frac{W\pi}{\omega_{\mathrm{IR}}} + \Delta\phi_k, \tag{102}$$

which allows us to determine the difference between the phases of the initial electron wave packet ($\Delta\phi_k$) in the interference region. The experimental results [365] showed that in the region close to the p_x direction [Fig. 12(b) the white rectangle in the right panel], photoionization of Ar is dominated by the contributions from the $m = \pm 1$ components.

4.2.2. Low-energy attosecond streaking

Attosecond streaking usually involves momentum shifts of high-energy photoelectrons, in which the central energy of the attosecond pulse is usually much higher than the ionization potential of the atoms or molecules and IR intensity is comparatively low. For a broadband single attosecond pulse with photon energy near the ionization threshold of the sample, a corresponding broadband electron wave packet will be created in the continuum with a significant fraction of the electrons

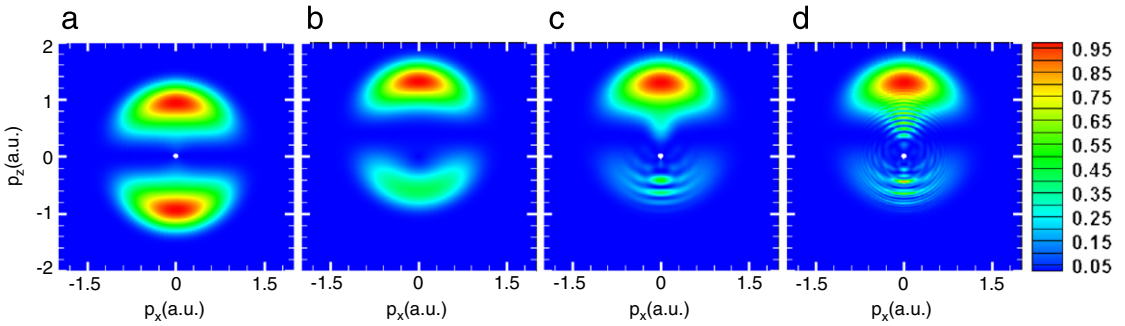

Fig. 13. (Color) (a) Momentum spectra of the photoelectrons by TDSE with the SAP alone. When an additional 2-cycle IR pulse is applied, the corresponding momentum spectra from different methods are compared : (b) SFA results and (c) TDSE results. Panel (d) shows the TDSE results when the duration of IR pulse is increased to 4 cycles.
Source: Taken from Ref. [465].

having relatively low energies. With such an attosecond pulse combined with an IR laser field, several differences can happen compared to the traditional attosecond streaking situation. One is that the Coulomb effect on the motion of these low energy electrons cannot be neglected, which means that the strong field approximation will break down in this region. Another very interesting application is that a moderately strong IR field can be used to control the continuum-electron dynamics by inducing photoelectrons scattering from the residual ion, which can be potentially used for holographic imaging of atoms and molecules. Different from the rescattering process induced by a single IR or mid-IR field, the ionization process and the subsequent control of the wave packets dynamics can be decoupled by using an xuv pulse combined with a synchronized IR field with a well-defined phase between them.

In Ref. [469], Smirnova et al. investigated the left–right asymmetries in the angle-resolved electron spectra ionized by an attosecond xuv pulse in the presence of an intense IR laser pulse. The effect of the Coulomb potential in the continuum after the absorption of the xuv photon and the effect of the laser-induced polarization of the electron wave packet prior to the absorption of the xuv photon was disentangled by using the Coulomb-corrected wave functions. Other theoretical developments [470,471] take electron–ion interaction effects into accounts in attosecond time-resolved photoelectron spectra. Laser-dressed scattering of an attosecond electron wave packet [472] was theoretically investigated by a quasi-classical model, based on classical electron trajectories. The external IR laser field controls the rescattering of an electron was demonstrated by measuring the photoelectron spectrum for different IR field intensities. The first experiment observation of the IR guided coherent electron wave packets (ionized by attosecond trains) scattering was achieved by the attosecond quantum stroboscope technique [367]. By using a lower carrier frequency single xuv attosecond pulse, the resultant rescattering of the low energy electrons under some conditions is demonstrated by the TDSE calculation [109,463,465,473,474] and by an intuitive simple semiclassical model [109].

In the following, we illustrate the ability of the IR field in controlling the continuum-electron dynamics through photoelectron scattering from the residual ion by TDSE calculations and a semiclassical model involving photoelectron trajectories [109]. Fig. 13 shows the momentum distribution calculated by TDSE and SFA method for a He atom interacting with a 126 as single attosecond pulse (SAP) and an IR laser pulse, with both assumed to be linearly polarized. The central frequency of attosecond pulse is 36 eV, which is slightly higher than ionization potential of the He ground state (24.6 eV). The attosecond pulse is placed at a zero of the IR laser electric field, which results in a maximum momentum shift of the electron that is promoted to the continuum by the SAP from the initial state. Amount of low-energy photoelectrons will be generated by this attosecond pulse and then steered by the synchronized IR field (with $\lambda = 750$ nm and $I_0 = 2 \times 10^{13}$ W/cm^2). Comparing the SFA calculation [Fig. 13(b)] and the TDSE result [Fig. 13(c)], one notices that SFA calculation indeed fails to capture the oscillation structures appeared in the low energy part of the momentum distribution. Increasing the duration of the IR field, the interference pattern becomes more complex [Fig. 13(d)], since multiple rescatterings with the core become possible for longer IR pulse. This electron–ion scattering process can be analyzed by a semiclassical model in terms of classical trajectories. The interference structures are determined by the phase difference accumulated by different trajectories leading to the same final energy. The quantum phase acquired by a free electron in an electromagnetic field is given by the Volkov phase, $e^{-iS_{\mathbf{p}}(t)}$, where $S_{\mathbf{p}}(t)$ denotes the semiclassical action of the trajectory given by

$$S_{\mathbf{p}}(t) = \frac{1}{2}\int_0^t d\tau\,[\mathbf{p} + \mathbf{A}_{\rm IR}(\tau)]^2\,, \tag{103}$$

with $\mathbf{p} + \mathbf{A}_{\rm IR}$ being the classical momentum of the photoelectron.

The photoelectron energy spectra for photoelectrons having negative ($p_z < 0$) and positive ($p_z > 0$) momenta along the laser polarization axis are shown respectively by the solid (red) lines in Fig. 14(a) and (b). By considering the phase difference between the forward rescattering or back rescattering trajectories and the directly outgoing photoelectrons, which is illustrated in Fig. 14(a) and (b), the position of the accurate TDSE interference peaks can be well reproduced by this semiclassical model at different IR wavelengths [Fig. 14(c) and (d)]. The low-energy attosecond streaking is thus shown to provide

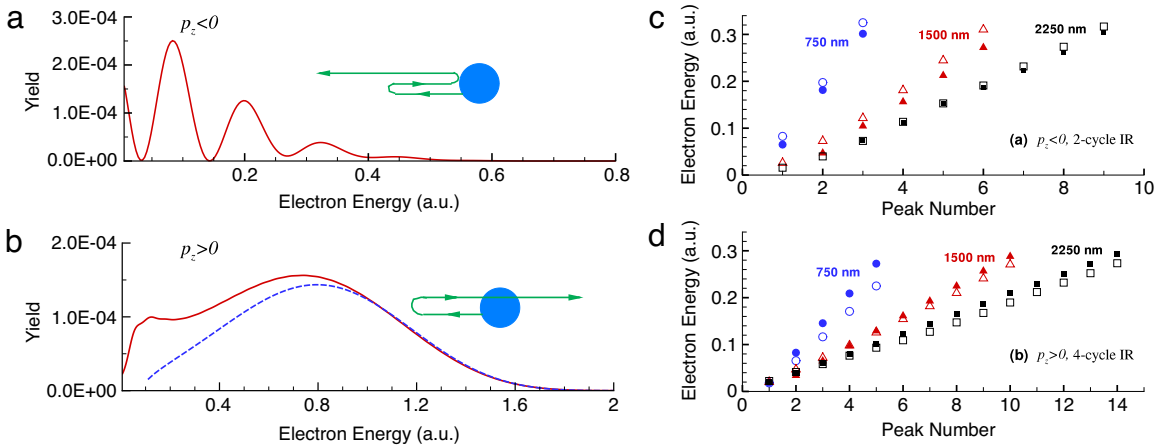

Fig. 14. (Color) Energy spectra of PEs ionized by the 750 nm and 2-cycle IR pulse: (a) $p_z < 0$ and (b) $p_z > 0$. Insets in (a) and (b) illustrate schematically PE trajectories that are initially ejected by the SAP with $p_z(0) < 0$, but are decelerated and at a later time experience respectively backward or forward rescattering. The dashed (blue) line in (b) is the PE spectrum calculated by SFA. (c) and (d): Comparisons of peak positions of the interference pattern in the PE spectrum for: $p_z < 0$ 2-cycle IR pulse case and $p_z > 0$ 4-cycle IR pulse case. In each frame, TDSE results (open symbols) are compared with predictions of the semiclassical model (filled symbols).
Source: Taken from Ref. [109].

an ideal tool to study and control the rescattering dynamics of the electrons in the Coulomb field of the ion. These results indicate the potential of such broadband xuv + IR field investigations of rescattering phenomena for holographic imaging of atoms and molecules, in which the target is "scanned" by the rescattered electrons and the directly-ionized electrons serve as a "reference" beam.

4.2.3. Attosecond streaking in relatively strong IR field

In streaking-like experiments, the intensity of the combined IR field is usually moderately strong enough to cause obvious streaking momentum shift but always keeps relatively low to avoid significant direct ionization by the IR itself. The ATI electrons of the IR field is usually considered as a contaminate to the streaking signal. However, an attosecond pulse combined with a strong IR field will bring new physics and new applications which call development of new theoretical methods and models to interpret the physical mechanism in this region.

The dynamics of the laser-driven tunneling and the recollision wave packet were investigated by using a strong IR pulse combined with an attosecond pulse [475]. When the recolliding electrons of the IR field revisit the parent ion, they can absorb an xuv photon, yielding high-energy electrons. This process provides a direct measurement of the electron energy at the moment of recollision. By changing the time delay between the driving IR laser and the attosecond pulse, the recollision energy of the electrons can be retrieved, which agrees well with the SFA calculation and the prediction of the simple man model.

With a high intensity IR pulse, the electron ionized by the xuv pulse can obtain larger streaking energy because of the larger IR vector potential, which may reach the energy range in the plateau region solely generated by the IR guided rescattering electrons. If these two kinds of electron wave packets have comparable amplitudes, they will interfere with each other. Under some proper conditions, these interference patterns can be analyzed by SFA [458]. Fig. 15 shows the TDSE calculated photoelectrons energy spectrum for $\theta = 0$ along the laser polarization direction of He atom in the presence of a four-cycle strong IR field (5×10^{14} W/cm^2) combined with a xuv pulse (other laser parameters can be found in the captions of Figs. 15 and 16). The two typical delays between the xuv pulse and the IR field at $t_1 = -67$ a.u. and $t_2 = 40$ a.u. respectively correspond to the third and fifth zero crossing of the four-cycle IR field. In Fig. 15(a) and (b), the energy spectra calculated by the IR field combined with different photon energy of the xuv pulses (the duration of the xuv pulses is almost kept as the same value of 1.5 fs) is compared with the spectrum obtained by the IR field only. The interference structures differ for different xuv photon energies and different time delays. This process can be described by

$$P = |M_{\mathrm{IR}} + M_{\mathrm{xuv+streaked}}|^2 , \tag{104}$$

where M_{IR} and $M_{\mathrm{xuv+streaked}}$ is respectively the transition amplitude of the above threshold ionization by the IR pulse alone and the xuv one-photon ionization streaked by the IR field. When these two transition amplitudes are comparable, they will interfere and lead to additional interference structures in the energy spectra. If the role of the Coulomb potential can be neglected, SFA can be applied to calculate Eq. (104). It is well the case when one uses a large xuv photon energy. The amplitude of the IR guided rescattering electrons can be easily obtained in the SFA by the saddle point method in terms of "quantum orbits" [45]. In the case of xuv photoionization in the presence of the strong IR field, SFA can also give a good description by Eq. (97). Fig. 16(a) and (b) show the comparison of the SFA and TDSE results for two delays with the xuv photon energy $\omega_{\mathrm{xuv}} = 6.0$ a.u. The good agreement between the SFA and TDSE results confirms the physical mechanism given by Eq. (104).

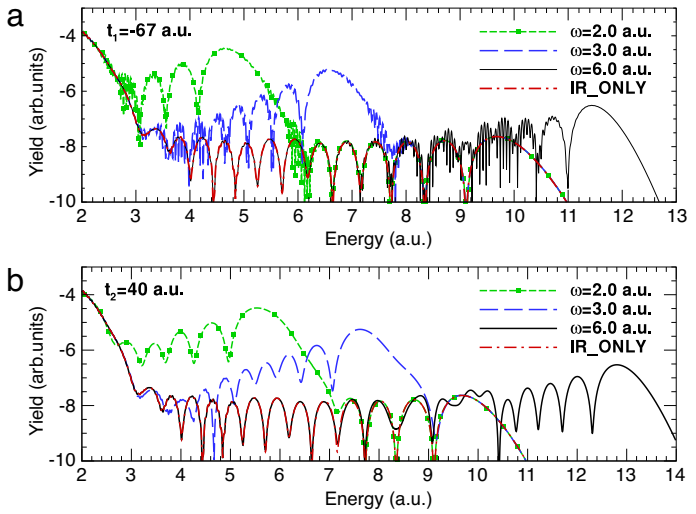

Fig. 15. (Color) Comparison of photoelectron spectrum for different xuv photon energies (the xuv intensity is 1×10^{11} W/cm^2). The IR field is a 4-cycle 800 nm IR pulse with intensity of 5×10^{14} W/cm^2. (a) and (b) energy spectrum ionized by the xuv pulse centered at time delay $t_1 = 40$ a.u. and time delay $t_2 = -67$ a.u. in the presence of the IR field, respectively.
Source: Taken from Ref. [458].

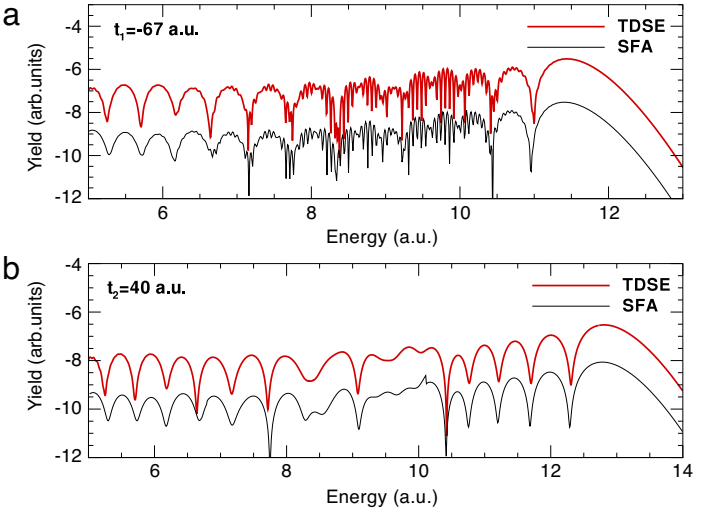

Fig. 16. (Color) Comparisons of the energy spectra calculated by TDSE (red upper thick line) and the SFA (black lower thin line) for the time delay t_1 and t_2, respectively. The photon energy and intensity of the xuv pulse is taken to be $\omega = 6.0$ a.u. and $I = 1 \times 10^{11}$ W/cm^2. The IR field is a 4-cycle 800 nm IR pulse with intensity of 5×10^{14} W/cm^2.
Source: Taken from Ref. [458].

By using a similar scheme, Liu and coworkers [459] proposed a method to fully characterize the temporal phase and amplitude of an isolated attosecond pulse. The CEP effects of the attosecond pulse were investigated in [463,476,477] for a single attosecond pulse, which suggests the importance of the electric waveform for a high intensity xuv pulse. As discussed before, the traditional attosecond streaking at a rather low IR intensity allows one to reconstruct the complete IR field and the temporal envelope and phase of the attosecond electron wave packet released by the xuv pulse. However, it can only characterize the intensity profile of the attosecond pulse after some algorithms from the streaking spectrogram. At high IR intensities, as showed in Ref. [459], it is possible to extract the CEP information of the attosecond pulse from the interferences just discussed above. Fig. 17(a) and (b) [459] show in the low energy region the energy spectrum do not depend on the attosecond pulse's CEP. The interference pattern in the middle energy range can be interpreted as the coherent interference between two electron wave packets

$$M(E, \tau) = |M_{\mathrm{IR}}|^2 + |M_{\mathrm{xuv}}|^2 + 2\,|M_{\mathrm{IR}}|\,|M_{\mathrm{xuv}}| \cos(\Delta\Phi)\,, \tag{105}$$

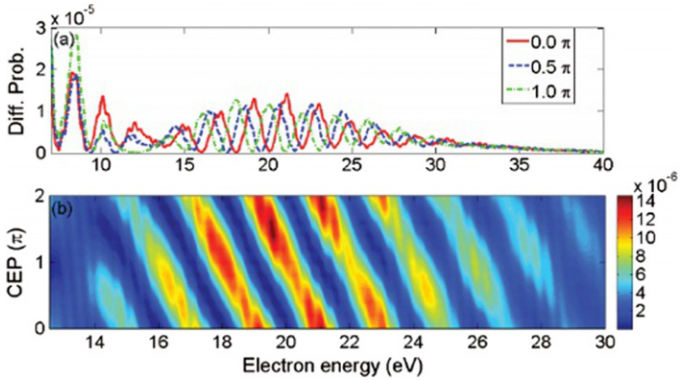

Fig. 17. (Color) Simulated photoelectron spectra generated by an isolated 250 as attosecond pulse at $\omega_{xuv} = 36$ eV in the presence of IR pulse with $\omega_{IR} = 1.63$ eV and $I = 4.5 \times 10^{13}$ W/cm^2. The time delay is $\tau = 0$. The CEP of the xuv field is 0 (red solid line), 0.5π (blue dashed line), and π (green dash-dotted line). (b) Interference fringes as a function of the electron energy in the CEP range $0 \sim 2\pi$. The IR intensity is $I = 4.5 \times 10^{13}$ W/cm^2.
Source: Taken from Ref. [459].

where $\Delta\Phi = \Delta\Phi_{xuv}(E, \tau) + \varphi_{xuv} - \Phi_{IR}(E)$. At lower IR intensities, using the FROG-CRAB algorithm, the phase and amplitude of the electron wave packet created by the xuv and the vector potential of the IR field can be determined. Then at higher IR laser intensities, based on the characterization of the IR field waveform, the initial xuv wave packet and using the TDSE calculations, the photoelectron spectra generated by the combination of the IR and xuv fields can be simulated for different CEPs of the attosecond pulse. The CEP φ_{xuv} of the attosecond pulse then can be obtained by finding the best matching between the directly simulated fringes and the interference pattern obtained using the retrieved parameters of the IR and xuv fields.

5. Photoionization time delay

The attosecond technologies allow one to quest the timing information of many physical processes on the attosecond time scale. One of the fundamental problems is that, subject to an absorption of a photon, whether it takes time or not for an electron to escape the potential that binds it within an atom, a molecule or a surface. If yes, how long is the time? How can one experimentally measure the time in a quantum system and how to theoretically interpret the data? Another related question still under current debate is the existence of the tunneling time for a matter wave or electromagnetic wave to pass through a barrier and the feasibility of its experimental measurement as a real quantity [478,479]. These questions are not only of practical importance, but also of conceptual challenge since they touch some basic issues of quantum mechanics such as the role of time variable, i.e, whether time is a quantum operator with a corresponding observable, or just a parameter as in the classical mechanics [480,481].

The aforementioned attosecond streaking [25,95,265,399] has shown its potential in answering the question of the time delay in photoelectric effects in atoms, molecules and solids. There are another two different schemes which can also extract the timing information of some electronic processes. The first one is the interferometric RABBIT technique in the context of ionization by attosecond pulse trains in the presence of a relatively weak IR field [26,438,482,483], in which case the intrinsic phases of quantum transition amplitudes can be accessed and thus time delays can be extracted. The second one is the so-called attosecond angular streaking by circularly polarized IR pulses [209,450,456,457,484], which was believe to measure the transversal time of the electron through the distorted Coulomb barrier, i.e., the tunneling time [485].

In this section, we will briefly discuss recent theoretical and experimental progress in photoionization time delays with the attosecond streaking technique. For a detailed and complete account of this subject, we refer the readers to recent reviews [482,486,487], where a systematic framework of theories is established and recent theoretical and experimental advances have been reviewed in details. Experimentally, the photoionization time delays have been measured in atoms and solids [97,99,438,443,437]. However, due to complexity of the experimental measurements and different sources of contribution to the time delays, any satisfactory agreement between theoretical predictions and experimental data has not yet achieved [482,486,487]. In the following, we only attempt to give a very brief overlook of the theoretical aspects of how one extracts the time delays in the context of attosecond streaking, taking the one-electron atomic and molecular systems as examples. At the end of this section, we will give a short introduction to the related and longstanding debate over the tunneling time.

5.1. Phaseshift and time delay

Instead of discussing the dispute of time itself as an operator and a physical observable, many authors tend to introduce the concepts of the time delay and investigate their applications in different physical context [488–492]. Particularly, Smith [493] proposed a new way to deal with the time delay in 1960 by introducing the concept of the dwell time of a particle in a given spatial region. His analysis to a stationary scattering was reduced to the Eisenbud–Wigner time delay [488,489],

as a difference between the interacting and the free dwell time. In this sense, one usually names the time delay as Eisenbud–Wigner–Smith (EWS) time delay in the scattering and photoionization community. For a particle collision of systems with one degree of freedom, Pollak and Miller [494] presented a new interpretation of the time delay as the time average of a flux–flux correlation function. Their formulation gives a complex time delay, whose real part is identical to the usual definition of Smith and the imaginary part is associated with the tunneling in the semiclassical limit. Nevertheless, the authors in Ref. [495] recently discussed the relationship and difference between the quantum dwell time of a quantum particle in a region of space and flux–flux correlations at the boundaries.

For an energy conservative quantum system, time enters the wave function through a phase-dependent term, which implies that time delays are directly related to the phase-shifts of the wave functions. Therefore, for a short range potential in which case the wavepackets can indeed truly be asymptotically regarded as free before and after the potential, the formal relation between the phaseshift and the time delay can be well established in the context of scattering theory [489,496]. Photoionization has been traditionally treated as a half scattering process, a similar relationship also exists for a short range potential.

To illustrate the above relationship, let us consider an incoming wave of 1D electronic wavepacket towards a short range potential

$$\Psi_{\text{in}}(x,t) = \int_0^\infty dE|A(E)| \exp\ [-i(Et + kx + \delta_0)], \tag{106}$$

where k is the wave number and δ_0 is a phase. After being scattered by a short range potential, the outgoing wave will be similarly given by

$$\Psi_{\text{out}}(x,t) = \int_0^\infty dE|A(E)| \exp\ \{-i[Et + kx + \delta_0 - \eta(E)]\}, \tag{107}$$

where the new term $\eta(E)$ is the energy-dependent phaseshift induced by the scattering process.

From a stationary phase argument, a connection between the quantum mechanical and classical description can be made by taking the first derivative of the phase with respect to E. For the incoming wave, one can get $t = -x/k = -x/v$. Similarly, for the outgoing wave, one can get $t = -x/k + \tau_{\text{EWS}}$ with the additional term given by

$$\tau_{\text{EWS}}(E) = \frac{\partial \eta(E)}{\partial E}, \tag{108}$$

which is the so-called EWS time delay. Please note that, the above reasoning has implicitly drawn a reference to the classical mechanics. Indeed, if one chooses to solve the Newton's equations for the cases of with or without the presence of a short range potential, a time delay of the particle motion will be also identified between the two cases.

For the case of 3D short range potential, the EWS time delay is dependent on the partial wave l and given by

$$\tau_{\text{EWS}}(E,l) = \frac{\partial \eta_l(E)}{\partial E}. \tag{109}$$

Things will become more complicated when a particle is scattered by a long range Coulomb potential because the outgoing wave is always in the presence of the potential. Therefore, the receding wave always asymptotically suffers a Coulomb distortion and never converges to a free particle. However, the asymptotical distortion is universal, independent of any specific short-range interactions, thus a general modification can be analytically derived [490,486]. For the 3D Coulomb potential case, remembering that the asymptotic form of the radial part of the partial wave at $r \to \infty$ takes the form

$$R_l(r,k,Z) \sim \sin\left[kr - \frac{l\pi}{2} + \frac{Z}{k}\ln(2kr) + \arg\Gamma\left(1 + l - i\frac{Z}{k}\right)\right], \tag{110}$$

one can thus define, similar to Eq. (109), a Coulomb EWS time delay

$$\tau^{\text{C}}_{\text{EWS}}(E,l) = \frac{\partial \sigma_l(E)}{\partial E}, \tag{111}$$

where $\sigma_l(E) = \arg\Gamma\left(1 + l - i\frac{Z}{k}\right)$. The Coulomb EWS $\tau^{\text{C}}_{\text{EWS}}(E,l)$ accounts for one part of the whole Coulomb time delay which is given by

$$t_{\text{Coul}}(E,l,r) = \frac{\partial}{\partial E}\left[\frac{Z}{k}\ln(2kr) + \sigma_l(E)\right] = \Delta t_{\text{Coul}}(E,r) + \tau^{\text{C}}_{\text{EWS}}(E,l), \tag{112}$$

in which, for the logarithmic distortion of the wavefront,

$$\Delta t_{\text{Coul}}(E,r) = \frac{Z}{\sqrt{(2E)^3}}\left[1 - \ln\left(2\sqrt{2E}r\right)\right], \tag{113}$$

defined as the Coulomb correction to the EWS time delay [486].

As carefully accounted in Ref. [486], for time-resolved photoionization, contributions due to long-range Coulomb interactions in the exit channel can be accounted for both classically and quantum mechanically to a high degree of accuracy, thereby allowing to clearly disentangle intrinsic short ranged delay times in complex systems from the Coulomb induced time shifts.

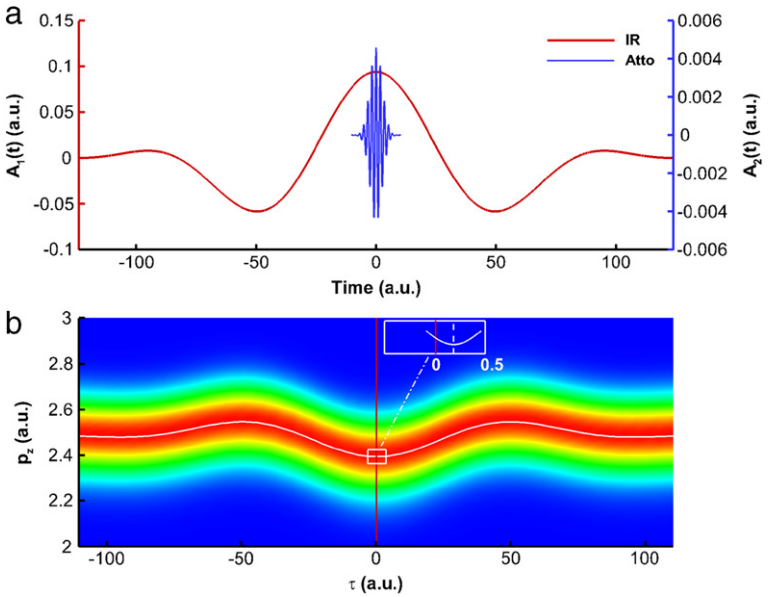

Fig. 18. Typical configurations of the attosecond streaking for extraction of the photoionization time delay: (a) the vector potential of the attosecond pulse (blue line) and the streaking IR pulse (red line); (b) a typical streaking spectrogram: the electron momentum distribution parallel to the laser polarization, p_z, as a function of the time delay τ between the two pulses, where the central white curve stands for the first moment of the momentum distribution $\bar{p}_z$. As can be seen from the insert of (b), the significant difference between the peaks of the $\bar{p}_z$ and the IR vector potential tells us the streaking time delay τ_S. (For interpretation of the references to color in this figure legend, the reader is referred to the web version of this article.)

5.2. Photoionization time delay

It is well known that photoionization can be treated as a half scattering problem. The current attosecond streaking technologies allow one to study the time delay problem of photoionization process, both experimentally and theoretically. The attosecond streaking maps the time information onto energy, which allows one to extract the time information with attosecond precision from the streaking spectrogram of the photoelectrons. In this section, we illustrate how one can extract the time delay from the numerical attosecond streaking experiments. As discussed in Ref. [486], over a wide range of photoelectron energies, the aforementioned RABBIT, where attosecond pulse trains and a weaker IR pulse are adopted, can amazingly give similar results with quantitative agreement, at least for the single-electron atom.

5.2.1. Extraction principle of the time delay

Upon absorption of an xuv photon from the attosecond pulse, if one assumes that the photoionization happens instantaneously without any time delay, then the final electron momentum after streaked by the IR field will be given by

$$\mathbf{p} = \mathbf{p}_0 - \mathbf{A}_L(t_0), \tag{114}$$

where the magnitude of $\mathbf{p}_0$ is given by $p_0 = \sqrt{2(\omega_{\rm xuv} - I_p)}$ and t_0 is the instantaneous release time of the electron from the potential. However, if there exist a time delay τ_S, the electron momentum at the detector should be given by

$$\mathbf{p} = \mathbf{p}_0 - \mathbf{A}_L(t_0 + \tau_S). \tag{115}$$

Therefore, from the theoretical point of view, the extraction of the time delay τ_S is quite straightforward. As a function of the delay time between the attosecond and the IR pulse, one can fit the shift of the linear momentum of the electron along the laser polarization direction $\hat{\mathbf{z}}$, with respect to the shape of the IR vector potential. In practice, for a better accuracy, one can evaluate the first moment of the electron p_z for a distribution $Q(p_z, t_0 + \tau_S)$, i.e.,

$$\bar{p}_z(t_0 + \tau_S) = \frac{\int p_z Q(p_z, t_0 + \tau_S) dp_z}{\int Q(p_z, t_0 + \tau_S) dp_z}. \tag{116}$$

One can then fit the quantity

$$\bar{A}(t_0 + \tau_S) = p_{0z} - \bar{p}_z(t_0 + \tau_S) \tag{117}$$

against the vector potential of the IR pulse along the laser polarization, i.e., $A_z^L(t_0)$. This procedure will uniquely determine the streaking time τ_S. In Fig. 18, we illustrate the field configuration of the attosecond streaking and the process of how to extract the time delay.

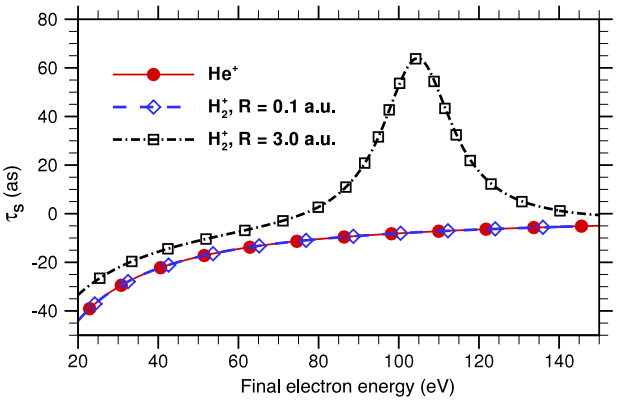

Fig. 19. (Color) The streaking time delay for H_2^+ at different internuclear distances, compared with the united atom case of He^+. *Source:* Taken from Ref. [503].

5.2.2. Single electron atom

The question arises about how to interpret the computed streaking time τ_S. It will be good to look at the one-electron system first. As mentioned before, the long range Coulomb potential will add the complexity of the problem. Therefore, the unambiguous test example will be the short range potential case. From many numerical calculations over a wide range of energies for different kinds of short range potentials, it turns out that [497–500] the streaking time τ_S is exactly the aforementioned EWS phase time, i.e.,

$$\tau_S = t_{EWS}. \tag{118}$$

However, for the Coulomb potential case, one will find that the extracted streaking time t_S is significantly different from the Coulomb EWS delay as given by Eq. (111). The difference between them are called the Coulomb–laser coupling (CLC) time shift [469,501,471,497]. For example, for ionization from the 1s state of H atom, the CLC time shift is given by

$$\tau_{CLC}\,(Z = 1, E, \omega_L) = \tau_S[\mathrm{H(1s)}] - \tau^C_{EWS}(E, l = 1). \tag{119}$$

Apparently, the CLC contribution to the time delay originates from the additional logarithmic phase distortion for the long range Coulomb potential. The coupling between the streaking IR laser field and the outgoing photoelectron transfers a finite part of the Coulomb correction term Δt_{Coul} onto the streaking time delay τ_S. Actually, the CLC contribution can also be accounted classically by CTMC method [497], or semiclassically by a matching procedure [502].

5.2.3. Simplest diatomic molecule

For a molecule, due to the multiple Coulomb centers, many strong field phenomena are different from an atomic case. For problem of the photoionization time delay in the attosecond streaking context, Ning and coworkers [503] studied the effects of the two-center for the simplest molecule H_2^+. In order to carry out the numerical attosecond streaking calculations, one need to solve the time-dependent Schrödinger equation of H_2^+ and compute the corresponding time-independent scattering states. The details of these numerical techniques can be found in previous work [504,254,505]. Note, however, that there exist other studies in the time-independent context for time delays in molecules [506–509].

In Fig. 19, we show the corresponding streaking time delays for two internuclear distances, $R = 0.1$ a.u. and $R = 3$ a.u., together with that of the He^+ case. For $R = 0.1$ a.u., one expects that the molecule is essentially atomic-like as He^+ so that one sees a quite smooth curve as the energy of the photoelectron is increased, which exactly overlaps with the result of He^+. However, for $R = 3$ a.u., we can see a pronounced peak around the electron energy of 105 eV. The immediate question is: does this peak also appear in the EWS time delay of the molecule?

The EWS time delay t_{EWS} for the H_2^+ molecule can be computed from the energy derivative of the phase of the exact dipole transition element

$$\tau_{EWS}(E, R, \theta_e, \theta_x) = \frac{\partial}{\partial E} \arg\left(\langle \psi_f^-\,(E, R, \theta_e)|\mathbf{d}\cdot\hat{\mathbf{e}}|\phi_0\rangle\right), \tag{120}$$

where E is the final continuum energy of the electron and θ_e is the electron ejection angle relative to the internuclear axis. The angle of the polarization axis of the xuv field, $\hat{e}$, relative to the internuclear axis is denoted by θ_x. The final results are shown in Fig. 20 with the $R = 3$ case marked with a white dashed line. Indeed, the peak appearing in the streaking time delay in Fig. 19 originates from the EWS time delay. Actually, this resonance peak corresponds to the minimum of the single-photon ionization cross section, where a smooth phaseshift of π occurs in the phase of transition amplitude [503].

The resonance in the photoionization time delays can be explained by the Cohen–Fano interference in the photoionization of two-center molecules [503]. Even after the vibronic ground state average and the molecular orientation angle average,

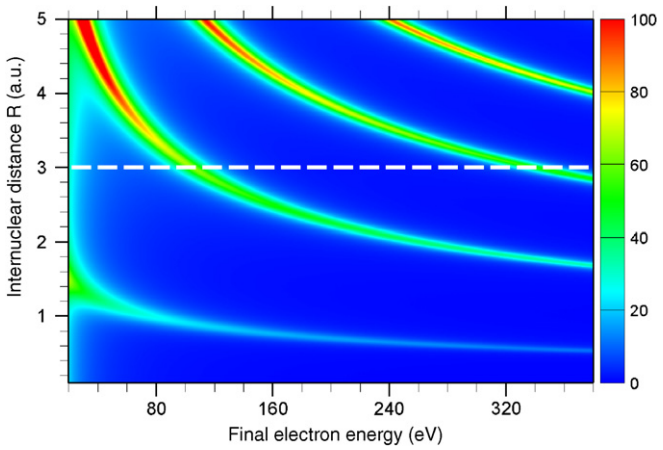

Fig. 20. (Color) EWS delays of H_2^+ in the (E, R) plane for the electron emission along the internuclear axis. The xuv pulse is polarized parallel to the internuclear axis.
Source: Taken from Ref. [503].

they showed that this resonance in the time delay is still feasible for an experimental observation. The study for the molecular case also shows that, the additive relationship

$$\tau_S = \tau_{EWS} + \tau_{CLC}, \tag{121}$$

first established for an atom, also works well for the simplest molecular case. The CLC term is quite universal and independent of the short range potentials. For the present case, t_{CLC} is identical for H_2^+ and He^+ for the same streaking pulse. Please note that, for a system with a permanent dipole, there will be an additional contribution term called the dipole–laser coupling [510,486].

5.2.4. Multielectron systems and solid

Compared to the situations of single-electron atoms and molecules discussed above, things are much more theoretically challenging for multielectron systems because *ab initio* simulations based on the numerical solution of the time-dependent Schrödinger equation is very difficult or formidable. However, first experimental measurements of photoionization time delays were carried out for multielectron rare gas atoms [99,438,443]. These work have triggered a lot of theoretical work [471,482,497,498,500,502,511–520]. Due to the complexity of the problem and limitation of this kind or another in different theories, there does not exist satisfactory agreement between the experimental measurements and the theoretical calculations. As an example, an *ab initio* simulation [514] for helium in the shakeup process demonstrated another important contribution to the streaking time delay, i.e., t_{CLC}^{e-e}, resulting from the back action of the excited bound state onto the continuum wave packet in the presence of the IR streaking field. Essentially, this term stems from the interplay of electron–electron and infrared–field interactions in the exit channel. Their work shows one aspect of the complexity in extracting and disentangling different contributions of time delays for multielectron systems.

Compared to the numerical extraction of the time delays, it is more tricky to measure the time delay experimentally. Usually, one needs to choose a reference system. When electrons in two different atomic subshells are ionized by the same attosecond pulse, the two quantum transitions to the continuum can be regarded to happen simultaneously. The experiment by Schultze et al. was carried out for Ne in such a situation. The measurement gave a relative time delay of $+21$ as for the 2p and 2s electron, which means that the formation of the 2s electron wavepacket precedes that of the 2p electron. However, up to now, all kinds of theoretical results, based on either time-independent [512,516,521–523] or time-dependent methods [515,519], are significantly smaller than the experimental value.

Another set of experiments by the RABBIT interferometry method [438,443] were carried out for Ar near the Cooper minimum [417], corresponding to the zeros in the photoionization dipole matrix element as a function of photoelectron energy. Around the Cooper minimum, the sign change of the dipole matrix element leads to a phase jump by $\pm\pi$ over a narrow range of energies [524], which means a very large EWS time shift. Again, large discrepancies exist between several theoretical calculations [516,518,523,525] and the experimental data [438,443].

Attosecond streaking has also find its application in studying the fast electronic dynamics of condensed matter [97,437]. In the first experiment [97], a time delay of 100 ± 70 as was found for the emission of 4f core levels relative to conduction band (CB) electrons from the W(110) surface at a photon energy of 91 eV. In the second experiment [437], measurements were repeated at higher photon energies of 106 and 120 eV, giving much smaller time delays around 30 as with a smaller uncertainty. The physical origin of this delay and its strong variation as a function of the photon energy has remained an open question and attracted a lot of theoretical investigations [471,500,526–533].

5.3. Debate on tunneling time

As mentioned in previous sections, the electron tunneling is the first step of many strong field processes. Actually, as a purely quantum effect, quantum tunneling represents one of the triumphs in quantum mechanics. The tunneling effect refers to the penetration of matter waves or transmission of particles through a high potential barrier, over which a classical particle is energetically prohibited to surmount. Merzbacher [534] presented a complete review for the early history of quantum tunneling in 1920s. The tunneling and its applications have been observed and discussed in many context such as α-particle emission from nuclei, fusion catalyzed by muons, the Esaki diode, and the scanning tunneling microscope. Despite of its conceptual [535] and practical [536] importance, our current understanding of the tunneling is far from being complete.

The most outstanding question that has been asked for more than 80 years [537] is how long a tunneling particle travels through a potential barrier [479,538,539]. The total traversal time was believed to include two parts, i.e., a long bouncing time inside the potential and a shorter escaping time from the barrier [540–543]. This question is still under fierce theoretical debates and no consensus has been reached so far. At the same time, experimental attempts in different contexts have continually been made to shed some light on different definitions of tunneling time from various framework. Intuitively, the estimation of the tunneling time is broken down into observing two events, i.e., the particle impinging on the barrier and the particle escaping out of the barrier, whose times need to be recorded and thus their difference decided. However, this intuitive picture faces many difficulties, to name just three. The first is that, time in quantum mechanics is not a well-defined operator, which has been realized from the early days of quantum theory by Pauli [544]. The reason is simply because the spectra of the conjugate operator H of a quantal system is bounded from below, thus the operator $\hat{t} = -i\frac{\partial}{\partial E}$ cannot be a self-adjoint operator. The second point is that, due to the wave–particle duality and the time–energy uncertainty principle $\Delta E \Delta t \sim \hbar$, there seems not to be a unique value of a traversal time for a wave packet or even for a particle [545,485]. The third difficulty lies in the fact that the system under investigation is a microscopic one and thus its measurement is a quantum measurement, which is capable to destroy the tunneling state itself under consideration. Nevertheless, there exist various theoretical attempts to construct time operators and develop frameworks to estimate arrival times in present time formalisms, which have been accounted in several reviews [546–548]. In addition, there have been many theoretical proposals to attach different versions of quantum clocks to the tunneling processes [538,539]. Along the vast theoretical investigations, quantum tunneling time have attracted a lot of experimental studies in different contexts [478,549–559]. Unfortunately, no definite confirmation has yet been made and there does not exist a consensus on a unique resolution of the tunneling time problem. From the early days, many of the studies have been focused on an incoming matter or optical wave (or a particle/photon) impinge on a potential barrier [560,561]. Most recently, with the fast development of time-resolved spectroscopy, more attentions have been paid to the time of photoionization of a bound state, either by absorbing a single photon or by tunneling through a distorted Coulomb potential barrier by a strong IR field [97,99,343,438,450,562–564].

As early as in 1932, Maccoll [537] noted that the tunneling process must be characterized by both the transmission rate and the speed of the transmission. Among many of the definitions of times, most of them are involved with a certain kind of derivative of the transmission amplitude $T = |T(E)|e^{i\theta(E)}$, e.g., (1) the Larmor time [539]: $\tau_{\rm LM} = -\partial\theta/\partial V$, (2) the Büttiker–Landauer time [565]: $\tau_{\rm BL} = -\partial \ln|T|/\partial V$, (3) the EWS phase time [489,488]: $\tau_{\rm EWS} = \partial\theta/\partial E$, and (4) the Pollack–Miller time [494]: $\tau_{\rm PM} = \partial \ln|T|/\partial E$, where V and E is respectively the height of the potential and the energy of the incident particle. Yamada [566] attempted to present a unified derivation of different definitions of tunneling time from the Gell-Mann–Hartle decoherence functionals. His derivation, working for the over-the-barrier propagation as well, reveals that the two types of derivatives with respect to V and E can be understood as resulting from two different definitions of the time that a Feynman path takes to traverse the barrier region, i.e., the dwell (resident) time and the passage time respectively. The EWS phase time belongs to the latter passage time. However, for a time-dependent potential, as recently reviewed by Landsman and Keller [485], these definitions do not give results comparable with the experimental measurements and probably need some kind of extensions. In addition, the probabilistic nature of the tunneling time may prohibit a direct measurement of it at the desired attosecond resolution.

6. Correlation dynamics in two-electron systems

The electron–electron correlation [567] has played an important role in many research fields since the development of quantum mechanics in 1920s. At that time, experimental physicists observed discrete atomic spectra. It was a rigorous challenge to explain these discrete atomic spectra from the classical theory. Initially, the simple hydrogen spectra can be quite successfully explained by the "old quantum theory" based on Bohr's quantum postulates. However, the old quantum theory failed in explaining the more complex atomic spectra of helium. Helium is the simplest two-electron atom, where the electron–electron correlation can be explored. In fact, the failure of the old quantum theory in the two-electron system prompted the birth of new quantum theory. The new quantum theory provide an effective frame to handle the dynamics of microscopic particles, including the electron–electron dynamics. However, accurate treatment for the many-body problem is an incredibly difficult task, which has long been the focus of the theoretical physicists [568].

It is valuable to explore those electron–electron correlation dynamics in various systems. The electron–electron correlation is responsible for a large number of many-body phenomena, including the superconductivity, the molecular structure formation, and the chemical reaction, etc. In this section, we review the recent progress of the studies on the

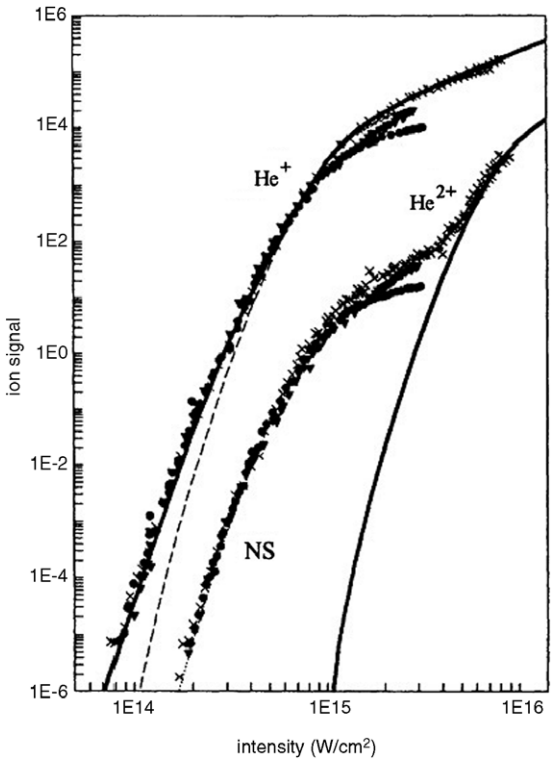

Fig. 21. Total cross section for the nonsequential two-photon double ionization of helium. Measured He ion yields for a linearly polarized laser of 100 fs at 780 nm. Calculations are shown as solid (SAE) and dashed (ac-tunneling) lines. The measured intensities are multiplied by 1.15. The solid curve on the right is the yield of He^{2+}, calculated according to a sequential ionization model.
Source: Taken from Ref. [204].

electron–electron correlation dynamics in the photon ionization process, including the double ionization process by strong infrared laser fields, the few-photon double ionization process by extreme ultraviolet radiation, and the pump–probe protocols to trace the electron–electron correlation dynamics.

6.1. Electron correlation in double ionization of atoms in strong IR fields

In the early stages, multiple ionization was usually described in a picture of sequential process. In this picture, multiple ionization is divided into a series of independent steps of single ionization. In each step, only one electron is treated to be active and can interact with the laser pulse field, and the influence of the remaining electrons can be reduced to a charge screening effect. However, this sequential picture is not always true. Early experiments have made it clear that interpretation of the experimental observations require to take into account a nonsequential channel, in which two electrons strongly interact with each other through the Coulomb repulsive force and the double ionization process cannot be divided into two single ionization events. Such electron correlation dynamics in the double (multiple) ionization process induced by strong infrared IR laser field have attracted considerable interest in the past two decades. Many reviews have focused on this topic [50,569–571]. In this section, we will only make a brief introduction for the main experimental observations which deviate from the sequential pictures and the corresponding mechanisms which have been built up to understand the electron correlation dynamics.

The first evidence for the breakdown of the sequential ionization picture is the observation that the double ionization yield can be six or more orders of magnitude greater than the prediction of theory based on the sequential ionization. In Fig. 21, the experimental data [204] are shown for the double ionization yield as a function of the laser intensity. We can see that the experimental measurements depart significantly from the predictions of the sequential model in the intermediate laser intensities, where a "knee" signature can be observed in the count of double ionization yield. Such kind of surprising departure from the sequential model gives rise to a fierce debate on the mechanism of nonsequential double ionization in 1990s [572,573]. Most mechanisms proposed to account for the nonsequential path involve high degree of electron correlation. Now, the recollision or a rescattering model [33,574–577,575,578–583] is widely accepted as the dominating mechanism. In the rescattering picture, one electron firstly tunnels through the potential barrier formed by the Coulomb potential and the instantaneous laser field at the instant that the electron field approaches the local maximum value. Then, the first freed electron experiences an acceleration process in the external laser field. In the acceleration process, the motion

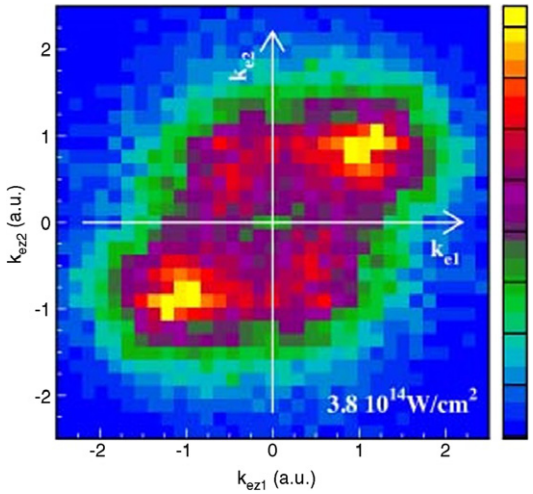

Fig. 22. (Color) The joint momentum distribution of the two electrons along the laser polarization, emitted in NSDI of Ar below saturation by a Ti:sapphire laser with a peak intensity of 3.8×10^{14} W/cm^2.
Source: Taken from Ref. [584].

of the electron can be treated classically, and the influence of the Coulomb potential is usually neglected. If the laser field is linearly polarized, the freed electron can be driven back to the ionic core, where it has obtained high enough energy to knock out another electron. Double ionization of this type thus reduces the electron correlation dynamics to the electron–ion impact process. Simple models based on the recollision picture well reproduce the observed "knee" structure. In addition, the recollision picture predicts that the nonsequential double ionization should be sensitive to the laser ellipticity. For a circularly polarized laser pulse, since the firstly freed electron cannot be driven back to the core, NSDI is expected to have negligible contribution. Such predictions have been confirmed by the experiments, and the "knee" character appearing in the linear polarization case does not appear in the circular polarization case.

Many other electron correlation mechanisms were also suggested to explain the nonsequential double ionization channel. For example, another frequently mentioned mechanism is the shake-off process [203]. In the shake-off picture, an electron is firstly ionized, then in a quite short time the other electron sees a sudden change of the potential from the core, and so the second electron also has probability to be shaken to the continuum. The shake-off mechanism is known to dominate in one-photon double ionization process in the high energy region induced by xuv pulses. Since the recollision mechanism was once blamed for that it could not interpret quantitatively the yield of double ionization, as a possible mechanism, the shake-off picture also once obtained considerable attention. However, similar to other mechanisms, the shake-off picture cannot explain characters observed in the more detailed recoil ion momentum distribution and the two-electron joint momentum distributions produced from the NSDI channel. In the shake-off picture, the two electrons are predicted to be ionized almost simultaneously at the local maxima of the electric field, where the vector potential of the field is zero. So the two electrons, as well as the recoil ion, can obtain negligible momentum from the laser field, and their momenta are expected to be peaked at zero. Such predictions conflict with the corresponding experimental observations. In contrast, these experimental observations are well understood in the recollision picture. In the recollision picture, double ionization happens when the first electron reencounters the ion core, which has a delay of 0.5∼1 optical cycles with respect to the ionization of the first electron. Thus the two electrons and the recoil ion are allowed to obtain considerable momentum from the laser field in the recollision picture, see Fig. 22 for one of experimental measurements.

The recollision picture is also supported by many theoretical analyses. Both classical and quantum theories have been used to analyze the NSDI process. It is found that the predictions of the classical calculations and quantum calculations are extremely similar. In addition, it is much easier to solve the time-dependent Newton equations than the time-dependent Schrödinger equation. Thus, the applications of the classical theory in NSDI have been extensively explored. In the classical methods, the initial conditions of the electrons are usually chosen in two ways. One of the "classical" methods in fact includes many quantum mechanical elements. One assumes that the first electron tunnels out the bound potential and its initial conditions are determined by its quantum mechanical wave function at the tunneling time [187]. The second electron is assumed to be in the ground state of a singly charged ion and its initial conditions is modeled by a microcanonical distribution. The motion of the first electron in the external laser field obeys the Newton's law. When the first electron is driven back to the core, the recollision leads to the ionization or excitation of the second electron. The other classical method completely give up all the quantum concepts, and it treats NSDI as a purely classical phenomenon [585]. In this method, the initial conditions of the position and velocity for both electrons are decided from microcanonical ensembles, and all the dynamics of the two electrons in this system are governed by the Newton's law of motion. It has been shown that the classical computation is quite powerful in reproducing important features in NSDI, including the "knee" structure

in the total double ionization yield, the peaks at nonzero momenta for the recoil ion, and two-electron joint momentum distributions [even the particular finger-like structures [586] in the electron momentum distribution].

The most rigorous theoretical treatment for NSDI is the numerical solution to the time-dependent Schrödinger equation. This approach does not involve any physical approximations, thus it can serve as a benchmark for other theoretical models. However, it is still a great challenge to perform *ab initio* TDSE in its full dimensions even for the simplest two-electron atom helium. The requirement for the computer resources will increase rapidly as the increase of the wavelength, the peak intensity, and the pulse duration of laser pulse. An earlier *ab initio* TDSE calculation in the full dimensions employed a laser-field wavelength of 390 nm [235]. Only recently, full-dimensional *ab initio* calculations were performed for the infrared wavelength of 780 nm in the context of xuv + IR [587], with the only inclusion of those essential partial waves involved in the dynamics. Thus, the high-accuracy quantitative *ab initio* full-dimensional calculation for the NSDI problem in the infrared wavelength region with the complete set of the partial waves is still lacking up to now. Most existing TDSE calculations are performed on the reduced space dimensions or rely on some assumptions [588]. Although such reduced TDSE calculations do not provide quantitative comparisons with experimental data, many qualitative features observed in experiments can be reproduced.

Other analytical quantum approaches such as S-matrix method have also been extensively explored [589–592]. An S-matrix element is the transition amplitude into a given final state from an initial state. This method requires that one has in mind a particular scenario of how double ionization proceeds, and the S-matrix element can be expressed according to the preconceived ionization paths. Compared with the numerical TDSE methods, such analytical methods are more suitable for identifying the mechanism of NSDI.

6.2. Electron correlation in two-photon double ionization of atoms

In the xuv light region, the photon energy is so large that only a few number of photons can provide enough energy for double ionization. After more than 30 years of extensive studies, as the most simple case, the one-photon double ionization of helium (PDI) have been well understood until the beginning of the 21st century. There exist several reviews of one-photon double ionization of helium [593,594]. In the past decade or more, a large number of interests are put on the two-photon double ionization of helium (TPDI). On one hand, the new light source, such as high-order harmonics [377] and free-electron lasers [595], have produced bright enough light to induce nonlinear double ionization process, which brings the process of TPDI experimentally observable. On the other hand, theoretical methods, which behave well in handling PDI process, can significantly disagree with each other when they are applied to TPDI of helium. For example, the total cross sections of TPDI of helium given by different theoretical calculations can differ by one order of magnitude [596–613]. However, experimental measurements still cannot provide a definite answer due to the large experimental uncertainty [614]. In the following, we mainly review the theoretical efforts on the TPDI process.

6.2.1. Numerical solution to TDSE of two-electron system

In the past decade, a number of sophisticated theoretical methods have been applied to the three-body Coulomb breakup problems, including the converged close-coupling method [615,616], R-matrix approach [617,618], exterior complex scaling method [257,258], and the time-dependent close-coupling (TDCC) methods [619]. The numerical methods have achieved unprecedented accuracy for this tough problem. In the following, we mainly present the main framework to solve the time-dependent Schrödinger equation of helium in its full dimensions.

The TDSE of helium in a linearly polarized laser field is given by

$$i\frac{\partial}{\partial t}\Psi(\mathbf{r}_1,\mathbf{r}_2,t)=H(t)\Psi(\mathbf{r}_1,\mathbf{r}_2,t), \tag{122}$$

where the Hamiltonian operator, in the dipole approximation (length gauge), can be written as

$$H(\mathbf{r}_1,\mathbf{r}_2,t)=\frac{\mathbf{p}_1^2}{2}+\frac{\mathbf{p}_2^2}{2}-\frac{2}{r_1}-\frac{2}{r_2}+\frac{1}{|\mathbf{r}_1-\mathbf{r}_2|}+(\mathbf{r}_1+\mathbf{r}_2)\cdot\mathbf{E}(t), \tag{123}$$

where $\mathbf{E}(t)$ is the electric field of the laser pulse.

In the close-coupling scheme, the two-electron wave function $\Psi(\mathbf{r}_1,\mathbf{r}_2,t)$ is expanded in the coupled spherical harmonics,

$$\Psi(\mathbf{r}_1,\mathbf{r}_2,t)=\sum_{L,M,l_1,l_2}\frac{R^{L,M}_{l_1,l_2}(r_1,r_2,t)}{r_1r_2}Y^{L,M}_{l_1,l_2}(\hat{r}_1,\hat{r}_2), \tag{124}$$

in which

$$Y^{L,M}_{l_1,l_2}(\hat{r}_1,\hat{r}_2)=\sum_{m_1,m_2}\langle l_1m_1l_2m_2|l_1l_2LM\rangle\times Y_{l_1,m_1}(\hat{r}_1)Y_{l_2,m_2}(\hat{r}_2), \tag{125}$$

where $\langle l_1m_1l_2m_2|l_1l_2LM\rangle$ is the usual Clebsch–Gordan coefficient.

For a linearly polarized laser field, the quantum number M is conservative. If the initial state is chosen to be the ground state of helium, $M = 0$ is always true. In the following we only consider this case and neglect the index M for simplicity.

Substitution of Eq. (124) into Eq. (122) leads to a set of coupled equations for the radial wavefunction $R^L_{l_1,l_2}(r_1, r_2, t)$,

$$i\frac{\partial}{\partial t}R^L_{l_1l_2}(r_1, r_2) = T_{l_1,l_2}R^L_{l_1l_2}(r_1, r_2) + \sum_{l'_1,l'_2,L'} W^L_{l_1,l_2,l'_1,l'_2}R^L_{l'_1l'_2}(r_1, r_2) + \sum_{l'_1,l'_2,L'} V^{LL'}_{l_1,l_2,l'_1,l'_2}R^{L'}_{l'_1l'_2}(r_1, r_2). \tag{126}$$

In the above equation, T_{l_1,l_2} comes from the contributions of the kinetic energy operator and the Coulomb attractive potential operator, explicitly given by

$$T_{l_1,l_2} = \sum_{i=1}^{2}\left(-\frac{1}{2}\frac{\partial^2}{\partial r_i^2} + \frac{l_i(l_i+1)}{2r_i^2} - \frac{Z}{r_i}\right). \tag{127}$$

$W^L_{l_1,l_2,l'_1,l'_2}$ represents the electron correlation term. Neumann expansion is employed to calculate the matrix element of the electron–electron repulsive potential, which is expressed as

$$\begin{aligned} W^L_{l_1,l_2,l'_1,l'_2} &= \sqrt{(2l_1+1)(2l'_1+1)(2l_2+1)(2l'_2+1)} \\ &\times \sum_{\lambda=0}^{\infty}(-1)^{L+\lambda}\frac{r^\lambda_<}{\lambda^{\lambda+1}_>}\begin{pmatrix} l_1 & \lambda & l'_1 \\ 0 & 0 & 0\end{pmatrix}\begin{pmatrix} l_2 & \lambda & l'_2 \\ 0 & 0 & 0\end{pmatrix}\begin{Bmatrix} l'_1 & l'_2 & L \\ l_2 & l_1 & \lambda\end{Bmatrix}, \end{aligned} \tag{128}$$

where $r_{>(<)}$ =max(min)(r_1, r_2). In the length gauge, the contribution of the electron–laser interaction term is

$$\begin{aligned} V^L_{l_1,l_2,l'_1,l'_2} &= E(t)\sqrt{(2L+1)(2L'+1)}\begin{pmatrix} L & 1 & L' \\ 0 & 0 & 0\end{pmatrix} \\ &\times\Bigg[r_1(-1)^{l_2}\sqrt{(2l_1+1)(2l'_1+1)}\begin{pmatrix} l_1 & 1 & l'_1 \\ 0 & 0 & 0\end{pmatrix}\begin{Bmatrix} l_1 & l_2 & L \\ L' & 1 & l'_1\end{Bmatrix}\delta_{l'_2l_2} \\ &+ r_2(-1)^{l_1}\sqrt{(2l_2+1)(2l'_2+1)}\begin{pmatrix} l_2 & 1 & l'_2 \\ 0 & 0 & 0\end{pmatrix}\begin{Bmatrix} l_2 & l_1 & L \\ L' & 1 & l'_2\end{Bmatrix}\delta_{l'_1l_1}\Bigg]. \end{aligned} \tag{129}$$

If the velocity gauge is used to describe the electron–laser interaction, the matrix element of it will be

$$\begin{aligned} V^L_{l_1,l_2,l'_1,l'_2} &= iA(t)\sqrt{(2L+1)(2L'+1)}\begin{pmatrix} L & 1 & L' \\ 0 & 0 & 0\end{pmatrix} \\ &\times\Bigg[\left(\frac{\partial}{\partial r_1} + \frac{l'_1(l'_1+1) - l_1(l_1+1)}{2r_1}\right)(-1)^{l_2}\sqrt{(2l_1+1)(2l'_1+1)}\times\begin{pmatrix} l_1 & 1 & l'_1 \\ 0 & 0 & 0\end{pmatrix}\begin{Bmatrix} l_1 & l_2 & L \\ L' & 1 & l'_1\end{Bmatrix}\delta_{l'_2l_2} \\ &+ \left(\frac{\partial}{\partial r_2} + \frac{l'_2(l'_2+1) - l_2(l_2+1)}{2r_2}\right)(-1)^{l_1}\sqrt{(2l_2+1)(2l'_2+1)} \\ &\times\begin{pmatrix} l_2 & 1 & l'_2 \\ 0 & 0 & 0\end{pmatrix}\begin{Bmatrix} l_2 & l_1 & L \\ L' & 1 & l'_2\end{Bmatrix}\delta_{l'_1l_1}\Bigg]. \end{aligned} \tag{130}$$

To solve the coupled equations for the radial wavefunction $R^L_{l_1,l_2}(r_1, r_2, t)$ [Eq. (126)], one needs to further discretize the radial coordinates r_1 and r_2 and employ some techniques to realize the time propagation. Those techniques have been introduced in Section 2.5.

6.2.2. Total and differential cross sections of TPDI

Definitions for the total and differential cross sections of TPDI

Two-photon double ionization of helium is usually studied in two regions according to whether the photon energy is larger than the second ionization potential. The first ionization potential and the second ionization potential of helium is $I_{p1} = 24.6$ eV and $I_{p2} = 54.4$ eV, respectively. If the photon energy ω is larger than the second ionization potential I_{p2}, the ejection of the two electrons by absorbing two photons can be treated as a sequential process, i.e. one electron is firstly freed with energy of $\omega - I_{p1}$ from the neutral helium atom by absorbing one photon and the other electron is then freed with energy of $\omega - I_{p2}$ from the remaining He^+. This physical picture is usually referred to as the sequential two-photon double ionization. When $(I_{p1} + I_{p2})/2 < \omega < I_{p2}$, the energy of one photon is not large enough to ionize He^+, but two photons can provide large enough energy for double ionization of helium. Thus, the above sequential picture does not hold any more, and the two electrons can be freed almost simultaneously by absorbing two photons. This latter physical picture is usually

referred to as the nonsequential or direct two-photon double ionization. The distinguishing of sequential and nonsequential two-photon double ionization is meaningful only when the pulse duration is long enough.

For the two-photon nonsequential double ionization, the total double ionization yield is proportional to the pulse length, i.e. the transition rate from the ground state to the double electron continuum is a constant. So we can define the two-photon cross section as the ratio of transition rate to the square of photon flux. Considering the interaction of a monochromatic laser field to the two electrons, the interaction Hamiltonian can be given by

$$\mathrm{V(t)} = \frac{1}{2} E_0 \left(\mathbf{r_1}\cdot\hat{\varepsilon} + \mathbf{r_2}\cdot\hat{\varepsilon}\right) e^{-i\omega t}, \tag{131}$$

where E_0 is the amplitude of the electric field strength, and $\hat{\varepsilon}$ is the unit vector which represents the direction of polarization of the electric field. Applying the second-order perturbation theory, according to Eq. (37), the transition rate can be expressed as

$$R^{(2)}(t) = \left(\frac{E_0}{2}\right)^4 2\pi\delta(\omega_{fi} - 2\omega) \times \left| \sum_k \frac{\langle E_f | \mathbf{r_1}\cdot\hat{\varepsilon} + \mathbf{r_2}\cdot\hat{\varepsilon} \, | E_k\rangle \, \langle E_k | \mathbf{r_1}\cdot\hat{\varepsilon} + \mathbf{r_2}\cdot\hat{\varepsilon} \, | E_i\rangle}{\omega_{ki} - \omega} \right|^2. \tag{132}$$

The photon flux is given by $I/\omega = \epsilon_0 c E^2/2\omega$. Dividing the transition rate by the square of photon flux, one can get

$$\frac{d\sigma}{dE_1 dE_2 d\Omega_1 d\Omega_2} = k_1 k_2 \frac{8\pi^3\omega^2}{c^2}\delta(\omega_{fi} - 2\omega) \times \left| \sum_k \frac{\langle E_f | \mathbf{r_1}\cdot\hat{\varepsilon} + \mathbf{r_2}\cdot\hat{\varepsilon} \, | E_k\rangle \, \langle E_k | \mathbf{r_1}\cdot\hat{\varepsilon} + \mathbf{r_2}\cdot\hat{\varepsilon} \, | E_i\rangle}{\omega_{ki} - \omega} \right|^2. \tag{133}$$

In the above equation, we have assumed that the final-state wave function $|E_f\rangle = |\Psi_{\mathbf{k_1 k_2}}\rangle$ is normalized according to $\left\langle \Psi_{\mathbf{k}'_1\mathbf{k}'_2} | \Psi_{\mathbf{k_1 k_2}} \right\rangle = \delta(\mathbf{k_1} - \mathbf{k}'_1, \mathbf{k_2} - \mathbf{k}'_2)$, where $\mathbf{k_1}$ and $\mathbf{k_2}$ are the momenta of the ejected two electrons and $E_1 = k_1^2/2$ and $E_2 = k_2^2/2$. In Eq. (133), integrating over dE_2, we obtain the triple-differential cross section (TDCS)

$$\frac{d\sigma}{dE_1 d\Omega_1 d\Omega_2} = k_1 k_2 \frac{8\pi^3\omega^2}{c^2} \times \left| \sum_k \frac{\langle E_f | \mathbf{r_1}\cdot\hat{\varepsilon} + \mathbf{r_2}\cdot\hat{\varepsilon} \, | E_k\rangle \, \langle E_k | \mathbf{r_1}\cdot\hat{\varepsilon} + \mathbf{r_2}\cdot\hat{\varepsilon} \, | E_i\rangle}{\omega_{ki} - \omega} \right|^2, \tag{134}$$

where $E_2 = 2\omega - I_{\mathrm{p1}} - I_{\mathrm{p2}} - E_1$. The total cross section σ can be obtained by integrating the TDCS over all energies and ejected angles of the two electrons.

Perturbation calculations in obtaining the total cross sections of TPDI

The calculation of the total cross section of two-photon double ionization of helium has recently attracted a large amount of attention. One can calculate the total cross section in the frame of lowest order perturbation theory (LOPT). Two difficulties exist in the theories based on LOPT. One difficulty is how to consider the electron correlation in the final wave functions, which is in fact the central difficultly in all theoretical methods. The other difficulty is that one should in principle perform infinite summing or integrating operations over the complete set of intermediate states.

In the early years, Kornberg and Lambropoulos [620] made a conjecture that the electron correlation is relatively unimportant in the multi-photon double ionization. They thus represented the final wave function by a product of single-particle continuum states. To overcome the problem of infinite summation, they performed a truncated summation, in which a finite number of discrete states 1s*n*p are included. With this two main approximations, they obtained the absolute generalized total cross sections for the nonsequential two-photon double ionization. The value they obtained is smaller than later most sophisticated calculations by about one order of magnitude. In 2000, Nikolopoulos and Lambropoulos [621] developed the multichannel theory for the two-photon single and double ionization of helium. Multichannel theory allows for a systematic way of incorporating correlation effects to the desired degree for the wave functions. The multichannel wave functions are constructed within the framework of discretized bases involving linear combinations of *B*-splines. This may be the first serious treatment for this problem.

In 2006, Kheifets and Ivanov [613] applied the convergent close-coupling (CCC) formalism to the problem of two-photon double ionization of helium. In principle, the electron correlation is fully included in the CCC final wave function. In that paper, they employed the so-called closure approximation to the LOPT by replacing the infinite sum of the perturbation theory with an averaged energy denominator. Though the integrated two-photon double ionization cross-section is substantially below non-perturbative literature results, the pattern of the angular correlation in the two-electron continuum is remarkably close to the nonperturbative time-dependent close-coupling calculation [622]. Two years later, they published another perturbative calculation of two-photon double electron ionization of helium [623], in which the final wave function was still described in the CCC formalism. In that work, the intermediate states were taken to be the discrete set of states resulting from the diagonalization of the atomic Hamiltonian. Both the length and Kramers–Henneberger gauges of the electromagnetic interaction were applied, and the results of the calculations using different gauges generally agreed within 25% with each other. This perturbative calculation gave results for the total cross section in agreement with their earlier non-perturbative calculations [610] and many other sophisticated calculations.

In 2007, Horner and McCurdy et al. [609] applied the method of exterior complex scaling to calculate the two-photon double ionization of helium. Their calculations started from the coupled (Dalgarno–Lewis) driven equations that describe two-photon absorption in LOPT. The electron correlation was treated essentially exactly in the initial, virtual intermediate, and final states. Their calculations showed a sharp rise of the total cross section as the photon energy increases to the threshold of the sequential double ionization (54.4 eV). This sharp rise is confirmed by various later calculations. Some arguments also arose about whether this sharp rise of total cross-section is the nature of nonsequential double ionization [600] or an unintended inclusion of the sequential two-photon double ionization process caused by the bandwidth of the applied field [608].

A more recent perturbative calculation is performed by Bachau [624], who focused on the case two-photon double ionization of helium at the sequential threshold. He concluded that the two-photon excitation-plus-ionization process of $nlk'l'$ Rydberg series plays a crucial role in the two-photon double ionization on the case of photon energies close to 54.4 eV. In 2007, Shakeshaft [625] described a method for calculating cross sections for two-photon single and double ionization of an atom without the use of the final-state continuum wave function.

Nonperturbation calculations in obtaining the total cross sections of TPDI

A large number of theories which describe two-photon double ionization in the nonperturbative framework have also been developed. In 2001, Mercouris et al. [626,627] developed their many-electron, many-photon theory (MEMPT) to calculate the total cross section of two-photon double ionization of helium. MEMPT is a nonperturbative and time-independent method. The MEMPT produces the rate of a particular field-induced process as the imaginary part of a frequency- and intensity-dependent complex eigenvalue obtained from the solution of a suitably constructed non-Hermitian Hamiltonian matrix. The total cross sections obtained by Mercouris et al. were comparable with the early perturbative calculation of Kornberg and Lambropoulos [620], but significantly lower than those of most later calculations.

Presently, the most accurate treatments for two-photon double ionization of helium are based on solving the time-dependent Schrödinger equation of helium with various technologies and strategies. The earlier applications of TDSE method in the problem of two-photon double ionization of helium can be found in [234,628]. In 2002, Colgan and Pindzola [629] used the time-dependent close-coupling method to calculate, for the first time, fully differential cross sections for the complete fragmentation of helium by two photons. They also reported differences with other calculations in the magnitude of the total-integral cross sections. These differences were initially attributed to a core-excited resonance enhancement of the two-photon process. Soon after the TDCC calculation, Feng and van der Hart [630] demonstrated that core excitation effects were relatively unimportant and did not account for the differences in the total cross section reported in [629]. Feng and van der Hart calculated the total cross section with the time-independent R-matrix Floquet theory, and the values they obtained agree with the TDCC calculations of Colgan and Pindzola [629]. Quite recently, the time-dependent R-matrix theory was also developed for the problem of two-photon double ionization of helium to calculate the total cross section [631].

In TDSE methods, numerically accurate final wave functions after interaction with the laser field can be obtained. The electron correlation can be accurately accounted for in the process of obtaining the final wave functions. Double ionization probability can be obtained by projecting the final wave function to the double continuum. Double continuum is needed to extract the double ionization probability both in the frameworks of TDSE and traditional LOPT. However, the requirement for the electron correlation in the double continuum can be different in the two frameworks. In the TDSE methods, the electron correlation in the double continuum can be not so important as in the LOPT methods, since the electron correlation has been fully included in the final wave function. For example, since the electron correlation is indispensable for one-photon double ionization to happen, many calculations have shown that, in TDSE methods it can produce high accurate results for one-photon double ionization process to project the final wave function to the completely uncorrelated double continuum, which is constructed by the product of the one-electron continuum [632,633]. The total cross section of two-photon double ionization have also been calculated in such projecting methods by a lot of authors [362,600,604,606,622,629,634,635].

In 2003, Laulan and Bachau calculated the double continuum states by treating the electronic term $1/r_{12}$ within the zero- and first-order perturbation theory. In the first-order perturbation theory, the electron correlation was partially included. Their results showed that cross sections calculated in zero- and first-order perturbation theory did not differ significantly, which indicated that the electron correlation did not play an important role in the double continuum when it was used to extract the double ionization information in the TDSE methods. However, the debate on the role of electron correlation arose when Foumouo et al. published their numerical calculations in 2006 [612]. They first used a spectral method of configuration interaction type to build up the eigenstates of the atomic Hamiltonian. Second, they propagated the total wave packet of the atom in time. Finally, they used the so-called J-matrix method to generate the continuum states on which they projected the final wave packet to extract information regarding the single and double ionization. The J-matrix method can produce quite accurate single continuum component of the continuum wave function, and the accuracy had been tested in the one-photon ionization of H^-. The doubly ionized wave packet was obtained by subtracting the single continuum component from the final total continuum wave function. This projection method took account of the electron correlation in the double continuum. In addition, they also performed the projection in which the electron correlation in the double continuum was neglected. Their calculations showed significant difference in the results of these two kinds of projection methods. The total two-photon double ionization cross sections in the fully correlated calculation were several times larger than those without the electron correlation taken into account in the double continuum. Their TDSE calculations without the electron correlation in the double continuum agreed with other previous TDSE calculations [622,629,634]. Their results of fully correlated calculations were reported to be closer to the earlier perturbative multichannel calculation of Nikolopoulos and

Lambropoulos [621]. Nikolopoulos and Lambropoulos have also developed the multichannel theory to the non-perturbative time-dependent calculations [611], which also gave comparable values to the fully correlated calculations of Foumouo et al. These calculations indicated that the electron-correlation played quite important role in the final wave functions.

These calculations published in Refs. [611,612,620] question the application of the uncorrelated projection method in the two-photon double ionization of helium. Indeed, though the uncorrelated projection method has been proved to work well in the one-photon double ionization, it may not work in the process of two-photon double ionization. The roles of the electron correlation in the one-photon and two-photon double ionizations can be different. However, it is too early to draw a clear, unmistakable conclusion for this question. Other calculations [597,601,603,609,610,623] which also fully took account of the electron correlation do not support the above three calculations [611,612,620]. Instead, these later calculations all tend to agree with the earlier results obtained by the uncorrelated projection methods [622,629,634]. These later calculations include the CCC methods employed by Ivanov and Kheifets [623], the ECS methods employed by McCurdy et al., and Fourier transform (FT) methods recently employed by Malegat et al. [597].

Both the CCC methods and the ECS methods have the time-dependent and time-independent versions. The time-independent perturbative versions of CCC [613,623] and ECS [607,609] have been mentioned above. The time-dependent nonperturbative versions of CCC [610] and ECS [601,603] methods were developed by the corresponding authors soon after the time-independent versions were published. These authors also obtained the final two-electron wave functions by solving the TDSE. In CCC methods, the correlated CCC double continuum is used to extract double ionization probability instead of the uncorrelated double continuum. In the ECS methods, the projection procedure is identical to perform the Fourier transform of the wave packet taken from the end of the pulse to infinity. This procedure involves a stationary driven Schrödinger equation with the wavepacket at the end of the pulse as the source term, which can be solved using the standard ECS approach. Recently, Malegat et al. presented another method for the analysis of the final wave packet. Their method, referred to as Fourier transform methods, consists in propagating the Fourier transform of the wavepacket to the asymptotic region where the different channels disentangle geometrically. The main procedures are: (i) identify a hypersphere $R = R_0$ that is reached by the wavepacket after the end of the pulse and crossed over by the wavepacket before unphysical reflections on the box boundaries reach R_0 again; (ii) form the Fourier transform of the wavepacket on this matching hypersphere; (iii) propagate this Fourier transform with respect to the hyperradius using the hyperradial propagators belonging to the hyperspherical R matrix with the semiclassical outgoing wave method; and (iv) obtain the double ionization cross section from the flux of the Fourier transform through the appropriate part of the final hypersphere, the latter being located in the genuine asymptotic region where the various channels disentangle geometrically. Though, in all these methods, the electron correlation was considered in the projection process, the results obtained still reasonably agreed to the uncorrelated projection methods.

In fact, if the final wave function is continually propagated freely for some times after the end of the laser pulse, the two electrons will be well separated, and the error, introduced by the neglect of electron correlation in the double continuum during projection, will be very small. Feist et al. have checked the convergence of the total cross section for the field-free propagation time τ [604]. They demonstrated that delaying the projection from $\tau = 1$ fs to $\tau = 21$ fs changed the total cross section by less than 2%. The concept of cross section is only meaningful for long enough pulses. Feist et al. also studied the influence of the pulse length and shape on the cross sections in time-dependent calculations. The dependence on the pulse duration of the cross sections extracted in the TDSE methods is more sensitive when the photon energy approaches the sequential threshold. The results of Feist et al. for the long pulse (total duration of 4 fs for a $\sin^2$ envelope shape) confirmed the sharp rise of the total cross section near the sequential threshold, which was also observed in the time-independent ECS calculations [609]. Even longer pulses were used by Pazourek et al. [599] to the calculation of total two-photon double ionization cross sections.

We make a brief summary for existing numerical results of the total cross section of two-photon double ionization. Presently, the mainstream debate can be divided into two groups. On one hand, many calculations [597,599–601,603,604,606,607,609,610,613,622,624,625,629–631,634,635] have achieved comparable results. On the other hand, some calculations [605,611,621] produced roughly one order of magnitude higher value. Some of the representative results are shown in Fig. 23. The center of the debate is on the role of electron correlation in the final wave function. It seems that almost all TDSE methods can produce accurate final wave functions, while the arguments arise when the double ionization information are extracted from the final wave functions. Though the calculation of Foumouo et al. [605] stressed the important role of the electron correlation in the final state, recent consensus turns to support that the method, in which the uncorrelated double continuum was used in the projection procedure, can provide meaningful and accurate information for double ionization [598,631,638]. Førre et al. [637] showed that the total cross section can be produced by a simple model. Their model, based on the time-independent LOPT, well reproduced the results of the *ab initio* calculations, see Fig. 24. In the model, the electron correlation in the final double continuum state have been completely neglected. Though so many theoretical efforts have been made on the two-photon double ionization of helium, this process is still puzzling. Indeed, recent calculations have shown some indications that we may have obtained the accurate total cross section. Until now, there only exist two experimental measurements. One measurement was performed at photon energy of 41.8 eV by Hasegawa et al. [377,636] with soft-X-ray radiation achieved by phase-matched high-order harmonics. The other measurement was performed at photon energy of 42.8 eV by Sorokin with soft-X-ray free-electron laser in Hamburg (FLASH) [595] et al. These experimental values are comparable with most of the theoretical data. However, due to the experimental uncertainties (e.g., the harmonic intensity in [377,636] or the assumptions on the pulse shape and focusing

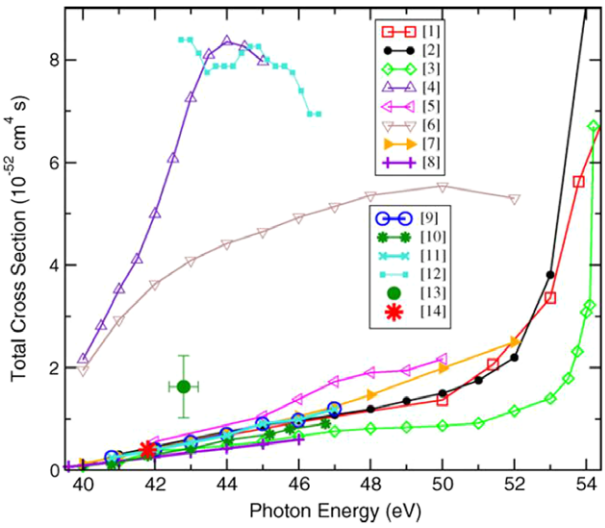

Fig. 23. (Color) Total two-photon double ionization cross sections of He as a function of the photon energy. [1] 2 fs results (Palacios et al. 2009 in Ref. [603]); [2] (Feist et al. 2008 in Ref. [604]); [3] (Horner et al. 2007 in Ref. [609]); [4] (Nikolopoulos and Lambropoulos 2007 in Ref. [611]); [5] (Ivanov and Kheifets 2007 in Ref. [610]); [6] (correlated final state) (Foumouo et al. 2006 in Ref. [612]); [7] (uncorrelated final state) (Foumouo et al. 2006 in Ref. [612]); [8] (Hu et al. 2005 in Ref. [622]); [9] (Piraux et al. 2003 [635]); [10] (Feng and van der Hart 2003 in Ref. [630]); [11] (Laulan and Bachau 2003 in Ref. [634]); [12] (Nikolopoulos and Lambropoulos 2001 in Ref. [621]); [13] (Sorokin et al. 2007 in Ref. [595]); [14] (Hasegawa et al. 2005 in Ref. [636]).
Source: Taken from Ref. [601].

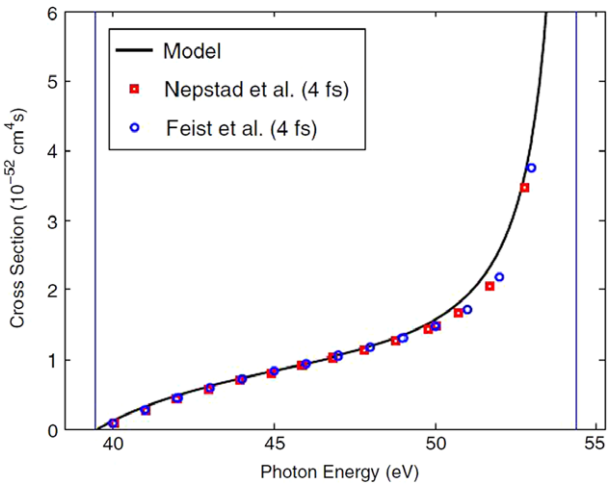

Fig. 24. (Color) Total cross section for the nonsequential two-photon double ionization of helium. Black line: model result in Ref. [637]); open (blue) circles: *ab initio* result of Feist et al. [604] obtained with a 4 fs pulse; and open (red) squares: corresponding *ab initio* result of Nepstad et al. [600]. The vertical lines define the two-photon direct double ionization region.
Source: Taken from Ref. [637].

conditions in [595]), the currently available experimental data are not sufficient to strongly support or rule out any of the theoretical results.

Differential cross sections of TPDI

More detailed information for the two-photon double ionization can be obtained by resolving the energies and ejection angles of the two electrons. The application of many-particle imaging techniques [e.g., reaction microscopes or cold target recoil ion momentum spectroscopy (COLTRIMS)] has allowed recording such differential signals experimentally [639]. In the late 1990s and the beginning of this century, a large number of experiments were performed to measure two-electrons' angular distributions in the one-photon double ionization of helium, with the excess energy varying from 0.1 eV to 450 eV. For reviews of the relative measurements, one can see Refs. [593,594,632]. However, kinematically complete experiments on the two-photon double ionization of helium have been lacking until now.

Presently, a few experiments can provide data on the recoil-ion-momentum distributions in two-photon double ionization. In 2008, Rudenko et al. [640] performed the first differential measurement, recoil-ion momentum distributions, for the most basic nonlinear two-electron light–matter interaction. The recoil-ion momentum distributions for two-photon

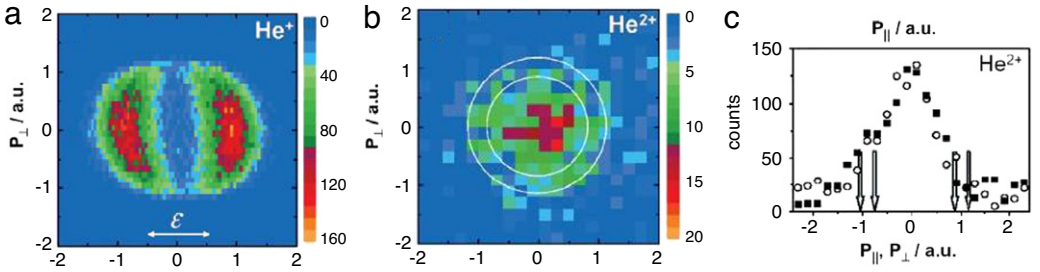

Fig. 25. (Color) Density plot of the measured recoil-ion momentum distributions for (a) single and (b) double ionization of He by 44 eV FLASH photons. The arrow in (a) indicates the direction of the FLASH polarization. Inner and outer circles in (b) mark the maximum He^{2+} momentum for the cases where one electron would have taken all the excess energy and for the equal energy sharing with the emission of both electrons in the same direction, respectively. (c) Projections of the 2D distribution of panel (b) onto the axis parallel (solid squares) and perpendicular (open circles) to the polarization directions. Arrows indicate the positions of the circles shown in panel (b).
Source: Taken from Ref. [640].

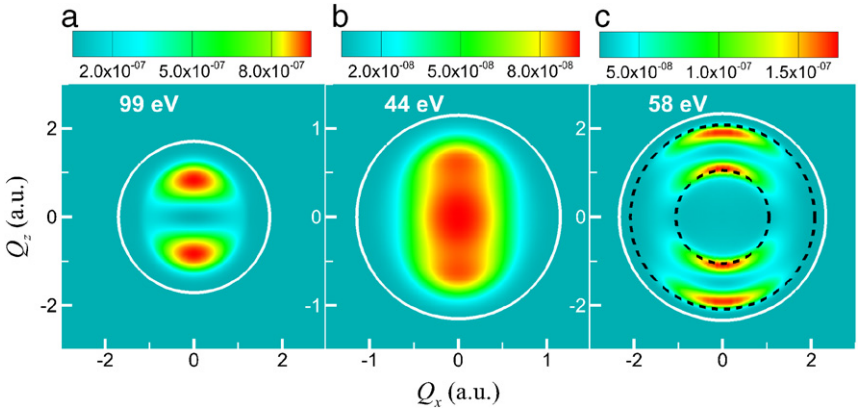

Fig. 26. (Color) Recoil-ion-momentum distribution in the *x*-*z* plane for (a) one-photon, (b) two-photon nonsequential, and (c) two-photon sequential double ionization. The dashed black circles in (c) are explained in the text. White circles indicate the maximum possible ion momentum in each process, which correspond to the ejection mode that the two electrons equally share the excess energy $E_{\mathrm{exc}} = n\omega - 79.0$ eV (n is the number of photons involved) and get ejected with the same direction.
Source: Taken from Ref. [641].

double ionization of He and Ne ($\omega = 44$ eV) were recorded with a reaction microscope at FLASH at an intensity of about 10^{14} W/cm^2. In Fig. 25, the measured recoil-ion momentum distributions for ionization of helium are shown. Since the linear momentum of the photon is negligible, the recoil-ion momentum in double ionization is the mirror image of the momentum sum of the two electrons, due to the law of conservation of momentum. The zero point of the recoil-ion momentum corresponds to that the two electrons are ejected with equal energy in the opposite directions. Such equal-energy back-to-back ejection modes of the two electrons are forbidden in the one-photon double ionization of helium [see Figs. 25(a) and 26(a)], while they are the most possible ejection modes in the nonsequential two-photon double ionization for photon energy far from the sequential threshold [see Figs. 25(b) and 26(b)].

Recently, many authors have also studied the recoil-ion momentum in the two-photon double ionization of helium by *ab initio* calculations [607,641–646]. It has been shown that the sequential and nonsequential two-photon double ionization can leave distinguishable signatures in the recoil-ion momentum distributions [607,641]. In Fig. 26(b) and (c), the recoil-ion momentum distributions for the nonsequential and sequential two-photon double ionization are shown respectively. Consistent with the experimental measurement shown in Fig. 25(b), the recoil-ion momentum distributions of the nonsequential two-photon double ionization show one dominating peak at zero momentum. For the sequential two-photon double ionization, the four-peak structures can be observed in the recoil-ion momentum distributions, see Fig. 26(c). Different from the nonsequential two-photon double ionization, where the two electrons favor to be ejected with similar energies, in the sequential two-photon double ionization the two electrons favor to be ejected with two particular energies, i.e. E_1 and E_2. When the two electrons with energies $E_1 = \omega - 24.6$ eV and $E_2 = \omega - 54.4$ eV are ejected in the same (opposite) direction, the recoil ion will be ejected with the momentum $Q = \sqrt{2E_1} + \sqrt{2E_2}$ ($Q = \sqrt{2E_1} - \sqrt{2E_2}$), which is marked as the bigger (smaller) black dashed circle. The black dashed circles roughly coincide with the positions of the four peaks. In 2010, the recoil ion momentum distributions for the two-photon double ionization at 52 eV were measured with FLASH [642]. The experimental data were compared with two numerical calculations [604,643,607,644].

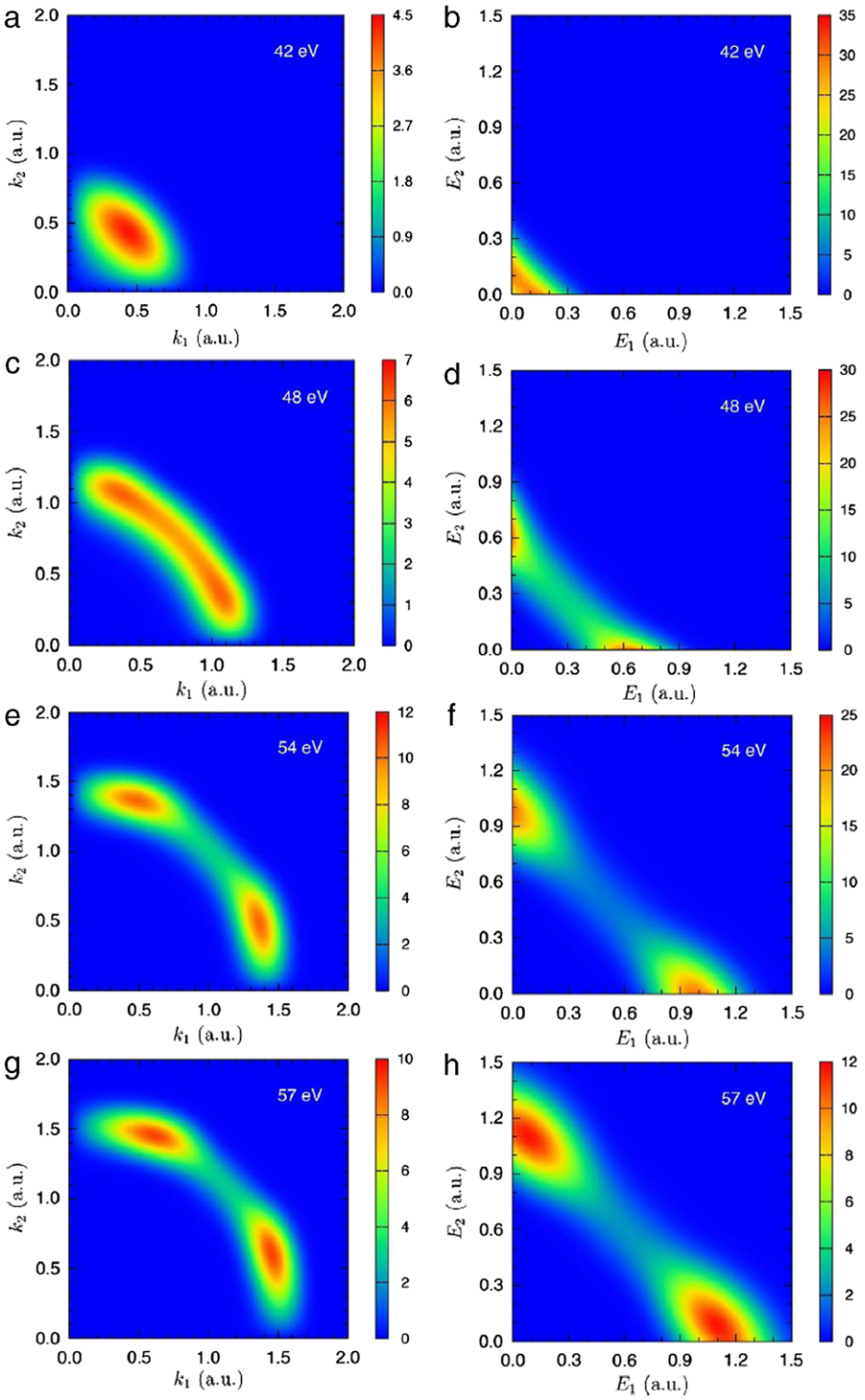

Fig. 27. (Color) Momentum (left column) and energy (right column) distributions of the two escaping electrons. The laser pulse has a sine-squared envelope around the peak intensity of 5×10^{14} W/cm^2 and a time duration of ten optical cycles. The central photon energies are 42, 48, 54, and 57 eV, respectively. The color bars are corresponding to units of 10^{-4} a.u.
Source: Taken from Ref. [606].

The signature of the sequential and nonsequential two-photon double ionization can also be directly identified from the energy distributions for the two electrons. Early discussions for this topic can be found in [620]. In Fig. 27, we show one numerical calculation by Guan et al. [606]. In the sequential region, clear double-peak structures can be identified. The

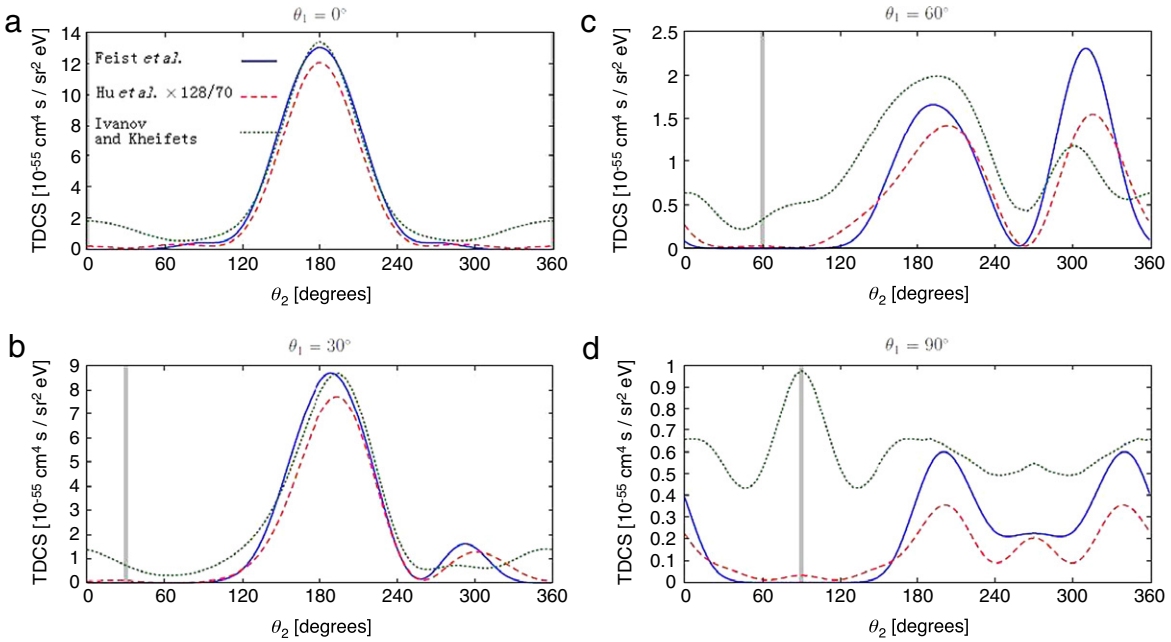

Fig. 28. (Color) Comparison of triply differential cross sections at 42 eV photon energy. The solid blue lines are the calculations of Feist et al. [604] The dashed red lines are the calculations of Hu et al. The solid blue lines are the calculations of Ivanov and Kheifets [610]. $E_1 = 2.5$ eV. The vertical gray line shows the ejection angle θ_1 of the first electron.
Source: Adapted from Ref. [604].

positions of the double peaks are expected to be $\omega - 24.6$ eV and $\omega - 54.4$ eV. However, several studies [603,647] have shown that such expectation will break down for short pulses. The shift of the sequential peak positions have been attributed to the interference of different ionization paths [647]. For the nonsequential double ionization far from the sequential threshold, the energy distributions are quite uniform, see Fig. 27(b). When the photon energy approaches the sequential threshold, the two electrons tend to be ejected with extremely unequal energy, see Fig. 27(c). Such character of the nonsequential two-photon double ionization is similar to the one-photon double ionization, in which the two ejected electrons favor equal-energy distribution for low photon energies and unequal-energy distribution for high photon energies.

The most detailed information for the nonsequential two-photon double ionization should be obtained by studying the triply differential cross sections, which is the ultimate goal of both the theoretical and experimental studies on this topic. Experimental measurements for TDCS are still lacking. Presently, we have already had several *ab initio* theoretical calculations. In Fig. 28, some of the calculations are shown. As mentioned above, present theoretical studies on the total cross section of the two-photon double ionization have not yet achieved a final completely consistent answer. It will be a more strict test for different theories to directly compare the TDCS of two-photon double ionization. These theoretical methods involved in Fig. 28 have achieved comparable results for the total cross section. Indeed, the magnitudes of the TDCS in these theories are also comparable. However, the shape of the TDCS can be quite different in different calculations, especially for the configuration [Fig. 28(d)] in which case the TDCS is small. For the two-electron angular distributions in the two-photon double ionization, a signature which is opposite to the one-photon double ionization has been discussed by many authors [605,632]. The signature is that angular correlations strongly favor back-to-back electron emission along the polarization axis in two-photon double ionization of helium, which can also be concluded form Fig. 28.

6.3. Probe and control of electron correlation dynamics

6.3.1. Measurements by combined xuv and IR pulses

The ultrafast phenomena including electron–electron correlation dynamics usually occur on the few-femtosecond to attosecond temporal scale. Attosecond pulses provide access to these temporal regimes. Most measurements take the protocols of combining a few-cycle IR pulse with a duration of a few femtoseconds and the synchronized (single or multiple) attosecond xuv pulses produced by it (for reviews, see Refs. [94,432,433]). Subfemtosecond time resolution can be achieved through nonlinear effects such as tunneling or streaking. Such technologies have also been used to study the electron–electron correlation dynamics in the double ionization process [520,648] or autoionization process [95,371,649,650].

In 1961, Fano theoretically described an asymmetric xuv absorption spectrum from helium [651]. Such asymmetric line shape has been named after Fano. When a helium atom in its ground state absorbs an xuv photon with a particular energy, a single electron can be emitted, leaving the other electron in the ground state, through direct photoionization.

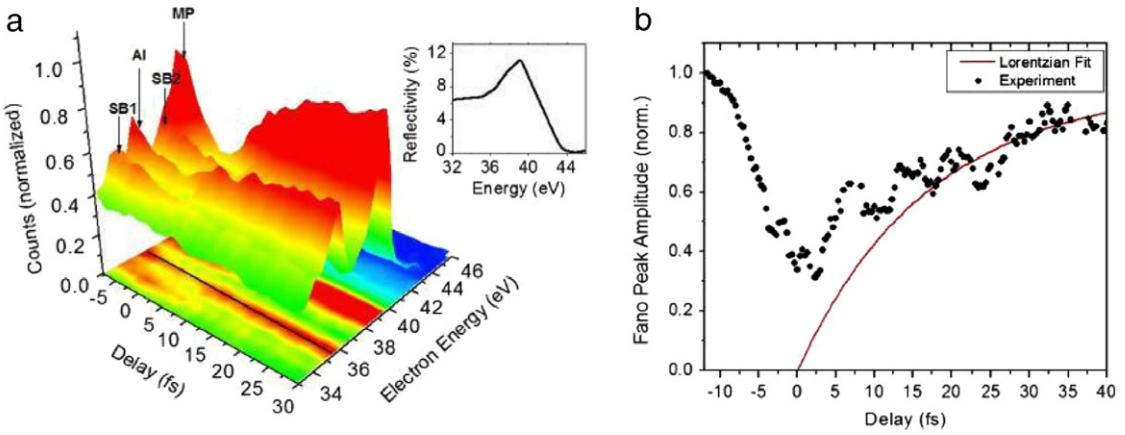

Fig. 29. (Color) Surface plot of a streaked spectrogram and autoionization Fano peak amplitude. (a) The electron spectra as a function of delay following the perturbed autoionization process. The inset shows the mirror reflectivity over the region of interest. The arrows indicate the locations of the sidebands (SB1 and SB2), the autoionization resonance (AI), and the peak reflectivity of the mirror (MP). (b) The autoionization signal as a function of delay for a 35.5 eV photoelectron.
Source: Taken from Ref. [649].

Alternatively, both electrons can be excited to the doubly excited state through absorption of a single photon. Due to the electron–electron correlation, the excited state can then "autoionize" with one electron returning to the ground state and the other electron being liberated from the atom. The quantum interference between the two paths of ionization gives the characteristic Fano line shape in the spectral domain, both in the photon absorption spectrum and ejected electron energy spectrum. The asymmetric Fano line shape, together with the symmetric Lorentzian line shape, are fundamental spectroscopic signatures that quantify the structural and dynamical properties of nuclei, atoms, molecules and solids. In the past few years, autoionization has become a hot research topic for theorists again because of the possibility of studying electron–electron interactions in the time domain experimentally [649,652–656].

In 2010, Gilbertson et al. [649] performed an experimental study on the electron dynamics in helium autoionization by combining attosecond extreme ultraviolet pulses with near infrared (NIR) femtosecond lasers. They showed that the interference between the two ionization channels was modified by the intense near infrared laser pulse. In Fig. 29, their measurements for the electron spectra as a function of delay are shown. The Fano peak height varies with the time delay. The signal along the line at 35.5 eV in the projection of the surface plot is shown in Fig. 29(b). The reduction of the Fano peak height can be explained by the depletion of the doubly excited state by the NIR laser field. By mapping the signal of the autoionization resonance peak as a function of delay, they showed that the lifetime of the doubly excited state can be measured. They used the Lorentzian lifetime of the resonance to fit the experimental data, and measured the lifetime of the double excited state 2s2p to be 17 fs. Their data represented the first time domain measurement of the lifetime of the autoionization process.

Next, we make a brief introduction for more recent pump–probe studies on the double excited states and autoionization by using the attosecond xuv pulses and IR field. In 2010, Argenti and Lindroth [650] made a simulation to show that quantum beating between doubly excited states can be monitored experimentally. In 2013, Ott et al. [657,658] have shown that asymmetric Fano line shape for the xuv absorption spectrum can be controlled by combining attosecond xuv pulses and IR pulses. They introduced a universal temporal-phase formalism, mapping the Fano asymmetry parameter q to a phase φ of the time-dependent dipole response function. The formalism was confirmed experimentally by laser-transforming Fano absorption lines of autoionizing helium into Lorentzian lines after the attosecond-pulse excitation. It was also possible to realize the inverse, i.e., the transformation of a naturally Lorentzian line into a Fano profile. In 2014, Kaldun et al. [659] further showed that a change in the Fano line shape, e.g., by interaction with short-pulsed laser fields, allows to extract dynamical modifications of the amplitude and phase of the coupled excited quantum states.

6.3.2. Double ionization by two attosecond pulses

Recently, many theoretical explorations have been made for applications of the attosecond pulses in probing and controlling the electron-correlation dynamics. Compared with strategies using IR laser field, only using attosecond pulses has the advantage that much fewer burdens are needed in the numerical calculations. Thus, the numerical simulations for the double ionization of two-electron system are usually rather accurate.

Probing the electron dynamics can be divided into two steps. One step is to pump the atoms to interesting states, and the second step is to probe the dynamics of these states. This means that normally at least two laser pulses (or other excitation source) is needed; one is used to induce the pump process, and the other is used to complete probe process. However, Feist et al. [106] have also argued that it is possible to interpret the two-photon double ionization of helium induced by a single attosecond as a pump–probe process. For an ultrashort pulse of attosecond duration the concept of "sequential

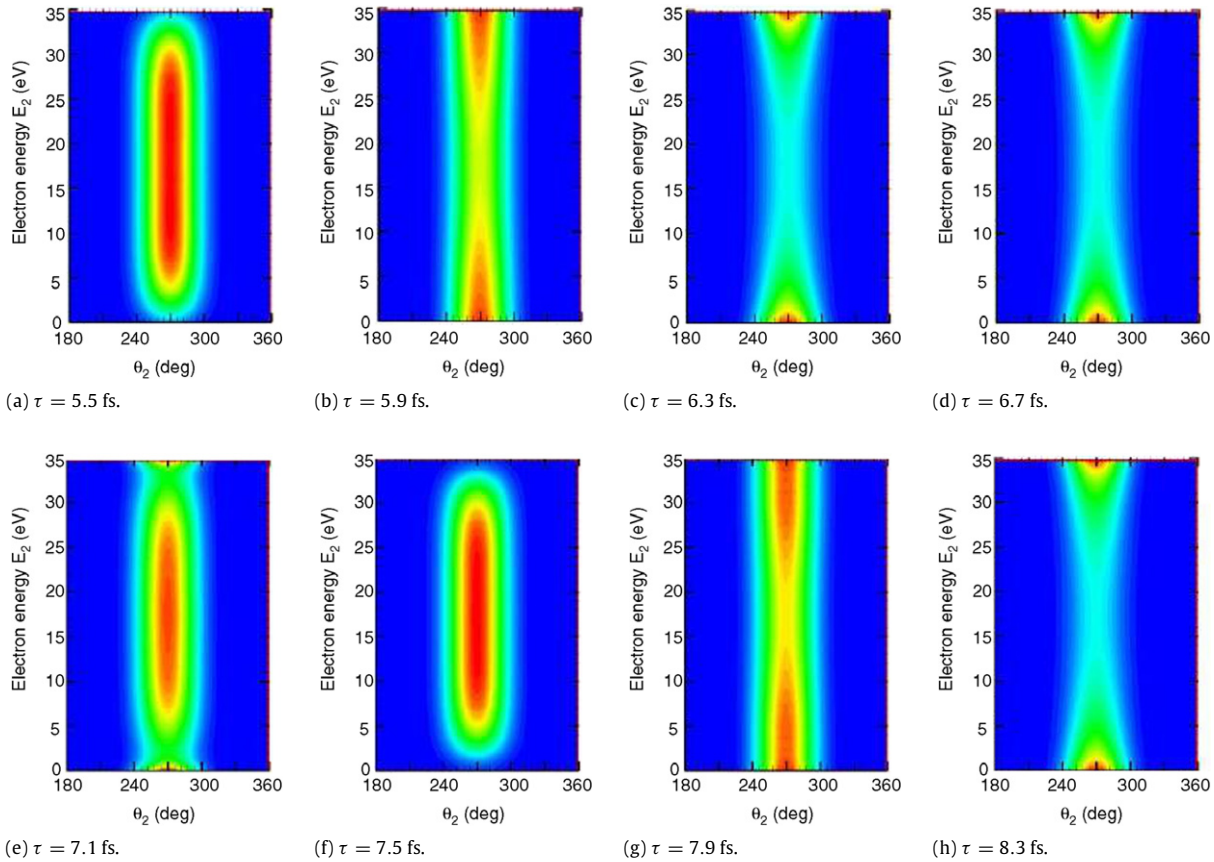

Fig. 30. (Color) The contour plots for triple-differential cross sections of He double ionization under the attosecond pump probe scheme, for the case of the pumping pulse $T_1 = 1.5$ fs.
Source: Taken from Ref. [104].

interactions", valid for long pulses, becomes meaningless. Instead, the two-electron emission occurs almost simultaneously, and the strength of electron correlation in the exit channel can be tuned by the pulse duration. This information is encoded in the final joint momentum distribution. They attributed the origin of the strong angular correlations observed for short pulses to three different sources: (i) Correlations in the helium ground state. Due to the Coulomb repulsion, the electrons in the ground state are not independent of each other. For ultrashort pulses, TPDI can thus be interpreted as a probe that maps out the initial-state correlations. (ii) Induced dipole polarization in the intermediate state. When the first electron leaves the core, its electric field induces polarization of the remaining ion, leading to an asymmetric probability distribution of the second electron. The second photon then probes the dynamics in this bound-free complex, such that TPDI can be interpreted as a pump–probe setup. (iii) Final-state electron–electron interaction in the continuum. After the second electron has been released within the short time interval as well, their mutual repulsion may redirect the electrons.

In 2006, Hu and Collins [104] performed a realistic modeling for the full dynamics of both the femtosecond pumping and the attosecond probing processes. Pumped by a broadband femtosecond UV pulse, one electron of ground-state helium can be launched into a superposition of low-lying excited states, thus forming a wave packet that begins to oscillate relative to the atomic core. They showed that such oscillation dynamics can be probed by a time-delayed attosecond extreme ultraviolet (EUV) pulse. The time-delayed attosecond pulse can doubly ionize the atom. By measuring either the energy sharing of the ionized electrons or the total ionization probability as a function of the time delay, the correlation (overlap) of the electrons at the instant of the probe can be determined. The different features of energy sharing between the two ejected electrons for various time delays are shown in Fig. 30.

In 2007, Morishita et al. [105] showed that attosecond pulses can be used to resolve the time-resolved correlated motion of the two electrons by measuring their six-dimensional momentum distributions in the double ionization. They assumed that the helium atoms have been pumped into a coherent state of two excited states. Then the attosecond pulse is used to doubly ionize the coherent state to probe the dynamics of it. They showed that in the hyperspherical coordinates, the shapes of the momentum distributions of the two ejected electrons were similar to the two electron density at the instant of double ionization, see Fig. 31.

In the double ionization process induced by two attosecond pulses, the two electrons can be ionized from different paths, and the superposition of those two-electron wave packets produce interesting interference patterns in the

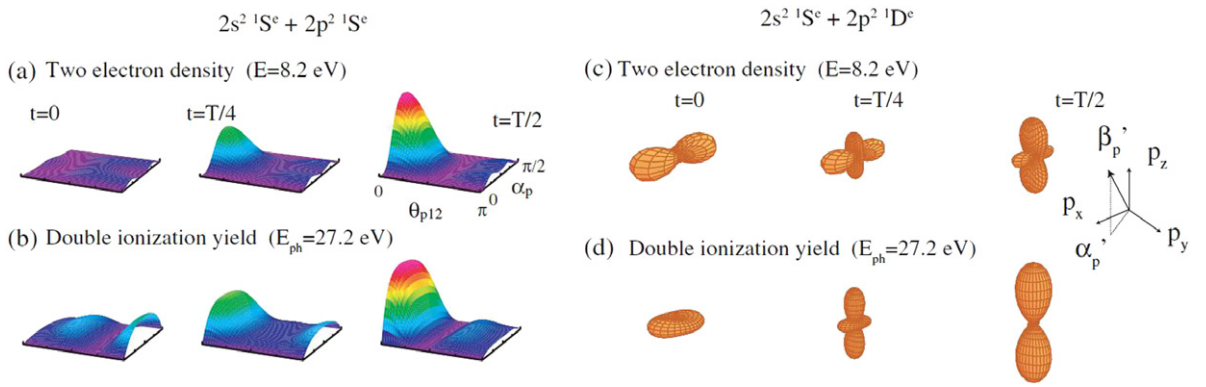

Fig. 31. (Color) (a) Time-dependent vibrational density of a coherent state made of $2s^2\ ^1S^e + 2p^2\ ^1S^e$ in momentum space as a function of (α_p, θ_{p12}) at the fixed total energy $E = 8.2$ eV, averaged over the rotational degrees of freedom. $T = 980$ as. (b) Double ionization yield of the vibrational wave packet by a 200 as, 27.2 eV pulse, averaged over the total electron energy. (c) Polar plot of the time-dependent rotational density of a coherent state made of $2s^2\ ^1S^e + 2p^2\ ^1D^e$ in momentum space, averaged over the vibrational degrees of freedom. $T = 2.0$ fs. (d) Polar plot of double ionization yield by a 200 as, 27.2 eV pulse, averaged over the total electron energy.
Source: Taken from Ref. [105].

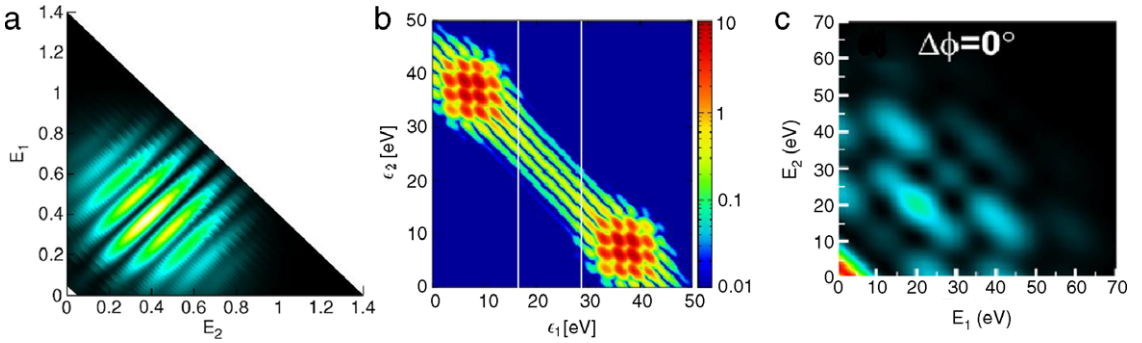

Fig. 32. (Color) Two-electron interference patterns by double pulses. (a) taken from Ref. [660]. The two pulses have duration of 500 as with time delay of 1 fs, and the central frequencies of the two pulses are 35 eV and 69 eV separately. (b) taken from Ref. [107]. The two pulses have duration of 1 fs with time delay of 1.5 fs, and the central frequencies of the two pulses are both 65.3 eV. (c) taken from Ref. [113]. The two pulses have duration of 191 as with time delay of 242 as, and the central frequencies of the two pulses are both 65 eV.

two-electron energy distributions, see Fig. 32. In the study of Palacios et al. [660], two attosecond pulses with different central frequencies are used. The two electrons are ionized by absorbing one photon from each pulse separately. There are two possible ionization paths. In the first path, the electron with energy of E_1 is ionized from the first pulse, and the electron with energy of E_2 is ionized from the second pulse. In the second path, the orders of the ejection of the two electrons are opposite, i.e. the electron with energy of E_2 is ionized from the first pulse, while the electron with energy of E_1 is ionized from the second pulse. Due to the large energy spectrum, the two ionization paths interfere to produce the patterns in Fig. 32(a). Such interference patterns do not depend on the relative CEP of the two attosecond pulses. Jiang et al. [113] have studied the cases that two attosecond pulses have the same central frequency. In resolving the interference patterns of this case [Fig. 32(c)], additional four ionization paths need to be considered except for the two ionization paths analyzed by Palacios et al. The two electrons can be both ionized from the same one attosecond pulse, and two ionization paths are possible when the two electrons are ionized from one pulse due to the exchange symmetry of the two electrons. Six ionization paths finally produce the grid-like interference patterns in Fig. 32(c), which is directly related to the relative CEP of the two attosecond pulses [113]. In the study of Feist et al. [107], a little longer pulses were used. As can be seen in Fig. 32(b), the grid-like interference patterns only appeared around the sequential peaks. In the region that the two electrons share roughly equal energy, interference lines are observed. The ionization paths through the double excited states will also contribute. Feist et al. [107] have shown that the dynamic of the double excited states can be revealed by varying the time delay of the two pulses to observe the change of the interference patterns in that region.

6.4. Electron correlation dynamics in molecular systems

The electron correlation dynamics in molecular systems can be more complex, due to the coupling with the nuclear motion. Molecular dynamics will bring us new physics and result in the observations which differ from the atomic case. In

this section, we review the studies on the electron-correlation dynamics in the molecular system and the applications of attosecond pulses to observe and control molecular dynamics.

6.4.1. One- and two-photon double ionization of H_2

For the simplest molecule H_2 (D_2), significant progresses have recently been achieved on the studies of one-photon and two-photon double ionization both in the experimental side and in the theoretical side. The double ionization of H_2 will lead to four particle fragments. Complete understanding of this process requires us to simultaneously measure the momenta of all the four fragments. This is a quite difficult task for the experimental physicists. In the early experimental measurements, only parts of the four fragments were detected. For example, Reddish et al. (1997) [661] and Wightman et al. (1998) [662] measured the angular distributions of the electron pairs without detecting the ions. In such a case, the orientation of the molecule relative to the laser polarization is random. Consequently, the angular distributions of the electron pairs for random oriented molecule H_2 (D_2) are quite similar to those of atomic He, and no obvious molecular effect was observed. In 2004, Weber et al. [663–665] completed the detection for all the fragments, in which special molecular dynamics were found. It has been shown that the angular distributions of the two electrons are quite sensitive to the molecular orientation and nuclear distance [663–667].

The numerical calculation of TDSE for H_2 is more challenging than helium. Fortunately, the numerical calculations appeared almost simultaneously with experiments to account for the dynamics of all the fragments in the one-photon double ionization process of H_2 (D_2). In one-photon double ionization process, the motions of the two electrons are expected to be much faster than the nuclear motion. So it has been assumed that the ionization always happens at a particular nuclear distance. In experiments, the nuclear distance is inferred from the momenta of the ions, while in numerical calculations the nuclear distance is assumed to be fixed at a constant. The first numerical calculations for the triply differential cross sections (TDCSs) were completed based on the exterior complex scaling [668–671] and the time-dependent close-coupling method [666,672] in the spherical coordinates. Very recently, another independent numerical calculation also in spherical coordinates was completed by Ivanov and Kheifets [673]. However, it is believed that the prolate spheroidal coordinates should be more suitable to handle this two-center problem than the spherical coordinates. The numerical calculations in the prolate spheroidal coordinates have also been performed [674–676]. Except for one calculation [674], which predicted a little lower TDCSs, all the other calculations have achieved generally consistent results. Most of the numerical methods mentioned above have also been applied to the study of two-photon double ionization of molecule H_2 [677–680].

6.4.2. Application of attosecond pulses to molecular systems

Application of attosecond pulses to molecular systems has recently drawn a considerable attention, for reviews see Refs. [114,681]. Attosecond pulses make it possible to observe and manipulate electron dynamics inside molecular systems and to elucidate the role of electron correlation in the ultrafast response of molecules to the incident light. In molecules, the electronic wave function is intimately connected to the chemical reactivity. So one of the important questions is whether investigations of chemical reactivity in pump–probe experiments with attosecond pulses allow the observation and control of novel reaction mechanisms that do not manifest themselves when molecules are exposed to pump–probe sequences with traditional femtosecond pulses.

The application of attosecond pulses to atomic systems appeared as soon as the first attosecond pulses were characterized in experiments. However, it was only very recent (until 2010) that the first attosecond pump–probe experiments on a molecular system were published by Sansone et al. [682]. Several theoretical predictions preceded the experiments. In the following, we firstly make an introduction for the earlier theoretical works on the application of attosecond pulses to molecular systems, and then review the recent relevant experiments.

The Born–Oppenheimer (BO) approximation is usually needed to simplify the description of the interaction between all the electrons and nuclei. The BO approximation is an important tool in quantum chemistry; without it only the lightest molecule, H_2, could be handled, and all computations of molecular wavefunctions for larger molecules make use of it. Even in the cases where the BO approximation breaks down, it is used as a point of departure for the computations. The BO approximation is based on the fact that the nuclear mass is much larger than the electronic mass. So the motion of the electron is much faster than the nucleus, and the electronic configuration is assumed to adapt instantaneously to the nuclear motion. The dependence of the electronic energy on the nuclear geometry defines the potential-energy surfaces (PES), which in turn determines the forces exerted on the nuclei.

In more detail, the BO approximation allows the wavefunction of a molecule to be broken into its electronic and nuclear (vibrational, rotational) components,

$$\Psi(\mathbf{r}, \mathbf{R}) = \chi(\mathbf{r}, \mathbf{R})\phi(\mathbf{R}), \tag{135}$$

where the vector $\mathbf{r}$ represents the electronic coordinates and the vector $\mathbf{R}$ represents the nuclear coordinates. In the above, $\Psi(\mathbf{r}, \mathbf{R})$ is the total molecular wavefunction, $\chi(\mathbf{r}, \mathbf{R})$ is the electronic wavefunction for a particular nuclear configuration (particular $\mathbf{R}$), and $\phi(\mathbf{R})$ is the nuclear wavefunction. It consists of two steps to obtain the molecule wavefunction in the BO approximation. In the first step, the following electronic Schrödinger equation is solved,

$$H_e(\mathbf{r}, \mathbf{R})\chi(\mathbf{r}, \mathbf{R}) = E_e(\mathbf{R})\chi(\mathbf{r}, \mathbf{R}). \tag{136}$$

$H_e(\mathbf{r}, \mathbf{R})$ is the electronic Hamiltonian, in which electron–nucleus interactions are included while the nuclear kinetic energies are excluded. The nuclear coordinates $\mathbf{R}$ enter as parameters. Varying these nuclear coordinates $\mathbf{R}$ in small steps and repeatedly solving the electronic Schrödinger equation, one obtains electronic energy eigenvalue E_ee as a function of $\mathbf{R}$. $E_e(\mathbf{R})$ is the previously mentioned potential-energy surface (PES). This manner of obtaining a PES is also referred to as the adiabatic approximation. In the second step of BO approximation, the following Schrödinger equation for nuclear motion is solved,

$$[T_n(\mathbf{R}) + E_e(\mathbf{R})]\phi(\mathbf{R}) = E\phi(\mathbf{R}). \tag{137}$$

$T_n(\mathbf{R})$ is the nuclear kinetic energy, and we see that the PES $E_e(\mathbf{R})$ in turn decides the nuclear motion.

Above discussions have shown that the nuclear motion is connected to the electronic dynamics. It is possible to use attosecond pulses to form a coherent superposition of excited electronic states, for which the electronic wave function can change significantly preceding any nuclear motion. This means that the nuclear motion can be controlled by forces that do not follow from a particular potential-energy surface (PES), and the forces which drive the nuclear motion can be a consequence of the time-dependent motion of the electronic wave packet. So it is possible to control both the nuclear motion and the chemical reactivity by controlling the composition of the electronic wave packet. This kind of dynamics has been called 'charge-directed chemical reactivity', which is of high interest at present.

Different theoretical works have been performed to study the formation of coherent superpositions of molecular electronic states. Remacle et al. have performed calculations where intense, short laser pulses are used to create coherent superposition states in LiH [683,684]. In their calculations, if a superposition of Σ-states is excited, the electronic motion along the molecular axis can be observed; if a combination of Σ- and Π- states is excited, a rotational electronic motion can be observed. Similar investigation has been performed for ABCU [685], a larger molecular system. Except for the linear laser pulses, Barth et al. have used circularly polarized UV pulses to generate rotational electron currents in planar, fixed-in-space molecules like Mg-porphyrin [686].

Having prepared a coherent superposition of electronic states in a molecular system, we still need to find a method to probe that dynamics in real time. The attosecond pulse serves as an effective tool. For an example, Bandrauk et al. [687] have shown that how the electronic dynamics in H_2^+ can be observed with an attosecond pulse.

A chirp encoded recollision method was proposed to probe the molecular dynamics [688,689]. This method is coined with a name PACER (probing attosecond dynamics via chirp encoded recollision). In this method, one can make use of the harmonics with different energies which encode the time information to reveal this nuclear motion. In this case, for different harmonic orders, the delay of pump and probe differs. The idea comes through the harmonic generated with different orders to get how the core vibrates. Basically, we measure the harmonic generation from a molecule and its isotopes. The difference between them comes from the nuclear motion. Heavy isotope moves slower and get a higher harmonic yield. The successful application has been achieved for the H_2 molecule [688,689]. When an electron is ionized, the core left behind can be treated as a H_2^+ molecule. The harmonic orders can reflect how fast the core moves along the H_2^+ potential curve. This kind of nuclear motion can also lower the two-center interference minimum [690]. For the molecule CH_4, the process from CH_4 to CH_4^+ is complex which cannot be easily retrieved [689,691]. The PACER method probes the nuclear motion within one optical cycle. While for many molecules heavier than hydrogen, nuclear vibrations happen in a longer time scale. To probe this motion, a longer pump–probe delay is necessary [692,693]. Some theoretical work has been done for more complex cases [694–697].

Those dynamics discussed above do not involve the electron correlation. Theoretical proposals have also been put forward to use the electron correlation to excite electronic wave packets in molecules [698]. In the many-electron molecular system, a sudden removal of an electron from the ground states will lead to the remaining ion in a nonstationary state that can be described as a coherent superposition of one-particle orbitals that are eigenstates of the ion. The ultrafast relaxation can then be observed after the sudden removal of an electron [699,700]. Breidbach and Cederbaum [701] have shown that the ultrafast relaxation can be observed after ionization of the 2p state of a Kr atom, the $1\pi_u$ orbital of a CO_2 molecule, and the $3\pi_u$ orbital of *N*-methylacetamide.

Usually, the photoionization will leave the remaining ion in a coherent superposition of several electronic states, which can lead to accompanying hole propagation that evolve on an ultrafast timescale. Relative investigation on the hole migration have been performed in the linear molecule N-methylacetamide [702], the simplest amino-acid, glycine [703], and small peptides [704] et al. The BO adiabatic approximation greatly simplify the theoretical studies. More generally, one may try to address the importance of non-adiabatic couplings of the electronic and nuclear dynamics. One such example was given by Kanno et al., who investigated the non-adiabatic couplings between the electronic and the vibration degrees of freedom in the chiral aromatic molecule 2,5-dichloropyrazine [705].

In the following, we turn from the theoretical side to the experimental side. In the first ever attosecond pump–probe experiment on a molecular system [682], Sansone et al. used xuv + IR to realize the pump–probe configuration. The attosecond pulses served as the pump laser pulse which excited and/or ionized the neutral diatomic molecule, and a time-delayed moderately intense, near-IR, few-cycle laser pulse served as the probe pulse. The IR pulse was used to influence the remaining electron in the molecular ion, leading to the transitions of the electron between the states $1s\sigma_g$ and $2p\sigma_u$. In such a manner, the localization of the one remaining bound electron in the $H + H^+$ dissociative ionization channel was influenced. Depending on the time delay of the two pulses and the kinetic energy of the detected H^+ fragment ion, the fragment ion prefers to move upward or downward along the laser polarization, forming an asymmetry in the ejection directions. Two mechanisms were revealed to be responsible for the observed electron localization. The first mechanism [Fig. 33(b)] is related to the coupling of the electronic and nuclear degrees of freedom. The IR laser pulse can drive transitions of the

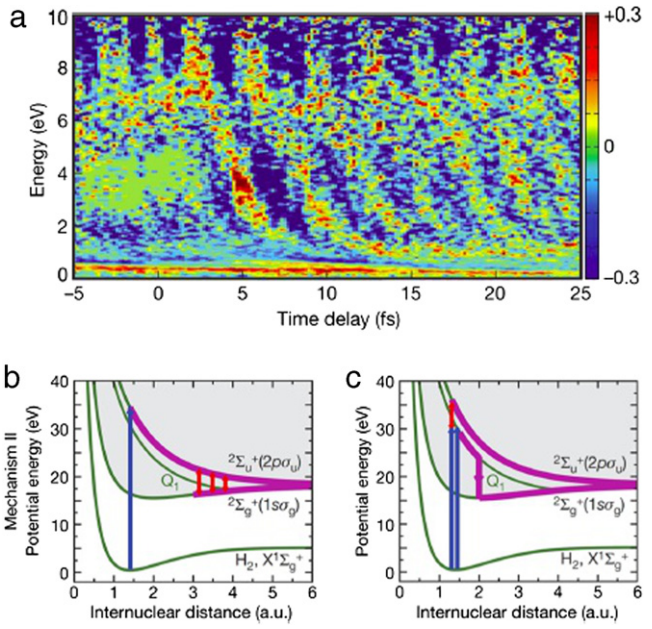

Fig. 33. (Color) Normalized asymmetry of D^+ fragments formed in two-color dissociative ionization of D_2 using an isolated XUV attosecond pulse that is followed at a variable time-delay by a few-cycle IR pulse. A non-trivial time-dependence of the normalized asymmetry on the kinetic energy release and the XUV–IR time delay is observed, which is caused by two mechanisms that lead to a preferential localization of the bound electron; (b) mechanism for the observation of electron localization caused by coupling of the electronic and nuclear degrees of freedom on the attosecond to few-femtosecond timescale under the influence of the IR laser which drives transitions between the $1s\sigma_g$ and the $2p\sigma_u$ states; (c) mechanism for the observation of electron localization caused by coupling of the electronic degrees of freedom; the action of the IR laser on the outgoing electron leads to a localization of the bound electron.
Source: Taken from Ref. [682].

electron between the states $1s\sigma_g$ and $2p\sigma_u$ in the molecular ion. The second mechanism [Fig. 33(c)] involves the coupling of the electronic degrees of freedom. Except for ionization, the attosecond pulses can also excite the molecule H_2 (D_2) to the doubly excited states Q_1, which will autoionize by the electron correlation. The existence of the IR laser pulse can alter the wavefunction of the outgoing electron, which finally leads to a localization of the bound electron.

After the first application of attosecond pulse on the pump–probe experiment of H_2 (D_2), the attosecond pulse has also been applied to other molecular systems such as N_2 [706], CO_2 [706], C_2H_4 [706], O_2 [707], and phenylalanine [708]. To realize the observation of theoretically predicted charge migration in molecular systems, it will be extremely attractive to design a protocol that an attosecond pump pulse to initiate the charge migration and an attosecond probe pulse to observe it. Presently, this is still challenging, since the present attosecond pulse is still not strong enough to realize such a protocol.

7. Summary and outlook

Thanks to the advances of attosecond pulses and relevant technologies, physicists have made another big step in ultrafast sciences after the huge success of the femtosecond sciences. The attosecond sciences have begun to show their potential in tracing and controlling the electronic dynamics on its natural time scale. In the last 15 years or so, we have witnessed many great progresses in the real time observation of many ultrafast processes in atoms, molecules, and solids, which are out of the reach of even the single-cycle femtosecond laser pulses.

In the present review, we have reviewed some basic theoretical methods and concepts behind the attosecond physics, together with some milestones experimental demonstration. We have reviewed those studies on the generation of the attosecond light resources, their applications to photoionization dynamics in a combined xuv and IR laser pulses, the extraction of photoionization time delays in the context of attosecond streaking, and the probe and control of the electron–electron correlation dynamics in two-electron systems. There have been some applications of attosecond technologies to more complex molecular systems [114,681] and condensed matter [97,435], but we have restrained ourselves from touching these topics as many other new concepts and methods beyond which the current review has covered.

We foresee increasing interests on the attosecond pulses for the extremely attractive applications in a broad fields. The applications of attosecond pulses will bring the eyesight of human into the inside of one atom or molecule to observe the electron dynamics. With the help of attosecond pulses, many dynamics, which previously could only exist in the theoretical description, can be traced and proven in experiments. For example, in the many-electron system, removal of one inner-shell electron or double excitation of two electron may leave the system in an unstable state, which will relax to a stable state in the time scale of femtosecond. Attosecond pulses are promising tools to trace such dynamics. The applications of attosecond

pulses to complex molecules can benefit chemical and biological sciences. The first experimental application of attosecond pulses to molecular system is quite recent, and great interest has been attracted after it. The charge migration dynamics predicted by theories may be explored extensively by the experimentalists in the near future. One challenging but useful goal on the application of attosecond pulse is to control the chemical reaction.

Due to the low flux of the current attosecond light sources, the majority of the current experimental applications rely on the combined usage of xuv and IR pulses. The ideal setup would be the attosecond-pump and attosecond-probe, which calls for a high flux attosecond sources under development in several laboratories worldwide. However, we have to emphasize, challenges and opportunities lie not only in the technologies for the experimentalists, but also in theoretical concepts and methods since attosecond physics touches many fundamental problems of quantum mechanics, such as particle–wave duality, quantum measurement, quantum tunneling, and the role of time in quantum mechanics, etc. [709]. Accurate theoretical description can only be achieved in simple atomic and molecular systems, and the description on more complex systems relies on a series of approximations. There is no doubt that attosecond technologies will continue to give us novel understanding and applications in physics, chemistry and biologies. However, to gain similar great triumphs as those in femtosecond technologies, there is still a long way to go and the combat calls joint efforts not only within the strong field and attosecond community, but also from different communities in various disciplines.

Acknowledgments

The authors thank the editor Jörg Eichler for numerous communications during the preparation of this review. LYP appreciates the five weeks' host of KITP at UCSB in 2014 and many useful discussions with Joachim Burgdörfer and Anthony F. Starace during his stay there. This work is supported by National Natural Science Foundation of China (NNSFC) under Grant No. 11322437, by the 973 Program under Grant No. 2013CB922402, by NNSFC under Grant Nos. 11174016, 11121091, and by Program for New Century Excellent Talents in University (NCET).

References

[1] J. Thomson, Bakerian lecture: Rays of positive electricity, Proc. R. Soc. A 89 (1913) 1.
[2] H. Geiger, E. Marsden, On a diffuse reflection of the α-particles, Proc. R. Soc. A 82 (1909) 495.
[3] E. Rutherford, The scattering of alpha and beta particles by matter and the structure of the atom, Philos. Mag. 21 (1911) 669.
[4] P. Krehl, S. Engemann, August toepler- the first who visualized shock waves, Shock Waves 5 (1995) 1.
[5] H. Abraham, J. Lemoine, Disparition instantanée du phenomene de kerr, C. R. Hebd. Seances Acad. Sci. 129 (1899) 206.
[6] T. Maiman, Stimulated optical radiation in ruby, Nature 187 (1960) 493.
[7] F.X. Kärtner, Few-Cycle Laser Pulse Generation and its Applications, Springer, 2004.
[8] T. Brabec, F. Krausz, Intense few-cycle laser fields: Frontiers of nonlinear optics, Rev. Modern Phys. 72 (2000) 545.
[9] T.S. Rose, M.J. Rosker, A.H. Zewail, Femtosecond real-time probing of reactions. iv. The reactions of alkali halides, J. Chem. Phys. 91 (1989) 7415.
[10] A. Zewail, Femtochemistry: Atomic-scale dynamics of the chemical bond, J. Phys. Chem. A 104 (2000) 5660.
[11] C. Joachain, M. Dorr, N. Kylstra, High-intensity laser-atom physics, in: B. Bederson, H. Walther (Eds.), Advances in Atomic Molecular and Optical Physics, in: Advances in Atomic Molecular and Optical Physics, vol. 42, 2000, p. 225.
[12] M. Protopapas, C. Keitel, P. Knight, Atomic physics with super-high intensity lasers, Rep. Progr. Phys. 60 (1997) 389.
[13] D. Umstadter, S. Sepke, S. Chen, Relativistic nonlinear optics, in: P.R. Berman, C.C. Lin (Eds.), Advances in Atomic Molecular and Optical Physics, in: Advances in Atomic Molecular and Optical Physics, vol. 52, 2005, p. 331.
[14] G.A. Mourou, T. Tajima, S.V. Bulanov, Optics in the relativistic regime, Rev. Modern Phys. 78 (2006) 309.
[15] E. Esarey, C.B. Schroeder, W.P. Leemans, Physics of laser-driven plasma-based electron accelerators, Rev. Modern Phys. 81 (2009) 1229.
[16] A. Di Piazza, C. Müller, K.Z. Hatsagortsyan, C.H. Keitel, Extremely high-intensity laser interactions with fundamental quantum systems, Rev. Modern Phys. 84 (2012) 1177.
[17] F. Grossmann, Theoretical Femtosecond Physics: Atoms and Molecules in Strong Laser Fields, Springer, 2008.
[18] J. Manz, L. Wöste (Eds.), Femtosecond Chemistry, VCH, 1995.
[19] M. Gu, D. Bird, D. Day, L. Fu, D. Morrish, Femtosecond Biophotonics: Core Technology and Applications, Cambridge University Press, 2010.
[20] R. Osellame, G. Cerullo, R. Ramponi (Eds.), Femtosecond Laser Micromachining, Springer, 2012.
[21] H. Fielding, Rydberg wavepackets in molecules: From observation to control, Annu. Rev. Phys. Chem. 56 (2005) 91.
[22] F.B. Dunning, J.J. Mestayer, C.O. Reinhold, S. Yoshida, J. Burgdörfer, Engineering atomic rydberg states with pulsed electric fields, J. Phys. B 42 (2009) 022001.
[23] P. Agostini, L. Dimauro, The physics of attosecond light pulses, Rep. Progr. Phys. 67 (2004) 813.
[24] A. Scrinzi, M. Ivanov, R. Kienberger, D. Villeneuve, Attosecond physics, J. Phys. B 39 (2006) R1.
[25] M. Hentschel, R. Kienberger, C. Spielmann, G. Reider, N. Milosevic, T. Brabec, P. Corkum, U. Heinzmann, M. Drescher, F. Krausz, Attosecond metrology, Nature 414 (2001) 509.
[26] P.M. Paul, E.S. Toma, P. Breger, G. Mullot, F. Auǵe, P. Balcou, H.G. Muller, P. Agostini, Observation of a train of attosecond pulses from high harmonic generation, Science 292 (2001) 1689.
[27] Z. Chang, Fundamentals of Attosecond Optics, CRC Press, 2011.
[28] D.H. Bilderback, P. Elleaume, E. Weckert, Review of third and next generation synchrotron light sources, J. Phys. B 38 (2005) S773.
[29] B.W.J. McNeil, N.R. Thompson, X-ray free-electron lasers, Nature Photon. 4 (2010) 814.
[30] M. Couprie, New generation of light sources: Present and future, J. Electron Spectrosc. Relat. Phenom. 196 (2014) 3.
[31] A.S. Pirozhkov, M. Kando, T.Z. Esirkepov, P. Gallegos, H. Ahmed, E.N. Ragozin, A.Y. Faenov, T.A. Pikuz, T. Kawachi, A. Sagisaka, J.K. Koga, M. Coury, J. Green, P. Foster, C. Brenner, B. Dromey, D.R. Symes, M. Mori, K. Kawase, T. Kameshima, Y. Fukuda, L. Chen, I. Daito, K. Ogura, Y. Hayashi, H. Kotaki, H. Kiriyama, H. Okada, N. Nishimori, T. Imazono, K. Kondo, T. Kimura, T. Tajima, H. Daido, P. Rajeev, P. Mckenna, M. Borghesi, D. Neely, Y. Kato, S.V. Bulanov, Soft-x-ray harmonic comb from relativistic electron spikes, Phys. Rev. Lett. 108 (2012) 135004.
[32] K.J. Schafer, B. Yang, L.F. Dimauro, K.C. Kulander, Above threshold ionization beyond the high harmonic cutoff, Phys. Rev. Lett. 70 (1993) 1599.
[33] P.B. Corkum, Plasma perspective on strong-field multiphoton ionization, Phys. Rev. Lett. 71 (1993) 1994.
[34] P. Corkum, Recollision physics, Phys. Today 64 (2011) 36.
[35] J. Itatani, J. Levesque, D. Zeidler, H. Niikura, H. Pepin, J. Kieffer, P. Corkum, D. Villeneuve, Tomographic imaging of molecular orbitals, Nature 432 (2004) 867.

[36] C.D. Lin, A.-T. Le, Z. Chen, T. Morishita, R. Lucchese, Strong-field rescattering physics-self-imaging of a molecule by its own electrons, J. Phys. B 43 (2010) 122001.
[37] S. Patchkovskii, Z. Zhao, T. Brabec, D.M. Villeneuve, High harmonic generation and molecular orbital tomography in multielectron systems: Beyond the single active electron approximation, Phys. Rev. Lett. 97 (2006) 123003.
[38] H. Niikura, P.B. Corkum, Attosecond and Angstrom science, in: P.R. Berman, C.C. Lin, E. Arimondo (Eds.), Advances in Atomic Molecular and Optical Physics, in: Advances in Atomic Molecular and Optical Physics, vol. 54, 2007, p. 511.
[39] C.I. Blaga, J. Xu, A. DiChiara, E. Sistrunk, K. Zhang, P. Agostini, T. Miller, L. Dimauro, C. Lin, Imaging ultrafast molecular dynamics with laser-induced electron diffraction, Nature 483 (2012) 194.
[40] T. Brabec (Ed.), Strong Field Laser Physics, Springer, 2008.
[41] K. Yamanouchi, S.L. Chin, P. Agostini, G. Ferrante (Eds.), Progress in Ultrafast Intense Laser Science Volume III, Springer, 2008.
[42] K. Yamanouchi, A. Becker, R. Li, S.L. Chin (Eds.), Progress in Ultrafast Intense Laser Science Volume IV, Springer, 2009.
[43] P. Agostini, F. Fabre, G. Mainfray, G. Petite, N.K. Rahman, Free–free transitions following six-photon ionization of xenon atoms, Phys. Rev. Lett. 42 (1979) 1127.
[44] W. Becker, F. Grasbon, R. Kopold, D. Milošević, G. Paulus, H. Walther, Above-threshold ionization: From classical features to quantum effects, in: B. Bederson, H. Walther (Eds.), Adv. At. Mol. Opt. Phys., in: Advances in Atomic, Molecular, and Optical Physics, vol. 48, Academic Press, 2002, p. 35.
[45] D.B. Milosevic, G.G. Paulus, D. Bauer, W. Becker, Above-threshold ionization by few-cycle pulses, J. Phys. B 39 (2006) R203.
[46] A. Mcpherson, G. Gibson, H. Jara, U. Johann, T.S. Luk, I.A. Mcintyre, K. Boyer, C.K. Rhodes, Studies of multiphoton production of vacuum ultraviolet-radiation in the rare-gases, J. Opt. Soc. Am. 4 (1987) 595.
[47] M. Ferray, A. L'Huillier, X. Li, L.A. Lompre, G. Mainfray, C. Manus, Multiple-harmonic conversion of 1064-nm radiation in rare-gases, J. Phys. B 21 (1988) L31.
[48] K. Midorikawa, High-order harmonic generation and attosecond science, Jpn. J. Appl. Phys. 50 (2011) 090001.
[49] J. Eden, High-order harmonic generation and other intense optical field-matter interactions: review of recent experimental and theoretical advances, Progr. Quantum Electron. 28 (2004) 197.
[50] W. Becker, X.J. Liu, P.J. Ho, J.H. Eberly, Theories of photoelectron correlation in laser-driven multiple atomic ionization, Rev. Modern Phys. 84 (2012) 1011.
[51] Y. Liu, S. Tschuch, A. Rudenko, M. Duerr, M. Siegel, U. Morgner, R. Moshammer, J. Ullrich, Strong-field double ionization of Ar below the recollision threshold, Phys. Rev. Lett. 101 (2008) 053001.
[52] Y. Liu, D. Ye, J. Liu, A. Rudenko, S. Tschuch, M. Duerr, M. Siegel, U. Morgner, Q. Gong, R. Moshammer, J. Ullrich, Multiphoton double ionization of Ar and Ne close to threshold, Phys. Rev. Lett. 104 (2010) 173002.
[53] K. Henrichs, M. Waitz, F. Trinter, H. Kim, A. Menssen, H. Gassert, H. Sann, T. Jahnke, J. Wu, M. Pitzer, M. Richter, M.S. Schöffler, M. Kunitski, R. Dörner, Observation of electron energy discretization in strong field double ionization, Phys. Rev. Lett. 111 (2013) 113003.
[54] X. Sun, M. Li, D. Ye, G. Xin, L. Fu, X. Xie, Y. Deng, C. Wu, J. Liu, Q. Gong, Y. Liu, Mechanisms of strong-field double ionization of xe, Phys. Rev. Lett. 113 (2014) 103001.
[55] Y. Liu, L. Fu, D. Ye, J. Liu, M. Li, C. Wu, Q. Gong, R. Moshammer, J. Ullrich, Strong-field double ionization through sequential release from double excitation with subsequent coulomb scattering, Phys. Rev. Lett. 112 (2014) 013003.
[56] S. Chelkowski, C. Foisy, A.D. Bandrauk, Electron-nuclear dynamics of multiphoton H_2^+ dissociative ionization in intense laser fields, Phys. Rev. A 57 (1998) 1176.
[57] J. Wu, H. Zeng, C. Guo, Comparison study of atomic and molecular single ionization in the multiphoton ionization regime, Phys. Rev. Lett. 96 (2006) 243002.
[58] C. Cornaggia, J. Lavancier, D. Normand, J. Morellec, P. Agostini, J.P. Chambaret, A. Antonetti, Multielectron dissociative ionization of diatomic molecules in an intense femtosecond laser field, Phys. Rev. A 44 (1991) 4499.
[59] X. Gong, Q. Song, Q. Ji, H. Pan, J. Ding, J. Wu, H. Zeng, Strong-field dissociative double ionization of acetylene, Phys. Rev. Lett. 112 (2014) 243001.
[60] X. Gong, P. He, Q. Song, Q. Ji, H. Pan, J. Ding, F. He, H. Zeng, J. Wu, Two-dimensional directional proton emission in dissociative ionization of H_2, Phys. Rev. Lett. 113 (2014) 203001.
[61] H. Niikura, F. Legare, R. Hasbani, A. Bandrauk, M. Ivanov, D. Villeneuve, P. Corkum, Sub-laser-cycle electron pulses for probing molecular dynamics, Nature 417 (2002) 917.
[62] H. Niikura, F. Legare, R. Hasbani, M. Ivanov, D. Villeneuve, P. Corkum, Probing molecular dynamics with attosecond resolution using correlated wave packet pairs, Nature 421 (2003) 826.
[63] J. Xu, C.I. Blaga, K. Zhang, Y.H. Lai, C.D. Lin, T.A. Miller, P. Agostini, L.F. Dimauro, Diffraction using laser-driven broadband electron wave packets, Nat. Commun. 5 (2014) 4635.
[64] H. Stapelfeldt, T. Seideman, Colloquium: Aligning molecules with strong laser pulses, Rev. Modern Phys. 75 (2003) 543.
[65] J. Yao, G. Li, X. Jia, X. Hao, B. Zeng, C. Jing, W. Chu, J. Ni, H. Zhang, H. Xie, C. Zhang, Z. Zhao, J. Chen, X. Liu, Y. Cheng, Z. Xu, Alignment-dependent fluorescence emission induced by tunnel ionization of carbon dioxide from lower-lying orbitals, Phys. Rev. Lett. 111 (2013) 133001.
[66] L.J. Frasinski, K. Codling, P. Hatherly, J. Barr, I.N. Ross, W.T. Toner, Femtosecond dynamics of multielectron dissociative ionization by use of a picosecond laser, Phys. Rev. Lett. 58 (1987) 2424.
[67] L. Frasinski, K. Codling, P. Hatherly, Covariance mapping—a correlation method applied to multiphoton multiple ionization, Science 246 (1989) 1029.
[68] D.T. Strickland, Y. Beaudoin, P. Dietrich, P.B. Corkum, Optical studies of inertially confined molecular iodine ions, Phys. Rev. Lett. 68 (1992) 2755.
[69] H. Stapelfeldt, E. Constant, P.B. Corkum, Wave packet structure and dynamics measured by coulomb explosion, Phys. Rev. Lett. 74 (1995) 3780.
[70] T. Seideman, M.Y. Ivanov, P.B. Corkum, Role of electron localization in intense-field molecular ionization, Phys. Rev. Lett. 75 (1995) 2819.
[71] A. Hishikawa, A. Iwamae, K. Hoshina, M. Kono, K. Yamanouchi, Mass-resolved two-dimensional momentum imaging of the Coulomb explosion of N_2 and SO_2 in an intense laser field, Chem. Phys. Lett. 282 (1998) 283.
[72] I.A. Bocharova, A.S. Alnaser, U. Thumm, T. Niederhausen, D. Ray, C.L. Cocke, I.V. Litvinyuk, Time-resolved coulomb-explosion imaging of nuclear wave-packet dynamics induced in diatomic molecules by intense few-cycle laser pulses, Phys. Rev. A 83 (2011) 013417.
[73] C. Wu, C. Wu, D. Song, H. Su, Y. Yang, Z. Wu, X. Liu, H. Liu, M. Li, Y. Deng, Y. Liu, L.-Y. Peng, H. Jiang, Q. Gong, Nonsequential and sequential fragmentation of CO_2^{3+} in intense laser fields, Phys. Rev. Lett. 110 (2013) 103601.
[74] Z. Zeng, Y. Cheng, X. Song, R. Li, Z. Xu, Generation of an extreme ultraviolet supercontinuum in a two-color laser field, Phys. Rev. Lett. 98 (2007) 203901.
[75] C. Jin, G. Wang, H. Wei, A.-T. Le, C.D. Lin, Waveforms for optimal sub-keV high-order harmonics with synthesized two- or three-colour laser fields, Nat. Commun. 5 (2014) 4003.
[76] N.G. Kling, K.J. Betsch, M. Zohrabi, S. Zeng, F. Anis, U. Ablikim, B. Jochim, Z. Wang, M. Kübel, M.F. Kling, K.D. Carnes, B.D. Esry, I. Ben-Itzhak, Carrier-envelope phase control over pathway interference in strong-field dissociation of H_2^+, Phys. Rev. Lett. 111 (2013) 163004.
[77] T. Rathje, A.M. Sayler, S. Zeng, P. Wustelt, H. Figger, B.D. Esry, G.G. Paulus, Coherent control at its most fundamental: carrier-envelope-phase-dependent electron localization in photodissociation of a H_2^+ molecular ion beam target, Phys. Rev. Lett. 111 (2013) 093002.
[78] C. Liu, M. Reduzzi, A. Trabattoni, A. Sunilkumar, A. Dubrouil, F. Calegari, M. Nisoli, G. Sansone, Carrier-envelope phase effects of a single attosecond pulse in two-color photoionization, Phys. Rev. Lett. 111 (2013) 123901.
[79] V. Roudnev, B.D. Esry, General theory of carrier-envelope phase effects, Phys. Rev. Lett. 99 (2007) 220406.
[80] W. Yang, X. Song, S. Gong, Y. Cheng, Z. Xu, Carrier-envelope phase dependence of few-cycle ultrashort laser pulse propagation in a polar molecule medium, Phys. Rev. Lett. 99 (2007) 133602.
[81] L.-Y. Peng, Q. Gong, A.F. Starace, Angularly resolved electron spectra of H^- by few-cycle laser pulses, Phys. Rev. A 77 (2008) 065403.

[82] Y. Liu, X. Liu, Y. Deng, C. Wu, H. Jiang, Q. Gong, Selective steering of molecular multiple dissociative channels with strong few-cycle laser pulses, Phys. Rev. Lett. 106 (2011) 073004.
[83] P. Ye, X. He, H. Teng, M. Zhan, S. Zhong, W. Zhang, L. Wang, Z. Wei, Full quantum trajectories resolved high-order harmonic generation, Phys. Rev. Lett. 113 (2014) 073601.
[84] G. Farkas, C. Toth, Proposal for attosecond light pulse generation using laser induced multiple-harmonic conversion processes in rare gases, Phys. Lett. A 168 (1992) 447.
[85] S.E. Harris, J.J. Macklin, T.W. Hänsch, Atomic-scale temporal structure inherent to high-order harmonic-generation, Opt. Commun. 100 (1993) 487.
[86] P.B. Corkum, N.H. Burnett, M.Y. Ivanov, Subfemtosecond pulses, Opt. Lett. 19 (1994) 1870.
[87] M. Protopapas, D.G. Lappas, C.H. Keitel, P.L. Knight, Recollisions, bremsstrahlung, and attosecond pulses from intense laser fields, Phys. Rev. A 53 (1996) R2933.
[88] P. Antoine, A. L'Huillier, M. Lewenstein, Attosecond pulse trains using high order harmonics, Phys. Rev. Lett. 77 (1996) 1234.
[89] P. Antoine, D.B. Milošević, A. L'Huillier, M.B. Gaarde, P. Salières, M. Lewenstein, Generation of attosecond pulses in macroscopic media, Phys. Rev. A 56 (1997) 4960.
[90] I.P. Christov, M.M. Murnane, H.C. Kapteyn, High-harmonic generation of attosecond pulses in the "single-cycle" regime, Phys. Rev. Lett. 78 (1997) 1251.
[91] D.G. Lappas, A. L'Huillier, Generation of attosecond xuv pulses in strong laser-atom interactions, Phys. Rev. A 58 (1998) 4140.
[92] G. Sansone, L. Poletto, M. Nisoli, High-energy attosecond light sources, Nature Photon. 5 (2011) 656.
[93] M. Chini, K. Zhao, Z. Chang, The generation, characterization and applications of broadband isolated attosecond pulses, Nature Photon. 8 (2014) 178.
[94] F. Krausz, M. Ivanov, Attosecond physics, Rev. Modern Phys. 81 (2009) 163.
[95] M. Drescher, M. Hentschel, R. Kienberger, M. Uiberacker, V. Yakovlev, A. Scrinzi, T. Westerwalbesloh, U. Kleineberg, U. Heinzmann, F. Krausz, Time-resolved atomic inner-shell spectroscopy, Nature 419 (2002) 803.
[96] M. Uiberacker, T. Uphues, M. Schultze, A.J. Verhoef, V. Yakovlev, M.F. Kling, J. Rauschenberger, N.M. Kabachnik, H. Schroeder, M. Lezius, K.L. Kompa, H.G. Muller, M.J.J. Vrakking, S. Hendel, U. Kleineberg, U. Heinzmann, M. Drescher, F. Krausz, Attosecond real-time observation of electron tunnelling in atoms, Nature 446 (2007) 627.
[97] A.L. Cavalieri, N. Müller, T. Uphues, V.S. Yakovlev, A. Baltuska, B. Horvath, B. Schmidt, L. Blm̈el, R. Holzwarth, S. Hendel, M. Drescher, U. Kleineberg, P.M. Echenique, R. Kienberger, F. Krausz, U. Heinzmann, Attosecond spectroscopy in condensed matter, Nature 449 (2007) 6229.
[98] E. Goulielmakis, M. Schultze, M. Hofstetter, V.S. Yakovlev, J. Gagnon, M. Uiberacker, A.L. Aquila, E.M. Gullikson, D.T. Attwood, R. Kienberger, F. Krausz, U. Kleineberg, Single-cycle nonlinear optics, Science 320 (2008) 1614.
[99] M. Schultze, M. Fieß, N. Karpowicz, J. Gagnon, M. Korbman, M. Hofstetter, S. Neppl, A.L. Cavalieri, R. Kienberger, U. Kleineberg, E. Goulielmakis, F. Krausz, V.S. Yakovlev, Delay in photoemission, Science 328 (2010) 1658.
[100] E. Goulielmakis, Z.-H. Loh, A. Wirth, R. Santra, N. Rohringer, V.S. Yakovlev, S. Zherebtsov, T. Pfeifer, A.M. Azzeer, M.F. Kling, S.R. Leone, F. Krausz, Real-time observation of valence electron motion, Nature 466 (2010) 739.
[101] A. Wirth, M.T. Hassan, I. Grguras, J. Gagnon, A. Moulet, T.T. Luu, S. Pabst, R. Santra, Z.A. Alahmed, A.M. Azzeer, V.S. Yakovlev, V. Pervak, F. Krausz, E. Goulielmakis, Synthesized light transients, Science 334 (2011) 195.
[102] A. Schiffrin, T. Paasch-Colberg, N. Karpowicz, V. Apalkov, D. Gerster, S. Muehlbrandt, M. Korbman, J. Reichert, M. Schultze, S. Holzner, J.V. Barth, R. Kienberger, R. Ernstorfer, V.S. Yakovlev, M.I. Stockman, F. Krausz, Optical-field-induced current in dielectrics, Nature 493 (2013) 70.
[103] M. Schultze, E.M. Bothschafter, A. Sommer, S. Holzner, W. Schweinberger, M. Fiess, M. Hofstetter, R. Kienberger, V. Apalkov, V.S. Yakovlev, M.I. Stockman, F. Krausz, Controlling dielectrics with the electric field of light, Nature 493 (2013) 75.
[104] S. Hu, L. Collins, Attosecond pump probe: Exploring ultrafast electron motion inside an atom, Phys. Rev. Lett. 96 (2006) 073004.
[105] T. Morishita, S. Watanabe, C.D. Lin, Attosecond light pulses for probing two-electron dynamics of helium in the time domain, Phys. Rev. Lett. 98 (2007) 083003.
[106] J. Feist, S. Nagele, R. Pazourek, E. Persson, B.I. Schneider, L.A. Collins, J. Burgdörfer, Probing electron correlation via attosecond xuv pulses in the two-photon double ionization of helium, Phys. Rev. Lett. 103 (2009) 063002.
[107] J. Feist, S. Nagele, C. Ticknor, B.I. Schneider, L.A. Collins, J. Burgdörfer, Attosecond two-photon interferometry for doubly excited states of helium, Phys. Rev. Lett. 107 (2011) 093005.
[108] S.X. Hu, L.A. Collins, B.I. Schneider, Attosecond photoelectron microscopy of H_2^+, Phys. Rev. A 80 (2009) 023426.
[109] M.H. Xu, L.Y. Peng, Z. Zhang, Q. Gong, X.M. Tong, E.A. Pronin, A.F. Starace, Attosecond streaking in the low-energy region as a probe of rescattering, Phys. Rev. Lett. 107 (2011) 183001.
[110] M.-H. Xu, L.-Y. Peng, Z. Zhang, Q. Gong, Tracing attosecond electron motion inside a molecule by interferences from photoelectron emission, J. Phys. B 44 (2011) 021001.
[111] G. Dixit, O. Vendrell, R. Santra, Imaging electronic quantum motion with light, Proc. Natl. Acad. Sci. 109 (2012) 11636.
[112] L.-Y. Peng, Z. Zhang, W.-C. Jiang, G.-Q. Zhang, Q. Gong, Probe of the electron correlation in sequential double ionization of helium by two-color attosecond pulses, Phys. Rev. A 86 (2012) 063401.
[113] W.-C. Jiang, W.-H. Xiong, T.-S. Zhu, L.-Y. Peng, Q. Gong, Double ionization of He by time-delayed attosecond pulses, J. Phys. B 47 (2014) 091001.
[114] F. Lepine, M.Y. Ivanov, M.J.J. Vrakking, Attosecond molecular dynamics: fact or fiction? Nature Photon. 8 (2014) 195.
[115] S.R. Leone, C.W. McCurdy, J. Burgdörfer, L.S. Cederbaum, Z. Chang, N. Dudovich, J. Feist, C.H. Greene, M. Ivanov, R. Kienberger, U. Keller, M.F. Kling, Z.-H. Loh, T. Pfeifer, A.N. Pfeiffer, R. Santra, K. Schafer, A. Stolow, U. Thumm, M.J.J. Vrakking, What will it take to observe processes in 'real time'? Nature Photon. 8 (2014) 162.
[116] T. Morishita, A.-T. Le, Z. Chen, C.D. Lin, Accurate retrieval of structural information from laser-induced photoelectron and high-order harmonic spectra by few-cycle laser pulses, Phys. Rev. Lett. 100 (2008) 013903.
[117] M. Okunishi, T. Morishita, G. Prumper, K. Shimada, C.D. Lin, S. Watanabe, K. Ueda, Experimental retrieval of target structure information from laser-induced rescattered photoelectron momentum distributions, Phys. Rev. Lett. 100 (2008) 143001.
[118] M.V. Frolov, D.V. Knyazeva, N.L. Manakov, A.M. Popov, O.V. Tikhonova, E.A. Volkova, M.-H. Xu, L.-Y. Peng, L.-W. Pi, A.F. Starace, Validity of factorization of the high-energy photoelectron yield in above-threshold ionization of an atom by a short laser pulse, Phys. Rev. Lett. 108 (2012) 213002.
[119] S. Hu, L. Collins, Imaging molecular structures by electron diffraction using an intense few-cycle pulse, Phys. Rev. Lett. 94 (2005) 073004.
[120] L. Keldysh, Ionization in field of a strong electromagnetic wave, Sov. Phys. - JETP 20 (1965) 1307.
[121] F. Faisal, Multiple absorption of laser photons by atoms, J. Phys. B 6 (1973) L89.
[122] H.R. Reiss, Effect of an intense electromagnetic-field on a weakly bound system, Phys. Rev. A 22 (1980) 1786.
[123] B. Borca, M. Frolov, N. Manakov, A. Starace, Threshold effects on angular distributions for multiphoton detachment by intense elliptically polarized light, Phys. Rev. Lett. 87 (2001) 133001.
[124] B. Borca, M. Frolov, N. Manakov, A. Starace, Threshold-related enhancement of the high-energy plateau in above-threshold detachment, Phys. Rev. Lett. 88 (2002) 193001.
[125] N. Manakov, M. Frolov, B. Borca, A. Starace, Multiphoton detachment of a negative ion by an elliptically polarized, monochromatic laser field, J. Phys. B 36 (2003) R49.
[126] M. Frolov, N. Manakov, E. Pronin, A. Starace, Model-independent quantum approach for intense laser detachment of a weakly bound electron, Phys. Rev. Lett. 91 (2003) 053003.
[127] A. Flegel, M. Frolov, N. Manakov, A. Starace, Cutoffs of high-energy plateaux for atomic processes in an intense elliptically polarized laser field, J. Phys. B 38 (2005) L27.
[128] M.V. Frolov, A.V. Flegel, N.L. Manakov, Description of harmonic generation in terms of the complex quasienergy. II. Application to time-dependent effective range theory, Phys. Rev. A 75 (2007) 063408.

[129] M.V. Frolov, A.V. Flegel, N.L. Manakov, Description of harmonic generation in terms of the complex quasienergy. I. General formulation, Phys. Rev. A 75 (2007) 063407.
[130] M.V. Frolov, N.L. Manakov, A.F. Starace, Wavelength scaling of high-harmonic yield: Threshold phenomena and bound state symmetry dependence, Phys. Rev. Lett. 100 (2008) 173001.
[131] M.V. Frolov, N.L. Manakov, A.F. Starace, Effective-range theory for an electron in a short-range potential and a laser field, Phys. Rev. A 78 (2008) 063418.
[132] M.V. Frolov, N.L. Manakov, T.S. Sarantseva, A.F. Starace, Analytic formulae for high harmonic generation, J. Phys. B 42 (2009) 035601.
[133] M.V. Frolov, N.L. Manakov, A.F. Starace, Analytic formulas for above-threshold ionization or detachment plateau spectra, Phys. Rev. A 79 (2009) 033406.
[134] M.V. Frolov, N.L. Manakov, T.S. Sarantseva, M.Y. Emelin, M.Y. Ryabikin, A.F. Starace, Analytic description of the high-energy plateau in harmonic generation by atoms: Can the harmonic power increase with increasing laser wavelengths? Phys. Rev. Lett. 102 (2009) 243901.
[135] M.V. Frolov, N.L. Manakov, A.A. Silaev, N.V. Vvedenskii, Analytic description of high-order harmonic generation by atoms in a two-color laser field, Phys. Rev. A 81 (2010) 063407.
[136] M.V. Frolov, N.L. Manakov, A.A. Silaev, N.V. Vvedenskii, A.F. Starace, High-order harmonic generation by atoms in a few-cycle laser pulse: Carrier-envelope phase and many-electron effects, Phys. Rev. A 83 (2011) 021405.
[137] M.V. Frolov, N.L. Manakov, T.S. Sarantseva, Analytic confirmation that the factorized formula for harmonic generation involves the exact photorecombination cross section, Phys. Rev. A 83 (2011) 043416.
[138] M.V. Frolov, N.L. Manakov, A.M. Popov, O.V. Tikhonova, E.A. Volkova, A.A. Silaev, N.V. Vvedenskii, A.F. Starace, Analytic theory of high-order-harmonic generation by an intense few-cycle laser pulse, Phys. Rev. A 85 (2012) 033416.
[139] M.V. Frolov, N.L. Manakov, T.S. Sarantseva, A.F. Starace, High-order-harmonic-generation spectroscopy with an elliptically polarized laser field, Phys. Rev. A 86 (2012) 063406.
[140] S.V. Borzunov, M.V. Frolov, M.Y. Ivanov, N.L. Manakov, S.S. Marmo, A.F. Starace, Zero-range-potential model for strong-field molecular processes: Dynamic polarizability and photodetachment cross section, Phys. Rev. A 88 (2013) 033410.
[141] M.V. Frolov, D.V. Knyazeva, N.L. Manakov, J.-W. Geng, L.-Y. Peng, A.F. Starace, Analytic model for the description of above-threshold ionization by an intense short laser pulse, Phys. Rev. A 89 (2014) 063419.
[142] O. Tolstikhin, Siegert-state expansion for nonstationary systems: Coupled equations in the one-channel case, Phys. Rev. A 73 (2006) 062705.
[143] O.I. Tolstikhin, Siegert-state expansion for nonstationary systems. II. The whole-axis problem, Phys. Rev. A 74 (2006) 042719.
[144] P.A. Batishchev, O.I. Tolstikhin, Siegert pseudostate formulation of scattering theory: Nonzero angular momenta in the one-channel case, Phys. Rev. A 75 (2007) 062704.
[145] K. Toyota, O.I. Tolstikhin, T. Morishita, S. Watanabe, Siegert-state expansion in the Kramers–Henneberger frame: Interference substructure of above-threshold ionization peaks in the stabilization regime, Phys. Rev. A 76 (2007) 043418.
[146] O.I. Tolstikhin, Siegert-state expansion for nonstationary systems. III. Generalized Born-Fock equations and adiabatic approximation for transitions to the continuum, Phys. Rev. A 77 (2008) 032711.
[147] O.I. Tolstikhin, Siegert-state expansion for nonstationary systems. IV. Three-dimensional case, Phys. Rev. A 77 (2008) 032712.
[148] O.I. Tolstikhin, T. Morishita, S. Watanabe, Adiabatic theory of ionization of atoms by intense laser pulses: One-dimensional zero-range-potential model, Phys. Rev. A 81 (2010) 033415.
[149] P.A. Batishchev, O.I. Tolstikhin, T. Morishita, Atomic Siegert states in an electric field: Transverse momentum distribution of the ionized electrons, Phys. Rev. A 82 (2010) 023416.
[150] O.I. Tolstikhin, T. Morishita, L.B. Madsen, Theory of tunneling ionization of molecules: Weak-field asymptotics including dipole effects, Phys. Rev. A 84 (2011) 053423.
[151] W.-C. Jiang, O.I. Tolstikhin, L.-Y. Peng, Q. Gong, Static-field-induced states and their manifestation in tunneling ionization dynamics of molecules, Phys. Rev. A 85 (2012) 023404.
[152] L. Hamonou, T. Morishita, O.I. Tolstikhin, Molecular Siegert states in an electric field, Phys. Rev. A 86 (2012) 013412.
[153] O.I. Tolstikhin, T. Morishita, Adiabatic theory of ionization by intense laser pulses: Finite-range potentials, Phys. Rev. A 86 (2012) 043417.
[154] O.I. Tolstikhin, H.J. Woerner, T. Morishita, Effect of nuclear motion on tunneling ionization rates of molecules, Phys. Rev. A 87 (2013) 041401.
[155] V.H. Trinh, O.I. Tolstikhin, L.B. Madsen, T. Morishita, First-order correction terms in the weak-field asymptotic theory of tunneling ionization, Phys. Rev. A 87 (2013) 043426.
[156] O.I. Tolstikhin, L.B. Madsen, T. Morishita, Weak-field asymptotic theory of tunneling ionization in many-electron atomic and molecular systems, Phys. Rev. A 89 (2014) 013421.
[157] V.N.T. Pham, O.I. Tolstikhin, T. Morishita, Molecular Siegert states in an electric field. II. Transverse momentum distribution of the ionized electrons, Phys. Rev. A 89 (2014) 033426.
[158] A. Gazibegovic-Busuladzic, D.B. Milosevic, W. Becker, Gauge dependence of the strong-field approximation: Theory vs. experiment for photodetachment of F^-, Opt. Commun. 275 (2007) 116.
[159] P.A. Korneev, S.V. Popruzhenko, S.P. Goreslavski, W. Becker, G.G. Paulus, B. Fetic, D.B. Milosevic, Interference structure of above-threshold ionization versus above-threshold detachment, New J. Phys. 14 (2012) 055019.
[160] A. Lohr, M. Kleber, R. Kopold, W. Becker, Above-threshold ionization in the tunneling regime, Phys. Rev. A 55 (1997) R4003.
[161] M. Lewenstein, P. Balcou, M. Ivanov, A. Lhuillier, P. Corkum, Theory of high-harmonic generation by low-frequency laser fields, Phys. Rev. A 49 (1994) 2117.
[162] S. Chelkowski, A. Bandrauk, Asymmetries in strong-field photoionization by few-cycle laser pulses: Kinetic-energy spectra and semiclassical explanation of the asymmetries of fast and slow electrons, Phys. Rev. A 71 (2005) 053815.
[163] S. Goreslavski, G. Paulus, S. Popruzhenko, N. Shvetsov-Shilovski, Coulomb asymmetry in above-threshold ionization, Phys. Rev. Lett. 93 (2004) 233002.
[164] M. Li, Y. Liu, H. Liu, Q. Ning, L. Fu, J. Liu, Y. Deng, C. Wu, L. Peng, Q. Gong, Subcycle dynamics of coulomb asymmetry in strong elliptical laser fields, Phys. Rev. Lett. 111 (2013) 023006.
[165] Y. Huismans, A. Rouzee, A. Gijsbertsen, J.H. Jungmann, A.S. Smolkowska, P.S.W.M. Logman, F. Lepine, C. Cauchy, S. Zamith, T. Marchenko, J.M. Bakker, G. Berden, B. Redlich, A.F.G. van der Meer, H.G. Muller, W. Vermin, K.J. Schafer, M. Spanner, M.Y. Ivanov, O. Smirnova, D. Bauer, S.V. Popruzhenko, M.J.J. Vrakking, Time-resolved holography with photoelectrons, Science 331 (2011) 61.
[166] X.-B. Bian, Y. Huismans, O. Smirnova, K.-J. Yuan, M.J.J. Vrakking, A. Bandrauk, Subcycle interference dynamics of time-resolved photoelectron holography with midinfrared laser pulses, Phys. Rev. A 84 (2011) 043420.
[167] X.-B. Bian, A. Bandrauk, Attosecond time-resolved imaging of molecular structure by photoelectron holography, Phys. Rev. Lett. 108 (2012) 263003.
[168] Y. Huismans, A. Gijsbertsen, A.S. Smolkowska, J.H. Jungmann, A. Rouzee, P.S.W.M. Logman, F. Lepine, C. Cauchy, S. Zamith, T. Marchenko, J.M. Bakker, G. Berden, B. Redlich, A.F.G. van der Meer, M.Y. Ivanov, T. M. Yan, D. Bauer, O. Smirnova, M.J.J. Vrakking, Scaling laws for photoelectron holography in the midinfrared wavelength regime, Phys. Rev. Lett. 109 (2012) 013002.
[169] M. Meckel, A. Staudte, S. Patchkovskii, D.M. Villeneuve, P.B. Corkum, R. Dörner, M. Spanner, Signatures of the continuum electron phase in molecular strong-field photoelectron holography, Nat. Phys. 10 (2014) 594.
[170] X.-B. Bian, A.D. Bandrauk, Orientation-dependent forward-backward photoelectron holography from asymmetric molecules, Phys. Rev. A 89 (2014) 033423.
[171] T. Nubbemeyer, K. Gorling, A. Saenz, U. Eichmann, W. Sandner, Strong-field tunneling without ionization, Phys. Rev. Lett. 101 (2008) 233001.
[172] H. Liu, Y. Liu, L. Fu, G. Xin, D. Ye, J. Liu, X.T. He, Y. Yang, X. Liu, Y. Deng, C. Wu, Q. Gong, Low yield of near-zero-momentum electrons and partial atomic stabilization in strong-field tunneling ionization, Phys. Rev. Lett. 109 (2012) 093001.

[173] Z. Lin, X. Jia, C. Wang, Z. Hu, H. Kang, W. Quan, X. Lai, X. Liu, J. Chen, B. Zeng, W. Chu, J. Yao, Y. Cheng, Z. Xu, Ionization suppression of diatomic molecules in an intense midinfrared laser field, Phys. Rev. Lett. 108 (2012) 223001.
[174] M. Li, L. Qin, C. Wu, L. Peng, Q. Gong, Y. Liu, Rescattering and frustrated tunneling ionization of atoms in circularly polarized laser fields, Phys. Rev. A 89 (2014) 013422.
[175] D. Arbo, S. Yoshida, E. Persson, K. Dimitriou, J. Burgdörfer, Interference oscillations in the angular distribution of laser-ionized electrons near ionization threshold, Phys. Rev. Lett. 96 (2006) 143003.
[176] Z. Chen, T. Morishita, A.-T. Le, M. Wickenhauser, X.M. Tong, C.D. Lin, Analysis of two-dimensional photoelectron momentum spectra and the effect of the long-range Coulomb potential in single ionization of atoms by intense lasers, Phys. Rev. A 74 (2006) 053405.
[177] D.G. Arbó, K.I. Dimitriou, E. Persson, J. Burgdörfer, Sub-poissonian angular momentum distribution near threshold in atomic ionization by short laser pulses, Phys. Rev. A 78 (2008) 013406.
[178] C.I. Blaga, F. Catoire, P. Colosimo, G.G. Paulus, H.G. Muller, P. Agostini, L.F. Dimauro, Strong-field photoionization revisited, Nat. Phys. 5 (2009) 335.
[179] F.H.M. Faisal, Strong-field physics ionization surprise, Nat. Phys. 5 (2009) 319.
[180] W. Quan, Z. Lin, M. Wu, H. Kang, H. Liu, X. Liu, J. Chen, J. Liu, X.T. He, S.G. Chen, H. Xiong, L. Guo, H. Xu, Y. Fu, Y. Cheng, Z.Z. Xu, Classical aspects in above-threshold ionization with a midinfrared strong laser field, Phys. Rev. Lett. 103 (2009) 093001.
[181] T.-M. Yan, S.V. Popruzhenko, M.J.J. Vrakking, D. Bauer, Low-energy structures in strong field ionization revealed by quantum orbits, Phys. Rev. Lett. 105 (2010) 253002.
[182] C. Liu, K.Z. Hatsagortsyan, Origin of unexpected low energy structure in photoelectron spectra induced by midinfrared strong laser fields, Phys. Rev. Lett. 105 (2010) 113003.
[183] C.Y. Wu, Y.D. Yang, Y.Q. Liu, Q.H. Gong, M. Wu, X. Liu, X.L. Hao, W.D. Li, X.T. He, J. Chen, Characteristic spectrum of very low-energy photoelectron from above-threshold ionization in the tunneling regime, Phys. Rev. Lett. 109 (2012) 043001.
[184] A. Kaestner, U. Saalmann, J.M. Rost, Electron-energy bunching in laser-driven soft recollisions, Phys. Rev. Lett. 108 (2012) 033201.
[185] L. Guo, S.S. Han, X. Liu, Y. Cheng, Z.Z. Xu, J. Fan, J. Chen, S.G. Chen, W. Becker, C.I. Blaga, A.D. DiChiara, E. Sistrunk, P. Agostini, L.F. Dimauro, Scaling of the low-energy structure in above-threshold ionization in the tunneling regime: Theory and experiment, Phys. Rev. Lett. 110 (2013) 013001.
[186] J. Dura, N. Camus, A. Thai, A. Britz, M. Hemmer, M. Baudisch, A. Senftleben, C.D. Schroeter, J. Ullrich, R. Moshammer, J. Biegert, Ionization with low-frequency fields in the tunneling regime, Sci. Rep. 3 (2013).
[187] T. Brabec, M. Ivanov, P. Corkum, Coulomb focusing in intense field atomic processes, Phys. Rev. A 54 (1996) R2551.
[188] J. Chen, J. Liu, L. Fu, W. Zheng, Interpretation of momentum distribution of recoil ions from laser-induced nonsequential double ionization by semiclassical rescattering model, Phys. Rev. A 63 (2001) 011404.
[189] G. Yudin, M. Ivanov, Physics of correlated double ionization of atoms in intense laser fields: Quasistatic tunneling limit, Phys. Rev. A 63 (2001) 033404.
[190] D.F. Ye, X. Liu, J. Liu, Classical trajectory diagnosis of a fingerlike pattern in the correlated electron momentum distribution in strong field double ionization of helium, Phys. Rev. Lett. 101 (2008) 233003.
[191] M.V. Ammosov, N.B. Delone, V.P. Krainov, Tunnel ionization of complex atoms and of atomic ions in an alternating electromagnetic field, Sov. Phys. - JETP 64 (1986) 1191–1194.
[192] M. Li, J.-W. Geng, H. Liu, Y. Deng, C. Wu, L.-Y. Peng, Q. Gong, Y. Liu, Classical-quantum correspondence for above-threshold ionization, Phys. Rev. Lett. 112 (2014) 113002.
[193] J.-W. Geng, L. Qin, M. Li, W.-H. Xiong, Y. Liu, Q. Gong, L.-Y. Peng, Nonadiabatic tunneling ionization of atoms in elliptically polarized laser fields, J. Phys. B 47 (2014) 204027.
[194] P. Salieres, B. Carre, L. Le Deroff, F. Grasbon, G. Paulus, H. Walther, R. Kopold, W. Becker, D. Milosevic, A. Sanpera, M. Lewenstein, Feynman's path-integral approach for intense-laser-atom interactions, Science 292 (2001) 902.
[195] M. Nandor, M. Walker, L. Van Wörkom, H. Muller, Detailed comparison of above-threshold-ionization spectra from accurate numerical integrations and high-resolution measurements, Phys. Rev. A 60 (1999) R1771.
[196] M.O. Scully, M.S. Zubairy, Quantum Optics, Cambridge University Press, 1997.
[197] P. Dirac, The quantum theory of the emission and absorption of radiation, Proc. R. Soc. A 114 (1927) 243.
[198] G.W.F. Drake (Ed.), Springer Handbooks of Atomic, Molecular, and Optical Physics, Springer, 2006.
[199] R. Panfili, J. Eberly, Comparing classical and quantum dynamics of strong-field double ionization, Opt. Express 8 (2001) 431.
[200] D.A. Wasson, S.E. Koonin, Molecular-dynamics simulations of atomic ionization by strong laser fields, Phys. Rev. A 39 (1989) 5676.
[201] G.G. Paulus, W. Becker, W. Nicklich, H. Walther, Rescattering effects in above-threshold ionization—a classical-model, J. Phys. B 27 (1994) L703.
[202] U. Mohideen, M.H. Sher, H.W.K. Tom, G.D. Aumiller, O.R. Wood, R.R. Freeman, J. Bokor, P.H. Bucksbaum, High-intensity above-threshold ionization of helium, Phys. Rev. Lett. 71 (1993) 509.
[203] D. Fittinghaoff, P. Bolton, B. Chang, K. Kunlander, Observation of nonsequential double ionization of helium with optical tunneling, Phys. Rev. Lett. 69 (1992) 2642.
[204] B. Walker, B. Sheehy, L.F. Dimauro, P. Agostini, K.J. Schafer, K.C. Kulander, Precision-measurement of strong-field double-ionization of helium, Phys. Rev. Lett. 73 (1994) 1227.
[205] B. Hu, J. Liu, S. Chen, Plateau in above-threshold-ionization spectra and chaotic behavior in rescattering processes, Phys. Lett. A 236 (1997) 533.
[206] N.I. Shvetsov-Shilovski, D. Dimitrovski, L.B. Madsen, Ionization in elliptically polarized pulses: Multielectron polarization effects and asymmetry of photoelectron momentum distributions, Phys. Rev. A 85 (2012) 023428.
[207] L.D. Landau, E.M. Liftshitz, Quantum Mechanics, Pergamon, Oxford, 1977.
[208] K. Dimitriou, D. Arbo, S. Yoshida, E. Persson, J. Burgdörfer, Origin of the double-peak structure in the momentum distribution of ionization of hydrogen atoms driven by strong laser fields, Phys. Rev. A 70 (2004) 061401.
[209] P. Eckle, A.N. Pfeiffer, C. Cirelli, A. Staudte, R. Doerner, H.G. Muller, M. Buettiker, U. Keller, Attosecond ionization and tunneling delay time measurements in helium, Science 322 (2008) 1525.
[210] A.N. Pfeiffer, C. Cirelli, A.S. Landsman, M. Smolarski, D. Dimitrovski, L.B. Madsen, U. Keller, Probing the longitudinal momentum spread of the electron wave packet at the tunnel exit, Phys. Rev. Lett. 109 (2012) 083002.
[211] R. Boge, C. Cirelli, A.S. Landsman, S. Heuser, A. Ludwig, J. Maurer, M. Weger, L. Gallmann, U. Keller, Probing nonadiabatic effects in strong-field tunnel ionization, Phys. Rev. Lett. 111 (2013) 103003.
[212] A.S. Landsman, C. Hofmann, A.N. Pfeiffer, C. Cirelli, U. Keller, Unified approach to probing coulomb effects in tunnel ionization for any ellipticity of laser light, Phys. Rev. Lett. 111 (2013) 263001.
[213] S.V. Popruzhenko, D. Bauer, Strong field approximation for systems with Coulomb interaction, J. Modern Opt. 55 (2008) 2573.
[214] S.V. Popruzhenko, G.G. Paulus, D. Bauer, Coulomb-corrected quantum trajectories in strong-field ionization, Phys. Rev. A 77 (2008) 053409.
[215] T.-M. Yan, D. Bauer, Sub-barrier Coulomb effects on the interference pattern in tunneling-ionization photoelectron spectra, Phys. Rev. A 86 (2012) 053403.
[216] R. Kopold, W. Becker, M. Kleber, Quantum path analysis of high-order above-threshold ionization, Opt. Commun. 179 (2000) 39.
[217] J. Javanainen, J.H. Eberly, Q. Su, Numerical simulations of multiphoton ionization and above-threshold electron spectra, Phys. Rev. A 38 (1988) 3430.
[218] S. Geltman, Ionization of a model atom by a pulse of coherent radiation, J. Phys. B 10 (1977) 831.
[219] S.-I. Chu, W.P. Reinhardt, Intense field multiphoton ionization via complex dressed states: application to the H atom, Phys. Rev. Lett. 39 (1977) 1195.
[220] A. Maquet, S.-I. Chu, W.P. Reinhardt, Stark ionization in dc and ac fields: An L^2 complex-coordinate approach, Phys. Rev. A 27 (1983) 2946.
[221] S.-I. Chu, J. Cooper, Threshold shift and above-threshold multiphoton ionization of atomic hydrogen in intense laser fields, Phys. Rev. A 32 (1985) 2769.
[222] K.C. Kulander, Multiphoton ionization of hydrogen—a time-dependent theory, Phys. Rev. A 35 (1987) 445.
[223] K.C. Kulander, Time-dependent Hartree–Fock theory of multiphoton ionization—helium, Phys. Rev. A 36 (1987) 2726.

[224] K.C. Kulander, Time-dependent theory of multiphoton ionization of xenon, Phys. Rev. A 38 (1988) 778.
[225] K.C. Kulander, B. Shore, Calculations of multiple-harmonic conversion of 1064-nm radiation in Xe, Phys. Rev. Lett. 62 (1989) 524.
[226] J. Eberly, Q. Su, J. Javanainen, K.C. Kulander, B. Shore, L. Rosofranco, High-order harmonic-generation during multiphoton ionization of gases, J. Modern Opt. 36 (1989) 829.
[227] K.C. Kulander, B. Shore, Generation of optical harmonics by intense pulses of laser-radiation.2. single-atom spectrum for xenon, J. Opt. Soc. Am. 7 (1990) 502.
[228] K.J. Schafer, K.C. Kulander, Energy analysis of time-dependent wave-functions—application to above-threshold ionization, Phys. Rev. A 42 (1990) 5794.
[229] K.C. Kulander, K. Schafer, J.L. Krause, Single-active electron calculation of multiphoton process in krypton, Int. J. Quant. Chem. (1991) 415.
[230] C. Cerjan, K.C. Kulander, Efficient time propagation for finite-difference representations of the time-dependent Schrödinger-equation, Comput. Phys. Commun. 63 (1991) 529.
[231] J.L. Krause, K. Schafer, K.C. Kulander, Optical harmonic-generation in atomic and molecular-hydrogen, Chem. Phys. Lett. 178 (1991) 573.
[232] K.C. Kulander, K. Schafer, J.L. Krause, Dynamic stabilization of hydrogen in an intense, high-frequency, pulsed laser field, Phys. Rev. Lett. 66 (1991) 2601.
[233] A. Lhuillier, K. Schafer, K. Kulander, Theoretical aspects of intense field harmonic-generation, J. Phys. B 24 (1991) 3315.
[234] J. Parker, L. Moore, K. Meharg, D. Dundas, K. Taylor, Double-electron above threshold ionization of helium, J. Phys. B 34 (2001) L69.
[235] J.S. Parker, B.J.S. Doherty, K.T. Taylor, K.D. Schultz, C.I. Blaga, L.F. Dimauro, High-energy cutoff in the spectrum of strong-field nonsequential double ionization, Phys. Rev. Lett. 96 (2006) 133001.
[236] H.G. Muller, An efficient propagation scheme for the time-dependent schrödinger equation in the velocity gauge, Laser Phys. 9 (1999) 138.
[237] D. Bauer, P. Koval, Qprop: A Schrödinger-solver for intense laser-atom interaction, Comput. Phys. Commun. 174 (2006) 396.
[238] J. Parker, E. Smyth, K. Taylor, Intense-field multiphoton ionization of helium, J. Phys. B 31 (1998) L571.
[239] E. Smyth, J. Parker, K. Taylor, Numerical integration of the time-dependent Schrödinger equation for laser-driven helium, Comput. Phys. Commun. 114 (1998) 1.
[240] K. Taylor, J. Parker, D. Dundas, E. Smyth, S. Vivirito, Laser-driven helium in full-dimensionality, Laser Phys. 9 (1999) 98.
[241] J. Parker, L. Moore, E. Smyth, K. Taylor, One- and two-electron numerical models of multiphoton ionization of helium, J. Phys. B 33 (2000) 1057.
[242] J. Parker, D. Glass, L. Moore, E. Smyth, K. Taylor, P. Burke, Time-dependent and time-independent methods applied to multiphoton ionization of helium, J. Phys. B 33 (2000) L239.
[243] F.W.J. Olver, D.W. Lozier, R.F. Boisvert, C.W. Clark (Eds.), NIST Handbook of Mathematical Functions, Cambridge University Press, 2010.
[244] T.N. Rescigno, C.W. McCurdy, Numerical grid methods for quantum-mechanical scattering problems, Phys. Rev. A 62 (2000) 032706.
[245] J. Lill, G. Parker, J. Light, Discrete variable representations and sudden models in quantum scattering-theory, Chem. Phys. Lett. 89 (1982) 483.
[246] J. Lill, G. Parker, J. Light, The discrete variable finite basis approach to quantum scattering, J. Chem. Phys. 85 (1986) 900.
[247] J. Light, I. Hamilton, J. Lill, Generalized discrete variable approximation in quantum-mechanics, J. Chem. Phys. 82 (1985) 1400.
[248] G. Corey, J. Tromp, Variational discrete variable representation, J. Chem. Phys. 103 (1995) 1812.
[249] C. Leforestier, R. Bisseling, C. Cerjan, M. Feit, R. Friesner, A. Guldberg, A. Hammerich, G. Jolicard, W. Karrlein, H. Meyer, N. Lipkin, O. Roncero, R. Kosloff, A comparison of different propagation schemes for the time dependent schrödinger equation, J. Comput. Phys. 94 (1991) 59.
[250] S. Billeter, W. Vangunsteren, A comparison of different numerical propagation schemes for solving the time-dependent Schrödinger equation in the position representation in one dimension for mixed quantum- and molecular dynamics simulations, Mol. Simulat. 15 (1995) 301.
[251] K. Burnett, V.C. Reed, J. Cooper, P.L. Knight, Calculation of the background emitted during high-harmonic generation, Phys. Rev. A 45 (1992) 3347–3349.
[252] X.-M. Tong, S.-I. Chu, Probing the spectral and temporal structures of high-order harmonic generation in intense laser pulses, Phys. Rev. A 61 (2000) 021802.
[253] L.-Y. Peng, A.F. Starace, Application of Coulomb wave function discrete variable representation to atomic systems in strong laser fields, J. Chem. Phys. 125 (2006) 154311.
[254] D. Yan, P.L.Y.Q. Gong, Grid method for computation of generalized spheroidal wave functions based on discrete variable representation, Phys. Rev. E 79 (2009) 036710.
[255] L.-Y. Peng, Q. Gong, An accurate Fortran code for computing hydrogenic continuum wave functions at a wide range of parameters, Comput. Phys. Commun. 181 (2010) 2098.
[256] S.-N. Song, J.-W. Geng, H.-B. Jiang, L.-Y. Peng, Comparative study of H(2s) and H($2p_0$) ionization dynamics in the over-barrier regime, Phys. Rev. A 89 (2014) 053411.
[257] C. McCurdy, M. Baertschy, T. Rescigno, Solving the three-body Coulomb breakup problem using exterior complex scaling, J. Phys. B 37 (2004) R137.
[258] P.L. Bartlett, A complete numerical approach to electron-hydrogen collisions, J. Phys. B 39 (2006) R379.
[259] H. Muller, Reconstruction of attosecond harmonic beating by interference of two-photon transitions, Appl. Phys. B 74 (2002) S17.
[260] E. Toma, H. Muller, Calculation of matrix elements for mixed extreme-ultraviolet-infrared two-photon above-threshold ionization of argon, J. Phys. B 35 (2002) 3435.
[261] S. Aseyev, Y. Ni, L. Frasinski, H. Muller, M. Vrakking, Attosecond angle-resolved photoelectron spectroscopy, Phys. Rev. Lett. 91 (2003) 223902.
[262] J. Itatani, F. Quéré, G.L. Yudin, M.Y. Ivanov, F. Krausz, P.B. Corkum, Attosecond streak camera, Phys. Rev. Lett. 88 (2002) 173903.
[263] M. Kitzler, N. Milosevic, A. Scrinzi, F. Krausz, T. Brabec, Quantum theory of attosecond xuv pulse measurement by laser dressed photoionization, Phys. Rev. Lett. 88 (2002) 173904.
[264] R. Kienberger, M. Hentschel, M. Uiberacker, C. Spielmann, M. Kitzler, A. Scrinzi, M. Wieland, T. Westerwalbesloh, U. Kleineberg, U. Heinzmann, M. Drescher, F. Krausz, Steering attosecond electron wave packets with light, Science 297 (2002) 1144.
[265] F. Quere, Y. Mairesse, J. Itatani, Temporal characterization of attosecond XUV fields, J. Modern Opt. 52 (2005) 339.
[266] E. Kosik, L. Corner, A. Wyatt, E. Cormier, I. Walmsley, L. Dimauro, Complete characterization of attosecond pulses, J. Modern Opt. 52 (2005) 361.
[267] A.K. Kazansky, I.P. Sazhina, N.M. Kabachnik, Angle-resolved electron spectra in short-pulse two-color XUV plus IR photoionization of atoms, Phys. Rev. A 82 (2010) 033420.
[268] S. Duesterer, L. Rading, P. Johnsson, A. Rouzee, A. Hundertmark, M.J.J. Vrakking, P. Radcliffe, M. Meyer, A.K. Kazansky, N.M. Kabachnik, Interference in the angular distribution of photoelectrons in superimposed XUV and optical laser fields, J. Phys. B 46 (2013) 164026.
[269] Y. Ge, Use of a laser as a femtosecond ruler to precisely measure an x-ray pulse, Phys. Rev. A 74 (2006) 015803.
[270] A.K. Kazansky, N.M. Kabachnik, Calculations of the double differential cross section for attosecond laser-assisted photoionization of atoms, J. Phys. B 39 (2006) 5173.
[271] D. Strickland, G. Mourou, Compression of amplified chirped optical pulses, Opt. Commun. 56 (1985) 219.
[272] R.L. Fork, C.H.B. Cruz, P.C. Becker, C.V. Shank, Compression of optical pulses to six femtoseconds by using cubic phase compensation, Opt. Lett. 12 (1987) 483.
[273] P. Maine, D. Strickland, P. Bado, M. Pessot, G. Mourou, Generation of ultrahigh peak power pulses by chirped pulse amplification, IEEE J. Quantum Electron. 24 (1988) 398.
[274] T.W. Hänsch, A proposed sub-femtosecond pulse synthesizer using separate phase-locked laser oscillators, Opt. Commun. 80 (1990) 71.
[275] T.W. Hänsch, Nobel lecture: Passion for precision, Rev. Modern Phys. 78 (2006) 1297.
[276] R.W. Minck, R.W. Terhune, W.G. Rado, Laser-stimulated raman effect and resonant four-photon interactions in gases h_2, d_2, and ch_4, Appl. Phys. Lett. 3 (1963) 181.
[277] A.E. Kaplan, Subfemtosecond pulses in mode-locked 2π solitons of the cascade stimulated raman scattering, Phys. Rev. Lett. 73 (1994) 1243.
[278] S.E. Harris, A.V. Sokolov, Subfemtosecond pulse generation by molecular modulation, Phys. Rev. Lett. 81 (1998) 2894.

[279] A.V. Sokolov, D.R. Walker, D.D. Yavuz, G.Y. Yin, S.E. Harris, Raman generation by phased and antiphased molecular states, Phys. Rev. Lett. 85 (2000) 562.
[280] A.V. Sokolov, D.R. Walker, D.D. Yavuz, G.Y. Yin, S.E. Harris, Femtosecond light source for phase-controlled multiphoton ionization, Phys. Rev. Lett. 87 (2001) 033402.
[281] D.D. Yavuz, D.R. Walker, M.Y. Shverdin, G.Y. Yin, S.E. Harris, Quasiperiodic raman technique for ultrashort pulse generation, Phys. Rev. Lett. 91 (2003) 233602.
[282] M.Y. Shverdin, D.R. Walker, D.D. Yavuz, G.Y. Yin, S.E. Harris, Generation of a single-cycle optical pulse, Phys. Rev. Lett. 94 (2005) 033904.
[283] Z.-M. Hsieh, C.-J. Lai, H.-S. Chan, S.-Y. Wu, C.-K. Lee, W.-J. Chen, C.-L. Pan, F.-G. Yee, A.H. Kung, Controlling the carrier-envelope phase of raman-generated periodic waveforms, Phys. Rev. Lett. 102 (2009) 213902.
[284] T. Suzuki, M. Hirai, M. Katsuragawa, Octave-spanning raman comb with carrier envelope offset control, Phys. Rev. Lett. 101 (2008) 243602.
[285] W.-J. Chen, Z.-M. Hsieh, S.W. Huang, H.-Y. Su, C.-J. Lai, T.-T. Tang, C.-H. Lin, C.-K. Lee, R.-P. Pan, C.-L. Pan, A.H. Kung, Sub-single-cycle optical pulse train with constant carrier envelope phase, Phys. Rev. Lett. 100 (2008) 163906.
[286] S. Baker, I.A. Walmsley, J.W.G. Tisch, J. Marangos, Femtosecond to attosecond light pulses from a molecular modulator, Nature Photon. 5 (2011) 664.
[287] P.A. Franken, A.E. Hill, C.W. Peters, G. Weinreich, Generation of optical harmonics, Phys. Rev. Lett. 7 (1961) 118.
[288] J.A. Armstrong, N. Bloembergen, J. Ducuing, P.S. Pershan, Interactions between light waves in a nonlinear dielectric, Phys. Rev. 127 (1962) 1918.
[289] N. Bloembergen, Y.R. Shen, Optical nonlinearities of a plasma, Phys. Rev. 141 (1966) 298.
[290] R.L. Carman, D.W. Forslund, J.M. Kindel, Visible harmonic emission as a way of measuring profile steepening, Phys. Rev. Lett. 46 (1981) 29.
[291] R.L. Carman, C.K. Rhodes, R.F. Benjamin, Observation of harmonics in the visible and ultraviolet created in co_2-laser-produced plasmas, Phys. Rev. A 24 (1981) 2649.
[292] J. Reintjes, C.Y. She, R.C. Eckardt, Generation of coherent radiation in the xuv by fifth- and seventh-order frequency conversion in rare gases, IEEE J. Quantum Electron. QE-14 (1978) 581.
[293] J. Bokor, P.H. Bucksbaum, R.R. Freeman, Generation of 35.5-nm coherent radiation, Opt. Lett. 8 (1983) 217.
[294] J. Wildenauer, Generation of the ninth, eleventh, and fifteenth harmonics of iodine laser radiation, J. Appl. Phys. 62 (1987) 41.
[295] J.J. Macklin, J.D. Kmetec, C.L. Gordon, High-order harmonic generation using intense femtosecond pulses, Phys. Rev. Lett. 70 (1993) 766.
[296] A. L'Huillier, P. Balcou, High-order harmonic generation in rare gases with a 1-ps 1053-nm laser, Phys. Rev. Lett. 70 (1993) 774.
[297] S.G. Preston, A. Sanpera, M. Zepf, W.J. Blyth, C.G. Smith, J.S. Wark, M.H. Key, K. Burnett, M. Nakai, D. Neely, A.A. Offenberger, High-order harmonics of 248.6-nm krf laser from helium and neon ions, Phys. Rev. A 53 (1996) R31.
[298] J.L. Krause, K.J. Schafer, K.C. Kulander, High-order harmonic generation from atoms and ions in the high intensity regime, Phys. Rev. Lett. 68 (1992) 3535.
[299] T. Popmintchev, M.-C. Chen, D. Popmintchev, P. Arpin, S. Brown, S. Alisauskas, G. Andriukaitis, T. Balciunas, O. Mucke, A. Pugzlys, A. Baltuska, B. Shim, S. Schrauth, A. Gaeta, C. Hernandez-Garcia, L. Plaja, A. Becker, A. Jaron-Becker, M.M. Murnane, H.C. Kapteyn, Bright coherent ultrahigh harmonics in the kev x-ray regime from mid-infrared femtosecond lasers, Science 336 (2012) 12878.
[300] T. Tanaka, Proposal for a pulse-compression scheme in x-ray free-electron lasers to generate a multiterawatt, attosecond x-ray pulse, Phys. Rev. Lett. 110 (2013) 084801.
[301] S. Corde, K. Ta phuoc, G. Lambert, R. Fitour, V. Malka, A. Rousse, A. Beck, E. Lefebvre, Femtosecond x rays from laser-plasma accelerators, Rev. Modern Phys. 85 (2013) 1.
[302] R.A. Ganeev, High-order harmonic generation in a laser plasma: a review of recent achievements, J. Phys. B 40 (2007) R213.
[303] U. Teubner, P. Gibbon, High-order harmonics from laser-irradiated plasma surfaces, Rev. Modern Phys. 81 (2009) 445.
[304] C. Thaury, F. Quere, High-order harmonic and attosecond pulse generation on plasma mirrors: basic mechanisms, J. Phys. B 43 (2010) 213001.
[305] D.C. Yost, T.R. Schibli, J. Ye, J.L. Tate, J. Hostetter, M.B. Gaarde, K.J. Schafer, Vacuum-ultraviolet frequency combs from below-threshold harmonics, Nat. Phys. 5 (2009) 815.
[306] E.P. Power, A.M. March, F. Catoire, E. Sistrunk, K. Krushelnick, P. Agostini, L.F. Dimauro, XFROG phase measurement of threshold harmonics in a Keldysh-scaled system, Nature Photon. 4 (2010) 352.
[307] J.A. Hostetter, J.L. Tate, K.J. Schafer, M.B. Gaarde, Semiclassical approaches to below-threshold harmonics, Phys. Rev. A 82 (2010) 023401.
[308] J.-C. Liu, M.C. Kohler, C.H. Keitel, K.Z. Hatsagortsyan, Coherent x-ray generation from below-threshold harmonics, Phys. Rev. A 84 (2011) 063817.
[309] W.-H. Xiong, J.-W. Geng, J.-Y. Tang, L.-Y. Peng, Q. Gong, Mechanisms of below-threshold harmonic generation in atoms, Phys. Rev. Lett. 112 (2014) 233001.
[310] T. Kanai, S. Minemoto, H. Sakai, Ellipticity dependence of high-order harmonic generation from aligned molecules, Phys. Rev. Lett. 98 (2007) 053002.
[311] V.A. Antonov, Y.V. Radeonychev, O. Kocharovskaya, Formation of a single attosecond pulse via interaction of resonant radiation with a strongly perturbed atomic transition, Phys. Rev. Lett. 110 (2013) 213903.
[312] P. Colosimo, G. Doumy, C.I. Blaga, J. Wheeler, C. Hauri, F. Catoire, J. Tate, R. Chirla, A.M. March, G.G. Paulus, H.G. Muller, P. Agostini, L.F. Dimauro, Scaling strong-field interactions towards the classical limit, Nat. Phys. 4 (2008) 386.
[313] B. Shan, Z. Chang, Dramatic extension of the high-order harmonic cutoff by using a long-wavelength driving field, Phys. Rev. A 65 (2002) 011804.
[314] K.L. Ishikawa, K. Schiessl, E. Persson, J. Burgdörfer, Fine-scale oscillations in the wavelength and intensity dependence of high-order harmonic generation: Connection with channel closings, Phys. Rev. A 79 (2009) 033411.
[315] J.A. Perez-Hernandez, L. Roso, L. Plaja, Harmonic generation beyond the Strong-Field Approximation: the physics behind the short-wave-infrared scaling laws, Opt. Express 17 (2009) 9891.
[316] K. Schiessl, K.L. Ishikawa, E. Persson, J. Burgdörfer, Quantum path interference in the wavelength dependence of high-harmonic generation, Phys. Rev. Lett. 99 (2007) 253903.
[317] P. Lan, E.J. Takahashi, K. Midorikawa, Wavelength scaling of efficient high-order harmonic generation by two-color infrared laser fields, Phys. Rev. A 81 (2010) 061802.
[318] H. Xu, H. Xiong, B. Zeng, W. Chu, Y. Fu, J. Yao, J. Chen, X. Liu, Y. Cheng, Z. Xu, Wavelength scaling of elliptical-polarization dependence of high-order harmonic generation, Opt. Lett. 35 (2010) 472.
[319] I. Yavuz, Z. Altun, T. Topcu, Wavelength scaling of high-order-harmonic-generation efficiency by few-cycle laser pulses: Influence of carrier-envelope phase, Phys. Rev. A 86 (2012) 043836.
[320] D.R. Austin, J. Biegert, Strong-field approximation for the wavelength scaling of high-harmonic generation, Phys. Rev. A 86 (2012) 023813.
[321] A.-T. Le, H. Wei, C. Jin, V.N. Tuoc, T. Morishita, C.D. Lin, Universality of returning electron wave packet in high-order harmonic generation with midinfrared laser pulses, Phys. Rev. Lett. 113 (2014) 033001.
[322] J. Tate, T. Auguste, H.G. Muller, P. Salieres, P. Agostini, L.F. Dimauro, Scaling of wave-packet dynamics in an intense midinfrared field, Phys. Rev. Lett. 98 (2007) 013901.
[323] A.D. Shiner, C. Trallero-Herrero, N. Kajumba, H.C. Bandulet, D. Comtois, F. Legare, M. Giguere, J.-C. Kieffer, P.B. Corkum, D.M. Villeneuve, Wavelength Scaling of High Harmonic Generation Efficiency, Phys. Rev. Lett. 103 (2009) 073902.
[324] C.-J. Lai, G. Cirmi, K.-H. Hong, J. Moses, S.-W. Huang, E. Granados, P. Keathley, S. Bhardwaj, F.X. Kärtner, Wavelength scaling of high harmonic generation close to the multiphoton ionization regime, Phys. Rev. Lett. 111 (2013) 073901.
[325] D. Milosevic, W. Becker, Role of long quantum orbits in high-order harmonic generation, Phys. Rev. A 66 (2002) 063417.
[326] A. Zair, M. Holler, A. Guandalini, F. Schapper, J. Biegert, L. Gallmann, U. Keller, A.S. Wyatt, A. Monmayrant, I.A. Walmsley, E. Cormier, T. Auguste, J.P. Caumes, P. Salieres, Quantum path interferences in high-order harmonic generation, Phys. Rev. Lett. 100 (2008) 143902.
[327] M. Lewenstein, P. Salieres, A. Lhuillier, Phase of the atomic polarization in high-order harmonic-generation, Phys. Rev. A 52 (1995) 4747.
[328] E. Frumker, N. Kajumba, J.B. Bertrand, H.J. Woerner, C.T. Hebeisen, P. Hockett, M. Spanner, S. Patchkovskii, G.G. Paulus, D.M. Villeneuve, A. Naumov, P.B. Corkum, Probing polar molecules with high harmonic spectroscopy, Phys. Rev. Lett. 109 (2012) 233904.
[329] M. Kitzler, M. Lezius, Spatial control of recollision wave packets with attosecond precision, Phys. Rev. Lett. 95 (2005) 253001.

[330] M. Fiess, B. Horvath, T. Wittmann, W. Helml, Y. Cheng, B. Zeng, Z. Xu, A. Scrinzi, J. Gagnon, F. Krausz, R. Kienberger, Attosecond control of tunneling ionization and electron trajectories, New J. Phys. 13 (2011) 033031.
[331] Y. Xiang, Y. Niu, H. Feng, Y. Qi, S. Gong, Coherent control of high-order harmonic generation by phase jump pulses, Opt. Express 20 (2012) 19289.
[332] L. Brugnera, F. Frank, D.J. Hoffmann, R. Torres, T. Siegel, J.G. Underwood, E. Springate, C. Froud, E.I.C. Turcu, J.W.G. Tisch, J.P. Marangos, Enhancement of high harmonics generated by field steering of electrons in a two-color orthogonally polarized laser field, Opt. Lett. 35 (2010) 3994.
[333] T. Siegel, R. Torres, D.J. Hoffmann, L. Brugnera, I. Procino, A. Zair, J.G. Underwood, E. Springate, I.C.E. Turcu, L.E. Chipperfield, J.P. Marangos, High harmonic emission from a superposition of multiple unrelated frequency fields, Opt. Express 18 (2010) 6853.
[334] S. Wang, W. Hong, P. Lan, Q. Zhang, P. Lu, Laser parameter influence on quantum path selection in a bichromatic field, J. Phys. B 42 (2009) 105601.
[335] X. Song, Z. Zeng, Y. Fu, B. Cai, R. Li, Y. Cheng, Z. Xu, Quantum path control in few-optical-cycle regime, Phys. Rev. A 76 (2007) 043830.
[336] C.M. Kim, C.H. Nam, Selection of an electron path of high-order harmonic generation in a two-colour femtosecond laser field, J. Phys. B 39 (2006) 3199.
[337] H. Du, L. Luo, X. Wang, B. Hu, Attosecond ionization control for broadband supercontinuum generation using a weak 400-nm few-cycle controlling pulse, Opt. Express 20 (2012) 27226.
[338] C. Serrat, Broadband spectral-phase control in high-order harmonic generation, Phys. Rev. A 87 (2013) 013825.
[339] F. Calegari, C. Vozzi, M. Negro, G. Sansone, F. Frassetto, L. Poletto, P. Villoresi, M. Nisoli, S. De silvestri, S. Stagira, Efficient continuum generation exceeding 200 eV by intense ultrashort two-color driver, Opt. Lett. 34 (2009) 3125.
[340] C. Kim, I. Kim, C. Nam, Generation of a strong attosecond pulse train with an orthogonally polarized two-color laser field, Phys. Rev. A 72 (2005) 033817.
[341] G. Doumy, J. Wheeler, C. Roedig, R. Chirla, P. Agostini, L.F. Dimauro, Attosecond synchronization of high-order harmonics from midinfrared drivers, Phys. Rev. Lett. 102 (2009) 093002.
[342] K.T. Kim, C. Zhang, A.D. Shiner, S.E. Kirkwood, E. Frumker, G. Gariepy, A. Naumov, D.M. Villeneuve, P.B. Corkum, Manipulation of quantum paths for space-time characterization of attosecond pulses, Nat. Phys. 9 (2013) 159.
[343] D. Shafir, H. Soifer, B.D. Bruner, M. Dagan, Y. Mairesse, S. Patchkovskii, M.Y. Ivanov, O. Smirnova, N. Dudovich, Resolving the time when an electron exits a tunnelling barrier, Nature 485 (2012) 343.
[344] J. Yao, Y. Cheng, J. Chen, H. Zhang, H. Xu, H. Xiong, B. Zeng, W. Chu, J. Ni, X. Liu, Z. Xu, Generation of narrow-bandwidth, tunable, coherent xuv radiation using high-order harmonic generation, Phys. Rev. A 83 (2011) 033835.
[345] G. Orlando, P.P. Corso, E. Fiordilino, F. Persico, A three-colour scheme to generate isolated attosecond pulses, J. Phys. B 43 (2010) 025602.
[346] J. Luo, W. Hong, Q. Zhang, Y. Li, P. Lu, Broadband isolated attosecond pulse with high spatiotemporal quality in pre-excited medium by multi-cycle two-color fields, Opt. Express 20 (2012) 21346.
[347] G.-T. Zhang, J. Wu, C.-L. Xia, X.-S. Liu, Enhanced high-order harmonics and an isolated short attosecond pulse generated by using a two-color laser and an extreme-ultraviolet attosecond pulse, Phys. Rev. A 80 (2009) 055404.
[348] G.-T. Zhang, X.-S. Liu, Generation of an extreme ultraviolet supercontinuum and isolated sub-50 as pulse in a two-colour laser field, J. Phys. B 42 (2009) 125603.
[349] Y. Xiang, J. Miao, Y. Niu, S. Gong, R. Li, Z. Xu, Isolated sub-100 attosecond pulse generation driven by a multi-cycle chirped laser pulse and a polarization gating, J. Phys. B 45 (2012) 115601.
[350] Y. Xiang, Y. Niu, S. Gong, Proposal for isolated-attosecond-pulse generation in the multicycle regime through modulation of the carrier wave, Phys. Rev. A 85 (2012) 023808.
[351] C.-L. Xia, X.-S. Liu, Quantum path control and isolated attosecond pulse generation with the combination of two circularly polarized laser pulses, Phys. Rev. A 87 (2013) 043406.
[352] C.-L. Xia, G.-T. Zhang, J. Wu, X.-S. Liu, Single attosecond pulse generation in an orthogonally polarized two-color laser field combined with a static electric field, Phys. Rev. A 81 (2010) 043420.
[353] L. Zhang, Z. Zeng, X. Song, H. Xiong, Y. Zheng, R. Li, Z. Xu, Single sub-100 attosecond pulse generation in a two-colour time-gating laser field, J. Phys. B 41 (2008) 115601.
[354] Y. Yu, X. Song, Y. Fu, R. Li, Y. Cheng, Z. Xu, Theoretical investigation of single attosecond pulse generation in an orthogonally polarized two-color laser field, Opt. Express 16 (2008) 686.
[355] J. Luo, Y. Li, Z. Wang, Q. Zhang, P. Lu, Ultra-short isolated attosecond emission in mid-infrared inhomogeneous fields without CEP stabilization, J. Phys. B 46 (2013) 145602.
[356] T. Hansch, A proposed sub-femtosecond pulse synthesizer using separate phase-locked laser-oscillators, Opt. Commun. 80 (1990) 71.
[357] M. Drescher, M. Hentschel, R. Kienberger, G. Tempea, C. Spielmann, G. Reider, P. Corkum, F. Krausz, X-ray pulses approaching the attosecond frontier, Science 291 (2001) 1923.
[358] T. Popmintchev, M.-C. Chen, P. Arpin, M.M. Murnane, H.C. Kapteyn, The attosecond nonlinear optics of bright coherent X-ray generation, Nature Photon. 4 (2010) 822.
[359] J. Mauritsson, P. Johnsson, R. Lopez-Martens, K. Varju, W. Kornelis, J. Biegert, U. Keller, M. Gaarde, K. Schafer, A. L'Huillier, Measurement and control of the frequency chirp rate of high-order harmonic pulses, Phys. Rev. A 70 (2004) 021801.
[360] K. Varju, Y. Mairesse, P. Agostini, P. Breger, B. Carre, L. Frasinski, E. Gustafsson, P. Johnsson, J. Mauritsson, H. Merdji, P. Monchicourt, A. L'Huillier, P. Salieres, Reconstruction of attosecond pulse trains using an adiabatic phase expansion, Phys. Rev. Lett. 95 (2005) 243901.
[361] M. Kovacev, S. Fomichev, E. Priori, Y. Mairesse, H. Merdji, P. Monchicourt, P. Breger, J. Norin, A. Persson, A. L'Huillier, C. Wahlstrom, B. Carre, P. Salieres, Extreme ultraviolet fourier-transform spectroscopy with high order harmonics, Phys. Rev. Lett. 95 (2005) 223903.
[362] S. Haessler, J. Caillat, P. Salieres, Self-probing of molecules with high harmonic generation, J. Phys. B 44 (2011) 203001.
[363] R. Lopez-Martens, K. Varju, P. Johnsson, J. Mauritsson, Y. Mairesse, P. Salieres, M. Gaarde, K. Schafer, A. Persson, S. Svanberg, C. Wahlstrom, A. L'Huillier, Amplitude and phase control of attosecond light pulses, Phys. Rev. Lett. 94 (2005) 033001.
[364] J. Mauritsson, P. Johnsson, E. Gustafsson, A. L'Huillier, K.J. Schafer, M.B. Gaarde, Attosecond pulse trains generated using two color laser fields, Phys. Rev. Lett. 97 (2006) 013001.
[365] T. Remetter, P. Johnsson, J. Mauritsson, K. Varju, Y. Ni, F. Lepine, E. Gustafsson, M. Kling, J. Khan, R. Lopez-Martens, K. Schafer, M. Vrakking, A. L'Huillier, Attosecond electron wave packet interferometry, Nat. Phys. 2 (2006) 323.
[366] P. Johnsson, J. Mauritsson, T. Remetter, A. L'Huillier, K.J. Schafer, Attosecond control of ionization by wave-packet interference, Phys. Rev. Lett. 99 (2007) 233001.
[367] J. Mauritsson, P. Johnsson, E. Mansten, M. Swoboda, T. Ruchon, A. L'Huillier, K.J. Schafer, Coherent electron scattering captured by an attosecond quantum stroboscope, Phys. Rev. Lett. 100 (2008) 073003.
[368] A. Mikkelsen, J. Schwenke, T. Fordell, G. Luo, K. Klunder, E. Hilner, N. Anttu, A.A. Zakharov, E. Lundgren, J. Mauritsson, J.N. Andersen, H.Q. Xu, A. L'Huillier, Photoemission electron microscopy using extreme ultraviolet attosecond pulse trains, Rev. Sci. Instrum. 80 (2009) 123703.
[369] F. Kelkensberg, C. Lefebvre, W. Siu, O. Ghafur, T.T. Nguyen-Dang, O. Atabek, A. Keller, V. Serov, P. Johnsson, M. Swoboda, T. Remetter, A. L'Huillier, S. Zherebtsov, G. Sansone, E. Benedetti, F. Ferrari, M. Nisoli, F. Lepine, M.F. Kling, M.J.J. Vrakking, Molecular dissociative ionization and wave-packet dynamics studied using two-color xuv and ir pump–probe spectroscopy, Phys. Rev. Lett. 103 (2009) 123005.
[370] E. Mansten, J.M. Dahlstrom, J. Mauritsson, T. Ruchon, A. L'Huillier, J. Tate, M.B. Gaarde, P. Eckle, A. Guandalini, M. Holler, F. Schapper, L. Gallmann, U. Keller, Spectral signature of short attosecond pulse trains, Phys. Rev. Lett. 102 (2009) 083002.
[371] J. Mauritsson, T. Remetter, M. Swoboda, K. Kluender, A. L'Huillier, K.J. Schafer, O. Ghafur, F. Kelkensberg, W. Siu, P. Johnsson, M.J.J. Vrakking, I. Znakovskaya, T. Uphues, S. Zherebtsov, M.F. Kling, F. Lepine, E. Benedetti, F. Ferrari, G. Sansone, M. Nisoli, Attosecond electron spectroscopy using a novel interferometric pump–probe technique, Phys. Rev. Lett. 105 (2010) 053001.

[372] M. Swoboda, T. Fordell, K. Klunder, J.M. Dahlstrom, M. Miranda, C. Buth, K.J. Schafer, J. Mauritsson, A. L'Huillier, M. Gisselbrecht, Phase measurement of resonant two-photon ionization in helium, Phys. Rev. Lett. 104 (2010) 103003.
[373] P. Rudawski, C.M. Heyl, F. Brizuela, J. Schwenke, A. Persson, E. Mansten, R. Rakowski, L. Rading, F. Campi, B. Kim, P. Johnsson, A. L'Huillier, A high-flux high-order harmonic source, Rev. Sci. Instrum. 84 (2013) 073103.
[374] F. Le kien, K. Midorikawa, A. Suda, Attosecond pulse generation using high harmonics in the multicycle regime of the driver pulse, Phys. Rev. A 58 (1998) 3311.
[375] Y. Tamaki, J. Itatani, Y. Nagata, M. Obara, K. Midorikawa, Highly efficient, phase-matched high-harmonic generation by a self-guided laser beam, Phys. Rev. Lett. 82 (1999) 1422.
[376] E. Takahashi, Y. Nabekawa, T. Otsuka, M. Obara, K. Midorikawa, Generation of highly coherent submicrojoule soft x rays by high-order harmonics, Phys. Rev. A 66 (2002) 021802.
[377] Y. Nabekawa, H. Hasegawa, E. Takahashi, K. Midorikawa, Production of doubly charged helium ions by two-photon absorption of an intense sub-10-fs soft x-ray pulse at 42 eV photon energy, Phys. Rev. Lett. 94 (2005) 043001.
[378] Y. Nabekawa, T. Shimizu, T. Okino, K. Furusawa, H. Hasegawa, K. Yamanouchi, K. Midorikawa, Conclusive evidence of an attosecond pulse train observed with the mode-resolved autocorrelation technique, Phys. Rev. Lett. 96 (2006) 083901.
[379] Y. Nabekawa, T. Shimizu, T. Okino, K. Furusawa, H. Hasegawa, K. Yamanouchi, K. Midorikawa, Interferometric autocorrelation of an attosecond pulse train in the single-cycle regime, Phys. Rev. Lett. 97 (2006) 153904.
[380] E.J. Takahashi, T. Kanai, K.L. Ishikawa, Y. Nabekawa, K. Midorikawa, Coherent Water Window X Ray by Phase-Matched High-Order Harmonic Generation in Neutral Media, Phys. Rev. Lett. 101 (2008) 253901.
[381] Y. Nabekawa, T. Shimizu, Y. Furukawa, E.J. Takahashi, K. Midorikawa, Interferometry of Attosecond Pulse Trains in the Extreme Ultraviolet Wavelength Region, Phys. Rev. Lett. 102 (2009) 213904.
[382] E.J. Takahashi, P. Lan, O.D. Muecke, Y. Nabekawa, K. Midorikawa, Infrared two-color multicycle laser field synthesis for generating an intense attosecond pulse, Phys. Rev. Lett. 104 (2010) 233901.
[383] G. Sansone, E. Benedetti, F. Calegari, C. Vozzi, L. Avaldi, R. Flammini, L. Polatto, P. Villoresi, C. Altucci, R. Velotta, S. Stagira, S.D. Silvestri, M. Nisoli, Isolated single-cycle attosecond pulses, Science 314 (2006) 443.
[384] F. Ferrari, F. Calegari, M. Lucchini, C. Vozzi, S. Stagira, G. Sansone, M. Nisoli, High-energy isolated attosecond pulses generated by above-saturation few-cycle fields, Nature Photon. 4 (2010) 875.
[385] M.J. Abel, T. Pfeifer, P.M. Nagel, W. Boutu, M.J. Bell, C.P. Steiner, D.M. Neumark, S.R. Leone, Isolated attosecond pulses from ionization gating of high-harmonic emission, Chem. Phys. 366 (2009) 9.
[386] H. Mashiko, M.J. Bell, A.R. Beck, M.J. Abel, P.M. Nagel, C.P. Steiner, J. Robinson, D.M. Neumark, S.R. Leone, Tunable frequency-controlled isolated attosecond pulses characterized by either 750 nm or 400 nm wavelength streak fields, Opt. Express 18 (2010) 25887.
[387] A. Baltuska, T. Udem, M. Uiberacker, M. Hentschel, E. Goulielmakis, C. Gohle, R. Holzwarth, V. Yakoviev, A. Scrinzi, T. Hansch, F. Krausz, Attosecond control of electronic processes by intense light fields, Nature 421 (2003) 611.
[388] T. Witting, F. Frank, W.A. Okell, C.A. Arrell, J.P. Marangos, J.W.G. Tisch, Sub-4-fs laser pulse characterization by spatially resolved spectral shearing interferometry and attosecond streaking, J. Phys. B 45 (2012) 074014.
[389] I. Thomann, A. Bahabad, X. Liu, R. Trebino, M.M. Murnane, H.C. Kapteyn, Characterizing isolated attosecond pulses from hollow-core waveguides using multi-cycle driving pulses, Opt. Express 17 (2009) 4611.
[390] A. Jullien, T. Pfeifer, M.J. Abel, P.M. Nagel, M.J. Bell, D.M. Neumark, S.R. Leone, Ionization phase-match gating for wavelength-tunable isolated attosecond pulse generation, Appl. Phys. B 93 (2008) 433.
[391] I. Sola, E. Mevel, L. Elouga, E. Constant, V. Strelkov, L. Poletto, P. Villoresi, E. Benedetti, J. Caumes, S. Stagira, C. Vozzi, G. Sansone, M. Nisoli, Controlling attosecond electron dynamics by phase-stabilized polarization gating, Nat. Phys. 2 (2006) 319.
[392] Z. Chang, Single attosecond pulse and xuv supercontinuum in the high-order harmonic plateau, Phys. Rev. A 70 (2004) 043802.
[393] H. Mashiko, S. Gilbertson, C. Li, S.D. Khan, M.M. Shakya, E. Moon, Z. Chang, Double optical gating of high-order harmonic generation with carrier-envelope phase stabilized lasers, Phys. Rev. Lett. 100 (2008) 103906.
[394] H. Mashiko, S. Gilbertson, M. Chini, X. Feng, C. Yun, H. Wang, S.D. Khan, S. Chen, Z. Chang, Extreme ultraviolet supercontinua supporting pulse durations of less than one atomic unit of time, Opt. Lett. 34 (2009) 3337.
[395] X. Feng, S. Gilbertson, H. Mashiko, H. Wang, S.D. Khan, M. Chini, Y. Wu, K. Zhao, Z. Chang, Generation of isolated attosecond pulses with 20 to 28 femtosecond lasers, Phys. Rev. Lett. 103 (2009) 183901.
[396] K. Zhao, Q. Zhang, M. Chini, Y. Wu, X. Wang, Z. Chang, Tailoring a 67 attosecond pulse through advantageous phase-mismatch, Opt. Lett. 37 (2012) 3891.
[397] M. Nisoli, G. Sansone, S. Stagira, S. De silvestri, C. Vozzi, M. Pascolini, L. Poletto, P. Villoresi, G. Tondello, Effects of carrier-envelope phase differences of few-optical-cycle light pulses in single-shot high-order-harmonic spectra, Phys. Rev. Lett. 91 (2003) 213905.
[398] C.A. Haworth, L.E. Chipperfield, J.S. Robinson, P.L. Knight, J.P. Marangos, J.W.G. Tisch, Half-cycle cutoffs in harmonic spectra and robust carrier-envelope phase retrieval, Nat. Phys. 3 (2007) 52.
[399] R. Kienberger, E. Goulielmakis, M. Uiberacker, A. Baltuska, V. Yakovlev, F. Bammer, A. Scrinzi, T. Westerwalbesloh, U. Kleineberg, U. Heinzmann, M. Drescher, F. Krausz, Atomic transient recorder, Nature 427 (2004) 817.
[400] S. Gilbertson, S.D. Khan, Y. Wu, M. Chini, Z. Chang, Isolated attosecond pulse generation without the need to stabilize the carrier-envelope phase of driving lasers, Phys. Rev. Lett. 105 (2010) 093902.
[401] H. Mashiko, K. Oguri, T. Sogawa, Attosecond pulse generation in carbon K-edge region (284 eV) with sub-250 mu J driving laser using generalized double optical gating method, Appl. Phys. Lett. 102 (2013) 171111.
[402] H. Vincenti, F. Quere, Attosecond lighthouses: How to use spatiotemporally coupled light fields to generate isolated attosecond pulses, Phys. Rev. Lett. 108 (2012) 113904.
[403] K.T. Kim, C. Zhang, T. Ruchon, J.-F. Hergott, T. Auguste, D.M. Villeneuve, P.B. Corkum, F. Quere, Photonic streaking of attosecond pulse trains, Nature Photon. 7 (2013) 651.
[404] H.-S. Chan, Z.-M. Hsieh, W.-H. Liang, A.H. Kung, C.-K. Lee, C.-J. Lai, R.-P. Pan, L.-H. Peng, Synthesis and measurement of ultrafast waveforms from five discrete optical harmonics, Science 331 (2011) 1165.
[405] D.D. Yavuz, Toward synthesis of arbitrary optical waveforms, Science 331 (2011) 1142.
[406] G. Laurent, W. Cao, I. Ben-Itzhak, C.L. Cocke, Attosecond pulse characterization, Opt. Express 21 (2013) 16914.
[407] Y. Mairesse, F. Quere, Frequency-resolved optical gating for complete reconstruction of attosecond bursts, Phys. Rev. A 71 (2005) 011401.
[408] J. Gagnon, E. Goulielmakis, V.S. Yakovlev, The accurate FROG characterization of attosecond pulses from streaking measurements, Appl. Phys. B 92 (2008) 25.
[409] D. Kane, Recent progress toward real-time measurement of ultrashort laser pulses, IEEE J. Quantum Electron. 35 (1999) 421.
[410] M. Chini, S. Gilbertson, S.D. Khan, Z. Chang, Characterizing ultrabroadband attosecond lasers, Opt. Express 18 (2010) 13006.
[411] C.-C. Chen, Y.-S. Chen, C.-B. Huang, M.-C. Chen, S.-D. Yang, Noniterative data inversion of phase retrieval by omega oscillating filtering for optical arbitrary waveform measurement, Opt. Lett. 38 (2013) 2011.
[412] M.B. Gaarde, J.L. Tate, K.J. Schafer, Macroscopic aspects of attosecond pulse generation, J. Phys. B 41 (2008) 132001.
[413] K.T. Kim, D.M. Villeneuve, P.B. Corkum, Manipulating quantum paths for novel attosecond measurement methods, Nature Photon. 8 (2014) 187.
[414] T. Morishita, A.-T. Le, Z. Chen, C.D. Lin, Accurate retrieval of structural information from laser-induced photoelectron and high-order harmonic spectra by few-cycle laser pulses, Phys. Rev. Lett. 100 (2008) 013903.
[415] G. Wang, C. Jin, A.-T. Le, C.D. Lin, Conditions for extracting photoionization cross sections from laser-induced high-order-harmonic spectra, Phys. Rev. A 86 (2012) 015401.

[416] J. Levesque, D. Zeidler, J.P. Marangos, P.B. Corkum, D.M. Villeneuve, High harmonic generation and the role of atomic orbital wave functions, Phys. Rev. Lett. 98 (2007) 183903.
[417] J.W. Cooper, Photoionization from outer atomic subshells. a model study, Phys. Rev. 128 (1962) 681.
[418] S. Pabst, L. Greenman, D.A. Mazziotti, R. Santra, Impact of multichannel and multipole effects on the Cooper minimum in the high-order-harmonic spectrum of argon, Phys. Rev. A 85 (2012) 023411.
[419] J. Higuet, H. Ruf, N. Thire, R. Cireasa, E. Constant, E. Cormier, D. Descamps, E. Mevel, S. Petit, B. Pons, Y. Mairesse, B. Fabre, High-order harmonic spectroscopy of the Cooper minimum in argon: Experimental and theoretical study, Phys. Rev. A 83 (2011) 053401.
[420] J.B. Bertrand, H.J. Woerner, P. Hockett, D.M. Villeneuve, P.B. Corkum, Revealing the cooper minimum of n_2 by molecular frame high-harmonic spectroscopy, Phys. Rev. Lett. 109 (2012) 143001.
[421] S. Pabst, R. Santra, Strong-field many-body physics and the giant enhancement in the high-harmonic spectrum of xenon, Phys. Rev. Lett. 111 (2013) 233005.
[422] A.D. Shiner, B.E. Schmidt, C. Trallero-Herrero, H.J. Woerner, S. Patchkovskii, P.B. Corkum, J.-C. Kieffer, F. Legare, D.M. Villeneuve, Probing collective multi-electron dynamics in xenon with high-harmonic spectroscopy, Nat. Phys. 7 (2011) 464.
[423] M. Lein, N. Hay, R. Velotta, J. Marangos, P. Knight, Role of the intramolecular phase in high-harmonic generation, Phys. Rev. Lett. 88 (2002) 183903.
[424] C. Vozzi, F. Calegari, E. Benedetti, J. Caumes, G. Sansone, S. Stagira, M. Nisoli, R. Torres, E. Heesel, N. Kajumba, J. Marangos, C. Altucci, R. Velotta, Controlling two-center interference in molecular high harmonic generation, Phys. Rev. Lett. 95 (2005) 153902.
[425] T. Kanai, S. Minemoto, H. Sakai, Quantum interference during high-order harmonic generation from aligned molecules, Nature 435 (2005) 470.
[426] O. Smirnova, Y. Mairesse, S. Patchkovskii, N. Dudovich, D. Villeneuve, P. Corkum, M.Y. Ivanov, High harmonic interferometry of multi-electron dynamics in molecules, Nature 460 (2009) 972.
[427] C. Vozzi, M. Negro, F. Calegari, G. Sansone, M. Nisoli, S. De silvestri, S. Stagira, Generalized molecular orbital tomography, Nat. Phys. 7 (2011) 822.
[428] S. Haessler, J. Caillat, W. Boutu, C. Giovanetti-Teixeira, T. Ruchon, T. Auguste, Z. Diveki, P. Breger, A. Maquet, B. Carre, R. Taieb, P. Salieres, Attosecond imaging of molecular electronic wavepackets, Nat. Phys. 6 (2010) 200.
[429] J.B. Bertrand, H.J. Woerner, P. Salieres, D.M. Villeneuve, P.B. Corkurni, Linked attosecond phase interferometry for molecular frame measurements, Nat. Phys. 9 (2013) 174.
[430] M.J.J. Vrakking, Attosecond imaging, Phys. Chem. Chem. Phys. 16 (2014) 2775.
[431] E. Goulielmakis, V.S. Yakovlev, A.L. Cavalieri, M. Uiberacker, V. Pervak, A. Apolonski, R. Kienberger, U. Kleineberg, F. Krausz, Attosecond control and measurement: Lightwave electronics, Science 317 (2007) 769.
[432] P.B. Corkum, F. Krausz, Attosecond science, Nat. Phys. 3 (2007) 381.
[433] M.F. Kling, M.J.J. Vrakking, Attosecond electron dynamics, Annu. Rev. Phys. Chem. 59 (2008) 463.
[434] L. Gallmann, C. Cirelli, U. Keller, Attosecond science: Recent highlights and future trends, Annu. Rev. Phys. Chem. 63 (2012) 447.
[435] F. Krausz, M.I. Stockman, Attosecond metrology: from electron capture to future signal processing, Nature Photon. 8 (2014) 205.
[436] E. Goulielmakis, M. Uiberacker, R. Kienberger, A. Baltuska, V. Yakovlev, A. Scrinzi, T. Westerwalbesloh, U. Kleineberg, U. Heinzmann, M. Drescher, F. Krausz, Direct measurement of light waves, Science 305 (2004) 1267.
[437] S. Neppl, R. Ernstorfer, E.M. Bothschafter, A.L. Cavalieri, D. Menzel, J.V. Barth, F. Krausz, R. Kienberger, P. Feulner, Attosecond time-resolved photoemission from core and valence states of magnesium, Phys. Rev. Lett. 109 (2012) 087401.
[438] K. Klunder, J.M. Dahlstrom, M. Gisselbrecht, T. Fordell, M. Swoboda, D. Guenot, P. Johnsson, J. Caillat, J. Mauritsson, A. Maquet, R. Taieb, A. L'Huillier, Probing single-photon ionization on the attosecond time scale, Phys. Rev. Lett. 106 (2011) 143002.
[439] N. Shivaram, H. Timmers, X.-M. Tong, A. Sandhu, Attosecond-resolved evolution of a laser-dressed helium atom: Interfering excitation paths and quantum phases, Phys. Rev. Lett. 108 (2012) 193002.
[440] K. Klunder, P. Johnsson, M. Swoboda, A. L'Huillier, G. Sansone, M. Nisoli, M.J.J. Vrakking, K.J. Schafer, J. Mauritsson, Reconstruction of attosecond electron wave packets using quantum state holography, Phys. Rev. A 88 (2013) 033404.
[441] M. Kling, C. Siedschlag, A. Verhoef, J. Khan, M. Schultze, T. Uphues, Y. Ni, M. Uiberacker, M. Drescher, F. Krausz, M. Vrakking, Control of electron localization in molecular dissociation, Science 312 (2006) 246.
[442] A. Buck, M. Nicolai, K. Schmid, C.M.S. Sears, A. Saevert, J.M. Mikhailova, F. Krausz, M.C. Kaluza, L. Veisz, Real-time observation of laser-driven electron acceleration, Nat. Phys. 7 (2011) 543.
[443] D. Guénot, K. Klünder, C.L. Arnold, D. Kroon, J.M. Dahlström, M. Miranda, T. Fordell, M. Gisselbrecht, P. Johnsson, J. Mauritsson, E. Lindroth, A. Maquet, R. Taïeb, A. L'Huillier, A.S. Kheifets, Photoemission-time-delay measurements and calculations close to the 3s-ionization-cross-section minimum in argon, Phys. Rev. A 85 (2012) 053424.
[444] F.O. Kirchner, A. Gliserin, F. Krausz, P. Baum, Laser streaking of free electrons at 25 keV, Nature Photon. 8 (2014) 52.
[445] H. Wang, M. Chini, S. Chen, C.-H. Zhang, F. He, Y. Cheng, Y. Wu, U. Thumm, Z. Chang, Attosecond time-resolved autoionization of argon, Phys. Rev. Lett. 105 (2010) 143002.
[446] M. Holler, F. Schapper, L. Gallmann, U. Keller, Attosecond Electron Wave-Packet Interference Observed by Transient Absorption, Phys. Rev. Lett. 106 (2011) 123601.
[447] M.B. Gaarde, C. Buth, J.L. Tate, K.J. Schafer, Transient absorption and reshaping of ultrafast XUV light by laser-dressed helium, Phys. Rev. A 83 (2011) 013419.
[448] R. Santra, V.S. Yakovlev, T. Pfeifer, Z.-H. Loh, Theory of attosecond transient absorption spectroscopy of strong-field-generated ions, Phys. Rev. A 83 (2011) 033405.
[449] L. Argenti, C. Ott, T. Pfeifer, F. Martin, Attosecond transient absorption spectroscopy of doubly-excited states in helium, J. Phys. Conf. Ser. 488 (2014) 032030.
[450] P. Eckle, M. Smolarski, P. Schlup, J. Biegert, A. Staudte, M. Schoeffler, H.G. Muller, R. Doerner, U. Keller, Attosecond angular streaking, Nat. Phys. 4 (2008) 565.
[451] J. Wu, M. Magrakvelidze, L.P.H. Schmidt, M. Kunitski, T. Pfeifer, M. Schoeffler, M. Pitzer, M. Richter, S. Voss, H. Sann, H. Kim, J. Lower, T. Jahnke, A. Czasch, U. Thumm, R. Doerner, Understanding the role of phase in chemical bond breaking with coincidence angular streaking, Nat. Commun. 4 (2013) 2177.
[452] W.T. Pollard, S.Y. Lee, R.A. Mathies, Wave packet theory of dynamic absorption-spectra in femtosecond pump–probe experiments, J. Chem. Phys. 92 (1990) 4012.
[453] R.A. Mathies, C.H.B. Cruz, W.T. Pollard, C.V. Shank, Direct observation of the femtosecond excited-state cis-trans isomerization in bacteriorhodopsin, Science 240 (1988) 777.
[454] Z.-H. Loh, M. Khalil, R.E. Correa, R. Santra, C. Buth, S.R. Leone, Quantum state-resolved probing of strong-field-ionized xenon atoms using femtosecond high-order harmonic transient absorption spectroscopy, Phys. Rev. Lett. 98 (2007) 143601.
[455] Z.-H. Loh, S.R. Leone, Ultrafast strong-field dissociative ionization dynamics of CH_2Br_2 probed by femtosecond soft x-ray transient absorption spectroscopy, J. Chem. Phys. 128 (2008) 204302.
[456] A.N. Pfeiffer, C. Cirelli, M. Smolarski, D. Dimitrovski, M. Abu-samha, L.B. Madsen, U. Keller, Attoclock reveals natural coordinates of the laser-induced tunnelling current flow in atoms, Nat. Phys. 8 (2012) 76.
[457] A.N. Pfeiffer, C. Cirelli, M. Smolarski, R. Doerner, U. Keller, Timing the release in sequential double ionization, Nat. Phys. 7 (2011) 428.
[458] J.-W. Geng, L.-Y. Peng, S.-N. Song, Q. Gong, Interference structures in photoelectron spectra of atoms ionized by XUV pulses in the presence of a strong IR field, Phys. Rev. A 88 (2013) 053418.
[459] C. Liu, M. Reduzzi, A. Trabattoni, A. Sunilkumar, A. Dubrouil, F. Calegari, M. Nisoli, G. Sansone, Carrier-envelope phase effects of a single attosecond pulse in two-color photoionization, Phys. Rev. Lett. 111 (2013) 123901.
[460] G. Yudin, M. Ivanov, Nonadiabatic tunnel ionization: Looking inside a laser cycle, Phys. Rev. A 64 (2001) 013409.

[461] M. Ivanov, M. Spanner, O. Smirnova, Anatomy of strong field ionization, J. Modern Opt. 52 (2005) 165.
[462] D.I. Bondar, Instantaneous multiphoton ionization rate and initial distribution of electron momentum, Phys. Rev. A 78 (2008) 015405.
[463] L.-Y. Peng, E.A. Pronin, A.F. Starace, Attosecond pulse carrier-envelope phase effects on ionized electron momentum and energy distributions: roles of frequency, intensity and an additional IR pulse, New J. Phys. 10 (2008) 025030.
[464] X.-F. Hou, L.-Y. Peng, Q.-C. Ning, Q. Gong, Attosecond streaking of molecules in the low-energy region studied by a wavefunction splitting scheme, J. Phys. B 45 (2012) 074019.
[465] J.-W. Geng, L.-Y. Peng, M.-H. Xu, Q. Gong, Attosecond streaking in the low-energy region, J. Phys. Conf. Ser. 488 (2014) 012003.
[466] K. Varju, P. Johnsson, J. Mauritsson, T. Remetter, T. Ruchon, Y. Ni, F. Lepine, M. Kling, J. Khan, K.J. Schafer, M.J.J. Vrakking, A. L'Huillier, Angularly resolved electron wave packet interferences, J. Phys. B 39 (2006) 3983.
[467] C. Liu, M. Nisoli, Attosecond electron interferometry for measurement of the quantum phase of free-electron wave packets, Phys. Rev. A 86 (2012) 053404.
[468] A. Chacon, M. Lein, C. Ruiz, Retrieval of the amplitude and phase of the dipole matrix element by attosecond electron-wave-packet interferometry, Phys. Rev. A 87 (2013) 023408.
[469] O. Smirnova, M. Spanner, M.Y. Ivanov, Coulomb and polarization effects in laser-assisted XUV ionization, J. Phys. B 39 (2006) S323. 10th International Conference on Multiphoton Processes (ICOMP 2005), Orford, CANADA, OCT 09-14, 2005.
[470] G.L. Yudin, S. Patchkovskii, P.B. Corkum, A.D. Bandrauk, Attosecond photoelectron interference in the separable Coulomb-Volkov continuum, J. Phys. B 40 (2007) F93.
[471] C.H. Zhang, U. Thumm, Electron-ion interaction effects in attosecond time-resolved photoelectron spectra, Phys. Rev. A 82 (2010) 043405.
[472] J. Gagnon, F. Krausz, V.S. Yakovlev, Laser-dressed scattering of an attosecond electron wave packet, Phys. Rev. A 82 (2010) 033435.
[473] A.K. Kazansky, N.M. Kabachnik, Theoretical description of atomic photoionization by an attosecond XUV pulse in a strong laser field: effects of rescattering and orbital polarization, J. Phys. B 40 (2007) 2163.
[474] A.K. Kazansky, A.V. Bozhevolnov, I.P. Sazhina, N.M. Kabachnik, Attosecond near-threshold photoionization in a strong laser field, Phys. Rev. A 90 (2014) 033409.
[475] O. Smirnova, S. Patchkovskii, M. Spanner, Direct XUV probing of attosecond electron recollision, Phys. Rev. Lett. 98 (2007) 123001.
[476] L.-Y. Peng, A.F. Starace, Attosecond pulse carrier-envelope phase effects on ionized electron momentum and energy distributions, Phys. Rev. A 76 (2007) 043401.
[477] L.-Y. Peng, F. Tan, Q. Gong, E.A. Pronin, A.F. Starace, Few-cycle attosecond pulse chirp effects on asymmetries in ionized electron momentum distributions, Phys. Rev. A 80 (2009) 013407.
[478] A.M. Steinberg, P.G. Kwiat, R.Y. Chiao, Measurement of the single-photon tunneling time, Phys. Rev. Lett. 71 (1993) 708.
[479] A.M. Steinberg, How much time does a tunneling particle spend in the barrier region? Phys. Rev. Lett. 74 (1995) 2405.
[480] J. Muga, R. Salamayato, I.L. Egusquiza (Eds.), Time in Quantum Mechanics - Vol. 1, Springer, 2008.
[481] J.G. Muga, A. Ruschhaupt, A. Campo (Eds.), Time in Quantum Mechanics - Vol. 2, Springer, Berlin. Heidelberg, 2009.
[482] J.M. Dahlström, A. L'huillier, A. Maquet, Introduction to attosecond delays in photoionization, J. Phys. B 45 (2012) 183001.
[483] J.M. Dahlström, D. Guénot, K. Klünder, M. Gisselbrecht, J. Mauritsson, A. L'Huillier, A. Maquet, R. Taïeb, Theory of attosecond delays in laser-assisted photoionization, Chem. Phys. 414 (2013) 53.
[484] A.N. Pfeiffer, C. Cirelli, M. Smolarski, U. Keller, Recent attoclock measurements of strong field ionization, Chem. Phys. 414 (2013) 84. Attosecond spectroscopy.
[485] A.S. Landsman, U. Keller, Attosecond science and the tunneling time problem, Phys. Rep. 547 (2015) 1.
[486] R. Pazourek, S. Nagele, J. Burgdörfer, Attosecond chronoscopy of photoemission, Rev. Modern Phys. (2015) submitted.
[487] A. Maquet, J. Caillat, R. Taeb, Attosecond delays in photoionization: time and quantum mechanics, J. Phys. B 47 (2014) 204004.
[488] L.E. Eisenbud, (Ph.D. thesis), Princeton University, 1948, unpublished.
[489] E.P. Wigner, Lower limit for the energy derivative of the scattering phase shift, Phys. Rev. 98 (1955) 145.
[490] P.A. Martin, Time delay of quantum scattering processes, Acta Phys. Austriaca Suppl. 23 (1981) 157.
[491] C.A.A. de Carvalho, H.M. Nussenzveig, Time delay, Phys. Rep. 364 (2002) 83.
[492] E.E. Kolomeitsev, D.N. Voskresensky, Time delays and advances in classical and quantum systems, J. Phys. G 40 (2013) 113101.
[493] F.T. Smith, Lifetime matrix in collision theory, Phys. Rev. 118 (1960) 349.
[494] E. Pollak, W.H. Miller, New physical interpretation for time in scattering theory, Phys. Rev. Lett. 53 (1984) 115.
[495] J. Muñoz, D. Seidel, J.G. Muga, Relation between quantum dwell times and flux–flux correlations, Phys. Rev. A 79 (2009) 012108.
[496] P. Grossel, The phase delay and its complex time: From stationary states up to wave packets, Ann. Phys. 330 (2013) 74.
[497] S. Nagele, R. Pazourek, J. Feist, K. Doblhoff-Dier, C. Lemell, K. Tokési, J. Burgdörfer, Time-resolved photoemission by attosecond streaking: extraction of time information, J. Phys. B 44 (2011) 081001.
[498] S. Nagele, R. Pazourek, M. Wais, G. Wachter, J. Burgdörfer, Time-resolved photoemission using attosecond streaking, J. Phys. Conf. Ser. 488 (2014) 012004.
[499] J. Su, H. Ni, A. Becker, A. Jaron-Becker, Theoretical analysis of time delays and streaking effects in xuv photoionization, J. Modern Opt. 60 (2013) 1484.
[500] C.-H. Zhang, U. Thumm, Streaking and wigner time delays in photoemission from atoms and surfaces, Phys. Rev. A 84 (2011) 033401.
[501] O. Smirnova, A.S. Mouritzen, S. Patchkovskii, M.Y. Ivanov, Coulomb-laser coupling in laser-assisted photoionization and molecular tomography, J. Phys. B 40 (2007) F197.
[502] M. Ivanov, O. Smirnova, How accurate is the attosecond streak camera, Phys. Rev. Lett. 107 (2011) 213605.
[503] Q.-C. Ning, L.-Y. Peng, S.-N. Song, W.-C. Jiang, S. Nagele, R. Pazourek, J. Burgdörfer, Q. Gong, Attosecond streaking of Cohen–Fano interferences in the photoionization of H_2^+, Phys. Rev. A 90 (2014) 013423.
[504] G. Hadinger, M. Aubert-Frécon, G. Hadinger, Continuum wavefunctions for one-electron two-centre molecular ions from the killingbeck-miller method, J. Phys. B 29 (1996) 2951.
[505] X.F. Hou, L.Y. Peng, Q.C. Ning, Q. Gong, Attosecond streaking of molecules in the low-energy region studied by a wavefunction splitting scheme, J. Phys. B 45 (2012) 074019.
[506] L. Tao, C.W. McCurdy, T.N. Rescigno, Grid-based methods for diatomic quantum scattering problems: A finite-element discrete-variable representation in prolate spheroidal coordinates, Phys. Rev. A 79 (2009) 012719.
[507] I.A. Ivanov, A.S. Kheifets, V.V. Serov, Attosecond time-delay spectroscopy of the hydrogen molecule, Phys. Rev. A 86 (2012) 063422.
[508] I.A. Ivanov, Double photoionization of the hydrogen molecule from the viewpoint of the time-delay theory, Phys. Rev. A 86 (2012) 023419.
[509] V.V. Serov, V.L. Derbov, T.A. Sergeeva, Interpretation of time delay in the ionization of two-center systems, Phys. Rev. A 87 (2013) 063414.
[510] J.C. Baggesen, L.B. Madsen, Polarization effects in attosecond photoelectron spectroscopy, Phys. Rev. Lett. 104 (2010) 043602.
[511] H. W. van der Hart, When does photoemission begin, Science 328 (2010) 1645.
[512] A.S. Kheifets, I.A. Ivanov, Delay in atomic photoionization, Phys. Rev. Lett. 105 (2010) 233002.
[513] S. Nagele, R. Pazourek, J. Feist, J. Burgdörfer, Time shifts in photoemission from a fully correlated two-electron model system, Phys. Rev. A 85 (2012) 033401.
[514] R. Pazourek, J. Feist, S. Nagele, J. Burgdörfer, Attosecond streaking of correlated two-electron transitions in helium, Phys. Rev. Lett. 108 (2012) 163001.
[515] L.R. Moore, M.A. Lysaght, J.S. Parker, H. W. van der Hart, K. T. Taylor, Time delay between photoemission from the 2p and 2s subshells of neon, Phys. Rev. A 84 (2011) 061404(R).
[516] A.S. Kheifets, Time delay in valence-shell photoionization of noble-gas atoms, Phys. Rev. A 87 (2013) 063404.
[517] T. Carette, J.M. Dahlström, L. Argenti, E. Lindroth, Multiconfigurational Hartree–Fock close-coupling ansatz: Application to the argon photoionization cross section and delays, Phys. Rev. A 87 (2013) 023420.

[518] G. Dixit, H.S. Chakraborty, M.E.-A. Madjet, Time delay in the recoiling valence photoemission of ar endohedrally confined in c_{60}, Phys. Rev. Lett. 111 (2013) 203003.
[519] J. Feist, O. Zatsarinny, S. Nagele, R. Pazourek, J. Burgdörfer, X. Guan, K. Bartschat, B.I. Schneider, Time delays for attosecond streaking in photoionization of neon, Phys. Rev. A 89 (2014) 033417.
[520] R. Pazourek, S. Nagele, J. Burgdörfer, Probing time-ordering in two-photon double ionization of helium on the attosecond time scale, arXiv:1405.1779v1, 2014.
[521] T. Mercouris, Y. Komninos, C.A. Nicolaides, The state-specific expansion approach to the solution of the polyelectronic time-dependent schrödinger equation for atoms and molecules in unstable states, Adv. Quantum Chem. 60 (2010) 333.
[522] V.S. Yakovlev, J. Gagnon, N. Karpowicz, F. Krausz, Attosecond streaking enables the measurement of quantum phase, Phys. Rev. Lett. 105 (2010) 073001.
[523] J.M. Dahlström, T. Carette, E. Lindroth, Diagrammatic approach to attosecond delays in photoionization, Phys. Rev. A 86 (2012) 061402(R).
[524] S.B. Schoun, R. Chirla, J. Wheeler, C. Roedig, P. Agostini, L.F. Dimauro, K.J. Schafer, M.B. Gaarde, Attosecond pulse shaping around a cooper minimum, Phys. Rev. Lett. 112 (2014) 153001.
[525] J.M. Dahlström, E. Lindroth, Study of attosecond delays using perturbation diagrams and exterior complex scaling, J. Phys. B 47 (2014) 124012.
[526] C. Lemell, B. Solleder, K. Tokési, J. Burgdörfer, Simulation of attosecond streaking of electrons emitted from a tungsten surface, Phys. Rev. A 79 (2009) 062901.
[527] A.K. Kazansky, P.M. Echenique, One-electron model for the electronic response of metal surfaces to subfemtosecond photoexcitation, Phys. Rev. Lett. 102 (2009) 177401.
[528] C.-H. Zhang, U. Thumm, Attosecond photoelectron spectroscopy of metal surfaces, Phys. Rev. Lett. 102 (2009) 123601.
[529] E.E. Krasovskii, V.M. Silkin, V.U. Nazarov, P.M. Echenique, E.V. Chulkov, Dielectric screening and band-structure effects in low-energy photoemission, Phys. Rev. B 82 (2010) 125102.
[530] E.E. Krasovskii, Attosecond spectroscopy of solids: Streaking phase shift due to lattice scattering, Phys. Rev. B 84 (2011) 195106.
[531] A.G. Borisov, D. Sánchez-Portal, A.K. Kazansky, P.M. Echenique, Resonant and nonresonant processes in attosecond streaking from metals, Phys. Rev. B 87 (2013) 121110.
[532] Q. Liao, U. Thumm, Attosecond time-resolved photoelectron dispersion and photoemission time delays, Phys. Rev. Lett. 112 (2014) 023602.
[533] Q. Liao, U. Thumm, Initial-state, mean-free-path, and skin-depth dependence of attosecond time-resolved ir-streaked xuv photoemission from single-crystalline magnesium, Phys. Rev. A 89 (2014) 033849.
[534] E. Merzbacher, The early history of quantum tunneling., Phys. Today 55 (2002) 44.
[535] M. Razavy, Quantum Theory of Tunneling, World Scientific, Singapore, 2003.
[536] D.K. Roy, Quantum Mechanical Tunneling and its Applications, World Scientific, Singapore, 1987.
[537] L.A. Maccoll, Note on the transmission and reflection of wave packets by potential barriers, Phys. Rev. 40 (1932) 621.
[538] E.H. Hauge, J.A. Støvneng, Tunneling times: a critical review, Rev. Modern Phys. 61 (1989) 917.
[539] R. Landauer, T. Martin, Barrier interaction time in tunneling, Rev. Modern Phys. 66 (1994) 217.
[540] D. Esteve, J.M. Martinis, C. Urbina, E. Turlot, M.H. Devoret, Observation of the temporal decoupling effect on the macroscopic quantum tunneling of a josephson junction, Phys. Scripta T29 (1989) 121.
[541] R. Landauer, Barrier traversal time, Nature 341 (1989) 567.
[542] Y. Ban, E.Y. Sherman, J.G. Muga, M. Büttiker, Time scales of tunneling decay of a localized state, Phys. Rev. A 82 (2010) 062121.
[543] E.A. Galapon, Only above barrier energy components contribute to barrier traversal time, Phys. Rev. Lett. 108 (2012) 170402.
[544] H. Geiger, K. Scheel (Eds.), Handbuch der Physik, Vol. 23, Springer, Berlin, Heidelberg, 1926.
[545] A.S. Landsman, U. Keller, Tunnelling time in strong field ionisation, J. Phys. B: At. Mol. Opt. Phys. 47 (2014) 204024.
[546] J.G. Muga, C.R. Leavens, Arrival time in quantum mechanics, Phys. Rep. 338 (2000) 353.
[547] V.S. Olkhovsky, E. Recami, J. Jakiel, Unified time analysis of photon and particle tunnelling, Phys. Rep. 398 (2004) 133.
[548] H.G. Winful, Tunneling time, the Hartman effect, and superluminality: A proposed resolution of an old paradox, Phys. Rep. 436 (2006) 1.
[549] J.M. Martinis, M.H. Devoret, D. Esteve, C. Urbina, Measuring the time spent traversing the barrier while tunneling, Phys. B: Condensed Matter 152 (1988) 159.
[550] P. Guéret, E. Marclay, H. Meier, Experimental observation of the dynamical image potential in extremely low gaas/alxga1-xas/gaas tunnel barriers, Appl. Phys. Lett. 53 (1988) 1617.
[551] C. Spielmann, R. Szipöcs, A. Stingl, F. Krausz, Tunneling of optical pulses through photonic band gaps, Phys. Rev. Lett. 73 (1994) 2308.
[552] M. Ueda, T. Ando, Electron-escape rate and barrier traversal time influenced by the electromagnetic environment, Phys. Rev. Lett. 72 (1994) 1726.
[553] P. Szriftgiser, D. Guéry-Odelin, M. Arndt, J. Dalibard, Atomic wave diffraction and interference using temporal slits, Phys. Rev. Lett. 77 (1996) 4.
[554] P. Balcou, L. Dutriaux, Dual optical tunneling times in frustrated total internal reflection, Phys. Rev. Lett. 78 (1997) 851.
[555] R. Chiao, A. Steinberg, Tunnelling times and superluminality, in: Progress in Optics, vol. 37, 1997, p. 345.
[556] T. Hils, J. Felber, R. Gähler, W. Gläser, R. Golub, K. Habicht, P. Wille, Matter-wave optics in the time domain: Results of a cold-neutron experiment, Phys. Rev. A 58 (1998) 4784.
[557] S. Yang, J. Page, Z. Liu, M. Cowan, C. Chan, P. Sheng, Ultrasound tunneling through 3d phononic crystals, Phys. Rev. Lett. 88 (2002) 104301.
[558] J.C. Martinez, E. Polatdemir, Measurement of tunneling time via electron interferometry, Appl. Phys. Lett. 84 (2004) 1320.
[559] D. Villegas, F. de Leon-Perez, R. Perez-Alvarez, Tunneling time of long-wavelength phonons through semiconductor heterostructures, Phys. Rev. B 71 (2005) 035322.
[560] H.G. Winful, Nature of "superluminal" barrier tunneling, Phys. Rev. Lett. 90 (2003) 023901.
[561] G.M. Gehring, A.C. Liapis, S.G. Lukishova, R.W. Boyd, Time-domain measurements of reflection delay in frustrated total internal reflection, Phys. Rev. Lett. 111 (2013) 030404.
[562] C.R. McDonald, G. Orlando, G. Vampa, T. Brabec, Tunnel ionization dynamics of bound systems in laser fields: How long does it take for a bound electron to tunnel? Phys. Rev. Lett. 111 (2013) 090405.
[563] G. Orlando, C.R. McDonald, N.H. Protik, T. Brabec, Identification of the keldysh time as a lower limit for the tunneling time, Phys. Rev. A 89 (2014) 014102.
[564] G. Orlando, C.R. McDonald, N.H. Protik, G. Vampa, T. Brabec, Tunnelling time, what does it mean? J. Phys. B: At. Mol. Opt. Phys. 47 (2014) 204002.
[565] M. Büttiker, R. Landauer, Traversal time for tunneling, Phys. Rev. Lett. 49 (1982) 1739.
[566] N. Yamada, Unified derivation of tunneling times from decoherence functionals, Phys. Rev. Lett. 93 (2004) 170401.
[567] G. Sansone, T. Pfeifer, K. Simeonidis, A.I. Kuleff, Electron correlation in real time, ChemPhysChem 13 (2012) 661.
[568] G. Tanner, K. Richter, J. Rost, The theory of two-electron atoms: between ground state and complete fragmentation, Rev. Modern Phys. 72 (2000) 497.
[569] C.F.d.M. Faria, X. Liu, Electron–electron correlation in strong laser fields, J. Modern Opt. 58 (2011) 1076.
[570] W. Becker, H. Rottke, Many-electron strong-field physics, Contemp. Physics 49 (2008) 199.
[571] R. Dorner, T. Weber, M. Weckenbrock, A. Staudte, M. Hattass, H. Schmidt-Bocking, R. Moshammer, J. Ullrich, Multiple ionization in strong laser fields, in: Advances in Atomic, Molecular, and Optical Physics, in: Advances in Atomic, Molecular, and Optical Physics, vol. 48, Academic Press Inc., 2002, p. 1.
[572] H. van der Hart, K. Burnett, Recollision model for double ionization of atoms in strong laser fields, Phys. Rev. A 62 (2000) 013407.
[573] M. Lein, E. Gross, V. Engel, Intense-field double ionization of helium: Identifying the mechanism, Phys. Rev. Lett. 85 (2000) 4707.
[574] B. Feuerstein, R. Moshammer, D. Fischer, A. Dorn, C.D. Schroter, J. Deipenwisch, J.R.C. Lopez-Urrutia, C. Hohr, P. Neumayer, J. Ullrich, H. Rottke, C. Trump, M. Wittmann, G. Korn, W. Sandner, Separation of recollision mechanisms in nonsequential strong field double ionization of argon: The role of excitation tunneling, Phys. Rev. Lett. 87 (2001) 043003.

[575] J. Liu, D.F. Ye, J. Chen, X. Liu, Complex dynamics of correlated electrons in molecular double ionization by an ultrashort intense laser pulse, Phys. Rev. Lett. 99 (2007) 013003.
[576] Y. Zhou, C. Huang, Q. Liao, P. Lu, Classical simulations including electron correlations for sequential double ionization, Phys. Rev. Lett. 109 (2012) 053004.
[577] L. Zhang, X. Xie, S. Roither, Y. Zhou, P. Lu, D. Kartashov, M. Schoeffler, D. Shafir, P.B. Corkum, A. Baltuska, A. Staudte, M. Kitzler, Subcycle control of electron–electron correlation in double ionization, Phys. Rev. Lett. 112 (2014) 193002.
[578] F. Mauger, C. Chandre, T. Uzer, From recollisions to the knee: A road map for double ionization in intense laser fields, Phys. Rev. Lett. 104 (2010) 043005.
[579] F. Mauger, C. Chandre, T. Uzer, Recollisions and correlated double ionization with circularly polarized light, Phys. Rev. Lett. 105 (2010) 083002.
[580] L.B. Fu, G.G. Xin, D.F. Ye, J. Liu, Recollision dynamics and phase diagram for nonsequential double ionization with circularly polarized laser fields, Phys. Rev. Lett. 108 (2012) 103601.
[581] F. Mauger, C. Chandre, T. Uzer, Strong field double ionization: The phase space perspective, Phys. Rev. Lett. 102 (2009) 173002.
[582] F. Mauger, A. Kamor, C. Chandre, T. Uzer, Mechanism of delayed double ionization in a strong laser field, Phys. Rev. Lett. 108 (2012) 063001.
[583] M. Forre, S. Selsto, R. Nepstad, Nonsequential two-photon double ionization of atoms: Identifying the mechanism, Phys. Rev. Lett. 106 (2011) 129905.
[584] T. Weber, H. Giessen, M. Weckenbrock, G. Urbasch, A. Staudte, L. Spielberger, O. Jagutzki, V. Mergel, M. Vollmer, R. Dorner, Correlated electron emission in multiphoton double ionization, Nature 405 (2000) 658.
[585] P.J. Ho, J.H. Eberly, Classical effects of laser pulse duration on strong-field double ionization, Phys. Rev. Lett. 95 (2005) 193002.
[586] A. Staudte, C. Ruiz, M. Schoeffler, S. Schoessler, D. Zeidler, T. Weber, M. Meckel, D.M. Villeneuve, P.B. Corkum, A. Becker, R. Doerner, Binary and recoil collisions in strong field double ionization of helium, Phys. Rev. Lett. 99 (2007) 263002.
[587] S.X. Hu, Boosting photoabsorption by attosecond control of electron correlation, Phys. Rev. Lett. 111 (2013) 123003.
[588] D.I. Bondar, G.L. Yudin, W.K. Liu, M.Y. Ivanov, A.D. Bandrauk, Nonsequential double ionization below laser-intensity threshold: Anticorrelation of electrons without excitation of parent ion, Phys. Rev. A 83 (2011) 013420.
[589] A. Becker, F. Faisal, Intense-field many-body S-matrix theory, J. Phys. B 38 (2005) R1.
[590] A. Becker, F. Faisal, Interpretation of momentum distribution of recoil ions from laser induced nonsequential double ionization, Phys. Rev. Lett. 84 (2000) 3546.
[591] R. Kopold, W. Becker, H. Rottke, W. Sandner, Routes to nonsequential double ionization, Phys. Rev. Lett. 85 (2000) 3781.
[592] X. Hao, J. Chen, W. Li, B. Wang, X. Wang, W. Becker, Quantum effects in double ionization of argon below the threshold intensity, Phys. Rev. Lett. 112 (2014) 073002.
[593] L. Avaldi, A. Huetz, Photodouble ionization and the dynamics of electron pairs in the continuum, J. Phys. B 38 (2005) S861.
[594] J. Briggs, V. Schmidt, Differential cross sections for photo-double-ionization of the helium atom, J. Phys. B 33 (2000) R1.
[595] A.A. Sorokin, M. Wellhoefer, S.V. Bobashev, K. Tiedtke, M. Richter, X-ray-laser interaction with matter and the role of multiphoton ionization: Free-electron-laser studies on neon and helium, Phys. Rev. A 75 (2007) 051402.
[596] S. Askeland, R. Nepstad, M. Forre, Two-photon double ionization of helium by attosecond laser pulses: Evidence of highly correlated electron motion, Phys. Rev. A 85 (2012) 035404.
[597] L. Malegat, H. Bachau, B. Piraux, F. Reynal, A novel estimate of the two-photon double-ionization cross section of helium, J. Phys. B 45 (2012) 175601.
[598] I.A. Ivanov, A.S. Kheifets, J. Dubau, On the account of final state correlation in double ionization processes, Eur. Phys. J. D 61 (2011) 563.
[599] R. Pazourek, J. Feist, S. Nagele, E. Persson, B.I. Schneider, L.A. Collins, J. Burgdörfer, Universal features in sequential and nonsequential two-photon double ionization of helium, Phys. Rev. A 83 (2011) 053418.
[600] R. Nepstad, T. Birkeland, M. Forre, Numerical study of two-photon ionization of helium using an ab initio numerical framework, Phys. Rev. A 81 (2010) 063402.
[601] A. Palacios, D.A. Horner, T.N. Rescigno, C.W. McCurdy, Two-photon double ionization of the helium atom by ultrashort pulses, J. Phys. B 43 (2010) 194003.
[602] E. Foumouo, H. Bachau, B. Piraux, $(2\gamma, 2e)$ total and differential cross-section calculations for helium with $\hbar\omega = 40$–50 eV, Eur. Phys. J. ST 175 (2009) 175.
[603] A. Palacios, T.N. Rescigno, C.W. McCurdy, Time-dependent treatment of two-photon resonant single and double ionization of helium by ultrashort laser pulses, Phys. Rev. A 79 (2009) 033402.
[604] J. Feist, S. Nagele, R. Pazourek, E. Persson, B.I. Schneider, L.A. Collins, J. Burgdörfer, Nonsequential two-photon double ionization of helium, Phys. Rev. A 77 (2008) 043420.
[605] E. Foumouo, P. Antoine, B. Piraux, L. Malegat, H. Bachau, R. Shakeshaft, Evidence for highly correlated electron dynamics in two-photon double ionization of helium, J. Phys. B 41 (2008) 051001.
[606] X. Guan, K. Bartschat, B.I. Schneider, Dynamics of two-photon double ionization of helium in short intense xuv laser pulses, Phys. Rev. A 77 (2008) 043421.
[607] D.A. Horner, C.W. McCurdy, T.N. Rescigno, Triple differential cross sections and nuclear recoil in two-photon double ionization of helium, Phys. Rev. A 78 (2008) 043416.
[608] P. Lambropoulos, L.A.A. Nikolopoulos, M.G. Makris, A. Mihelic, Direct versus sequential double ionization in atomic systems, Phys. Rev. A 78 (2008) 055402.
[609] D.A. Horner, F. Morales, T.N. Rescigno, F. Martin, C.W. McCurdy, Two-photon double ionization of helium above and below the threshold for sequential ionization, Phys. Rev. A 76 (2007) 030701.
[610] I.A. Ivanov, A.S. Kheifets, Two-photon double ionization of helium in the region of photon energies 42–50 eV, Phys. Rev. A 75 (2007) 033411.
[611] L.A.A. Nikolopoulos, P. Lambropoulos, Time-dependent theory of double ionization of helium under XUV radiation, J. Phys. B 40 (2007) 1347.
[612] E. Foumouo, G.L. Kamta, G. Edah, B. Piraux, Theory of multiphoton single and double ionization of two-electron atomic systems driven by short-wavelength electric fields: An ab initio treatment, Phys. Rev. A 74 (2006) 063409.
[613] A.S. Kheifets, I.A. Ivanov, Convergent close-coupling calculations of two-photon double ionization of helium, J. Phys. B 39 (2006) 1731.
[614] L.A.A. Nikolopoulos, P. Lambropoulos, Comment on "Production of doubly charged helium ions by two-photon absorption of an intense sub-10-fs soft X-ray pulse at 42 eV photon energy", Phys. Rev. Lett. 97 (2006) 169301.
[615] D. Fursa, I. Bray, Convergent close-coupling calculations of electron-helium scattering, J. Phys. B 30 (1997) 757.
[616] I. Bray, D. Fursa, A. Kheifets, A. Stelbovics, Electrons and photons colliding with atoms development and application of the convergent close-coupling method, J. Phys. B 35 (2002) R117.
[617] T. Gorczyca, N. Badnell, Photoionization-excitation of helium using an R-matrix with pseudostates method, J. Phys. B 30 (1997) 3897.
[618] K. Bartschat, E. Hudson, M. Scott, P. Burke, V. Burke, Electron-atom scattering at low and intermediate energies using a pseudo-state R-matrix basis, J. Phys. B 29 (1996) 115.
[619] M.S. Pindzola, F. Robicheaux, S.D. Loch, J.C. Berengut, T. Topcu, J. Colgan, M. Foster, D.C. Griffin, C.P. Ballance, D.R. Schultz, T. Minami, N.R. Badnell, M.C. Witthoeft, D.R. Plante, D.M. Mitnik, J.A. Ludlow, U. Kleiman, The time-dependent close-coupling method for atomic and molecular collision processes, J. Phys. B 40 (2007) R39.
[620] M. Kornberg, P. Lambropoulos, Photoelectron energy spectrum in 'direct' two-photon double ionization of helium, J. Phys. B 32 (1999) L603.
[621] L. Nikolopoulos, P. Lambropoulos, Multichannel theory of two-photon single and double ionization of helium, J. Phys. B 34 (2001) 545.
[622] S. Hu, J. Colgan, L. Collins, Triple-differential cross-sections for two-photon double ionization of He near threshold, J. Phys. B 38 (2005) L35.
[623] I.A. Ivanov, A.S. Kheifets, Perturbative calculation of two-photon double electron ionization of helium, J. Phys. B 41 (2008) 095002.
[624] H. Bachau, Theory of two-photon double ionization of helium at the sequential threshold, Phys. Rev. A 83 (2011) 033403.
[625] R. Shakeshaft, Two-photon single and double ionization of helium, Phys. Rev. A 76 (2007) 063405.

[626] T. Mercouris, C. Haritos, C. Nicolaides, Theory and computation of the rate of multiphoton two-electron ionization via the direct mechanism, J. Phys. B 34 (2001) 3789.
[627] T. Mercouris, C.A. Nicolaides, He in dichromatic weak or strong ac fields of $\lambda_1 = 248$ nm and $\lambda_2 = (1/m)248$ nm ($m = 2, 3, 4$), Phys. Rev. A 63 (2000) 013411.
[628] M. Pindzola, F. Robicheaux, Two-photon double ionization of He and H^-, J. Phys. B 31 (1998) L823.
[629] J. Colgan, M. Pindzola, Core-excited resonance enhancement in the two-photon complete fragmentation of helium, Phys. Rev. Lett. 88 (2002) 173002.
[630] L. Feng, H. van der Hart, Two-photon double ionization of He, J. Phys. B 36 (2003) L1.
[631] H. W. van der Hart, Time-dependent R-matrix theory applied to two-photon double ionization of He, Phys. Rev. A 89 (2014) 053407.
[632] W.-C. Jiang, L.-Y. Peng, W.-H. Xiong, Q. Gong, Comparison study of electron correlation in one-photon and two-photon double ionization of helium, Phys. Rev. A 88 (2013) 023410.
[633] Z. Zhang, L.-Y. Peng, Q. Gong, T. Morishita, Momentum space analysis of multiphoton double ionization of helium by intense attosecond xuv pulses, Opt. Express 18 (2010) 8976.
[634] S. Laulan, H. Bachau, Correlation effects in two-photon single and double ionization of helium, Phys. Rev. A 68 (2003) 013409.
[635] B. Piraux, J. Bauer, S. Laulan, H. Bachau, Probing electron–electron correlation with attosecond pulses, Eur. Phys. J. D 26 (2003) 7.
[636] H. Hasegawa, E. Takahashi, Y. Nabekawa, K. Ishikawa, K. Midorikawa, Multiphoton ionization of He by using intense high-order harmonics in the soft-x-ray region, Phys. Rev. A 71 (2005) 023407.
[637] M. Forre, S. Selsto, R. Nepstad, Nonsequential two-photon double ionization of atoms: Identifying the mechanism, Phys. Rev. Lett. 105 (2010) 163001.
[638] L. Argenti, R. Pazourek, J. Feist, S. Nagele, M. Liertzer, E. Persson, J. Burgdörfer, E. Lindroth, Photoionization of helium by attosecond pulses: Extraction of spectra from correlated wave functions, Phys. Rev. A 87 (2013) 053405.
[639] J. Ullrich, R. Moshammer, A. Dorn, R. Dorner, L.P.H. Schmidt, H. Schniidt-Bocking, Recoil-ion and electron momentum spectroscopy: reaction-microscopes, Rep. Progr. Phys. 66 (2003) 1463.
[640] A. Rudenko, L. Foucar, M. Kurka, T. Ergler, K.U. Kuehnel, Y.H. Jiang, A. Voitkiv, B. Najjari, A. Kheifets, S. Luedemann, T. Havermeier, M. Smolarski, S. Schoessler, K. Cole, M. Schoeffler, R. Doerner, S. Duesterer, W. Li, B. Keitel, R. Treusch, M. Gensch, C.D. Schroeter, R. Moshammer, J. Ullrich, Recoil-ion momentum distributions for two-photon double ionization of helium and neon by 44 ev free-electron laser radiation, Phys. Rev. Lett. 101 (2008) 073003.
[641] W.-C. Jiang, Y. Tong, Q. Gong, L.-Y. Peng, Recoil-ion-momentum spectrum for few-photon double ionization of helium, Phys. Rev. A 89 (2014) 043422.
[642] M. Kurka, J. Feist, D.A. Horner, A. Rudenko, Y.H. Jiang, K.U. Kuehnel, L. Foucar, T.N. Rescigno, C.W. McCurdy, R. Pazourek, S. Nagele, M. Schulz, O. Herrwerth, M. Lezius, M.F. Kling, M. Schoeffler, A. Belkacem, S. Duesterer, R. Treusch, B.I. Schneider, L.A. Collins, J. Burgdörfer, C.D. Schröter, R. Moshammer, J. Ullrich, Differential cross sections for non-sequential double ionization of He by 52 eV photons from the Free Electron Laser in Hamburg, FLASH, New J. Phys. 12 (2010) 073035.
[643] D.A. Horner, T.N. Rescigno, C.W. McCurdy, Nuclear recoil cross sections from time-dependent studies of two-photon double ionization of helium, Phys. Rev. A 81 (2010) 023410.
[644] D.A. Horner, T.N. Rescigno, C.W. McCurdy, Decoding sequential versus nonsequential two-photon double ionization of helium using nuclear recoil, Phys. Rev. A 77 (2008) 030703.
[645] S.A. Abdel-Naby, M.S. Pindzola, J. Colgan, Nuclear-recoil differential cross sections for the double photoionization of helium, Phys. Rev. A 86 (2012) 013424.
[646] S.A. Abdel-Naby, M.F. Ciappina, M.S. Pindzola, J. Colgan, Nuclear-recoil differential cross sections for the two-photon double ionization of helium, Phys. Rev. A 87 (2013) 063425.
[647] K. Stefanska, F. Reynal, H. Bachau, Two-photon double ionization of He(1s(2)) and He(1s2s(1)S) by xuv short pulses, Phys. Rev. A 85 (2012) 053405.
[648] E.P. Mansson, D. Guenot, C.L. Arnold, D. Kroon, S. Kasper, J.M. Dahlstrom, E. Lindroth, A.S. Kheifets, A. L'Huillier, S.L. Sorensen, M. Gisselbrecht, Double ionization probed on the attosecond timescale, Nat. Phys. 10 (2014) 207.
[649] S. Gilbertson, M. Chini, X. Feng, S. Khan, Y. Wu, Z. Chang, Monitoring and controlling the electron dynamics in helium with isolated attosecond pulses, Phys. Rev. Lett. 105 (2010) 263003.
[650] L. Argenti, E. Lindroth, Ionization branching ratio control with a resonance attosecond clock, Phys. Rev. Lett. 105 (2010) 053002.
[651] U. Fano, Effects of configuration interaction on intensities and phase shifts, Phys. Rev. 124 (1961) 1866.
[652] T. Mercouris, Y. Komninos, C.A. Nicolaides, Time-dependent formation of the profile of the He 2s2p P-1(o) state excited by a short laser pulse, Phys. Rev. A 75 (2007) 013407.
[653] X. Tong, C. Lin, Double photoexcitation of He atoms by attosecond xuv pulses in the presence of intense few-cycle infrared lasers, Phys. Rev. A 71 (2005) 033406.
[654] M. Wickenhauser, J. Burgdörfer, F. Krausz, M. Drescher, Time resolved Fano resonances, Phys. Rev. Lett. 94 (2005) 023002.
[655] Z. Zhao, C. Lin, Theory of laser-assisted autoionization by attosecond light pulses, Phys. Rev. A 71 (2005) 060702.
[656] J.D. Lee, Model for the attosecond resonant photoemission of copper dichloride: Evidence for high-order fano resonances and a time-domain core-hole clock, Phys. Rev. Lett. 111 (2013) 027401.
[657] C. Ott, A. Kaldun, P. Raith, K. Meyer, M. Laux, J. Evers, C.H. Keitel, C.H. Greene, T. Pfeifer, Lorentz meets fano in spectral line shapes: a universal phase and its laser control, Science 340 (2013) 716.
[658] C.D. Lin, W.-C. Chu, Controlling atomic line shapes, Science 340 (2013) 694.
[659] A. Kaldun, C. Ott, A. Blaettermann, M. Laux, K. Meyer, T. Ding, A. Fischer, T. Pfeifer, Extracting phase and amplitude modifications of laser-coupled fano resonances, Phys. Rev. Lett. 112 (2014) 103001.
[660] A. Palacios, T.N. Rescigno, C.W. McCurdy, Two-electron time-delay interference in atomic double ionization by attosecond pulses, Phys. Rev. Lett. 103 (2009) 253001.
[661] T. Reddish, J. Wightman, M. MacDonald, S. Cvejanovic, Triple differential cross section measurements for double photoionization of D_2, Phys. Rev. Lett. 79 (1997) 2438.
[662] J. Wightman, S. Cvejanovic, T. Reddish, (gamma,2e) cross section measurements of D_2 and He, J. Phys. B 31 (1998) 1753.
[663] T. Weber, A.O. Czasch, O. Jagutzki, A.K. Mueller, V. Mergel, A. Kheifets, E. Rotenberg, G. Meigs, M.H. Prior, S. Daveau, A. Landers, C.L. Cocke, T. Osipov, R. Diez Muino, H. Schmidt-Boecking, R. Doerner, Complete photo-fragmentation of the deuterium molecule, Nature 443 (2006) 1014.
[664] T. Weber, A. Czasch, O. Jagutzki, A. Muller, V. Mergel, A. Kheifets, E. Rotenberg, G. Meigs, M. Prior, S. Daveau, A. Landers, C. Cocke, T. Osipov, R. Muino, H. Schmidt-Bocking, R. Dorner, Complete photo-fragmentation of the deuterium molecule, Nature 431 (2004) 437.
[665] T. Weber, A. Czasch, O. Jagutzki, A. Muller, V. Mergel, A. Kheifets, J. Feagin, E. Rotenberg, G. Meigs, M. Prior, S. Daveau, A. Landers, C. Cocke, T. Osipov, H. Schmidt-Bocking, R. Dorner, Fully differential cross sections for photo-double-ionization of D_2, Phys. Rev. Lett. 92 (2004) 163001.
[666] T.J. Reddish, J. Colgan, P. Bolognesi, L. Avaldi, M. Gisselbrecht, M. Lavollee, M.S. Pindzola, A. Huetz, Physical interpretation of the "Kinetic Energy Release" effect in the double photoionization of H_2, Phys. Rev. Lett. 100 (2008) 193001.
[667] M. Gisselbrecht, M. Lavollee, A. Huetz, P. Bolognesi, L. Avaldi, D. Seccombe, T. Reddish, Photodouble ionization dynamics for fixed-in-space h_2, Phys. Rev. Lett. 96 (2006) 153002.
[668] D.A. Horner, S. Miyabe, T.N. Rescigno, C.W. McCurdy, F. Morales, F. Martin, Classical two-slit interference effects in double photoionization of molecular hydrogen at high energies, Phys. Rev. Lett. 101 (2008) 183002.
[669] D.A. Horner, W. Vanroose, T.N. Rescigno, F. Martin, C.W. McCurdy, Role of nuclear motion in double ionization of molecular hydrogen by a single photon, Phys. Rev. Lett. 98 (2007) 073001.
[670] W. Vanroose, D.A. Horner, F. Martin, T.N. Rescigno, C.W. McCurdy, Double photoionization of aligned molecular hydrogen, Phys. Rev. A 74 (2006) 052702.
[671] W. Vanroose, F. Martin, T. Rescigno, C. McCurdy, Complete photo-induced breakup of the H_2 molecule as a probe of molecular electron correlation, Science 310 (2005) 1787.

[672] J. Colgan, M.S. Pindzola, F. Robicheaux, Triple differential cross sections for the double photoionization of H_2, Phys. Rev. Lett. 98 (2007) 153001.
[673] I.A. Ivanov, A.S. Kheifets, Time-dependent calculations of double photoionization of the aligned H_2 molecule, Phys. Rev. A 85 (2012) 013406.
[674] L. Tao, C.W. McCurdy, T.N. Rescigno, Grid-based methods for diatomic quantum scattering problems. III. Double photoionization of molecular hydrogen in prolate spheroidal coordinates, Phys. Rev. A 82 (2010) 023423.
[675] W.-C. Jiang, L.-Y. Peng, J.-W. Geng, Q. Gong, One-photon double ionization of H_2 with arbitrary orientation, Phys. Rev. A 88 (2013) 063408.
[676] X. Guan, K. Bartschat, B.I. Schneider, Breakup of the aligned H_2 molecule by xuv laser pulses: A time-dependent treatment in prolate spheroidal coordinates, Phys. Rev. A 83 (2011) 043403.
[677] J. Colgan, M.S. Pindzola, F. Robicheaux, Two-photon double ionization of the hydrogen molecule, J. Phys. B 41 (2008) 121002.
[678] X. Guan, K. Bartschat, B.I. Schneider, Two-photon double ionization of H_2 in intense femtosecond laser pulses, Phys. Rev. A 82 (2010) 041404.
[679] I.A. Ivanov, A.S. Kheifets, Two-photon double ionization of the H_2 molecule: Cross sections and amplitude analysis, Phys. Rev. A 87 (2013) 023414.
[680] F. Morales, F. Martin, D.A. Horner, T.N. Rescigno, C.W. McCurdy, Two-photon double ionization of H_2 at 30 eV using exterior complex scaling, J. Phys. B 42 (2009) 134013.
[681] F. Lepine, G. Sansone, M.J.J. Vrakking, Molecular applications of attosecond laser pulses, Chem. Phys. Lett. 578 (2013) 1.
[682] G. Sansone, F. Kelkensberg, J.F. Perez-Torres, F. Morales, M.F. Kling, W. Siu, O. Ghafur, P. Johnsson, M. Swoboda, E. Benedetti, F. Ferrari, F. Lepine, J.L. Sanz-Vicario, S. Zherebtsov, I. Znakovskaya, A. L'Huillier, M.Y. Ivanov, M. Nisoli, F. Martin, M.J.J. Vrakking, Electron localization following attosecond molecular photoionization, Nature 465 (2010) 763.
[683] F. Remacle, M. Nest, R.D. Levine, Laser steered ultrafast quantum dynamics of electrons in LiH, Phys. Rev. Lett. 99 (2007) 183902.
[684] F. Remacle, R. Kienberger, F. Krausz, R.D. Levine, On the feasibility of an ultrafast purely electronic reorganization in lithium hydride, Chem. Phys. 338 (2007) 342.
[685] B. Mignolet, A. Gijsbertsen, M.J.J. Vrakking, R.D. Levine, F. Remacle, Stereocontrol of attosecond time-scale electron dynamics in ABCU using ultrafast laser pulses: a computational study, Phys. Chem. Chem. Phys. 13 (2011) 8331.
[686] I. Barth, J. Manz, Y. Shigeta, K. Yagi, Unidirectional electronic ring current driven by a few cycle circularly polarized laser pulse: Quantum model simulations for Mg-porphyrin, J. Am. Chem. Soc. 128 (2006) 7043.
[687] A. Bandrauk, S. Chelkowski, H. Nguyen, Attosecond localization of electrons in molecules, Int. J. Quant. Chem. 100 (2004) 834.
[688] M. Lein, Attosecond probing of vibrational dynamics with high-harmonic generation, Phys. Rev. Lett. 94 (2005) 053004.
[689] S. Baker, J. Robinson, C. Haworth, H. Teng, R. Smith, C. Chirila, M. Lein, J. Tisch, J. Marangos, Probing proton dynamics in molecules on an attosecond time scale, Science 312 (2006) 424.
[690] S. Baker, J.S. Robinson, M. Lein, C.C. Chirila, R. Torres, H.C. Bandulet, D. Comtois, J.C. Kieffer, D.M. Villeneuve, J.W.G. Tisch, J.P. Marangos, Dynamic two-center interference in high-order harmonic generation from molecules with attosecond nuclear motion, Phys. Rev. Lett. 101 (2008) 053901.
[691] S. Patchkovskii, Nuclear dynamics in polyatomic molecules and high-order harmonic generation, Phys. Rev. Lett. 102 (2009) 253602.
[692] W. Li, X. Zhou, R. Lock, S. Patchkovskii, A. Stolow, H.C. Kapteyn, M.M. Murnane, Time-resolved dynamics in N_2O_4 probed using high harmonic generation, Science 322 (2008) 1207.
[693] H.J. Woerner, J.B. Bertrand, B. Fabre, J. Higuet, H. Ruf, A. Dubrouil, S. Patchkovskii, M. Spanner, Y. Mairesse, V. Blanchet, E. Mevel, E. Constant, P.B. Corkum, D.M. Villeneuve, Conical intersection dynamics in NO_2 probed by homodyne high-harmonic spectroscopy, Science 334 (2011) 208.
[694] A.-T. Le, T. Morishita, R.R. Lucchese, C.D. Lin, Theory of high harmonic generation for probing time-resolved large-amplitude molecular vibrations with ultrashort intense lasers, Phys. Rev. Lett. 109 (2012) 203004.
[695] M. Spanner, J. Mikosch, A.E. Boguslavskiy, M.M. Murnane, A. Stolow, S. Patchkovskii, Strong-field ionization and high-order-harmonic generation during polyatomic molecular dynamics of N_2O_4, Phys. Rev. A 85 (2012) 033426.
[696] M.Y. Emelin, M.Y. Ryabikin, A.M. Sergeev, Monitoring long-term evolution of molecular vibrational wave packet using high-order harmonic generation, New J. Phys. 10 (2008) 025026.
[697] X.-B. Bian, A.D. Bandrauk, Probing nuclear motion by frequency modulation of molecular high-order harmonic generation, Phys. Rev. Lett. 113 (2014) 193901.
[698] L. Cederbaum, J. Zobeley, Ultrafast charge migration by electron correlation, Chem. Phys. Lett. 307 (1999) 205.
[699] B. Cooper, V. Averbukh, Single-photon laser-enabled auger spectroscopy for measuring attosecond electron-hole dynamics, Phys. Rev. Lett. 111 (2013) 083004.
[700] J. Leeuwenburgh, B. Cooper, V. Averbukh, J.P. Marangos, M. Ivanov, High-order harmonic generation spectroscopy of correlation-driven electron hole dynamics, Phys. Rev. Lett. 111 (2013) 123002.
[701] J. Breidbach, L. Cederbaum, Universal attosecond response to the removal of an electron, Phys. Rev. Lett. 94 (2005) 033901.
[702] H. Hennig, J. Breidbach, L. Cederbaum, Electron correlation as the driving force for charge transfer: Charge migration following ionization in N-methyl acetamide, J. Phys. Chem. A 109 (2005) 409.
[703] A.I. Kuleff, L.S. Cederbaum, Charge migration in different conformers of glycine: The role of nuclear geometry, Chem. Phys. 338 (2007) 320.
[704] F. Remacle, R. Levine, An electronic time scale in chemistry, Proc. Natl. Acad. Sci. 103 (2006) 6793.
[705] M. Kanno, H. Kono, Y. Fujimura, S.H. Lin, Nonadiabatic response model of laser-induced ultrafast pi-electron rotations in chiral aromatic molecules, Phys. Rev. Lett. 104 (2010) 108302.
[706] C. Neidel, J. Klei, C.-H. Yang, A. Rouzée, M.J.J. Vrakking, K. Klünder, M. Miranda, C.L. Arnold, T. Fordell, A. L'Huillier, M. Gisselbrecht, P. Johnsson, M.P. Dinh, E. Suraud, P.-G. Reinhard, V. Despré, M.A.L. Marques, F. Lépine, Probing time-dependent molecular dipoles on the attosecond time scale, Phys. Rev. Lett. 111 (2013) 033001.
[707] W. Siu, F. Kelkensberg, G. Gademann, A. Rouzee, P. Johnsson, D. Dowek, M. Lucchini, F. Calegari, U. De Giovannini, A. Rubio, R.R. Lucchese, H. Kono, F. Lepine, M.J.J. Vrakking, Attosecond control of dissociative ionization of O_2 molecules, Phys. Rev. A 84 (2011) 063412.
[708] L. Belshaw, F. Calegari, M.J. Duffy, A. Trabattoni, L. Poletto, M. Nisoli, J.B. Greenwood, Observation of ultrafast charge migration in an amino acid, J. Phys. Chem. Lett. 3 (2012) 3751.
[709] R. Omnes, Consistent interpretations of quantum-mechanics, Rev. Modern Phys. 64 (1992) 339.